ESTIMATION OF HYDROLOGICAL PROPERTIES OF SOUTH AFRICAN SOILS

by

JOHN LESLIE HUTSON.

(M.Sc. Agric. (Natal))

Submitted in partial fulfilment

of the requirements for the degree of

Doctor of Philosophy

in the

Department of Soil Science and Agrometeorology

University of Natal,

PIETERMARITZBURG.

SEPTEMBER 1983.

DECLARATION

In the execution of the research reported in this thesis, specific assistance and information, other than from my supervisors, was received from:

Dr C.N. MacVicar and pedologists of the Soil and Irrigation Research Institute, who provided soil samples and classification data from the South African Land Type Survey;

Mrs M. Sobczyk and staff of the Analytical Section, S.I.R.I., who performed the organic carbon analyses;

Dr A. Cass, Mr M. Hensley, Mr M. Johnston, Mr R. Mottram, Dr D. Scotney and Mr D. Turner, who provided soil water retentivity data;

Participants in the Israel-South African workshop on the soil-tree-atmosphere continuum, Addo, November, 1981, who sampled the lysimeters and determined root distributions, and to staff at the Citrus and Sub-tropical Fruit Research Institute Research Station, Addo, who recorded tensiometer, lysimeter and rainfall data.

J.L. Hutson

Dr A. Cass

Supervisor

CONTENTS

CONTENTS
(Contd.)

CONTENTS
(Contd.)

CONTENTS
(Contd.)

ABSTRACT

A computer simulation model of the soil water regime can be a useful research, planning and management tool, providing that the data required by the model are available. Finite difference solutions of the general flow equation can be applied to complex field situations if soil profile characteristics are reflected by appropriate retentivity ($\theta(\psi)$) and hydraulic conductivity ($K(\psi)$) functions.

The validity of a flow simulation model depends upon the degree to which simulated flow corresponds to the flow pattern in real soils. Macroscopic flow in apedal soils is likely to obey Darcy's law but in structured or swelling soils, macro-pores and shrinkage voids lead to non-Darcian flow. Physical composition and structural stability properties of a wide range of South African soils were used to assess swelling behaviour and depth-related textural changes. The applicability of a one-dimensional Darcian flow model to various soil types was evaluated.

Core retentivity data for South African soils were used to derive regression equations for predicting $\theta(\psi)$ from textural criteria and bulk density. A sigmoidal, non-hysteretic two-part retentivity function having only two constants in addition to porosity was developed for use in water flow simulation models. Values of the constants, shapes of the retentivity curves and soil textural properties were related by fitting the retentivity function to retentivity data generated using regression equations. Hydraulically inhomogeneous soils may be modelled by varying the values of the retentivity constants through the profile to reflect changing soil properties.

Equations for calculating $K(\theta)$ or $K(\psi)$ from retentivity data were derived by applying each of three capillary models to both exponential and two-part retentivity functions. Comparison of these equations showed that the definition and value of semi-empirical constants in the capillary models were as important as the choice of model in determining $K(\theta)$. $K(\psi)$ was calculated using retentivity constants corresponding to a range of bulk density, clay and silt content combinations. Three retentivity constant-soil property systems were evaluated. These were derived from retentivity data for South African soils between 1) -10 and -1500 kPa, 2) 0 and -50 kPa and 3) from published retentivity data for British soils. Only that derived from retentivity data accurate in the 0 to -50 kPa range led to $K(\psi)$ relationships in which saturated K and the slope $\delta K/\delta\psi$ decreased as bulk density, clay or silt content increased. Absolute values of K were unreliable and measured values are essential for matching purposes.

A method for evaluating the constants in a $K(\psi)$ or $K(\theta)$ function from the rate of outflow or inflow of water after a step change in potential at the base of a soil core was described. Simple exponential $\theta(\psi)$ and $K(\psi)$ functions were assumed to apply to each pressure potential range. Retentivity parameters were obtained by fitting the $\theta(\psi)$ function to the measured retentivity curve. A value for K_s, the remaining unknown parameter in the $K(\psi)$ function, was obtained by matching measured outflow and inflow data to a family of simulated curves. These were computed using measured retentivity parameters, core dimensions and ceramic plate conductivity, and a range of K_s values. An advantage of this method is that

there are no limitations on core length, plate impedance or pressure potential range which cannot be ascertained by prior simulation.

Regression equations relating texture to retentivity, and a conductivity model were applied in a simulation study of the water regime in a weighing lysimeter in which gains and losses of water were measured accurately. Active root distribution was assumed proportional to root mass distribution. Relative $K(\psi)$ curves for each node were computed using one of the conductivity equations derived earlier. Daily water potentials for a month were simulated using three conductivity matching factors. By matching simulated ψ values to tensiometer potentials measured at five depths an appropriate matching factor was chosen. The effects of an over- or underestimate of $K(\psi)$ were demonstrated.

This work simplifies the prediction and use of retentivity and conductivity relationships in soil water flow simulation models. These models can be used for assessing the water regime in both irrigated and dry-land crop production. Other applications include catchment modelling, effluent disposal and nutrient and solute transport in soil.

ACKNOWLEDGEMENTS

I wish to thank the following persons who assisted during this investigation:

Dr A.Cass and Prof. J.M. de Villiers, who supervised this investigation;

The Department of Agriculture for permission to submit the results of this research in the form of a thesis;

Dr M.C.F du Plessis, Director of the Soil and Irrigation Research Institute and Mr G.C. Green, former Deputy-Director, for their support and encouragement;

Mr B.J.J. Joubert, Mrs M.M. Kruger and Mrs A.M. Odendaal for technical and analytical assistance;

Colleagues, especially Mr H.M. du Plessis, for valuable discussion and their keen interest;

Mrs R. Els, who typed this dissertation;

Jane, my wife, for her enthusiastic interest, assistance and encouragement.

INTRODUCTION

Pressure on limited land resources, owing to sophistication of agricultural practices, urbanization and pollution, has increased demand for information about the chemical and physical behaviour of soils. A growing awareness of the dynamic and interactive nature of the environment has stimulated the use of computer simulation modelling as an aid in planning and research.

Soils are usually described in terms of various static or equilibrium physical, chemical and morphological properties, some of which are used as criteria for pedological classification systems. These properties reflect the static characteristics of soil materials and profiles but cannot define the plant root environment, which is influenced by external factors and is rarely, if ever, at moisture, chemical or temperature equilibrium. Soil temperature fluctuates diurnally at the surface, decreasing in amplitude with depth until only seasonal changes are noticeable. Most soils are subjected to a succession of hydrological events, starting with infiltration of rain or irrigation water, continuing with redistribution, drainage and evapotranspiration, and ending with the next application of water to the soil surface. Successive cycles may vary both in duration and amount of water applied. Accompanying water content changes are changes in chemical composition of soil water, caused by concentration, dilution, transport, ion exchange, weathering, dissolution and precipitation. Plant roots, especially of annual crops, explore a varying soil volume. If the spatial variability of soils is superimposed, it is clear that accurate description and forecasting of the plant environment is a most difficult task.

Soil scientists have a range of resources to aid in their research and advisory tasks. These include quantitative or qualitative knowledge

of soil processes, and data concerning the nature and properties of specific soils. To solve problems, soil properties, processes and management practices must be integrated. The advent of computer simulation modelling has enabled soil scientists to extrapolate their knowledge from simple to complex situations. Computer models are no longer used only by research scientists but have also become an advisory tool. This is especially true of salt and water transport models, which are applied in irrigation scheduling, salinity control, effluent disposal and in assessing return flow quality.

Hillel (1977) cautioned against the indiscriminate and blind use of simulation models: "It must be remembered that simulation per se cannot solve a real problem. It can only simulate a solution. Its results are predetermined by the input, although the full consequences of this determinism are often unforeseen for complex systems. A simulation can indeed provide new perspectives on the problem, but its predictions are always somewhat doubtful, even when the model is basically sound. When a model is not sound, i.e., when its premises or data are wrong, there is great danger that it will gain a false aura of respectability merely because it was processed on a computer, which still conveys a sense of magic to many laymen. Simulation is not a panacea. It is not a substitute for experimentation, but a possibly more rational basis for experimentation. We need detailed, sound, and comprehensive experimentation as a basis for devising models, as well as for supplying the necessary parameters, and for validating (or refuting!) their results. Reciprocally, such results can help economize experimentation by guiding it to where it is needed most."

In this thesis some aspects of soil water flow modelling are examined, with special emphasis on validity and the problem of obtaining soil retentivity and hydraulic conductivity data for South African soils. The primary objectives are to:

1) survey the properties of South African soil types which are related to hydrological behaviour;
2) examine the data required by a one-dimensional finite difference flow model;
3) develop regression equations relating retentivity to soil type and physical composition;
4) derive a retentivity function suitable for modelling purposes and relate function parameters to soil properties;
5) examine methods of predicting hydraulic conductivity, especially those which utilize retentivity data;
6) describe a method of estimating hydraulic conductivity from absorption or desorption data;
7) demonstrate the use of some of these techniques in a simulation study.

By estimating retentivity and conductivity parameters which reflect soil properties, this work should simplify the use of soil water flow models. Moreover, this work facilitates the simulation of the effect of changes in texture and bulk density through the profile.

CHAPTER 1

A MODEL FOR SIMULATING WATER FLOW IN SOIL

1.1 INTRODUCTION

Soil hydrology is an important factor determining the success of both irrigated and rain-fed crop production enterprises. In South Africa, lack of water is probably the greatest limitation of crop yields. In irrigated areas, the application of too much water is often the cause of waterlogging and salinity. In future, demands on water resources by industry will increase, forcing greater efficiency in irrigation. Improved soil water management requires a knowledge of the rate at which water can be added to soil, how this water is distributed through the profile, how much is available to plants and at which rate it drains out of the root zone. Traditional approaches to defining the amount of water available to plants are inadequate in the face of improved irrigation technology and management requirements.

For most agricultural purposes, the profile water content is allowed to vary between limits determined primarily by the requirements of the crop, but also by the nature of the soil and the type of irrigation practised. Drainage is kept to the minimum necessary for salinity control. Soil water management consists largely of maintaining root zone water contents within the desired bounds for as long a period as possible. In order to do this, a model with the following capabilities is essential:

1) prediction of spatial and temporal changes in water potential, content and flux;
2) simulation of inhomogeneous soils, which exhibit gradual or abrupt changes in hydrological characteristics with depth, should be possible;

3) simulation of short-term events, such as infiltration, as well as long-term changes;
4) flexibility of surface and bottom boundary conditions;
5) accommodation of variable irrigation and rainfall patterns, application intensities, evapotranspiration rates, rooting depths and withdrawal patterns.

There are several types of soil water models. The simplest are the water balance or overflow models. A record of gains and losses of water in each of several soil layers is maintained. Field capacity and wilting point are specified for each layer. When the water content of a layer reaches field capacity any excess water is assumed to percolate to the layer beneath. Models based on numerical solutions of the flow equation enable temporal changes in water content to be predicted. In agriculture, finite-difference techniques are commonly used. The flow equation is solved for each of a number of discrete layers which enables water flux density distribution in the profile to be calculated.

A distinction should be drawn between long-term, large-area simulations and simulations of water flow at a well-defined point. Scale influences the nature of the data collected, its accuracy and variability. Many of the considerations linked to scale are listed in Table 1.1. Finite difference models are more suited to short-term simulations involving transient phenomena such as infiltration, rather than long-term water balance studies. Long-term simulations require excessive computer time and satisfactory results may be obtained using a simpler type model. Finite-difference models can be used to generate some basic relationships for simpler models, for example, rate of drainage in relation to profile water content.

Although they are adaptable to a wide range of situations, finite difference flow models are highly idealized. They are discrete models

TABLE 1.1 Aspects of model accuracy and data collection in relation to the size of modelling unit

Modelling unit	Data	Sampling intensity	Soil variability	Extraneous factors	Accuracy
Region	Estimation from survey data	Low	Large	Many	Qualitative
Field		↓	↓	↓	↓
Plot					
Column					
Core	Direct measurement	High	Small	Few	Quantitative

of continuous systems, which in addition usually neglect temperature, vapour and chemical effects.

Despite these limitations the models enable complex phenomena to be simulated. Most soil water flow problems cannot be solved or evaluated by any other method, so that a computer model which can be operated rapidly using easily obtainable or estimated data is an invaluable tool for soil scientists.

A suitable model for this project was developed from the water-flow section of a computer simulation model of dynamic bio-physico-chemical processes in soils (Dutt, Shaffer and Moore, 1972 and Ayars, 1976). The complete model has subprograms for predicting salt transport, chemical changes and nitrogen transformations. It was used by the U.S. Bureau of Reclamation for predicting irrigation return flow quality and is used for the same purpose in South Africa. There is a demand for soil hydrological data required for its operation. The water flow subroutine is a one-dimensional implicit finite difference model, which is both accurate and efficient in computer time (Haverkamp, Vauclin, Touma, Weiringa and Vachaud, 1977). The major disadvantages of Dutt's model are the use of the water content form of the general flow equation and the assumption of a permanent water table at a fixed depth. Water content is discontinuous across boundaries between soil layers having different retentivity characteristics, which complicates simulation of flow through layered soils. Water potential, on the other hand, is continuous across boundaries, simplifying flow simulation in multi-layered profiles.

Dutt's original model was converted to the potential/hydraulic conductivity form, modified where necessary and many more boundary condition options were included. Development and improvement of the potential form of the model included input from Hanks and Bowers (1962), Hillel (1977), Nimah and Hanks (1973), Feddes, Bresler

and Newman (1974), van der Ploeg (1974), Feddes, Kowalik, Kolinska-Malinka and Zaradny (1976) and Hillel and Talpaz (1977).

The following sections contain a description of the flow equation used in the model, its solution and some boundary conditions. A listing of the programs used is provided in Appendix 1.

1.2 THE MODEL

1.2.1 Finite difference form of the general flow equation

The soil water flow equation for vertical flow, derived from Darcy's law and the equation of continuity, is:

$$\frac{\delta\theta}{\delta t} = \frac{\delta}{\delta Z}\left(D\frac{\delta\theta}{\delta Z} + K\right) - S \qquad (1.1)$$

where θ is fractional water content;

D is soil water diffusivity;

K is hydraulic conductivity;

t is time;

Z is depth, positive downwards;

and S is a sink term representing water lost per unit time by transpiration.

If pressure potential is the dependant variable then Eq. 1.1 may be rewritten as:

$$\frac{\delta\psi}{\delta t} C_\theta = \frac{\delta}{\delta Z}\left(K\frac{\delta\psi}{\delta Z} + K\right) - S \qquad (1.2)$$

where C_θ is the differential water capacity;

ψ is the pressure potential

and $K = DC_\theta$.

To simulate flow and redistribution of water in soil by finite difference techniques, the profile is divided into a number of horizontal

segments and the total time period divided into short time intervals (Fig 1.1). The top node (j = 1) and the lowest node (j = q) are outside the soil profile and are used for maintaining the desired boundary conditions. A finite difference form of Eq. 1.2 may be written for each depth node,

$$\frac{C_j^{i-\frac{1}{2}}\,(h_j^i - h_j^{i-1})}{\Delta t} = \frac{(h_{j-1}^{i-1} + h_{j-1}^{i} + 2\Delta Z - h_j^{i-1} - h_j^{i})\,K_{j-\frac{1}{2}}^{i-\frac{1}{2}}}{2(\Delta Z)^2} - \frac{(h_j^{i-1} + h_j^{i} + 2\Delta Z - h_{j+1}^{i-1} - h_{j+1}^{i})\,K_{j+\frac{1}{2}}^{i-\frac{1}{2}}}{2(\Delta Z)^2} - S_j^i \qquad (1.3)$$

in which $C_j^{i-\frac{1}{2}} = (\frac{\delta\theta}{\delta h})_j^{i-\frac{1}{2}}$

Eq. 1.3 describes the change in water content in the segment surrounding node j during a time interval Δt. Soil water pressure potentials are expressed in weight potential units (height of a water column equivalent to the pressure potential). The superscript i-1 denotes the beginning and i the end of the time interval. The subscript j denotes the node under consideration, j-1 the node above and j+1 the node below. Node intervals (ΔZ) are assumed constant in all the models used in this thesis, but this is not a necessary condition. $K^{i-\frac{1}{2}}$ and $C^{i-\frac{1}{2}}$ are estimates of the effective K and C values during the time interval.

The model is operated by solving Eq. 1.3 for all nodes. Potential values at the start of the time interval (h^{i-1} terms) are known while the h^i terms are the unknown potential values at the end of the time period.

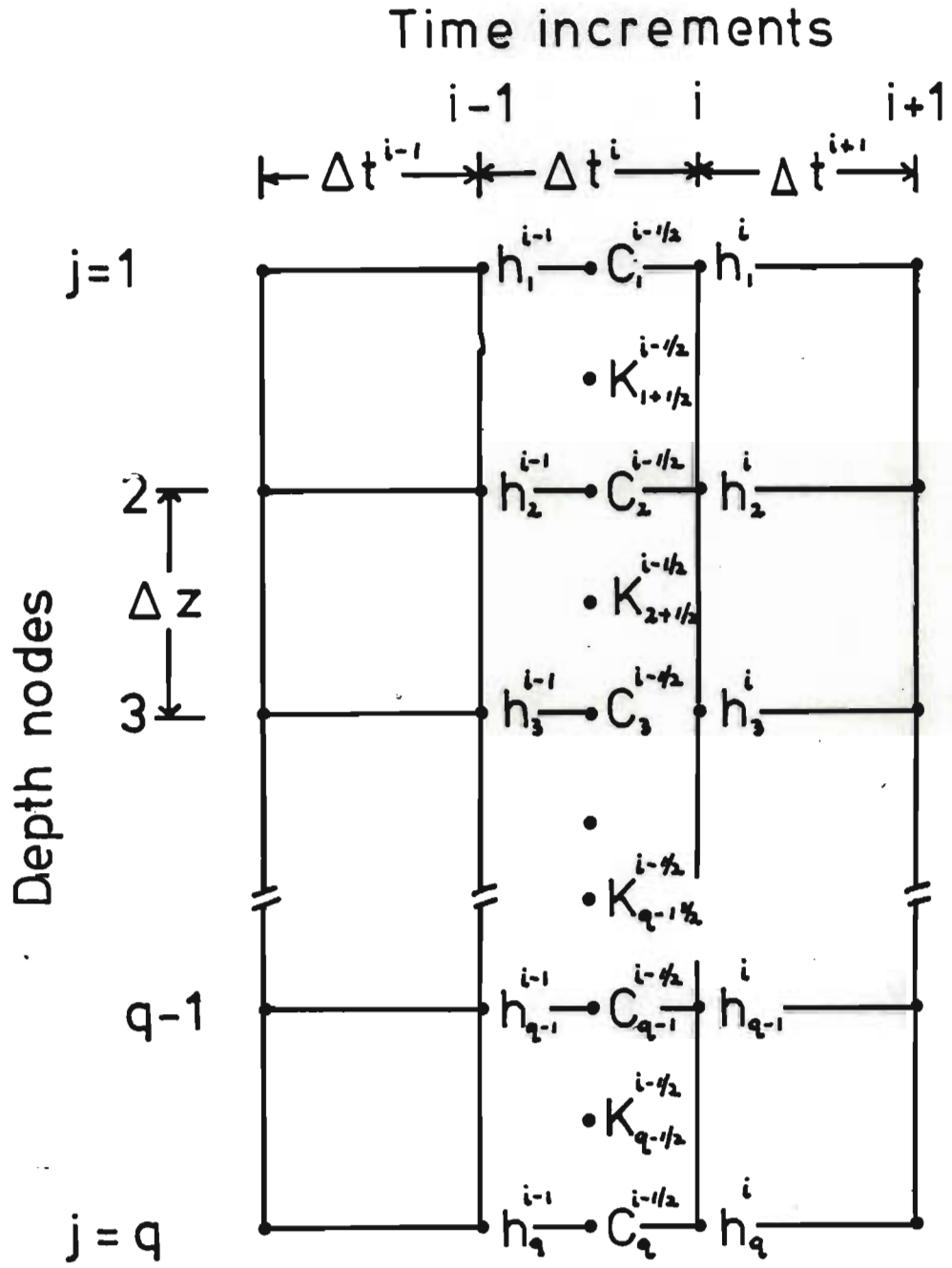

FIGURE 1.1 Solution mesh for soil water flow model

1.2.2 Solution of finite difference equations

An equation of the form of Eq. 1.3 may be written for each node at the beginning of each time period. For q nodes there are thus q equations containing q unknown h^i values. If all the unknown h^i terms are gathered on the left hand side and all the known terms on the right hand side, Eq. 1.3 becomes:

$$- K_{j-\frac{1}{2}}^{i-\frac{1}{2}} h_{j-1}^{i} + \left(\frac{2(\Delta Z)^2}{\Delta t} C_j^{i-\frac{1}{2}} + K_{j-\frac{1}{2}}^{i-\frac{1}{2}} + K_{j+\frac{1}{2}}^{i-\frac{1}{2}}\right) h_j^i - K_{j-\frac{1}{2}}^{i-\frac{1}{2}} h_{j+1}^i$$

$$= K_{j-\frac{1}{2}}^{i-\frac{1}{2}} h_{j-1}^{i-1} + \left(\frac{2(\Delta Z)^2}{\Delta t} C_j^{i-\frac{1}{2}} - K_{j-\frac{1}{2}}^{i-\frac{1}{2}} - K_{j+\frac{1}{2}}^{i-\frac{1}{2}}\right) h_j^{i-1} \qquad (1.4)$$

$$+ K_{j+\frac{1}{2}}^{i-\frac{1}{2}} h_{j+1}^{i-1} + 2\Delta Z \left(K_{j-\frac{1}{2}}^{i-\frac{1}{2}} - K_{j+\frac{1}{2}}^{i-\frac{1}{2}}\right) - 2(\Delta Z)^2 S_j^i.$$

Eq. 1.4 may be simplified by combining constants and writing in the general form.

$$\alpha_j^i h_{j-1}^i + \beta_j^i h_j^i + \gamma_j^i h_{j+1}^i = \delta_j^i. \qquad (1.5)$$

All the terms included in the constants α_j^i, β_j^i, γ_j^i and δ_j^i have known or estimated values. The q equations form a tridiagonal matrix, which may be solved by means of a rapid Gaussian elimination method. The recursive formula by which the h^i terms may be calculated is (Dutt et al., 1972; Amerman, 1971)

$$h_j^i = g_j^i + m_j^i h_{j+1}^i \qquad (1.6)$$

in which $$g_j^i = \left[\frac{\delta_j^i + \alpha_j^i g_{j-1}^i}{\beta_j^i - \alpha_j^i m_{j-1}^i}\right]$$

and $$m_j^i = \gamma_j^i/(\beta_j^i - \alpha_j^i m_{j-1}^i).$$

In the first stage of the solution g and m values are calculated for nodes 2 to q. Initial values of g_1 and m_1 are chosen to fulfil the desired surface boundary conditions. In the second stage, h^i values are calculated, starting at the bottom of the profile by substituting the boundary value h_q^i into Eq. 1.6 and working towards the surface. The h^i values become starting values for the next time period.

Water contents at each node may be calculated from a known relationship between θ and h or from the equation,

$$\theta_j^i = (h_j^i - h_j^{i-1})\ C_j^{i-\frac{1}{2}} + \theta_j^{i-1} \qquad (1.7)$$

1.2.3 Calculation of water flux

Water flow between nodes during a time interval i-1 to i is calculated from:

$$U_j^i = (K_{j+\frac{1}{2}}^{i-\frac{1}{2}} - K_{j+\frac{1}{2}}^{i-\frac{1}{2}} (h_{j+1}^i + h_{j+1}^{i-1} - h_j^i - h_j^{i-1})/2\Delta Z)\ \Delta t \qquad (1.8)$$

where U_j^i is flow. Positive values of U indicate downward movement and negative values, upward movement. Flux density (F) is defined as

$$F_j^i = U_j^i/\Delta t. \qquad (1.9)$$

The largest flux density in the profile was used to define the length of the next time interval (Hanks and Bowers, 1962),

$$t^{i+1} - t^i = \frac{\Delta\theta\Delta Z}{F_{max}} \qquad (1.10)$$

in which F_{max} is the maximum F_j^i value and $\Delta\theta$ is the maximum allowable water content change. Eq. 1.10 was used to define Δt between the limits of 10^{-10} day, set at the initiation of infiltration and a maximum Δt, usually 0,05 or 0,1 day.

1.2.4 Estimating differential water capacity

A value for $C_j^{i-1/2}$ is required for each node in order to solve Eq. 1.4. Hanks and Bowers (1962), Dutt et al., (1972) and Ayars (1976), who used a finite-difference form of Eq. 1.1, faced an equivalent problem in estimating diffusivity D, since D = K/C. They calculated D from a probable mean water content during the time interval, assuming that the rate of change of water content will be similar to that of the previous time interval.

Amerman (1971) described an iterative procedure which requires more computer time than a simple prediction, but which gave good results. Initial values of $C_j^{i-\frac{1}{2}}$ are calculated using pressure potentials h_j^{i-1}, known for the beginning of a time interval. Using these $C_j^{i-\frac{1}{2}}$ values, h_j^i values are predicted for the end of the time interval. Revised $C_j^{i-\frac{1}{2}}$ values are then predicted from calculated $h_j^{i-\frac{1}{2}}$ values for the time interval, where

$$h_j^{i-\frac{1}{2}} = 0{,}58\ (h_j^i - h_j^{i-1}) + h_j^{i-1}). \qquad (1.11)$$

Two iterations are sufficient except during periods of rapid change in h, when three iterations are used.

1.2.5 Averaging hydraulic conductivity

Effective $K_{j-\frac{1}{2}}^{i-\frac{1}{2}}$ values must be estimated from the known h_j^{i-1} and h_{j-1}^{i-1} values and the as yet unknown h_j^i and h_{j-1}^i values.

In practice, using an iterative procedure similar to that for the C values is not warranted since averaging K between depth nodes using h^{i-1} values produces virtually identical results. Any rapid changes in hydraulic conductivity owing to infiltration causes time intervals to be shortened so that errors in the estimation of $K^{i-\frac{1}{2}}$ will apply to very short time periods.

Dutt et al. (1972) calculated K from average θ between nodes using a defined relationship between K and θ. This leads to unrealistically low values of $K_{j-\frac{1}{2}}$ for steep gradients of θ. Ayars (1976) calculated K at each node and averaged these while Hillel (1977) used an average conductivity weighted according to the relative thickness of the segments. In this model, a simple arithmetic average was used as all segments were the same thickness,

$$K_{j-\frac{1}{2}}^{i-\frac{1}{2}} = (K_j^{i-1} + K_{j-1}^{i-1})/2$$

$$K_{j+\frac{1}{2}}^{i-\frac{1}{2}} = (K_j^{i-1} + K_{j+1}^{i-1})/2 . \qquad (1.12)$$

When conductivity gradients are steep, an integrated mean conductivity (Klute, 1972) may be a better estimate of effective conductivity between nodes,

$$\bar{K} = \frac{1}{\Delta h} \int_{h_{j-1}}^{h_j} K(h)\, dh . \qquad (1.13)$$

1.3 BOUNDARY CONDITIONS

Solution of the sequence of simultaneous equations represented by Eq. 1.4 require that the surface and bottom boundary conditions be known. The boundary conditions are defined in terms of pressure potential or flux density and are chosen to suit particular soil

conditions.

1.3.1 Surface boundary conditions

The desired flux density or potential at the soil surface is maintained by adjusting h_1^i.

1) Constant potential

During a period of ponded infiltration, the pressure potential of the first node is set to zero, or a positive value if a depth of ponded water is to be simulated:

$$h_1^i \geq 0; \qquad g_1^i = 0; \qquad m_1^i = 0 \tag{1.14}$$

2) Flux

A flux controlled surface boundary exists during periods of evaporation, non-ponded infiltration and zero flux. For any time period, the surface flow (U_1^i) has first to be calculated by a sub-routine. Evaporation for example, may vary diurnally and be further influenced by surface moisture conditions. Evaporation models will not be described here.

The soil surface is situated midway between nodes j = 1 and j = 2. Writing Eq. 1.9 for surface flux density,

$$F_1^i = K_{1+\frac{1}{2}}^{i-\frac{1}{2}} - K_{1+\frac{1}{2}}^{i-\frac{1}{2}} (h_2^i + h_2^{i-1} - h_1^i - h_1^{i-1})/2\Delta Z \tag{1.15}$$

Setting $m_1^i = 1$, Eq. 1.6 becomes

$$g_1^i = h_1^i - h_2^i.$$

Substituting g_1^i for the unknown value of $h_1^i - h_2^i$ in Eq. 1.15 and rearranging,

$$g_1^i = 2\Delta Z \ (F_1^i - K_{1+\frac{1}{2}}^{i-\frac{1}{2}}) \ / K_{1+\frac{1}{2}}^{i-\frac{1}{2}} + h_2^{i-1} - h_1^{i-1} \tag{1.16}$$

enables a value of h_1^i to be calculated (Eq. 1.6) at the end of the tridiagonal matrix algorithm which satisfies the surface flux condition. When surface flux is zero,

$$g_1^i = -2\Delta Z + h_2^{i-1} - h_1^{i-1} \tag{1.17}$$

1.3.2 Bottom boundary conditions

The bottom boundary condition is maintained by adjusting the potential of the bottom node to satisfy the desired potential or flux criteria.

1) Constant pressure potential

A permanent water table in the profile is simulated by setting the pressure potential h_j^i to zero or a positive value,

$$h_q^i = (q - i_w) \ \Delta Z \tag{1.18}$$

in which i_w is the node number corresponding to the phreatic surface.

Under certain circumstances, a constant negative pressure potential is assigned to the lowest node, for example, during suction drainage when the drainage system has a negligible impedance.

2) Free-draining profile

In a free-draining profile below the root zone, the hydraulic potential gradient is approximately unity. F_{q-1}^i is thus numerically equal to

$K^i_{q-\frac{1}{2}}$. From Eq. 1.8 and 1.9,

$$F^i_{q-1} = K^i_{q-\frac{1}{2}} = K^i_{q-\frac{1}{2}} - K^i_{q-\frac{1}{2}} \, (h^i_q + h^{i-1}_q - h^i_{q-1} - h^{i-1}_{q-1})/2\Delta Z. \quad (1.19)$$

Since $h^i_{q-1} = g^i_{q-1} + m^i_{q-1} \, h^i_q$

$$h^i_q = (g^i_{q-1} - h^{i-1}_q + h^{i-1}_{q-1})/(1 - m^i_{q-1}). \quad (1.20)$$

Since g^i_{q-1} and m^i_{q-1} are calculated before a value for h^i_q is required and h^{i-1}_q and h^{i-1}_{q-1} are known, h^i_q may be calculated to satisfy the flux condition.

3) Zero flux

A soil profile underlain by an impermeable layer will have zero flux across the bottom boundary under all conditions.

$$K^i_{q-\frac{1}{2}} - K^i_{q-\frac{1}{2}} \, (h^i_q + h^{i-1}_q - h^i_{q-1} - h^{i-1}_{q-1})/2\Delta Z = 0. \quad (1.21)$$

Since $h^i_{q-1} = g^i_{q-1} + m^i_{q-1} \, h^i_q$

$$h^i_q = (2\Delta Z - h^{i-1}_q + h^{i-1}_{q-1} + g^i_{q-1})/(1 - m^i_{q-1}). \quad (1.22)$$

4) Lysimeter tank

A lysimeter may be represented by a combination of conditions (1) and (3). Water can drain from the tank when the bottom layer is saturated or has a pressure potential greater than that of a suction drainage system. No water can move into the tank from the drainage system so when h^i_q is less than the potential of the drainage system a zero flux condition is maintained at the bottom boundary.

1.4 COMPONENTS OF THE FIELD WATER BALANCE

1.4.1 Introduction

In the previous section a model for simulating vertical water flow in soil was described. Data concerning the supply of water to the soil and losses from it must be provided in order to operate the model.

Soil water balance is determined by rainfall, runoff, irrigation, drainage, capillary rise into the root zone, retention in plant biomass, evaporation, transpiration and condensation of vapour. The net effect of these water balance components is reflected in the change in soil water storage ΔW. The soil water flow model predicts drainage and capillary rise but the remaining components of the water balance must be measured and supplied as data or be predicted from sub-models. Thus a complete simulation model of the soil-plant-atmosphere system consists of a system of linked sub-models (Fig. 1.2). The sub-models are linked to the water flow model through three variables:

1) the sink term S_j^i, which accounts for losses of water by transpiration;
2) the surface flux density F_j^i, positive during infiltration and negative during evaporation;
3) surface potential, which has the value h_j^i during ponded infiltration.

Prediction of the values S_j^i, F_j^i and h_j^i is ancillary to the main objective of this thesis, which concerns retentivity and conductivity of South African soils. The way in which the water balance components were treated in the model listed in Appendix 1 is described briefly. The sub-models may be replaced by more sophisticated models if desired.

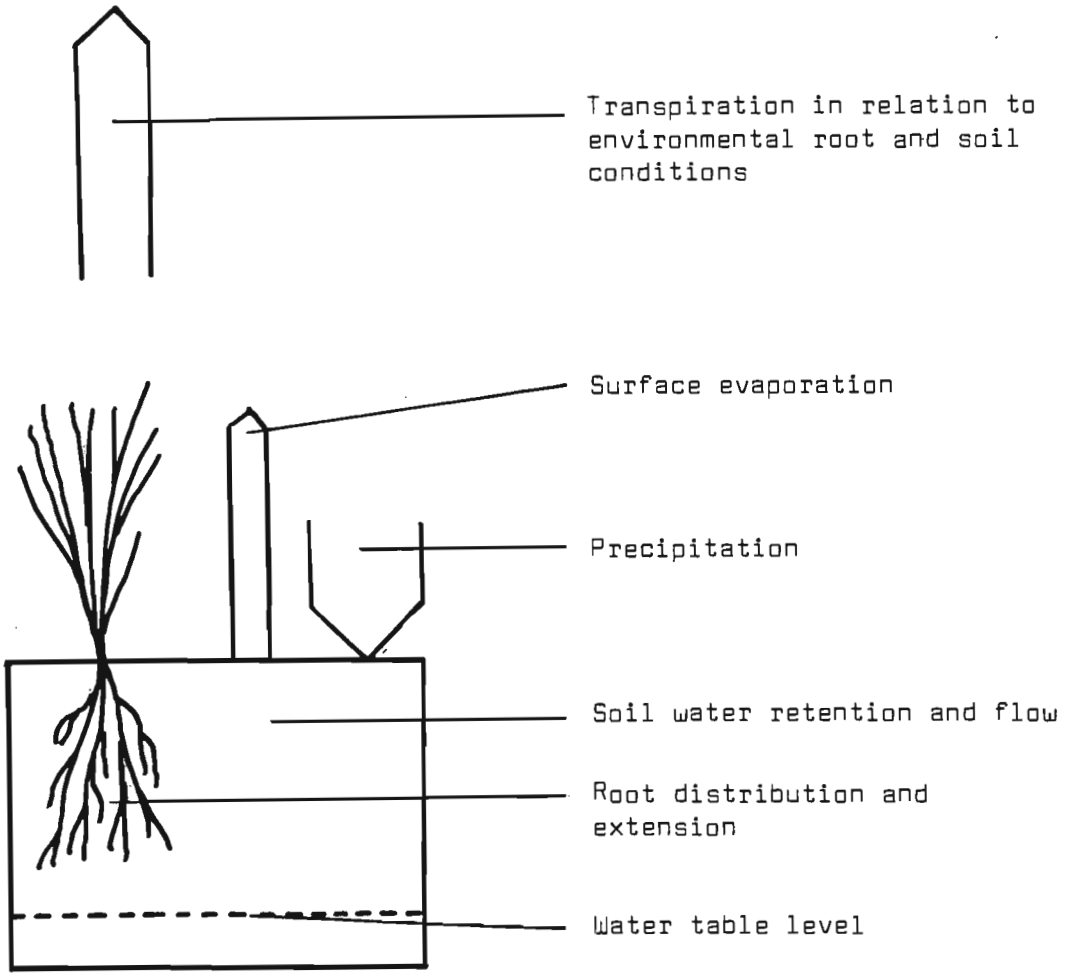

FIGURE 1.2 Components of the soil plant atmosphere system which determine water distribution and flux.

The importance of peripheral components of the field water balance must not be underestimated. Withdrawal of water by plant roots largely determines water distribution in the profile once infiltration is complete and redistribution of water has slowed. Supply and loss of soil water are the triggers which initiate water flow in the profile. Only in simulation of laboratory processes or controlled experiments in the absence of plants can a soil water flow model be used in isolation.

1.4.2 Surface water applications

Rainfall and irrigation applications are defined only by the depth and day of application. Ponded infiltration under negligible hydraulic head ($h_j^i = 0$) begins at the start of the day of application. The value of U_1^i is thus maintained at the maximum possible value. This procedure was used by Dutt et al. (1972) and Ayars (1976) but if desired can be improved by:

1) specifying a time-dependant rate of application to simulate storms;
2) specifying times of commencement of fixed-rate irrigation to simulate irrigation under non-ponded conditions.

If the rate of water application exceeds the infiltration rate then the excess water, less an amount retained in surface depressions, is assumed lost as run-off.

1.4.3 Evaporation

Evaporation is assumed to occur from 07h12 to 16h48 (0,3 to 0,7 day) and to be negligible during periods of infiltration or when h_1^i drops below -3 000 kPa. Evaporation rate varies sinusoidally with time reaching a maximum specified density (F_{max}) at noon.

The surface flux density during a time period is calculated from:

$$F_1^i = -F_{max} \cdot \max (0, \sin (2\pi (t - 0,25))) \qquad (1.23)$$

where t is the fraction of a day elapsed by the middle of the time interval i - 1 to i.

Equation 1.23 may be improved by incorporating equations (Savage and McGee, 1980) for predicting the photoperiods and times of sunrise and sunset as a function of location and day of the year.

1.4.4 Transpiration

Transpiration is assumed to take place between 0,3 and 0,7 day only, but at a constant rate throughout this period. The total amount of water withdrawn from the profile is distributed amongst the segments in proportion to a specified root distribution. Transpiration data is entered into the model as weekly totals (T mm). The value of the sink term S_j^i is calculated from:

$$S_j^i = 2,5\ TR\Delta t/7 \qquad (1.24)$$

where i refers only to time intervals occurring between 0,3 and 0,7 day and R is the fraction of roots in segment j.

The value of S_j^i reduces to zero if h_j^i falls below a defined minimum potential (usually -1500 kPa). The amount by which the potential transpiration from a segment exceeds S_j^i is accumulated as a water deficit.

Inclusion of a sub-model to predict evaporation and transpiration from climatic data could be useful. Other improvements could be:

1) a sub-model which predicts root distribution with time so that the growth of an annual crop may be simulated;

2) inclusion of root and soil water potentials as factors influencing S_j^i (see for example, Nimah and Hanks, 1973; Tillotson, Robbins, Wagenet and Hanks, 1980).

1.4.5 Mass balance check

Cumulative totals of evaporation, infiltration, transpiration, calculated bottom boundary flux density (drainage minus capillary rise) are used in conjunction with the change in profile water content to calculate a mass balance. This provides a useful check on the operation of the model and whether the node intervals and time intervals are sufficiently small.

1.5 PORTRAYING SOIL PROPERTIES

The only means of expressing the properties of a real soil in a simulation model is through the choice of profile depth, node intervals and the hydrological properties (retentivity and conductivity) of each segment.

1.5.1 Profile depth and node intervals

The depth of soil simulated should be greater than the root zone depth or of sufficient depth to ensure that the assumption of unit potential gradient under free drainage is reasonable. Any horizons which may impede flow and hence influence water content in the root zone should be included, even if they occur beneath the root zone.

Segment thickness will influence the accuracy of predicted values. Amerman (1971) suggests that the influence of segment thickness on accuracy should be tested by running a model using several segment thicknesses. A solution for zero segment thickness may be obtained

by extrapolation and used for evaluating the relative accuracy of other mesh sizes.

The model described in Section 1.2 makes no provision for non-uniform segment thicknesses or node spacings through the profile. Greater flexibility in describing profile characteristics is gained if the node spacing (ΔZ in Eq. 1.3) can be varied to suit conditions in different parts of the profile (Tillotson, et al., 1980). For example node spacings could be decreased near the soil surface where water contents change rapidly and where, owing to crusting, soil hydrological properties may be unique, or at textural transitions or plough pans, where sharp changes in both root distribution and soil properties occur. Thicker segments may be used in areas of steady flow or where pressure potentials do not vary rapidly with depth or time.

1.5.2 Soil hydrological properties

Each segment of a finite-difference water flow model represents a thin layer of the field soil. The only way in which the properties of that slice of soil can be reflected in the model is through the definition of hydrological properties, namely, porosity, and $\theta(h)$ and $K(h)$ functions. Soil texture, clay type, structure, compaction and similar properties are thus represented indirectly in the model through their effect on hydrological properties.

Ideally, each segment should be assigned its own hydrological properties so that either gradual or abrupt changes in soil properties may be simulated. Experimental measurement of $\theta(h)$ and $K(h)$ relationships for each segment is usually impracticable. Some means of predicting these relationships from easily measured soil properties would be useful, especially if it were possible to interpolate values for intermediate segments.

The way in which the K(h) and θ(h) relationships are incorporated into the model is important. If sufficient K(h) and θ(h) data are available then regression equations may be used, ensuring that they properly describe K(h) and θ(h) over the whole soil water content range. At no stage should the equations predict infinite θ values or negative K values, for example.

In order to comply with these constraints, the approach adopted in this investigation was:

1) a single retentivity function was chosen which was valid for the whole water content range;
2) the parameter values of this function were related to soil properties; and
3) conductivity functions were derived from the θ(h) function which can be matched to measured data if available.

This approach has several advantages. Any amount of measured data can be utilized. If no data are available, parameter values may be estimated from soil type, density and texture. Sufficient measured data enable the parameters to be evaluated using curve-fitting techniques. Small amounts of measured data can be used for matching purposes. No alterations need be made to the water flow program for different soils. The K(h) and θ(h) functions are incorporated in the main body of the program and the parameter values are supplied as input data. The effects of parameter changes on the shapes of curves are easily visualized if few parameters are used. Interpolated parameter values for intermediate segments are easily obtained, resulting in simulated θ(h) curves representing gradual changes in soil profile properties.

1.6 DISCUSSION

A one-dimensional model cannot simulate all field and laboratory phenomena. Furrow and drip irrigation require two- and three-dimensional models respectively. These require much more computer time than one-dimensional models. Although they require hydrological data similar to that required by one-dimensional models, factors such as anisotropy may have to be included.

The model described has proved useful for simulating the water regime in irrigation experiments, both in the field and in lysimeters. The modeller is generally able to adjust input data, usually retentivity and conductivity functions or root distribution to obtain a better correlation between predicted and simulated data. Validity of a model cannot be evaluated using a few comparisons. Modelling can only become an acceptable and trusted advisory and planning aid after it has been applied in many situations, its limitations accepted and possible sources of error fully understood.

CHAPTER 2

SOME PHYSICAL FEATURES OF SOUTH AFRICAN SOILS RELEVANT TO THEIR HYDROLOGICAL BEHAVIOUR

2.1 INTRODUCTION

An approach to modelling vertical water flow in soils was described in Chapter 1. The accuracy with which this model can predict water movement in real soils depends upon:

1) the accuracy with which profile hydrological properties are portrayed in the model;
2) correct and complete modelling of all water transport mechanisms;
3) field variability of soil properties;
4) stability of the soil matrix;
5) accurate simulation of water absorption by plant roots;
6) position of the profile in the catchment area which may determine depth to water table or lateral flow.

One-dimensional finite difference models are widely used as independent models or as sub-routines in larger soil models. Multi-dimensional models and models incorporating temperature and vapour flux have been developed but are too complex for routine use, especially in situations where data must be estimated or obtained rapidly. An object of this work, namely promotion of modelling as a practical tool in soil water management, demands a simpler model using estimated or easily measured data, but the limitations of such a model should always be appreciated. In general, validity of the model decreases as the real system becomes more complex and processes extraneous to

the model play an increasing role in water balance and movement. Some of these factors can be inferred from the South African soil classification system (MacVicar et al., 1977) and will be discussed in this chapter.

In 1972 the Soil and Irrigation Research Institute embarked upon a reconnaissance scale land type survey of South Africa to identify areas of land having uniform climate, terrain form and soil pattern. Soil samples from modal profiles were submitted for physical, chemical and minerological analysis. Some of the physical data provide valuable information concerning properties of diagnostic horizons and soil forms which influence hydrological behaviour. The broad features of soils that determine model validity and guide the choice of hydrological relationships for qualitative simulations are discussed. These include:

1) textural features of soil forms and diagnostic horizons;
2) organic carbon levels in South African soils;
3) structural stability characteristics of diagnostic horizons;
4) soil classification in relation to soil hydrology.

2.2 PHYSICAL FEATURES OF DIAGNOSTIC HORIZONS

2.2.1 Introduction

Preliminary modelling may be undertaken without detailed soil analyses. For example, the water regimes in two different soil types subjected to the same rainfall pattern may be compared, or possible hydrological differences between several soil forms may be investigated. For these models representative hydrological data may be estimated from defined properties of the soil types and available soil survey information.

Soil survey information usually consists of classification to series or phase level, particle size distribution, organic matter content and chemical properties. During the South African Land Type

Survey, additional analyses were performed. These data provide valuable information regarding the range of properties exhibited by diagnostic horizons and soil forms. In this section, textural properties, organic carbon contents and structural stability of soil horizons and forms are examined.

The physical composition of soils is usually defined by a size distribution of mineral particles and the organic matter content. Pore geometry cannot be defined easily but much research (see Chapter 3) has been done on relationships between soil textural properties, water retentivity and plant-available water. Formal soil classification systems such as the Binomial System for South Africa (MacVicar et al., 1977) use particle size distribution as a criterion for distinguishing soil series. Textural classifications based purely on the relative proportions of sand-, silt-, and clay-sized particles are often used. Many aspects of the physical behaviour of soil, notably water retentivity, compactibility and strength, are inferred from textural properties.

In South Africa, the International Soil Science Society (ISSS) particle size classification system is used, with the addition of a medium sand fraction. The size limits are:

clay	< 0,002 mm
silt	0,002 - 0,02 mm
fine sand	0,02 - 0,2 mm
medium sand	0,2 - 0,5 mm
coarse sand	0,5 - 2 mm

Textural classes were defined by Loxton (1961). The textural triangle (Fig. 2.1) was adapted from that of the USDA Soil Survey, after compensating for the different silt size limits used in the

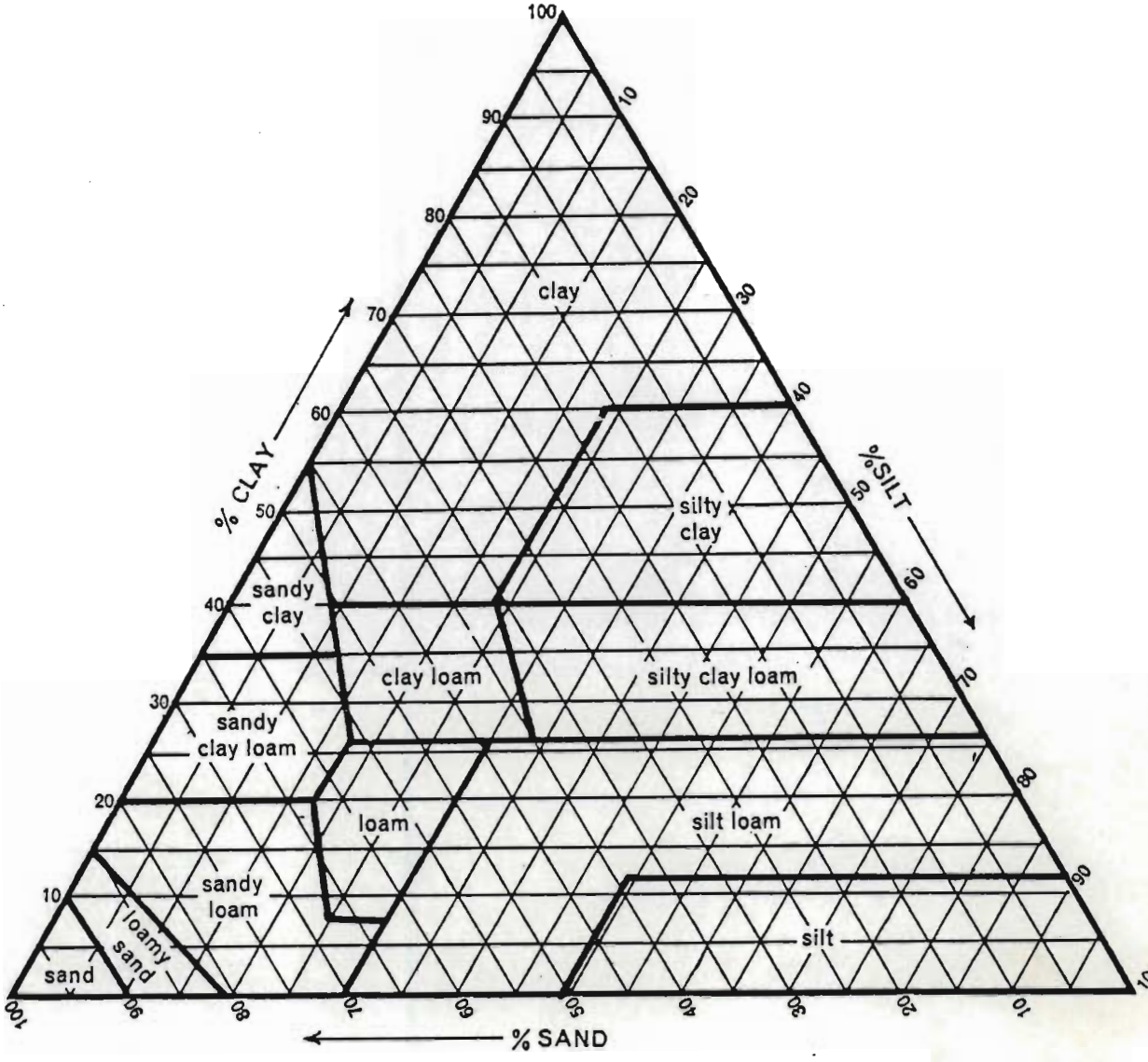

FIGURE 2.1 Textural triangle for determining textural class from proportions of sand, silt and clay (after Loxton, 1961).

USDA system.

Organic matter, usually measured as organic carbon, is an important soil constituent owing to its relatively high cation exchange capacity and surface area, its effect on the surface properties of mineral particles and the role it plays in aggregation and water retentivity.

Clay mineralogy plays an important role in determining soil physical properties. Smectitic clays increase total surface area and are usually the cause of swelling and shrinking. The presence of smectites is indicated by the degree of structural development of a horizon, which reaches an extreme in the highly smectitic vertic horizons. High exchangeable sodium levels can lead to extreme swelling and particle dispersion.

The structure of most soils changes to some extent during wetting and drying cycles. The extent of this change, or the structural stability of the soil, depends upon the nature and composition of the soil material. Observation of field behaviour combined with a knowledge of soil mineralogy and sodium levels have provided soil scientists with a rough picture of the structural stability of South African soils. Sandy soils, soils having a high organic matter content and sesquioxide-rich soils generally have a high structural stability during wetting and drying while the stability of soils containing swelling clays or high exchangeable sodium levels is low. Low structural stability may reduce the suitability of soil for both agricultural and engineering purposes. Dispersive soils are often the cause of erosion and have been implicated in the failure of earth dams (Donaldson, 1975).

Air-to-water permeability ratio (AWR) measurements were introduced by Reeve (1953) as a method for evaluating structural stability. The principle of the method is that when water is added to dry soil the geometry of the solid matrix changes owing to swelling, dispersion and

slaking. These effects tend to reduce the pore space or shift the pore size distribution, decreasing the average pore diameter. The ratio of the permeability of dry soil to the permeability after wetting is thus a measure of structural degradation. The permeability of soils before wetting with water may be measured using air or a non-polar liquid (Van Shaik, 1974), air being more commonly used. A completely stable, porous material has an AWR of 1 while 20 roughly indicates the instability threshold in soils. High AWR values may be caused by swelling, dispersion or a combination of the two processes.

2.2.2 Methods

2.2.2.1 Sampling

Areas of land having marked uniformity of terrain and soil pattern, called pedosystems, were delineated by field staff using reconnaissance soil survey techniques. Soils were sampled subjectively such that good coverage of the range of soil conditions in each pedosystem was obtained. Generally, one sample from each diagnostic horizon was forwarded to the Soil and Irrigation Research Institute for analysis.

2.2.2.2 Particle size distribution

After air-drying, samples were crushed in a mechanical crusher and sieved through a 1,68 mm mesh sieve, later replaced by a 2 mm mesh sieve. Details of the particle size analysis method are described by Day (1965). Organic matter was removed from an air-dry soil sample (10 g) by oxidation with 30% H_2O_2 (10 ml). Carbonates were destroyed by adding sufficient HCl (15%). The soil suspension was flocculated with 10% $CaCl_2$ (10 ml) and suction filtered. Soluble salts were leached from the soil by repeated washing with deionized water. Dispersion was accomplished by means of stirring (7 000 rpm for 10 minutes) after adding dispersing agent (10 ml). At first

0,4% NaOH was used as a dispersant. On certain kinds of materials, especially samples from sesquioxic apedal horizons, dispersion was inadequate and clay percentages low. A sodium hexametaphosphate /Na_2CO_3 dispersant was used in later analyses. This was prepared by dissolving 35,7 g sodium hexametaphosphate and 7,9 g Na_2CO_3 in water, making up to 1 ℓ and adjusting pH to between 8 and 9. The hexametaphosphate dispersant was chosen in preference to a 4% NaOH solution which gave better dispersion on some sesquioxic soils but which flocculated other samples. As a result of a comparative study some earlier analyses were repeated.

The sand fractions were separated by sieving after successive cycles of sedimentation and siphoning to remove suspended clay and silt. Results are expressed as a percentage of original oven-dry soil mass, moisture content of the air-dry sample being determined on a separate sample. All size fractions were determined individually and none was estimated by difference. Totals were required to lie between 94 and 104% unless carbonates, water soluble salts or organic matter were present in appreciable amounts.

Clay and silt percentages only were used to allocate each sample to a textural class according to the boundaries defined by Loxton (1961). Samples falling on a boundary line were placed in the finer of the two classes.

2.2.2.3 Organic carbon

The Walkley-Black wet oxidation procedure (Allison, 1965) was used to determine organic carbon content.

2.2.2.4 Air-to-water permeability ratio

The method followed was similar to that described by Reeve (1953, 1965). Since a large number of samples was tested a

standard method was used and a single determination carried out on each sample. According to Reeve (1965), 75% of individual determinations can be expected to lie within ± 10% of the mean, and 80% within ± 20% of the mean.

Permeameters were constructed using transparent plastic tubing with an internal diameter of 42 mm and a height of 120 mm to which a perforated plastic base was cemented. A nylon mesh disc covered with several fibreglass tissue discs retained the soil while allowing free passage of air and water through holes in the base. Dry soil was crushed and sieved (2 mm mesh), then mixed and dumped into the permeameter through a funnel to reduce aggregate segregation. A 65 g plastic cylinder was placed on the surface of the soil and the permeameter was dropped 100 times from a height of 20 mm on to a hard surface to compact the soil to a final depth of 30 to 40 mm.

Permeability to air was determined using a falling pressure method. Permeability to water was determined on the same sample after deionized water had percolated through the sample for 4 hours. A hydraulic gradient of 2 was used for all water permeability measurements. A computer program, incorporating temperature correction factors for density and viscosity of water and air, was used to calculated AWR values which were rounded to the nearest whole number to a maximum value of 1 000.

2.2.3 Results and discussion

2.2.3.1 Sampling

Data sampled in this survey could be biased owing to the personal judgement involved in selecting sampling sites and determining sampling intensity. Sampling frequency of the various soil forms was not necessarily related to the occurrence or total area of each soil

type. There was no estimate of variability within each soil body or any guarantee that the sites chosen as type profiles really were representative. However, the large number of soil samples (3 000) probably represents soil materials occurring in South Africa.

The number of profiles sampled in each of the agricultural regions of South Africa (Fig. 2.2), and the distribution of the samples amongst the various soil forms and diagnostic horizons (Tables 2.1 and 2.2) indicate the predominance of soils having red and yellow-brown apedal B horizons. Most belong to the Hutton, Clovelly or Avalon forms. Nearly 48% of the profiles sampled have red or yellow-brown apedal horizons and 25% of the samples were from these horizons. Very few samples were obtained from certain forms, either because of their rare occurrence or agricultural insignificance. No samples of the Kranskop form were available and fewer than five profiles were sampled for each of 11 forms.

Fortunately, the majority of South African soils are apedal and hence have few characteristics which can invalidate models of the type described in Chapter 1.

2.2.3.2 Particle size distribution

The distribution of clay contents within diagnostic horizons is plotted in the form of relative frequency distributions (Fig. 2.3). The histograms are arranged in order of increasing mean clay content. Many of the distributions appear approximately normal but some are negatively skewed. Some distributions may not be representative of their parent populations as the number of samples was low. The spatial distribution of soils according to clay content is not necessarily similar to the sample distribution as each sample represents an unknown area of land.

FIGURE 2.2 Agricultural regions in South Africa:

1) Highveld
2) Karroo
3) Natal
4) Eastern Cape
5) Free State
6) Transvaal
7) Winter Rainfall

TABLE 2.1 Distribution of sampled soil diagnostic horizons in agricultural regions of South Africa

Diagnostic horizon	Highveld	Eastern Cape	OFS	Natal	Transvaal	Winter rain	Karroo	Total
Topsoils:								
Organic	1	1		2				4
Humic		2		4	5			11
Vertic	9	2	4	17	14			46
Melanic	11	2	12	22	12			59
Orthic	142	64	199	178	202	161	37	983
Subsoils:								
E	12	12	13	28	16	30		111
G	7	2	2	8	10	1		30
Red apedal	44	18	89	74	188	60	24	497
Yellow-brown apedal	55	7	36	65	62	27	3	255
Red structured	2	5	15	24	33	10	2	91
Soft plinthic	44	2	20	31	13	6		116
Hard plinthic	2		1			1		4
Gleycutanic	5	10	9	17	8	12		61
Prismacutanic	15	8	34	24	3	11	3	98
Pedocutanic	24	13	41	55	24	11	6	174
Lithocutanic	7	7	3	23	10	7		57
Neocutanic	10	5	9	14	4	16	1	59
Ferrihumic		2				5		7
Regic sand		4	2	15		16		37
Stratified alluvium	1		1	6		9	1	18
Other non-diagnostic	56	7	64	30	24	52	49	282
TOTAL	447	173	554	637	628	435	126	3 000

TABLE 2.2 Distribution of sampled soil forms in agricultural regions of South Africa

Form	Highveld	Eastern Cape	OFS	Natal	Transvaal	Winter rainfall region	Karroo	Total
Arcadia	5	1	3	5	5			19
Avalon	26	2	6	13	15			62
Bainsvlei	3		1					4
Bonheim	7	2	4	12	8		1	34
Cartref		2		2	2			6
Champagne	1	1		3				5
Clovelly	16	3	20	16	21	15	2	93
Constantia						3		3
Dundee			2	2		6	1	11
Estcourt	10	3	7	7	2	7		36
Fernwood		3	2	11		9		25
Glencoe	5			3	6			14
Glenrosa	5	6	3	8	6	7		35
Griffin				14	11	1		26
Houwhoek						2		2
Hutton	33	11	64	30	139	42	36	355
Inanda				2	3			5
Inhoek	1							1
Katspruit		1		3	2	1		7
Kranskop								0
Kroonstad	1	8	5	9	7	10		40
Lamotte		1				3		4
Longlands	1	1	1	8	5	1		17
Magwa		1		1	1			3
Mayo	1			3	1			5
Milkwood	1		5	3	3			12
Mispah			8	2		8	6	24
Nomanci		1		1	1			3
Oakleaf	8	3	7	3	3	10	1	35
Pinedene	1			1		2		4
Rensburg	3			5	6			14
Shepstone				1				1
Shortlands	1	4	12	16	31	8	2	74
Sterkspruit	7	3	26	9	1	4	2	52
Swartland	6	3	9	12	6	9	3	48
Tabankulu				1				1
Valsrivier	7	3	24	5	5	1	2	47
Vilafontes				2		3		5
Wasbank	1			1	3	2		7
Westleigh	10		8	2	1	4		25
Willowbrook			2		1			3
TOTAL	160	63	219	216	295	158	56	1 167

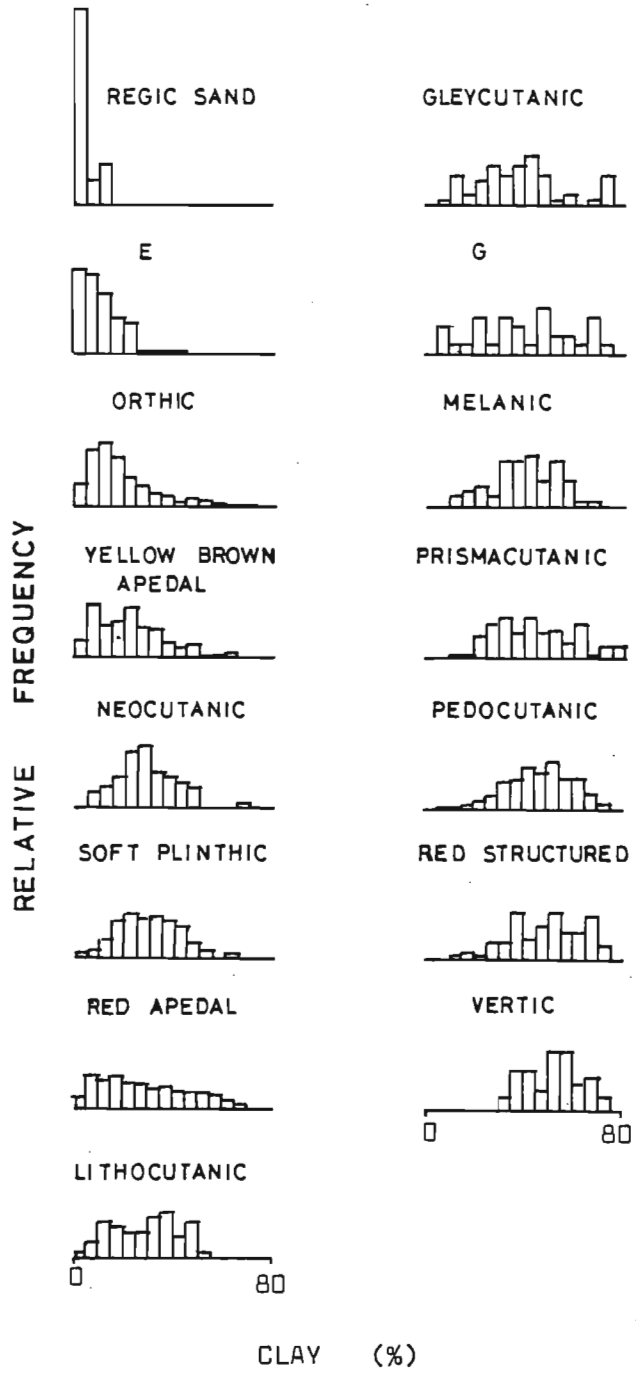

FIGURE 2.3 Relative distribution of clay within diagnostic horizons for 5% clay class intervals (range = 0-80%) within diagnostic horizons No. of samples in each histogram listed in Table 2.1

The distribution of samples amongst soil textural classes (Table 2.3) indicates the low silt content of South African soils. None was classified as a silt and very few were placed in the loam, silty clay loam and silty loam classes. Sixty-one per cent of the samples were distributed amongst three textural classes, sandy loam (20%), sandy clay loam (19%) and clay (22%).

In the present binomial soil classification system, a maximum of five clay content classes are used to subdivide soil forms into series. These are 0 - 6%, 6 - 15%, 15 - 35%, 35 - 55% and above 55% clay. The 0 - 6% and 6 - 15% clay content classes are subdivided into a further three classes each according to sand grade. Silt content is not reflected in the classification system. Improvements to the classification system should be aimed at improved characterization of particles in the range 2 to 100 μm. This could involve a departure from the ISSS particle size classification system used at present and the adoption of either the USDA or BSI system which defines more particle sizes between 20 and 200 μm.

If textural classes were used to subdivide the soil forms into series then there would be 11 classes, excluding silt, an extremely rare textural class in South Africa. The textural triangle used at present could perhaps be modified, improving discrimination in the three textural classes which now accommodate 61% of the samples studied in this investigation.

2.2.3.3 Organic carbon

Relative frequency distributions (Fig. 2.4) show that in general the organic carbon content of South African soils is low; mean values are generally less than 0,6%. Apart from the few organic and humic horizons sampled, organic carbon contents are highest in

TABLE 2.3 Relative frequency distribution of diagnostic horizons among textural classes

Horizon	Textural class											
	Sa	LmSa	SaLm	Lm	SiLm	Si	SaClLm	ClLm	SiClLm	SaCl	SiCl	Cl
Topsoils:												
Vertic								5		9	9	77
Melanic			7				16	9		12	2	54
Orthic	14	18	32	3	1		15	4	1	3	2	9
Subsoils:												
E	21	28	36	4	3		6	2		1		
G		7	7				17	10		7	10	43
Red apedal	10	10	17	1			21	3	2	6	2	28
YBr apedal	15	14	16	1			31	3	1	6	3	10
Red structured			2				10	5	2	7	1	73
Soft plinthic	2	4	19	1			38	4	1	15		13
Gleycutanic		5	8				23	13		15	2	32
Prismacutanic			1				24			13	2	52
Pedocutanic		1	1		1		14	4	2	11	5	62
Lithocutanic		5	23		4		21	11	2	9	2	25
Neocutanic	2		15	3	3		41	12	2	12		10
Regic sand	86	8	6									
Strat. alluvium	22	28	39	6			6					
Overall frequency %	10,7	11,8	20,4	1,8	0,6	0,0	18,8	4,4	1,0	6,0	2,1	22,4

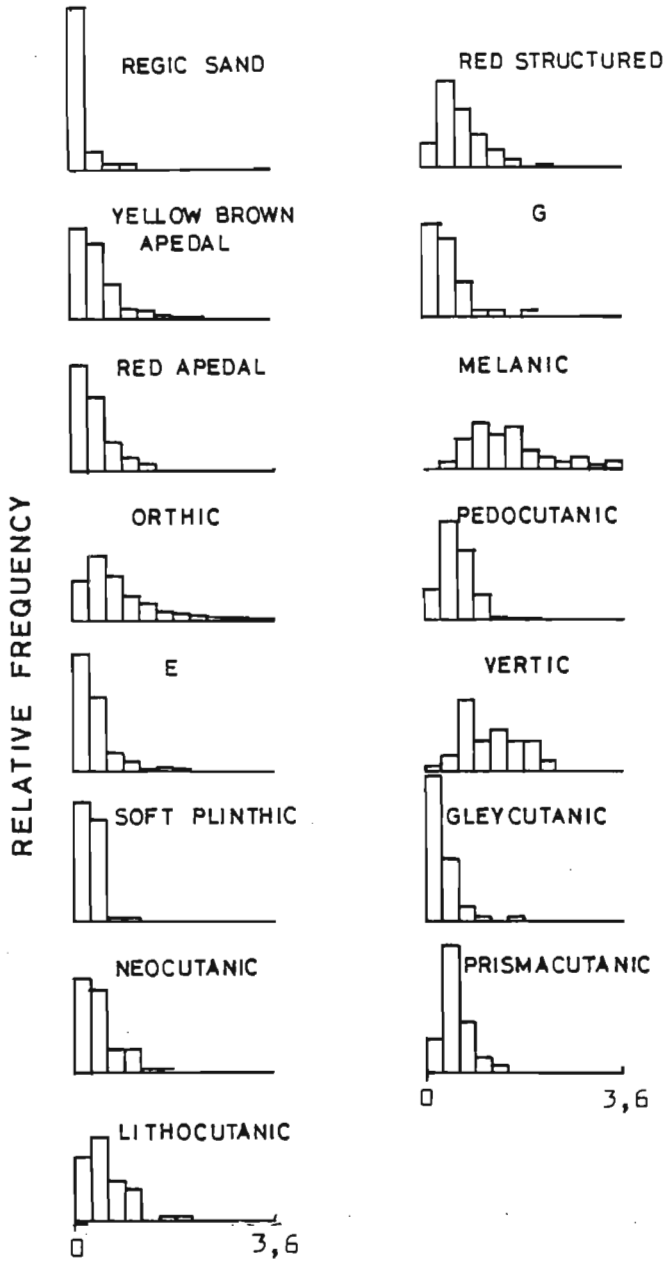

FIGURE 2.4 Relative organic carbon distributions for 0,3% carbon class intervals (range 0-3,6% C) within diagnostic horizons. Number of samples in each histogram listed in Table 2.1

melanic and vertic horizons. This may reflect that most vertic and melanic samples were from Natal and the Eastern Transvaal where the climate is conducive to the accumulation of organic matter.

2.2.3.4 Air-to-water permeability ratio

The relationship between air and water permeabilities for red apedal and red structured horizons (Fig. 2.5) demonstrates the range of air and water permeability values encompassed by a narrow AWR range. Low permeability to water does not necessarily indicate low stability although high water permeability values are usually associated with high air permeability and hence low AWR values.

Frequency histograms were prepared for each diagnostic horizon having 30 or more samples. Log AWR values were accumulated in 12 classes from 0 to 3 with intervals of 0,25 (Fig. 2.6). On the basis of median and quartile AWR values (Table 2.4) diagnostic horizons were grouped into three classes, namely a high stability group, one exhibiting variable stability, and a low stability class.

The most stable group contains those horizons which are generally highly weathered, containing little swelling clay and stabilized by sesquioxides or organic matter (Fig. 2.6). Results for organic, humic and ferrihumic horizons (not shown in Fig. 2.6) indicate that they would fall in this group. The E horizon is an eluvial one from which most sesquioxides and some clay have been removed. The remaining clay is probably mobile owing to the absence of aggregating agents but the coarse texture and predominance of large pores allow suspended clay to move without causing pore blockage or reducing permeability. The intermediate group contains less-weathered soil material which would be expected to contain moderately developed structure. The unstable group consists of soil materials which contain either large quantities

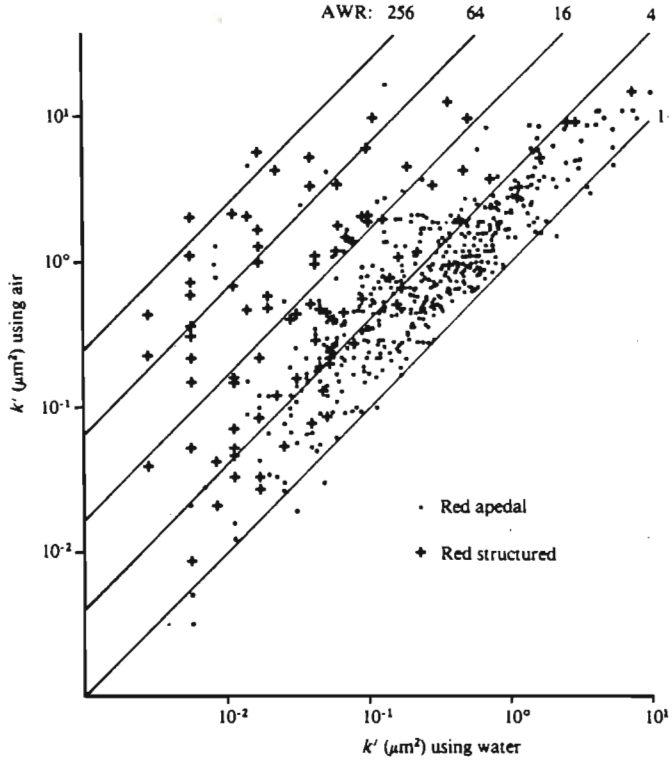

FIGURE 2.5 Air and water permeability values for red apedal and red structured horizons

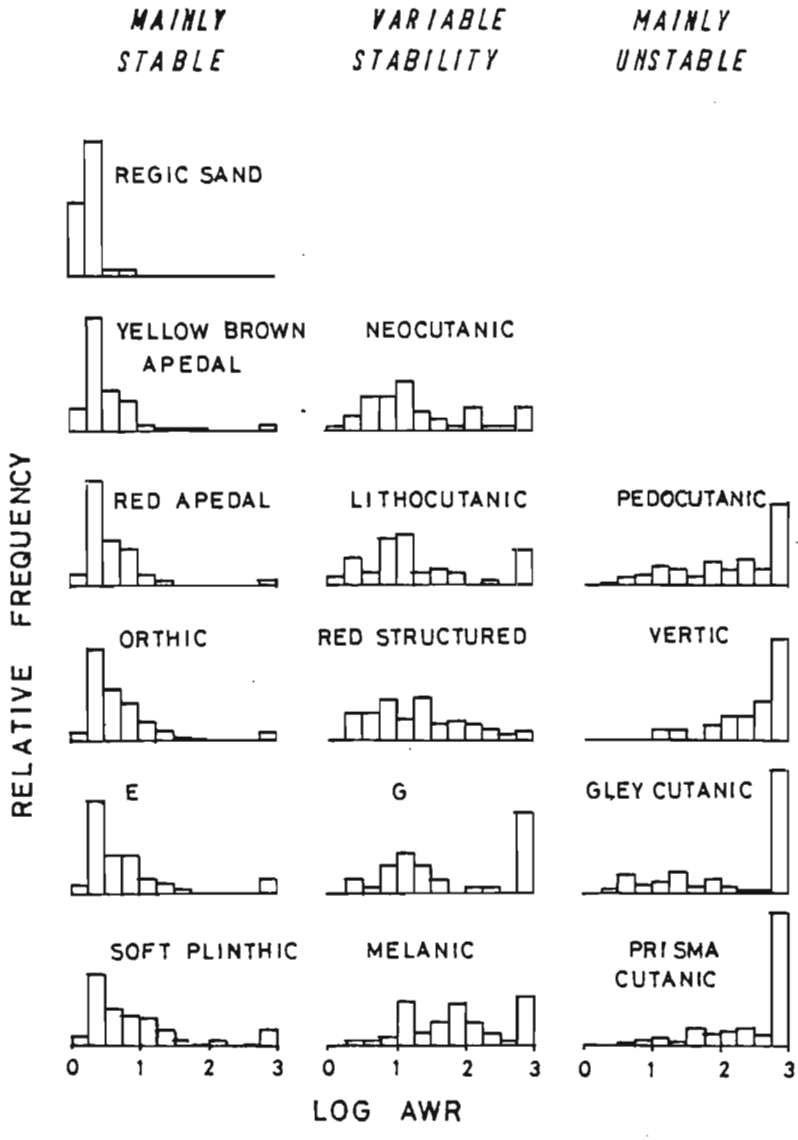

FIGURE 2.6 Relative distribution of log AWR values within diagnostic horizons grouped according to degree of stability. Number of samples in each histogram listed in Table 2.4

TABLE 2.4 Distributions of AWR, showing lower quartile (Q_1), median (Q_2) and upper quartile (Q_3) values for each diagnostic horizon

Diagnostic horizon	No. of samples	Q_1	Q_2	Q_3
High stability				
Regic sand	36	1	2	2
Yellow-brown apedal	257	2	3	5
Red apedal	490	2	3	6
Orthic	977	3	4	7
E	109	2	4	8
Soft plinthic	112	3	5	12
Intermediate stability				
Neocutanic	58	6	13	89
Lithocutanic	57	6	13	41
Red structured	90	6	18	60
G	32	12	36	1 000
Melanic	58	16	65	235
Low stability				
Pedocutanic	171	45	236	1 000
Vertic	46	167	467	1 000
Gleycutanic	62	29	1 000	1 000
Prismacutanic	96	170	1 000	1 000

of swelling clays or high exchangeable sodium levels. In these horizons structure is moderately to strongly developed.

There is a fairly wide distribution of AWR values within each histogram, which comprise data for supposedly similar soil materials. This is not unexpected since a range of soil materials can meet the classification criteria for each diagnostic horizon. These criteria are not based solely on factors influencing structural stability. Other possible causes of variability in the data may be classification and analytical errors. Nonetheless, the results indicate whether a soil from a known diagnostic horizon is likely to be unstable or not.

AWR values could possibly be used as an aid in distinguishing horizons that appear morphologically similar, such as red apedal and red structured horizons, and melanic and vertic horizons. Of all red apedal samples, 73% had AWR values of 5 or less whereas only 23% of red structured horizons had AWR values in this range. Only 40% of melanic samples had AWR values above 100 while 85% of vertic samples were in this range. A fixed threshold cannot be defined to distinguish between horizons but AWR values can be used as additional evidence for classification purposes.

Any soil material having a high AWR value is likely to be unsuitable for engineering purposes. Dam walls and embankments constructed from such material will either swell and shrink, erode rapidly or be subject to dispersive piping. Such behaviour is not always reflected by common engineering test procedures, such as Atterberg limits. As a rapid screening technique the AWR value is useful for identifying such soils and has several advantages over other methods of determining structural stability. Differences in sample preparation and packing change both air and water permeabilities by approximately the same proportion, so that their effect on the air-water permeability

ratio is not nearly as great. The apparatus is simple to construct and the method is rapid and simple for routine use.

2.3 HYDROLOGICAL GROUPING OF SOIL PROFILES

2.3.1 Flow mechanisms in diagnostic horizons

The validity of a soil water simulation model is governed partly by the accuracy with which soil properties and the hydrological environment are portrayed in the model, and partly by assumptions regarding water flow mechanisms. In this section water flow patterns in diagnostic horizons are discussed in relation to the probable hydrological environment.

Most profile water balance models assume rain, irrigation, evapotranspiration and vertical drainage to be the only sources of gain or loss of water. Contributions from lateral flow or phreatic water are usually ignored. Soil morphological properties provide evidence of the occurrence of permanent or seasonal water tables or lateral flow.

It is usually assumed that, on a macroscopic scale, water flow in soil obeys Darcy's law. Microscopic spatial variations in potential which may lead to varying flow geometries and velocities are averaged to produce a mean macroscopic flux. This assumption is less valid in pedal or aggregated soils in which varying flow velocities occur on a macroscopic scale. Water applied to the soil surface initially moves rapidly through larger macropores (interpedal flow) but more slowly through finer matrix pores (intrapedal flow). There is thus a short-circuiting effect which causes water to be transmitted rapidly into the profile along larger pores and cracks, leaving the fine peds relatively dry. This type of flow, called two-region or macropore/micropore flow, affects initial infiltration and solute transfer. Models describing two-region flow and solute transfer are being developed (e.g. Bevan and Germann, 1981; Skopp, Gardner and Tyler, 1981).

Flow patterns in soils may be further complicated by swelling. Swelling soils that are initially dry may exhibit two-region flow until larger voids or shrinkage cracks close. Changing pore geometries means that $K(\psi)$ and $\theta(\psi)$ relationships vary according to the wetting history of the soil and exhibit non-reversible hysteresis.

The validity of a Darcian model such as that described in Chapter 1 depends upon:

1) whether macropore flow is significant;
2) the swelling behaviour of the soil;
3) lateral flow and water table effects.

Diagnostic horizons may be evaluated in terms of expected flow patterns and in situ hydrology using profile morphology, field and laboratory tests diagnostic horizon definitions and criteria (MacVicar et al., 1977) and concepts of genesis of the various horizons (MacVicar et al., 1977; Van der Eyk, MacVicar and De Villiers, 1969).

Single-region Darcian models will be most applicable to horizons which have a micropore system. All water should enter and leave the horizon vertically if a one-dimensional finite difference model is being used. Horizons subject to permanent or intermittent saturation may be modelled providing that the height of the water table is known or can be simulated. If water table height is determined by overall catchment hydrology then the model will not be valid for long periods of time unless the phreatic level is monitored in the field and specified in the model. The upper layers of such profiles may be modelled successfully if they are not influenced by water table level.

Lateral flow will invalidate a one-dimensional model. Since appreciable lateral flow takes place only during periods of saturation

the model may be applicable at other times.

The majority of important agricultural soils in South Africa are free-draining and non-structured. Among these are the orthic, red apedal and yellow-brown apedal horizons. This means that simulation models could be a valuable tool for obtaining quantitative solutions to soil water problems in these soils.

2.3.2 Profile characteristics in modelling

A water flow model such as that described in Chapter 1 can be applied more successfully to some soils than to others. Simpler profiles, in terms of variability, structure and structural stability are more easily portrayed in the model by means of appropriate retentivity and conductivity functions. If the only means of characterizing a soil layer in a model is through these hydrological functions then the complexity of the profile for modelling purposes will be related to the vertical variability of retentivity and conductivity.

Five profile types are identified for modelling purposes.

1) Free-draining structurally stable profiles in which textural transitions are gradual. In the simplest case one set of hydrological functions may be used at all depths, but these soils usually exhibit gradual, depth-related changes in hydrological properties which necessitate corresponding gradual changes in hydrological function parameters.

2) Stratified profiles having several horizontal layers of different texture and gradual or abrupt transitional zones. Such soils are generally alluvial. Man-made examples of this type, such as mine slimes dams, can be the subject of simulation studies. They are more complex than type (1) as the vertical variability within the profile is greater and there is a possibility of lateral movement of water

along bedding planes.

3) Profiles having a layer or horizon of low permeability situated below the root zone, caused by clay accumulation, partial or complete induration or rock. Plinthic, hardpan and some gleyed horizons are examples of this type. Modelling is complicated as the effects of such layers on water table level and drainage is uncertain.

4) Duplex profiles which exhibit an abrupt textural and/or consistency change across a horizon boundary. In South Africa the clay fraction of duplex subsoils is generally dispersed owing to high exchangeable sodium levels. Such soils cannot be simulated using a one-dimensional model owing to the likelihood of lateral flow, the possibility of macropore flow in the structured horizon and the effects of soil solution composition on structural stability and hydrological properties.

5) Swelling soils which crack on drying. Initial infiltration into these profiles is assisted by flow through macropores. The subsequent movement and evaporation of water is more complex in these soils than in apedal soils.

One-dimensional models are most valid for profiles of type 1. Type 3 profiles are also suited to modelling provided that water table levels can be specified. Profiles of types 2, 4 and 5 are less easily modelled, especially when horizons are strongly differentiated or structure is well-developed.

2.4 TEXTURAL VARIABILITY WITHIN SOIL FORMS

2.4.1 Introduction

The retentivity and conductivity features of a soil profile must be reflected in a computer model. Soil hydrological properties are related to soil texture and bulk density; thus, textural and bulk density changes down a soil profile indicate their vertical variability. Texture plays a minor role in the definitions of diagnostic horizons in the South African soil classification system, thus a wide range of soil textures can be accommodated within each soil form. At series level, texture of the B horizon alone, is an important differentiating criterion.

In this section the Land Type Survey data are used to demonstrate the range of textures commonly encountered in South African soil profiles. Usually only one sample per horizon, representative of the horizon thickness, was available. Thus it is possible to compare average clay content in A and B horizons for example. The nature of the transition between horizons, whether abrupt or gradual, can be inferred from the definitions of soil forms and other more detailed analyses.

It is essential that vertical textural changes be reflected in soil water flow models. The usual extent of these changes is demonstrated in this section.

2.4.2 Procedure

Clay content was used as an index of texture. Only certain forms could be studied as there were insufficient data for the remainder. Scattergrams of clay contents in adjacent horizons were prepared for several soil forms (Fig. 2.7).

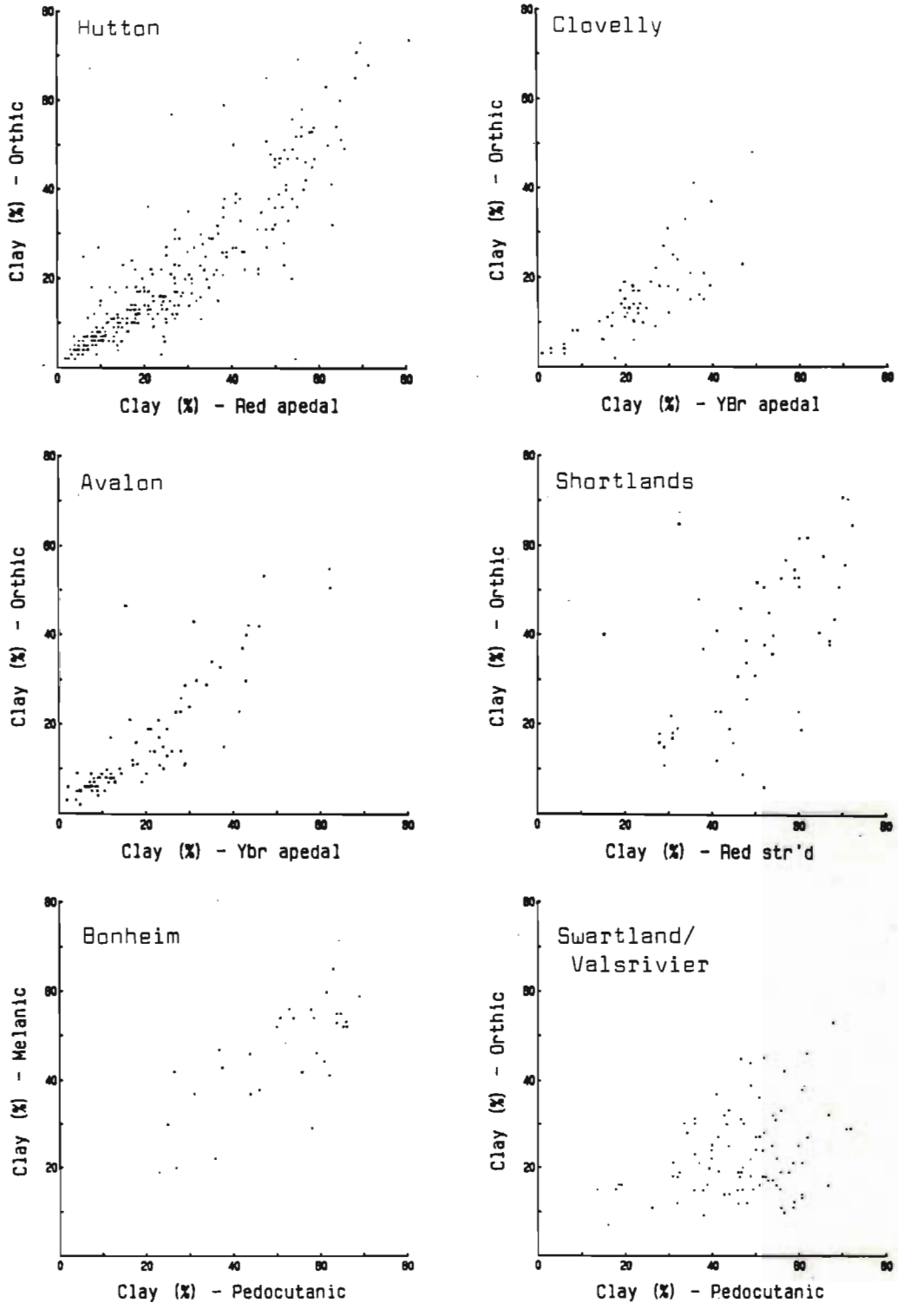

FIGURE 2.7 Distribution of clay in adjacent horizons for some soil forms

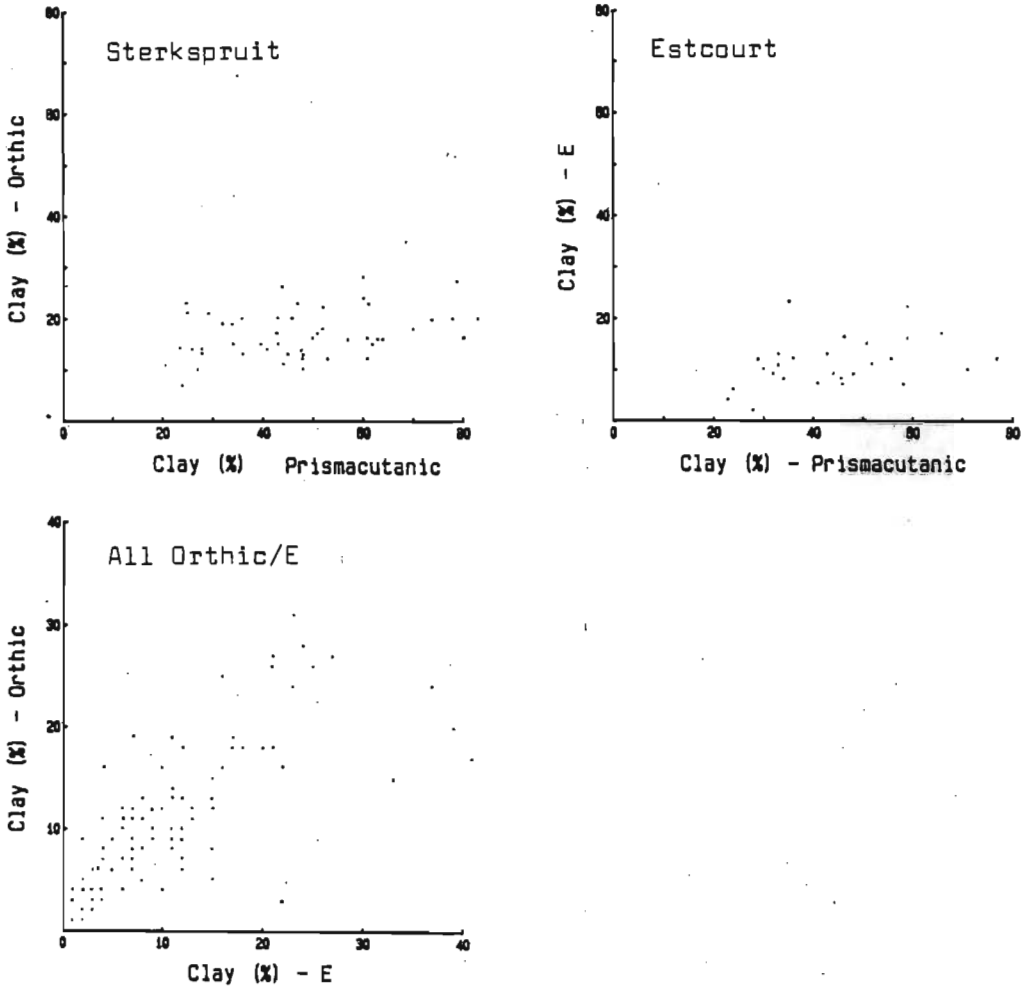

FIGURE 2.7: (Continued)

2.4.3 Results and discussion

In apedal soils, represented in Fig. 2.7 by the Hutton, Clovelly and Avalon forms, the ratio of clay content in the orthic horizon to that in the apedal B varies between 0,5 and 1. Yellow-brown apedal soils of high clay content are less common than clayey red apedal soils. The few yellow-brown apedal horizons having high clay content display smaller differences between orthic and B horizon than do the Hutton profiles, but it is doubtful whether this is significant or not. The ratio of clay content in yellow-brown apedal horizons to that in underlying soft plinthic horizons varies from about 0,7 to 1,3. Permeability in soft plinthic horizons is likely to be low owing to high bulk densities and the presence of particles and concretions larger than 2 mm in diameter, which can comprise an appreciable proportion of the total soil mass.

Soils of the Shortlands form generally have high clay contents but the ratios of clay content in the orthic horizon to that in the red structured B horizon are similar to those of the Hutton form.

Forms having orthic horizons overlying pedocutanic horizons, such as the Valsrivier and Swartland profiles, exhibit a wide range of clay content ratios between the A and B horizons. Bonheim profiles display small differences between their melanic A and pedocutanic B horizons. The available data give no indication of the nature of the transitions between orthic and pedocutanic horizons but the horizon definitions allow an abrupt transition. Structure is always more strongly developed in the pedocutanic B than in the orthic A horizon.

Duplex soils, of the Estcourt, Kroonstad or Sterkspruit forms, generally meet the defined textural transition between E and B horizons. Permeability at the transition will drop sharply. Intermittent satu-

ration above the transition together with lateral flow accentuates the development of E horizons. E horizons usually contain slightly less clay than the overlying orthic horizon and should be relatively permeable. Modelling water flow in these soils is difficult as lateral flow in the E horizon depends upon the hydrology of the surrounding catchment.

These results show that most profiles are not uniform with depth and usually display considerable variation in texture. Hydrological properties will also vary and these variations must be reflected in models. Relating retentivity and conductivity function parameters to textural criteria and bulk density provides a means of reflecting soil properties in models. The functions and their parameters are discussed in Chapters 3 and 4.

2.5 CONCLUDING REMARKS

In simple soil models the hydrological characteristics of the profile are often assumed uniform with depth, so that only one $K(\psi)$ and one $\theta(\psi)$ function need be specified. Most soils exhibit gradual or abrupt changes in texture through the profile. In addition, the presence of macropores and swelling behaviour can mean that macroscopic flow will not obey Darcy's law.

The data presented in this chapter demonstrate the major physical features of South African soils which influence their hydrological properties and behaviour. Structure is reflected in the swelling behaviour of soils which was characterized by air-to-water permeability measurements. The hydrological effects of structure and swelling are difficult to incorporate in soil water flow models. Textural variation, which was illustrated for several soil forms, can be incorporated in a model through appropriate $K(\psi)$ and $\theta(\psi)$

functions for each node in a finite difference model.

The validity of a model will depend upon the extent to which the simulated profile and its Darcian flow behaviour deviates from the more complex hydrological behaviour of real soils. The horizon and profile classifications presented are an attempt to assess this difference in complexity.

CHAPTER 3

ESTIMATING AND DESCRIBING WATER RETENTIVITY OF SOUTH AFRICAN SOILS

3.1 INTRODUCTION

Soil hydrology is of crucial importance in a country such as South Africa, where lack of moisture limits rain fed crop production and increasing areas of land are irrigated from a limited water supply. Patterns of infiltration, redistribution, evapotranspiration and drainage of soil water determine, and in turn are influenced by, cropping and management practices. Attempts to modify soil physical properties in order to promote better plant growth are often aimed at some aspect of soil hydrology.

A knowledge of the energy status and mobility of soil water in relation to water content enables the amount of plant-available water stored in a soil profile to be estimated, the analytical or numerical solution of soil water problems and the simulation of hydrologic processes by means of mathematical models. The energy status or pressure potential of water in soil in relation to water content may be portrayed by means of a retentivity curve. In soils having a rigid matrix the pressure potential is equal to the matric potential, while in swelling soils the pressure potential is a function of both water content and "envelope pressure" or overburden potential. The relationship between water content and pressure potential is not unique, owing to hysteresis in the filling and emptying of pores, and, in swelling soils, changes in pore geometry caused by changing overburden potential and water content. Some investigations have shown that retentivity curves determined under transient and static conditions may differ. In practice, for all but detailed research purposes, these effects are usually ignored and a unique non-hysteretic relationship between water content and pressure potential is assumed.

The concept of retentivity as an intrinsic and stable soil property, defined by a retentivity curve in which water content is a single-valued function of potential is erroneous but convenient. It is justified by the difficulty of measuring and describing hysteretic retentivity functions and by the spatial variability of soil properties, which usually mask the more subtle aspects of soil hydrology. Retentivity curves are determined in the laboratory by measuring the water content of soil cores or clods at increasing pneumatic potentials, or in the field by means of tensiometer potential and water content measurements. Both laboratory and field measurements are laborious and time-consuming, prompting the search for simpler methods of estimating retentivity from soil type, composition and bulk density.

Requests for approximate retentivity data for planning purposes, irrigation scheduling and system design are received frequently and predictive methods are required to satisfy such requests. The limitations of these techniques and the likely errors involved have to be appreciated by both supplier and recipient of such information. For example, soil of a particular particle size distribution can exhibit a range of retentivity curves depending on factors such as bulk density, structure and aggregation etc. Nevertheless, the range of possible retentivity curves is governed by the nature of the soil material.

Concepts concerning plant available water and its relationship to retentivity have been refined, making much early work obsolete. Traditionally, the upper (field capacity) and lower (wilting point) limits of plant available water were estimated from water contents at certain pressure potentials, generally -10 kPa or -33 kPa for the upper limit and -1500 kPa for the lower limit. It is now more widely appreciated that plant available water depends upon factors in addition to retentivity, among which are profile morphology, plant rooting pattern, transpiration demand and hydraulic conductivity. Wilcox (1962)

defined the upper limit of available water as "that moisture range in the soil that is available for consumptive use, including all consumptive use from the time of irrigation but excluding loss of water by drainage below root level". Field measurements of field capacity are preferable to estimates based on fixed water potentials.

Much research effort has been expended in attempting to relate water retentivity and plant available water to easily-measured soil properties and in developing mathematical functions to fit retentivity curves. These efforts have met with only partial success, and considering the complex and variable nature of soil, little improvement can be expected. It is not possible to characterize retentivity solely in terms of soil type and composition because of the effect of many other factors, such as particle shape, bulk density, clay mineralogy, organic matter content, structure, degree of aggregation, etc. Some of these factors defy precise quantitative description, consequently their effect can be assessed in qualitative terms only.

The object of this section is firstly, to determine the extent to which retentivity of South African soils can be predicted from a knowledge of soil type, composition and bulk density and secondly, to develop and determine the range of the parameters of a retentivity function to facilitate the mathematical description of retentivity for modelling purposes.

3.2 RETENTIVITY AND PLANT AVAILABLE WATER IN RELATION TO SOIL COMPOSITION AND BULK DENSITY

3.2.1 Introduction

There is a large number of published regression equations relating retentivity and plant available water to particle size distribution, organic matter content and bulk density. They are intended

for calculating the approximate shape of retentivity curves or approximate available water content (AW) in situations in which experimental determinations are not warranted. The equations are not always comparable owing to the several systems of particle size classification used (Figure 3.1) and varying assumptions regarding the limits of plant available water. The emphasis in this review is on:

1) the extent to which variation in retentivity and AW can be explained by particle size distribution, organic matter content and bulk density;
2) which particle size classes are most strongly associated with retentivity and AW;
3) the potential associated with field-measured field capacity in free-drained soils.

Results reported in the literature may be classified into, and are discussed in roughly the following groups:

1) in which field capacity (FC) and permanent wilting point (PWP) were assumed to be represented by certain pressure potentials, the choice of which may have been guided by field measurements;
2) in which AW was measured at each site using a ponding and drainage method for estimating FC and a sunflower wilting test for PWP;
3) where retentivity at each of several water potentials was related to soil composition;
4) relationships between retentivity and composition of South African soils.

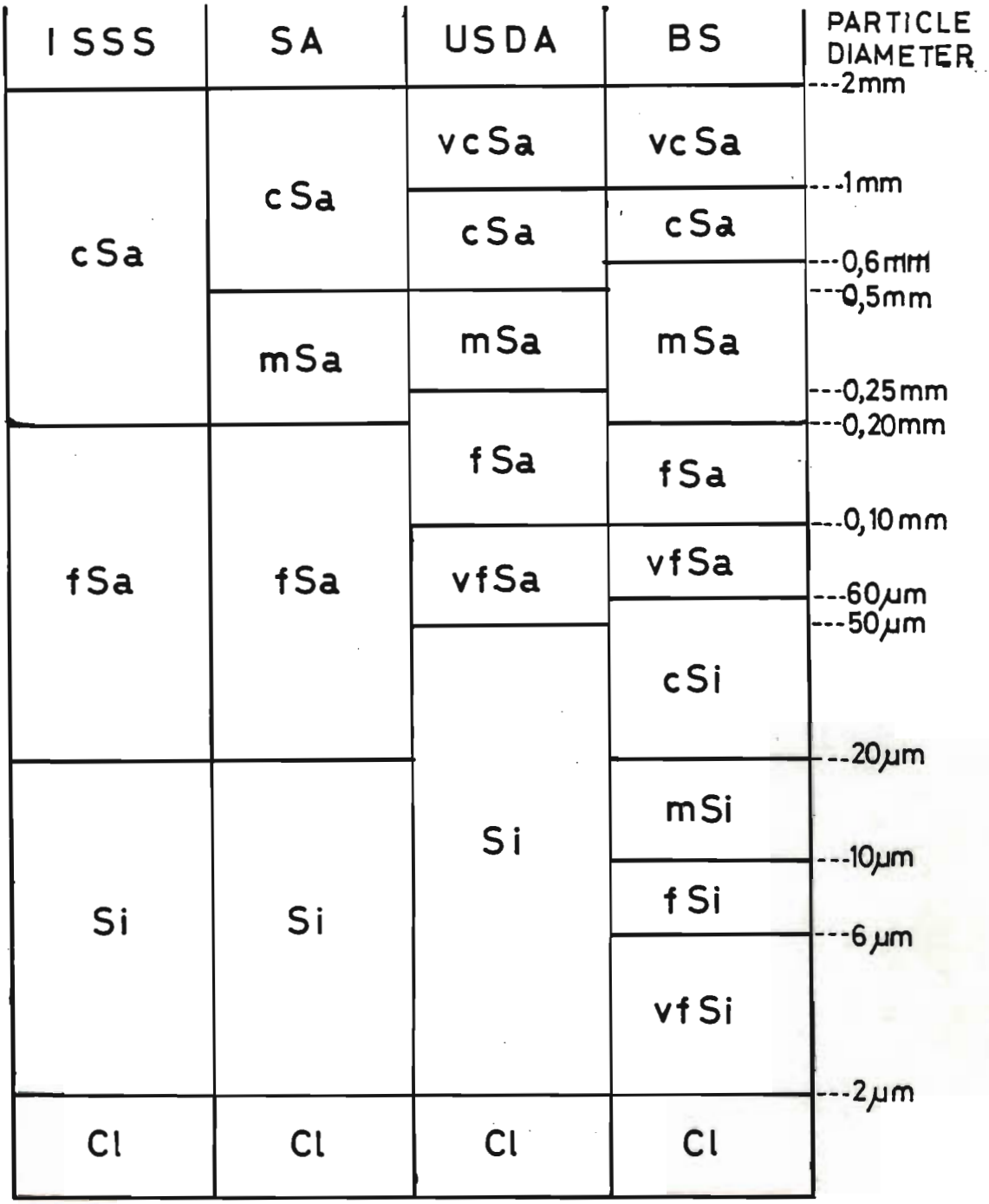

FIGURE 3.1 Particle size classification systems according to the International Society of Soil Science (ISSS), South Africa (SA), United States Department of Agriculture (USDA) and British Standards (BS)

Cl	Clay	vc	Very coarse
Si	Silt	c	Coarse
Sa	Sand	m	Medium
		f	Fine

Unless otherwise stated, water content is expressed throughout as wetness W, in kg water per kg of solid phase after drying, or as a volume fraction of liquid θ, expressed in m^3 liquid per m^3 bulk volume. Abbreviations used in equations correspond to those in Fig. 3.1, with the addition of organic carbon C, and organic matter M. Units are mass per cent (kg of particles of the designated size class per 100 kg of dry soil). Particle sizes are expressed as equivalent spherical diameter.

In earlier work, many researchers did not determine regression equations and reported correlation coefficients only (Bartelli and Peters, 1959; Lund, 1959; Jamison and Kroth, 1958). Petersen, Cunningham and Matelski (1968) determined retentivity at -33 kPa using cores and at -1500kPa using fragmented samples on 1267 Pennsylvanian soils of all textural classes. Bulk density was most closely correlated with retentivity at -33 kPa and clay content with retentivity at -1500 kPa. They derived a regression equation

$$\theta_{-1500} = 0{,}0174 + 0{,}0076\ C1 - 0{,}00005\ C1^2 \qquad (3.1)$$

but did not report either a correlation coefficient or standard error. Their multiple regression equations relating AW to particle size criteria are of limited value as AW was estimated as the difference between water contents at -33 kPa and -1500 kPa which have been shown to be unreliable indices of AW in field soils.

Salter and Williams (1965a,b) measured FC in free-draining profiles of British soils 48 hours after ponding and PWP by means of the sunflower wilting test. These water contents were matched to pressure potential values using retentivity curves measured on cores and fragmented soil. They recommended that core samples be used in preference to sieved soil and found that water retained between -33 kPa and -1500 kPa

underestimated AW by 9 to 76%. Salter, Berry and Williams (1966), using the same data, related AW to organic carbon content and particle size distribution. AW was most closely correlated with ISSS fine sand (20 - 200 µm), USDA silt (2 - 50 µm) and the 20 - 50 µm fraction, but poorly correlated with clay content.

Similar measurements were reported by Shaykewich and Zwarich (1968) for 112 Canadian soils from all textural groups. They considered their regression equations useful for predicting bulk density (ρ_b), FC and PWP but not for AW.

MacLean and Yager (1972) measured retentivity at pressure potentials of -5; -10; -33 and -1500 kPa on 143 cores from 31 Zambian soils, including oxisols and vertisols. FC was determined in the field 48 hours after ponding and PWP by the sunflower wilting test. Water retained at -5 kPa was more closely correlated with FC (R^2 = 0,955) than was that retained at -10 or -33 kPa. Measured PWP was closely correlated with water content at -1500 kPa (R^2 = 0,957). Water retained between -5 kPa and -1500 kPa overestimated AW by an average of 4% (R^2 = 0,78) and that retained between -33 kPa and -1500 kPa underestimated AW by an average of 35%. AW was most closely correlated with the 20 to 60 µm and 2 to 60 µm particle size classes. Depth had an influence on AW and was included in their regression analysis.

Rivers and Shipp (1972, 1978) studied the relationship between AW and texture of sands and loamy sands. Sand grade has a greater impact on AW in these soils than in soils of finer texture. FC was determined after 48 hours drainage from a saturated profile and retentivity was determined at -5; -7,5; -10 and -1500 kPa, using fragmented samples. The water content closest to the in situ field capacity water content was that corresponding to the -10 kPa pressure potential. AW was significantly correlated with the < 100 µm particle size class in all textural classes except fine sands and coarse sands but there

was a considerable variation in correlation coefficients both between and within textural classes at different locations. Therefore no single particle size range should be used as an indicator of AW in sandy soils without local field measurements as a control.

Retentivity at a range of pressure potentials between saturation and -1500 kPa was correlated with particle size distribution, bulk density (ρ_b) and organic carbon by Hall, Reeve, Thomasson and Wright (1977) who used data obtained from 2500 cores from 825 British soil profiles. They derived regression equations predicting water content at each of five pressure potentials, using British Standards Institute particle size classes. For topsoils,

		R^2	
θ_{-5}	$= 0,47 + 0,0025\ Cl + 0,0010\ Si + 0,0112\ C - 0,1652\ \rho_b$	0,69	
θ_{-10}	$= 0,3747 + 0,0032\ Cl + 0,0012\ Si + 0,0115\ C - 0,0125\ \rho_b$	0,70	
θ_{-40}	$= 0,2666 + 0,0036\ Cl + 0,0012\ Si + 0,010\ C - 0,0764\ \rho_b$	0,70	(3.2)
θ_{-200}	$= 0,0870 + 0,0045\ Cl + 0,0011\ Si + 0,0103\ C$	0,74	
θ_{-1500}	$= 0,0294 + 0,0083\ Cl - 0,000054\ Cl^2$	0,73	

and for subsoils,

θ_{-5}	$= 0,3720 + 0,0035\ Cl + 0,0012\ Si - 0,1173\ \rho_b$	0,68	
θ_{-10}	$= 0,2787 + 0,0041\ Cl + 0,0015\ Si - 0,0832\ \rho_b$	0,74	
θ_{-40}	$= 0,2081 + 0,0045\ Cl + 0,0013\ Si - 0,0596\ \rho_b$	0,77	(3.3)
θ_{-200}	$= 0,0757 + 0,0048\ Cl + 0,0011\ Si$	0,79	
θ_{-1500}	$= 0,0148 + 0,0084\ Cl - 0,000054\ Cl^2$	0,83	

The amount of water released between -5 kPa and -1500 kPa was assumed to approximate AW, and was most closely correlated with bulk density, organic matter and in subsoils, the 2 to 100 µm fraction. The silt fraction explained little of the variation of AW in topsoils.

Gupta and Larson (1979) compacted 43 mixtures of soil materials to various bulk densities. Regression coefficients (Table 3.1) were calculated for the regression equation

$$\theta_\psi = aSa + bSi + cCl + dM + e\rho_b \qquad (3.4)$$

where θ_ψ is fractional water content (m^3/m^3) at a pressure potential ψ and M is organic matter (mass %).

No systematic study of water retentivity in relation to soil composition has been conducted for South African soils, although retentivity and AW data has been reported for soils of certain geographical, crop production or irrigation areas. The development of a uniform soil classification system for the whole country (MacVicar et al., 1977) makes the compilation of predictive equations easier and more useful.

Hill and Summer (1967) studied the effect of bulk density on AW in eight Natal sugarbelt soils and emphasized the need for field measurement of FC and the use of undisturbed cores for retentivity measurements. Van der Meden and Johnston (Johnston, 1973) carried out a series of FC and retentivity measurements on soils in the Natal sugarbelt, but did not attempt to relate their results to soil composition. Hensley (1980) is conducting a series of AW determinations on a range of South African soils. Van der Watt (1971) calculated regression equations from retentivity and particle size distribution data for 56 sieved samples:

W_{-10} (g/100 g) = 4,99 + 0,456 Cl R^2=0,94 (3.5)

W_{-33} (g/100 g) = 4,54 - 0,0403 (0,2-1 mm) + 0,344 Cl R^2=0,94 (3.6)

W_{-1500} (g/100 g) = 2,28 - 0,0329 (0,2-1 mm) + 0,213 Cl R^2=0,94 (3.7)

TABLE 3.1 Regression and correlation coefficients for prediction of soil water content (mm/m) at specified pressure potentials according to Eq. 3.4 (Gupta and Larson, 1979)

Potential kPa	Regression coefficients (x10³)					R
	a	b	c	d	e	
-4	7,053	10,242	10,070	6,333	-321,2	0,950
-7	5,678	9,228	9,135	6,103	-269,6	0,959
-10	5,018	8,548	8,833	4,966	-242,3	0,961
-20	3,890	7,066	8,408	2,817	-187,8	0,962
-33	3,075	5,886	8,039	2,208	-143,4	0,962
-60	2,181	4,557	7,557	2,191	- 92,8	0,964
-100	1,563	3,620	7,154	2,388	- 57,6	0,966
-200	0,932	2,643	6,636	2,717	- 22,1	0,967
-400	0,483	1,943	6,128	2,925	- 2,0	0,962
-700	0,214	1,538	5,908	2,855	15,3	0,954
-1000	0,076	1,334	5,802	2,653	21,5	0,951
-1500	0,059	1,142	5,766	2,228	26,7	0,947

Van der Merwe (1973) measured retentivity on 69 Orange Free State soils and found using the ISSS particle size classification,

$$W_{-10} = 0,2662 + 0,162 / \ln(1 + Cl + Si) \qquad R^2 = 0,87 \quad (3.8)$$

$$W_{-1500} = 0,00218 + 0,003068\ (Cl + Si) \qquad R^2 = 0,88 \quad (3.9)$$

Turner (1976) measured retentivity using resin-coated clods from 32 Natal clay and clay loam, red and yellow-brown apedal soils. Clay contents were generally above 40%, bulk densities low and organic carbon contents high. Regression coefficients for the equation,

$$\theta_\psi = a + bCl + cfSa + dC + e\rho_b \qquad (3.10)$$

using ISSS size limits, are listed in Table 3.2.

Burger, Bennie, Botha and Du Preez (1979) studied the relationship between retentivity, texture, bulk density and soil strength on six laboratory-compacted sands and loamy sands from the Vaalharts irrigation scheme. As their regression equations were obtained using very few samples from a narrow range of textures they are probably useful only for soils of that area.

Mottram, Hutson and Goodman (1981) reported regression equations predicting retentivity of soil cores from Mkuze Game Reserve, Natal. Those accounting for the greatest proportion of the variation of θ at -5 kPa and -1500 kPa were, for topsoils,

$$\theta_{-5} = 0,2111 + 0,0044\ Cl + 0,0029\ Si + 0,0106\ M - 0,1191\ \rho_b \qquad R^2 = 0,81 \quad (3.11)$$

$$\theta_{-1500} = 0,1526 + 0,0028 Cl + 0,0005 Si + 0,0232 M - 0,106\ \rho_b \qquad R^2 = 0,80 \quad (3.12)$$

TABLE 3.2 Regression and correlation coefficients for predicting water content of Natal apedal soils according to Eq. 3.10 (Turner, 1976)

Potential kPa	Regression coefficients (x10³)					R
	a	b	c	d	e	
-1	1288,6	-0,66	-1,98	6,66	-588,9	0,951
-3	1067,5	-4,17	-6,55	16,78	-281,8	0,901
-10	938,7	-4,24	-7,07	24,67	-213,1	0,909
-30	766,2	-3,09	-6,70	25,24	-155,3	0,915
-100	665,4	-2,40	-6,58	25,02	-124,1	0,929
-1500	588,3	-2,09	-6,00	21,16	-116,0	0,898

TABLE 3.3 Sources of retentivity data

Code	Laboratory	Analyst	Reference
1	Soil & Irrigation Research Inst.	JL Hutson & BJ Joubert	Unpublished data
2	Natal University	DP Turner	Turner (1976)
3	Natal University	M Hensley	Hensley (1969)
4	Sugar Assoc. Expt. Stn. Mt Edgecombe	E von der Meden & MA Johnston	Johnston (1973 & unpublished expt station reports
5	Natal University	A Cass	Dekker, Jeffrey & Scotney (1980)
6	Natal University	DM Scotney	Scotney (1970)
7	Summer Grain Sub-centre, Cedara	R Mottram	Mottram, et al. (1981) & unpublished data
8	University of Fort Hare	M Hensley	Hensley (1980) & unpublished data
9	Soil & Irrigation Research Inst.	JL Hutson	Unpublished land type survey data

and for subsoils,

$$\theta_{-5} = 0,3536 + 0,003\,Cl + 0,0087\,Si - 0,198\,\rho_b \qquad R^2 = 0,72 \qquad (3.13)$$

$$\theta_{-1500} = 0,0193 + 0,0031\,Cl + 0,0059\,Si + 0,029\,\rho_b \qquad R^2 = 0,81 \qquad (3.14)$$

Several general conclusions may be drawn from this review.

1) Particle size distribution, bulk density and organic matter account for between 60 and 90% of the variability of retentivity, the R^2 value decreasing as potential increases. The effect of structure, which can neither be measured quantitatively nor included in the regression, is minimal at low pressure potentials.

2) Plant available water is predicted less reliably than retentivity, the independent variables accounting for between 50 and 80% of the variability. The fraction of particles between 2 and 100 µm diameter and bulk density are most closely correlated with AW, while clay content appears to have little influence on AW.

3) FC is best approximated by water content at potentials of about -5 kPa. The data reported was obtained from what was described as "free-draining profiles". Any profile features which inhibit downward movement of water will tend to increase FC and the potential at FC. Estimates of FC based upon water retained at -10 to -33 kPa are therefore too low.

3.2.2 Retentivity of South African soils in relation to composition and bulk density

3.2.2.1 Introduction

In order to use soil survey data to predict hydrological properties it is necessary to investigate retentivity of South African

soils in relation to their physical composition and classification. The regression equations derived by Burger et al., (1979) and Turner (1976) were based on relatively few data from narrow ranges of soil type. In this section retentivity data from several sources are combined and used to derive equations relating water content at several potentials to some particle size criteria and bulk density.

3.2.2.2 Procedure

The data base contained water retentivity data from several sources, the two main groups being that from the Land Type Survey (3000 samples), which consisted of water retentivity at -1500 kPa and -500 kPa determined on sieved samples, and retentivity determined at a range of potentials using cores or clods (500 samples). The sources of data are listed in Table 3.3 and the data available from each source are summarized in Table 3.4.

Since different sets of potentials were used by the various laboratories, for example some used -30 kPa while others used -33 kPa, each retentivity curve was plotted on semi-logarithmic axes and the points were joined by a smooth curve. Values of θ at -1; -3; -10; -30; -100; -500 and -1500 kPa, or those that fell within the measured range and near an experimental point, were obtained directly or by interpolation. These values, together with analytical and classification data, were stored on magnetic tape for further processing.

Histograms and scattergrams were prepared to establish the range of soils in the data base. Simple and multiple regression analyses were used to determine the proportion of the variance of retentivity at each potential which can be explained by particle size criteria and bulk density. The multiple regression model used was

TABLE 3.4 Retentivity and analytical data available from each data source

Source code	1	2	3	4	5	6	7	8	9
No. of samples	163	41	45	82	21	48	89	11	3000
Classification	+	*	+	*	*	*	*	*	*
Stability class	*	*	*	*	*	*	*	*	*
Particle size data:									
Clay < 2 µm	*	*	*	*	*	-	*	*	*
Silt 2-20 µm	*	*	*	*	+	-	*	*	*
fSa 0,02-0,2mm	*	*	*	*	-	-	*	*	*
mSa 0,2-0,5mm	*	*	+	+	-	-	*	*	*
cSa 0,5-2mm	*	*	+	+	-	-	*	*	*
Gravel > 2mm	+	-	-	-	-	-	-	-	-
Organic carbon	+	*	-	-	-	-	-	-	-
Bulk density	*	*	*	*	*	*	*	*	-
θ at: -1kPa	*	*	*	+	-	*	-	*	e
-3kPa	*	*	*	*	-	*	-	*	
-10kPa	*	*	*	*	*	*	*	*	
-30kPa	*	*	*	+	*	*	*	*	
-50kPa	*	-	-	-	-	-	-	-	
-100kPa	-	*	*	+	*	*	*	*	
-500kPa	-	*	*	+	-	*	-	*	
-1500kPa	-	*	*	+	*	*	*	*	
Textural class	*	*	*	*	+	-	*	*	*
Sample type	a	b	a	a	b	c	a	a	d

Symbols: * Data available for all samples + some data missing

- No data available

a Cores b Clods c Cores + sieved samples at -500kPa and -1500kPa d Sieved samples

e W (g/g) at -33kPa, -80kPa, -500kPa, -1500kPa

$$\gamma_\psi = \beta_o + \beta_1 Z_1 + \beta_2 Z_2 + ... \beta_n Z_n + \varepsilon \qquad (3.15)$$

where γ is θ or W at potential ψ,

β_i are regression coefficients,

Z_i are independent variables, and

ε is an error term.

Separate analyses were performed on the following sets of data:

(1) all core and clod data (sources 1 to 8) excluding unstable soils (soils regarded as unstable are those classified as vertic, prismacutanic, gleycutanic and pedocutanic);

(2) core data from source 1 only;

(3) data from the Land Type Survey, which consisted of water contents of sieved soils at -1500 kPa. Although these soils, 3000 samples in all, were classified according to the Binomial System (MacVicar et al., 1977), preliminary analysis showed that little was accomplished by performing separate regression analyses for each diagnostic horizon. A broad classification based upon structural stability as reflected by the air-water permeability ratio was used to group the samples as follows:

a) all samples;

b) air-water permeability ratios (AWR) less than 10;

c) AWR between 10 and 100;

d) all vertics, which generally have AWR values greater than 100;

e) prismacutanic, pedocutanic and gleycutanic soils, which generally have extremely high AWR values.

3.2.2.3 Results and discussion

The distribution of samples according to textural class is shown in two-way frequency tables (Tables 3.5 and 3.6). The relatively few samples from vertic, prismacutanic, pedocutanic and gleycutanic horizons were excluded from the regression analysis as they are structurally unstable and structure and swelling effects may dominate retentivity. Since retentivity data were usually not available over the whole range of potentials for each sample, the number of samples used in the regression analysis at each potential varied from 409 at -10 kPa to only 147 at -500 kPa.

The distribution of bulk density values (Fig. 3.2) is not necessarily a reflection of bulk density values in South African soils in general. The soils of low bulk density were from high rainfall areas in Natal. From the few organic carbon analyses available (e.g. Turner, 1976) it appears as though low bulk density values are associated with high organic carbon contents. This was also observed by Hall et al., (1977). Results of regression analysis are recorded in Tables 3.7 to 3.10. Scatter diagrams of observed versus predicted values are shown in Fig. 3.3 for some of the equations. Combined data from sources 1 to 8 had a wide range of physical properties which show a pattern similar to that found in published literature.

As pressure potential decreases, the proportion of the variance of water content accounted for by regression increases since retentivity is increasingly related to water film thickness and surface area whereas pore size distribution, aggregation and the geometry of the solid matrix play a lesser role. Of the independent variables included in the regression, clay content accounts for the greatest proportion of the variance in θ and W (Fig. 3.4). Silt content increases in importance as potential increases but bulk density has a negligible influence until saturation is approached. Bulk density

TABLE 3.5 Textural distribution of soils

Source code	Sa	LmSa	SaLm	Lm	Si	SaClLm	ClLm	SiClLm	SaCl	SiCl	Cl
1	6	3	55	4		53	14	10	2		16
2			1	3			5	4	1		27
3	20	24	1								
4	2	14	13			15	6		4	2	26
5	1	1	4			1	1				5
6	No particle size data available										
7	4	9	9	1	1	10	3		2	3	47
8			2			6				1	2

TABLE 3.6 Textural distribution of soils for which retentivity data were available (data sources 1 - 8 excluding unstable soils)

Pressure potential kPa	Sa	LmSa	SaLm	Lm	Si	SaClLm	ClLm	SiClLm	SaCl	SiCl	Cl	Total
-1	26	29	63	7		60	19	13	3	1	45	266
-3	28	41	72	7		70	21	13	4	3	57	316
-10	33	51	84	8	1	83	24	13	6	5	101	409
-30	33	49	79	8	1	82	24	13	6	5	101	401
-50	6	3	55	4		53	14	10	2		16	163
-100	27	46	24	4	1	26	10	3	4	5	85	235
-500	22	36	12	4		17	7	3	2	3	41	147
-1 500	27	46	24	5	1	29	10	3	4	5	85	239

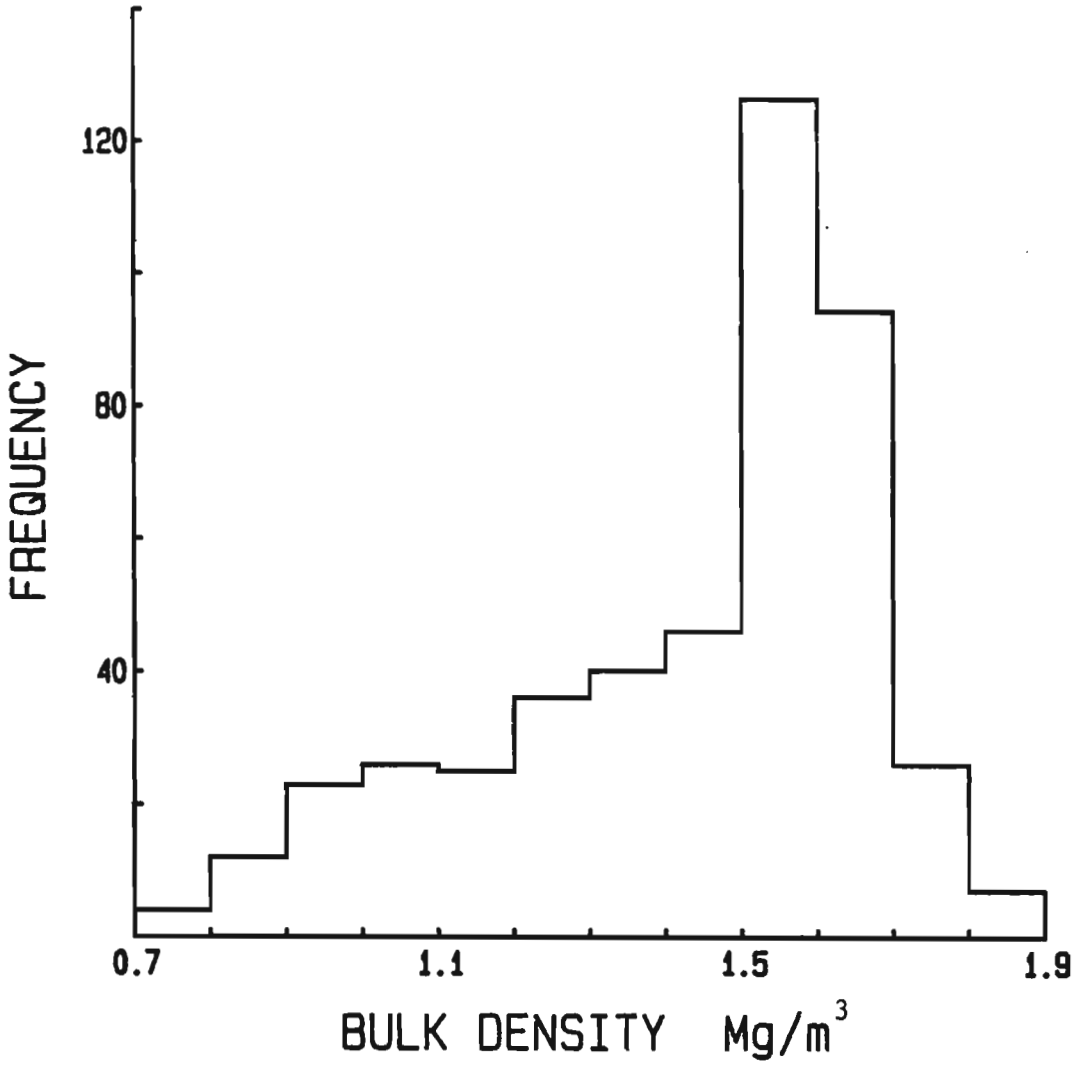

FIGURE 3.2 Distribution of bulk density values (sources 1 to 8)

TABLE 3.7 Regression equations for predicting θ and W at -1500kPa for South African soils, together with variance accounted for (R^2) and standard error (s) of the estimate of θ or W

Sample source		R^2	s
Sources 1 to 8	$\theta_{-1500}=0,0344+0,00382Cl$	0,733	0,056
Core and clod data	$\theta_{-1500}= 0,00741+0,00735Cl-0,000045Cl^2$	0,771	
(excluding unstable soils)	$\theta_{-1500}=0,06023+0,0032Cl+0,00308Si$ $-0,02598\rho b$	0,785	0,051
	$W_{-1500}=-0,00948+0,00370Cl+0,00289Si$	0,791	
Source 9	$W_{-1500}=0,00871+0,00378Cl$	0,788	0,037
	$W_{-1500}=0,00429+0,00419Cl-6,2x10^{-6}Cl^2$	0,789	
	$W_{-1500}=-0,00073+0,00348Cl+0,00184Si$	0,815	0,034
	$W_{-1500}=0,00341+0,00340Cl+0,00154Si$ $+0,0195C$	0,827	0,033
AWR: <10	$W_{-1500}=0,00032+0,00279Cl$ $0,00170Si+0,0160C$	0,877	0,022
AWR: 10-100	$W_{-1500}=0,00524+0,00342Cl+0,00136Si$ $+0,00852C$	0,744	0,036
Vertic	$W_{-1500}=0,01953+0,00404Cl+0,00190Si$ $+0,0256C$	0,454	0,053
Prismacutanic Pedocutanic Gleycutanic	$W_{-1500}=0,01077+0,00348Cl+0,00148Si$	0,711	0,034

TABLE 3.8 Regression coefficients for the model $\theta = \beta_o+\beta_1 Cl+\beta_2 Si+\beta_3 \rho_b$ applied to data from sources 1 to 8, excluding unstable soils, variance accounted for (R^2), and standard error of the estimate of θ (s)

ψ kPa	β_o	β_1	β_2	β_3	R^2	s
-10	0,0558	0,00365	0,00554	0,0303	0,681	0,066
-30	-0,0150	0,00384	0,00572	0,0463	0,764	0,055
-100	0,0290	0,00361	0,00441	0,0049	0,769	0,059
-500	0,1588	0,00347	0,00170	-0,0838	0,823	0,047
-1500	0,0602	0,00322	0,00308	-0,0260	0,785	0,051

TABLE 3.9 Regression coefficients for the model $\theta = \beta_o+\beta_1 Cl+\beta_2 Si+\beta_3 \rho_b$ applied to data from source 1 only, excluding unstable soils

ψ kPa	β_o	β_1	β_2	β_3	R^2	s
-1	0,4862	0,00136	0,00148	-0,1169	0,365	0,032
-3	0,2590	0,00234	0,00252	-0,0140	0,552	0,034
-10	0,0660	0,00439	0,00431	0,0267	0,852	0,030
-30	0,0200	0,00506	0,00490	0,0194	0,909	0,025
-50	0,0035	0,00515	0,00514	0,0184	0,930	0,023

TABLE 3.10 Regression coefficients for the model $\theta = \beta_o+\beta_1 Cl+\beta_2 Si +\beta_3$ fSa + $\beta_4 \rho_b$ applied to data from source 1, excluding unstable soils

ψ kPa	β_o	β_1	β_2	β_3	β_4	R^2	s
-1	0,4244	0,00246	0,00188	0,00134	-0,1284	0,449	0,030
-3	0,1620	0,00408	0,00317	0,00212	-0,0328	0,687	0,029
-10	-0,0029	0,00562	0,00477	0,00151	0,0133	0,882	0,029
-30	-0,0035	0,00548	0,00507	0,00051	0,0148	0,921	0,025
-50	-0,0146	0,00548	0,00526	0,00040	0,0149	0,932	0,022

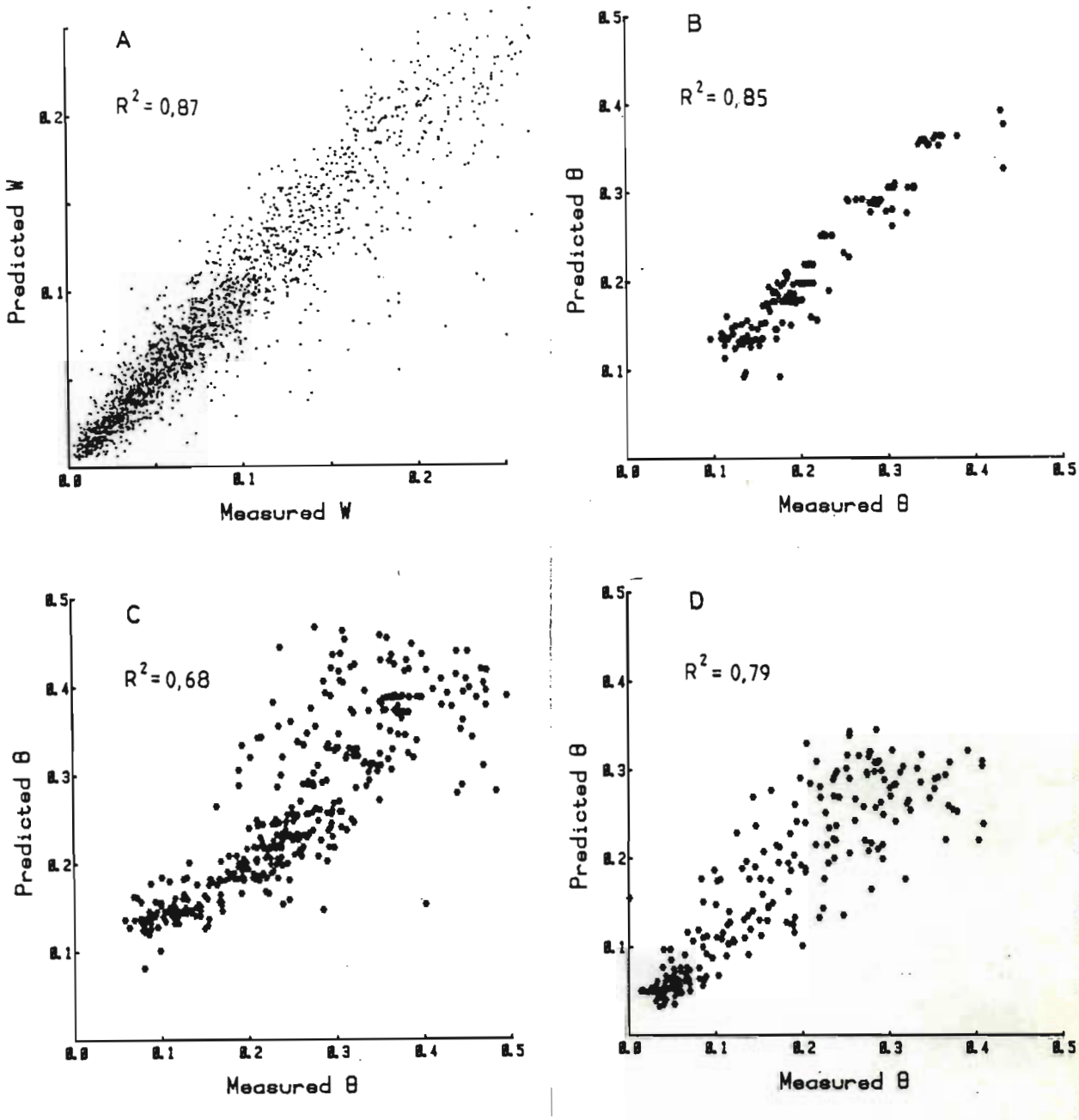

FIGURE 3.3 Observed and predicted values of W (g/g) and θ (m^3/m^3) for selected regression equations

A: $W_{-1500} = 0,0003 + 0,0028\ Cl + 0,0017\ Si + 0,016\ C$

(based on Land Type Survey; AWR < 10)

B: $\theta_{-10} = 0,0660 + 0,0044\ Cl + 0,0043\ Si + 0,0267\ \rho_b$

(based on source 1 data)

C: $\theta_{-10} = 0,0558 + 0,0037\ Cl + 0,0055\ Si + 0,0303\ \rho_b$

(based on sources 1 to 8 data)

D: $\theta_{-1500} = 0,0602 + 0,0032\ Cl + 0,0031\ Si - 0,0260\ \rho_b$

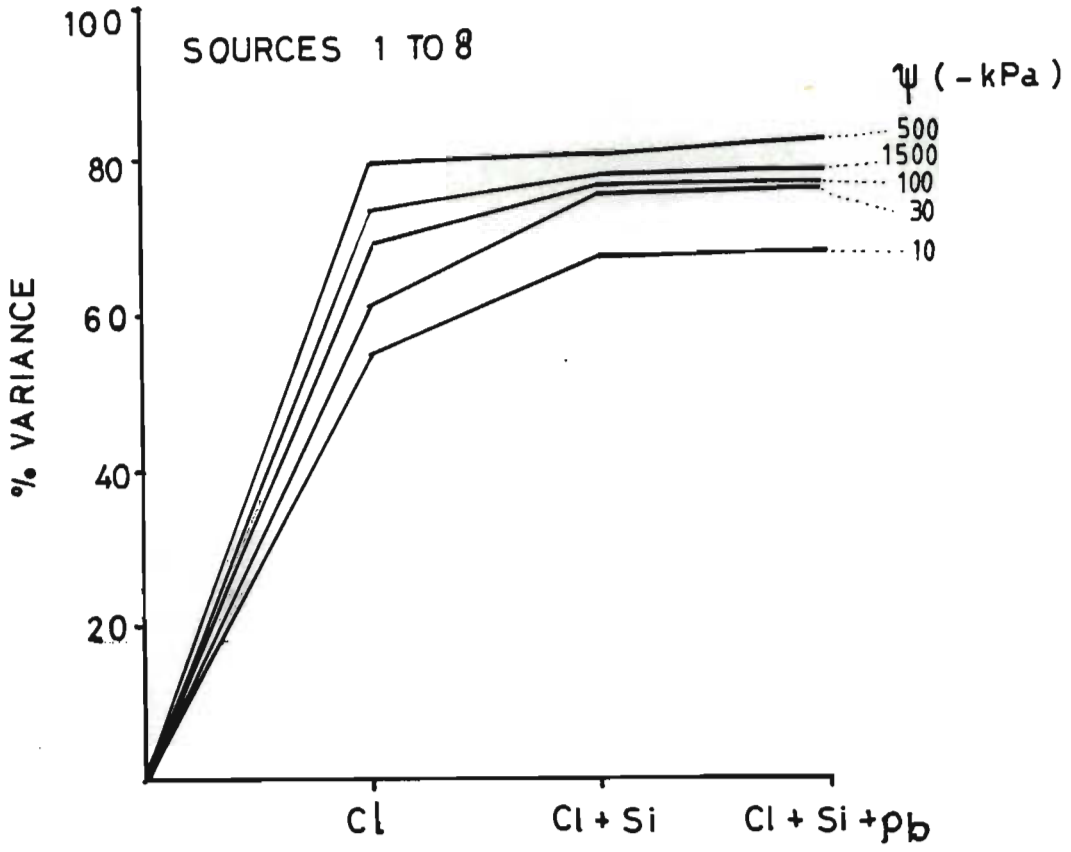

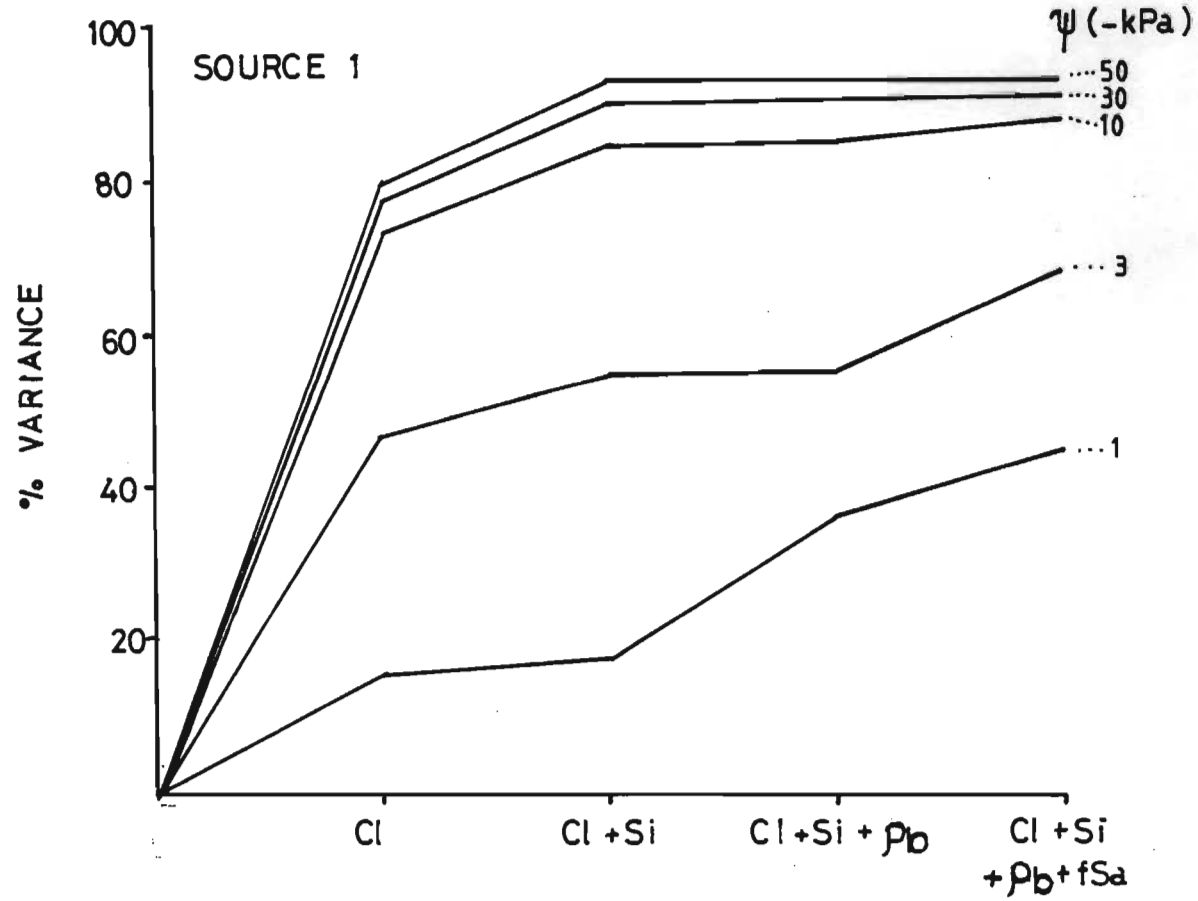

FIGURE 3.4 Variation of retentivity accounted for by particle size criteria and bulk density

could have been excluded from the regression analysis but the small effect that it does have supports the observation of Hill and Sumner (1967) that increasing bulk density increases retentivity at higher potentials and decreases it slightly at low potentials (Table 3.8). Obviously water content at saturation is related solely to bulk density. Including fine sand in the regression analysis increased R^2 values slightly at pressure potentials of -1 and -3 kPa for data from source 1 (Tables 3.9 and 3.10), but did not improve estimation when included in the analysis of the combined data from sources 1 to 8.

These equations do not enable very precise predictions. Standard errors of the estimates of θ (core samples) and W (sieved samples) are about 0,05 or 5% volumetric water content. Higher correlation coefficients are obtained if the range of soil types included in the regression analysis is reduced, and especially if smectitic and other structured soils are ignored. Regression analysis of the Land Type Survey data (Table 3.7) demonstrates this point. As the air-to-water permeability ratio (an index of swelling and smectitic clay content) increases, the correlation coefficient decreases, the regression coefficient β_1 increases and standard error of the estimate increases. Similarly, using core data from source 1 only, comprised mainly of soils from the Horticultural Research Institute (Pretoria), and Addo Research Station (near Port Elizabeth), leads to greater estimation precision. Apart from the effects of variable and ill-defined aspects of soil structure, clay mineralogy, particle shape, etc., other factors contributing to low correlation coefficients are:

(1) differences in analytical techniques between laboratories, including aspects such as temperature and pressure control;

(2) the presence of unknown amounts of gravel > 2 mm diameter in the soil cores which is not included in the particle size analysis, and

(3) sampling procedures, and type and size of sample;

(4) non-equilibrium owing to poor contact between core and plate or shrinkage of soil away from the plate.

These results demonstrate the difficulty of making precise predictions of retentivity from soil survey data. Field or laboratory measurements are essential if accurate data are required. Regression equations merely provide a good first estimate and can be most useful for planning and evaluation purposes.

3.3 A RETENTIVITY FUNCTION FOR USE IN SIMULATION MODELS

3.3.1 Introduction

Retentivity functions, or equations relating water content to water potential, are essential for modelling purposes. Simulation modelling is hampered by a lack of relevant soil hydrologic data for each segment of the simulated profile. Unless these data can be estimated, profile characterization is restricted to a few layers as the experimental determination of more data becomes too laborious.

A method of describing and estimating retentivity for use in models is developed in this section. A retentivity function, in which the volume fraction of water θ_ψ is a single-valued function of pressure potential ψ, is developed and the parameters of the function are related to soil properties. Investigations into the variability of soil hydrological properties (Nielson, Biggar and Erh, 1973; Cameron, 1978) have shown that many measurements are required in order to obtain reliable estimates of retentivity and hydraulic conductivity. Most models necessarily neglect important but poorly defined facets of soil water behaviour, such as hysteresis, vapour diffusion, swelling, temperature and solute effects. For these reasons it is often acceptable to estimate retentivity and conductivity relationships, ensuring that

predominant soil profile features are reflected in the estimated data.

One method of describing the wide range of possible retentivity curves is to assume that a general retentivity equation may be fitted to all possible retentivity curves sufficiently accurately for simulation purposes, the parameters being related to soil type. For practical purposes the retentivity function should not have more than two or three constants otherwise it becomes too difficult to relate them to soil properties. It must be appreciated that there will be varying degrees of agreement between the family of curves generated by such an equation and the range of curves exhibited by real soils.

Many retentivity functions have been used, for example,

$$\theta = \left[\frac{1}{1 + (\alpha\psi)^{n}}\right]^{m} \qquad \text{(van Genuchten, 1980)} \qquad (3.16)$$

$$\psi = a\,\theta^{-b} \qquad \text{(Gardner et al., 1970)} \qquad (3.17)$$

$$S_e = (\psi_e/\psi)^{\lambda} \qquad \text{(Brooks and Corey, 1966)} \qquad (3.18)$$

$$\theta = \theta_e + \alpha \ln (\psi - \psi_e + 1) \qquad \psi \geqq \psi_e$$

$$\theta = \theta_e + \beta \ln (\psi_e - \psi + 1) \qquad \psi \leqq \psi_e \text{ (Rogowski, 1971)} \qquad (3.19)$$

where θ is the volume fraction of water,

θ_e is the volume fraction at the air-entry potential, ψ_e,

ψ is pressure potential, and

S_e is effective saturation.

S_e is defined as

$$S_e = \frac{\theta - \theta_r}{\theta_s - \theta_r} \tag{3.20}$$

where θ_s is the volume fraction of water at saturation and θ_r is residual saturation. θ_r is defined as the value of θ at which $d\theta/d\psi \rightarrow 0$ or $K \rightarrow 0$ but is often used as a curve-fitting parameter. Mathematical spline functions have also been used (Erh, 1972).

The Brooks and Corey function has been widely tested, modified and incorporated in analytical solutions to water flow problems. Lenhard and Bloomberg (1979) found it applicable to retentivity relationships of a forest soil under various compaction treatments. Russo and Bresler (1980a, b) used it in their study of the variability and scaling of hydraulic properties of field soils. Although physical significance is attached to parameters ψ_e and θ_r, most authors have used them as curve-fitting parameters. Campbell (1974) described a similar equation in which residual saturation was ignored,

$$\psi = \psi_e \, (\theta/\theta_s)^{-b}. \tag{3.21}$$

Campbell's equation has only two constants in addition to θ_s and is thus easily fitted to measured retentivity data. Clapp and Hornberger (1978) fitted Campbell's function to U S Soil Survey retentivity data and found that the exponent b was related to soil texture. Their data (Table 3.11) indicate that ψ_e may be related to silt content. If ψ_e represented a true air-entry potential then $-\psi_e$ would be inversely proportional to the radius of the largest pore. Texture would influence ψ_e insofar as it determines largest pore size.

Ghosh (1980) applied Eq. 3.21 to 27 Indian soils and found that the value of b could be predicted from an empirical function of sand, silt and clay content. His range of b values, from 1 to 6, was lower than that found by Clapp and Hornberger (1978), suggesting that a narrow range of soil types was used.

Exponential retentivity functions have a sharp discontinuity at $\psi = \psi_e$ which causes problems in soil water simulation models since $\theta = \theta_s$ and $d\theta/d\psi = 0$ over the potential range 0 to ψ_e. Real soils do not exhibit such abrupt changes in retentivity and retentivity curves are sigmoidal. To obtain a more realistic representation of retentivity, Su and Brooks (quoted by Ayars, 1976) used a combination of two functions to describe a sigmoidal retentivity curve:

$$\psi = \psi_i \left[\frac{S - S_r}{a}\right]^{-m} \left[\frac{1 - S}{b}\right]^{bm/a} \qquad (3.22)$$

where ψ_i is water potential at the inflection point, S is saturation, S_r is residual saturation, m is a shape factor of the curve, a is the domain of saturation associated with the concave portion of the curve and b is the domain of saturation associated with the convex portion of the curve.

Clapp and Hornberger (1978) replaced the exponential function by a parabolic function at water contents near saturation, so that for the interval $S_i \leq S \leq 1$

$$\psi = -m\,(S - n)(S - 1) \qquad (3.23)$$

The parameters m and n were calculated so that the curve passed through θ_s and the term $d\psi/dS$ of both Eq. 3.21 and 3.23 were equal at the inflection point (S_i, ψ_i). Either S_i or ψ_i may be chosen to locate an inflection point which corresponds to available data. Expressions for m and n in terms of b and ψ_i are

$$m = \frac{\psi_i}{(1 - S_i)^2} - \frac{\psi_i b}{S_i (1 - S_i)} \tag{3.24}$$

$$n = 2S_i - (\psi_i b/mS_i) - 1 \tag{3.25}$$

For obtaining the data in Table 3.11 Clapp and Hornberger (1978) maintained S_i at 0,92.

Eq. 3.22 or 3.23 provide flexibility for describing sigmoidal retentivity curves but require additional parameters. The object of this work was to develop a retentivity function that is easy to use in simulation models, that describes retentivity realistically over the whole water content range, and which has parameters which can be related to soil properties. A function was required which has no more than two parameters in addition to θ_s, is sigmoidal, continuous and passes through θ_s at $\psi = 0$. In the following sections a two-part retentivity function based on Eq. 3.21 is derived, the function is fitted to retentivity data for South African soils and the relationship between the function parameters and soil properties is examined.

3.3.2 Theory

The retentivity equation proposed by Campbell (1974) is exponential, having a sharp discontinuity at ψ_e, $\theta/\theta_s = 1$. The potential at this discontinuity was assumed by Campbell to be an air-entry potential. A better representation of retentivity in real

TABLE 3.11 Representative values for retentivity parameters (after Clapp and Hornberger, 1978)

Soil texture USDA Classes	Mean Clay %	b	Mean ψ_e mm water	Mean θ_s m/m
Sa	3	4,05 ± 1,78	-121 ± 143	0,395 ± 0,056
LmSa	6	4,38 ± 1,47	- 90 ± 124	0,410 ± 0,068
SaLm	9	4,90 ± 1,75	-218 ± 310	0,435 ± 0,086
SiLm	14	5,30 ± 1,96	-786 ± 512	0,485 ± 0,059
Lm	19	5,39 ± 1,87	-478 ± 512	0,451 ± 0,078
SaClLm	28	7,12 ± 2,43	-299 ± 378	0,420 ± 0,059
SiClLm	34	7,75 ± 2,77	-356 ± 378	0,477 ± 0,057
ClLm	34	8,52 ± 3,44	-630 ± 510	0,476 ± 0,053
SaCl	43	10,40 ± 1,64	-153 ± 173	0,426 ± 0,057
SiCl	49	10,40 ± 4,45	-490 ± 621	0,492 ± 0,064
Cl	63	10,40 ± 3,70	-405 ± 397	0,482 ± 0,050

soils is made by replacing the exponential function by a parabolic function at high potentials, as did Clapp and Hornberger (1978). In this section a two-part retentivity equation is developed in which no parameters additional to those used in the exponential part of the function are introduced.

Campbell's equation (Eq. 3.21) is rewritten as

$$\psi = a\ (\theta/\theta_s)^{-b} \tag{3.26}$$

in which the constant a replaces ψ_e, removing the implication that it is an air-entry potential rather than a curve-fitting parameter. A parabolic equation for which the term $d\theta/d\psi = 0$ at $\psi = 0$ is

$$\psi = \left[\left(\frac{1 - \theta/\theta_s}{c}\right)\right]^{\frac{1}{2}} \tag{3.27}$$

where c is a constant. This is an arbitrary choice of equation, the merits of which are ease of matching to the exponential function and simplicity.

At the point of inflection (ψ_i, θ_i) where the two curves coincide (Fig. 3.5),

$$\psi_i = \left[\frac{1 - \theta_i/\theta_s}{c}\right]^{\frac{1}{2}} = a\ (\theta_i/\theta_s)^{-b} \tag{3.28}$$

and

$$\frac{d\psi}{d\theta} = \frac{-1}{2c^{\frac{1}{2}}\theta_s}\ (1 - \theta_i/\theta_s)^{-\frac{1}{2}} = \frac{-ab}{\theta_s}\ (\theta_i/\theta_s)^{-b-1}. \tag{3.29}$$

From Equation 3.28

$$c = (1 - \theta_i/\theta_s)\ /\ a^2\ (\theta_i/\theta_s)^{-2b}. \tag{3.30}$$

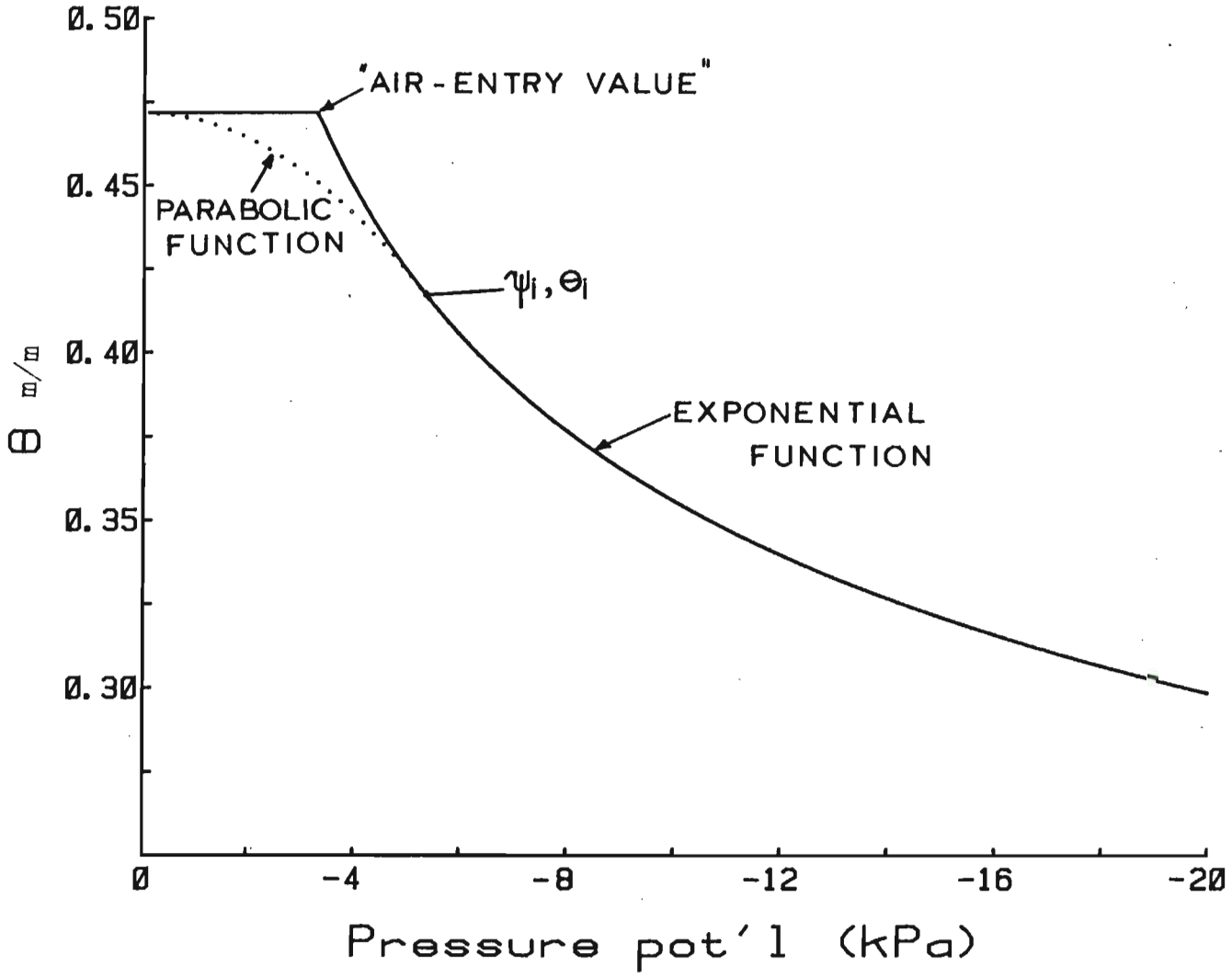

FIGURE 3.5 A two-part retentivity function in which θ_s = 0,472; b = 3,92 and a = -350 mm water (-3,42 kPa)

Substituting for c in Eq. 3.29 and rearranging,

$$\theta_i = 2b\theta_s/(1 + 2b) . \tag{3.31}$$

Substituting Eq. 3.31 in Eq. 3.26

$$\psi_i = a \left(\frac{2b}{1 + 2b}\right)^{-b} . \tag{3.32}$$

Combining Eq. 3.30 and 3.27 gives a parabolic retentivity curve in terms of $\underline{a}$, $\underline{b}$ and θ_s for the pressure potential range $0 > \psi > \psi_i$

$$\psi = a \frac{(1 - \theta/\theta_s)^{\frac{1}{2}} (\theta_i/\theta_s)^{-b}}{(1 - \theta_i/\theta_s)^{\frac{1}{2}}} . \tag{3.33}$$

Pertinent equations for the two-part retentivity function, including those for differential water capacity, are summarized in Table 3.12.

Soil water potential is expressed unambiguously as energy per unit mass (J/kg). It is conveniently expressed as energy per unit volume in units of pressure (Pa) at a specified temperature, or as a hydraulic potential (energy per unit weight) at a specified gravitational acceleration, in terms of the height of a liquid column corresponding to the given pressure. The constant a is expressed throughout this work in hydraulic potential units as mm of water, assuming that 1 kPa corresponds to 102,2 mm of water.

It is useful to examine the combinations of $\underline{a}$ and $\underline{b}$ which give rise to a constant saturation level at a specified pressure potential. If, for example, a relationship between clay content and saturation level at -1500 kPa (S_{-1500}) is assumed then a family of retentivity curves which has a constant S_{-1500} value corresponding to a desired clay

TABLE 3.12 Two-part retentivity function: equations for water content, pressure potential and differential water capacity. The 3 portions of the curve are indicated as I - point of inflection; II - exponential portion and III - parabolic portion

	Conditions	Water content	Pressure potential	Differential water capacity
I	$\theta=\theta_i$	$\theta_i = \frac{2b\theta_s}{1+2b}$	$\psi_i=a(\frac{2b}{1+2b})^{-b}$	
II	$\theta\leqq\theta_i$ $\psi\geqq\psi_i$	$\theta=\theta_s(\psi/a)^{-1/b}$	$\psi=a(\theta/\theta_s)^{-b}$	$\frac{d\theta}{d\psi} = -\frac{\theta_s\psi^{-(1/b+1)}}{ba^{-1/b}}$
III	$\theta\geq\theta_i$ $\psi\geq\psi_i$	$\theta=\theta_s - \frac{\theta_s\psi^2(1-\theta_i/\theta_s)}{a^2(\theta_i/\theta_s)^{-2b}}$	$\psi = \frac{a(1-\theta/\theta_s)^{\frac{1}{2}}(\theta_i/\theta_s)^{-b}}{(1-\theta_i/\theta_s)^{\frac{1}{2}}}$	$\frac{d\theta}{d\psi} = \frac{-2\theta_s(1-\theta_i/\theta_s)}{a^2(\theta_i/\theta_s)^{-2b}}$

content is defined by all combinations of a and b which satisfy the equation

$$a\, S_{-1500}^{-b} = -1500 \times 102{,}2 \text{ mm}. \qquad (3.34)$$

In this way an approximate relationship between soil properties and the values of the retentivity parameters may be established.

An example of the relationship between a, b, θ_{-1500} and θ_{-10} is shown in Fig. 3.6. Each solid line defines combinations of parameters a and b which give a constant value of θ_{-1500}/θ_s while the dashed lines join points having similar S_{-10} values. The advantages of such graphs are:

1) moving along a line of constant S_{-1500} the effect of a change of a and b on the shape of the retentivity curve as characterized by S_{-10} may be seen;
2) if the value of, say, S_{-1500} is correlated with clay content, the graph provides a means of relating retentivity parameters to soil properties;
3) the value of S_{-10} may be linked to pore size distribution, since any factors causing a shift in pore size distribution towards smaller pores, thus increasing retentivity at potentials between saturation and -1500 kPa will increase S_{-10}.

Similar graphs may be prepared for other pressure potentials if desired.

3.3.3 The application of the two-part retentivity function to South African soils

3.3.3.1 Introduction

In the previous section a two-part retentivity function was

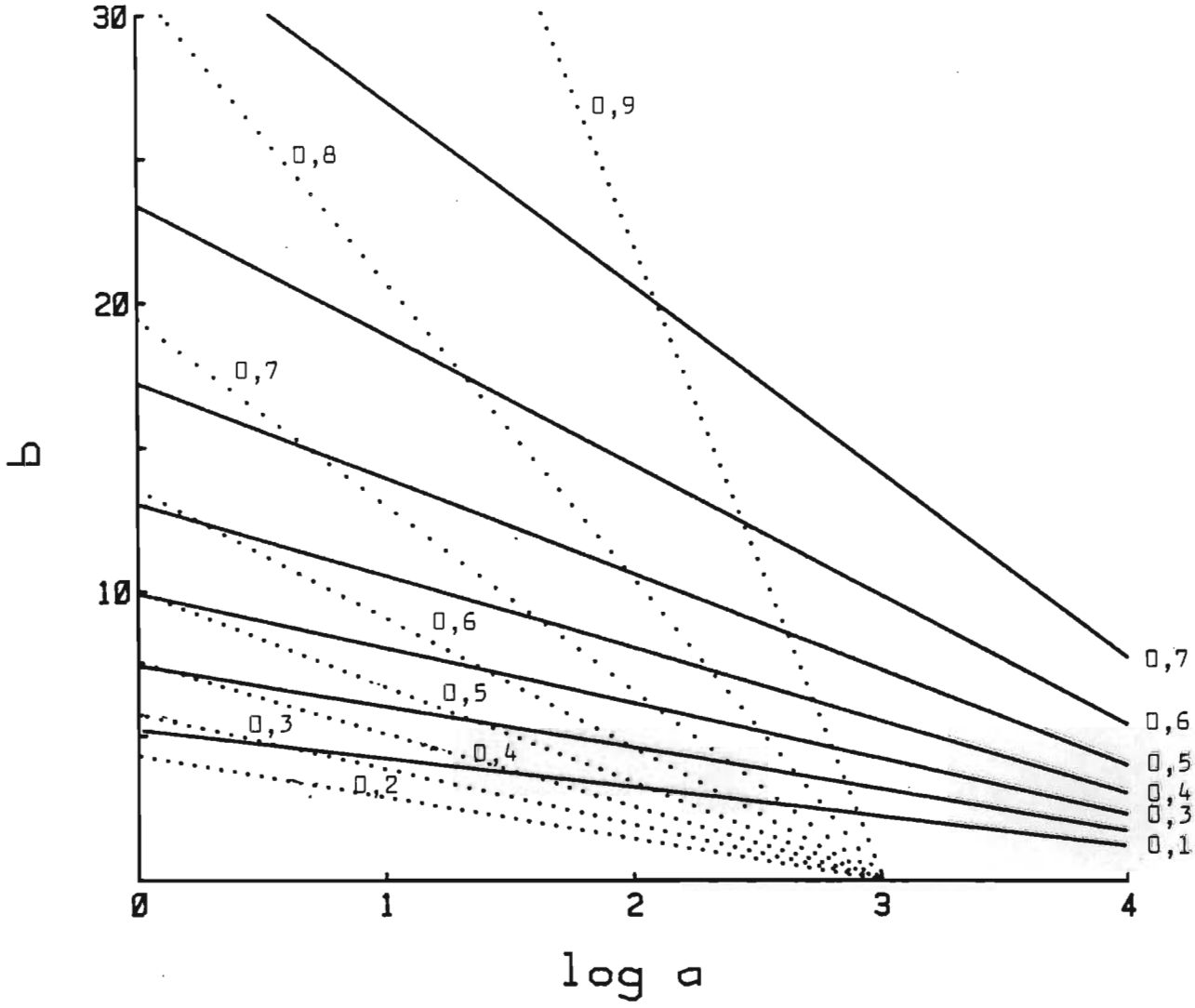

FIGURE 3.6 The relationship between S_{-1500}, S_{-10} and the retentivity constants a and b.

—— denotes combinations of a and b having the indicated S_{-1500} value;

--- denotes combinations of a and b having the indicated S_{-10} value

proposed, based upon a widely used exponential function. The two-part function is ideal for use in mathematical simulation modelling as it is applicable over the whole range of water content, from saturation to beyond wilting point. It is sigmoidal, has no abrupt discontinuities, and at saturation the term $d\theta/d\psi$ is zero.

Two aspects of the applicability and use of the function are studied in this section:

(1) the precision with which the function can be fitted to measured retentivity data,

(2) the relationship between soil properties and the function parameters.

3.3.3.2 Procedure

Since the two-part retentivity function (Table 3.12) is non-linear, an iterative procedure was developed to fit the function to the measured retentivity data. A modified form of the steepest descent procedure described by Draper and Smith (1966) was used to find the point within the three-dimensional parameter space at which the sum of squares was a minimum. Smallest step changes of parameter values were $\Delta\theta_s = 0{,}001$; $\Delta b = 0{,}002$ and $\Delta(\log a) = 0{,}0004$. If, in swelling soils, θ at high potentials was greater than θ_s calculated from dry bulk density, θ_s was excluded from the sum of squares (SS) and the function was fitted over the remaining points. An estimated value of θ_s was obtained as a curve-fitting parameter. Appendix 1 contains a listing of the program used for fitting the function.

As a demonstration of the effect of the number and distribution of measured retentivity points the function was fitted to two sets of retentivity data for a Fernwood sand and Shorrocks sandy loam. The first set contained all available retentivity data between θ_s and -50 kPa,

while the second consisted of interpolated values at 0; -10; -30 and -50 kPa only.

The function was fitted to all the data from sources 1 to 8 inclusive (Tables 3.3 and 3.4). For each soil a linear regression analysis of predicted water content $\hat{\theta}_\psi$, on measured θ_ψ was performed, from which the SE indicated the goodness of fit.

To show the relationship between soil properties and function parameters a number of retentivity curves were generated using regression equations relating retentivity to some properties of South African soils (Table 3.8). All combinations of clay content, silt/clay ratio and bulk density at the levels listed in Table 3.13 were used to generate θ values at 0; -10; -30; -100; -500 and -1500 kPa. Thus for each combination a retentivity curve was generated. The two-part retentivity function was fitted to each generated curve to obtain values for the parameters a and b.

For comparison a similar procedure was followed using Eq. 3.3 (Hall et al., 1977) which apply to soils from England and Wales. The South African and English regression equations are not strictly comparable as the silt class definitions differ.

3.3.3.3 Results and discussion

Among the factors which influence the precision of fit of the retentivity function are the number of retentivity points, their range and distribution, the method used to fit the function to the data and the quality of the measured data. If the measured data do not lie on a smooth curve then the function will be fitted as a best-fit through a scatter of points. Methods of determining retentivity are important. The best means of obtaining data forming a smooth progression of points is to use a pressure cell such as a Tempe cell, in which the core is

TABLE 3.13 Values of clay content, silt/clay ratio and bulk density used in all possible combinations to generate retentivity data

Clay %	Silt/clay	Bulk density Mg/m^3
5	0,33	1,2
15	0,66	1,4
25	1,00	1,6
35		1,8
45		
55		
65		

not disturbed at all between pressure increments, nor is there rewetting. The worst method, if a smooth curve is the objective, is to use a different core at each potential.

The effect of the first factor is illustrated in Fig. 3.7 in which fitted curves and parameters are displayed for retentivity data from a Fernwood sand and Shorrocks sandy loam, using

1) all measured points;
2) interpolated values of retentivity at 0; -10; -30; and -50 kPa only.

These curves demonstrate inaccuracies likely when extrapolating beyond the range of measured data, and show that a better fit may be obtained over a desired portion of the retentivity curve if one is willing to neglect the remainder. There is a fairly wide range of parameter combinations that describe similar curves and the absence of a measured point at a high potential can have a large influence on the retentivity function parameters obtained. In general, the absence of retentivity points near saturation increases the values of $\underline{a}$ (less negative) and $\underline{b}$.

The precision of fit of the retentivity function to the available measured retentivity data is indicated by the distribution of standard errors of the estimate of θ_ψ, which was calculated separately for each set of data (Fig. 3.8). The mean SE was 0,0172 and the median value 0,010. Scattergrams of predicted water content ($\hat{\theta}_\psi$) versus θ_ψ (Fig. 3.9a - h) indicate the fit obtained at each pressure potential for all soils.

The retentivity function fits the majority of the sets of experimental data satisfactorily. SE values are generally within the limits of error and variability experienced in soil water measurements. There

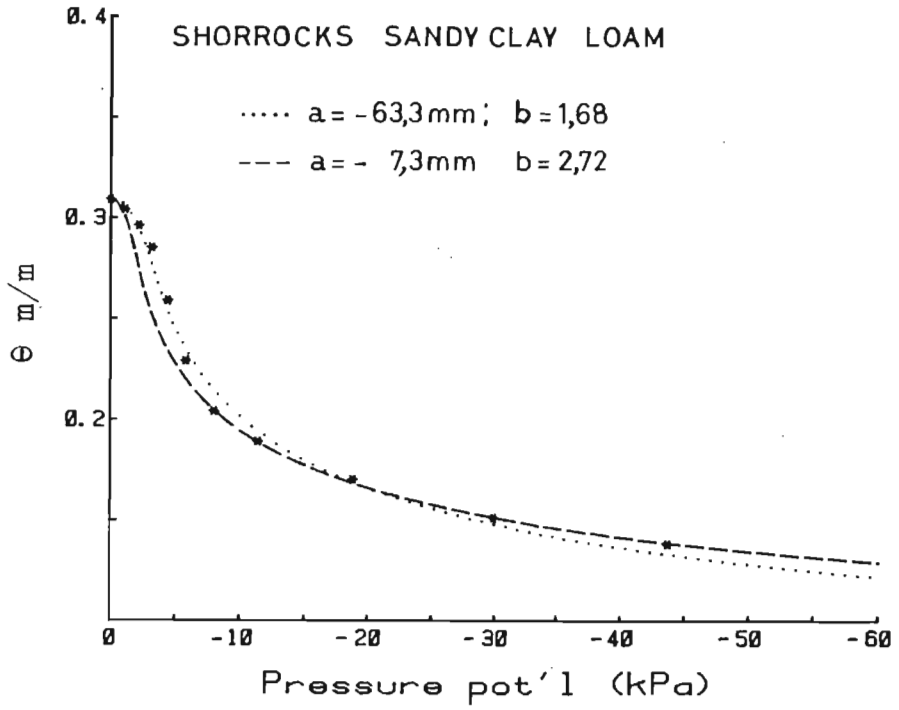

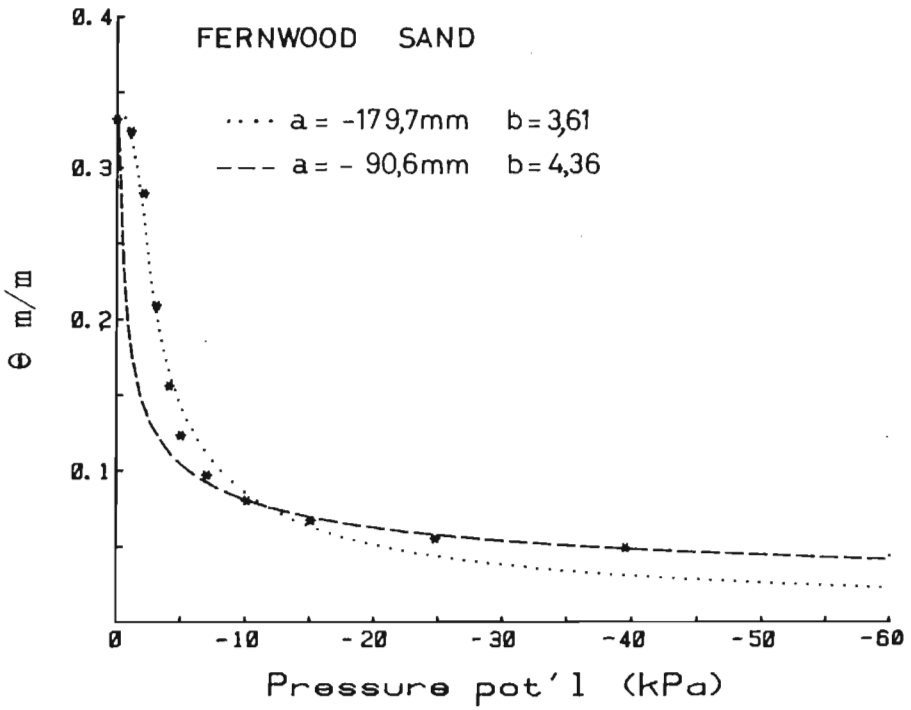

FIGURE 3.7 The effect of the number and distribution of retentivity values on the fitted two-part function. Best fit through experimental data points * indicated ...; best fit through interpolated values at -10; -30 and -50 kPa indicated by ---- line

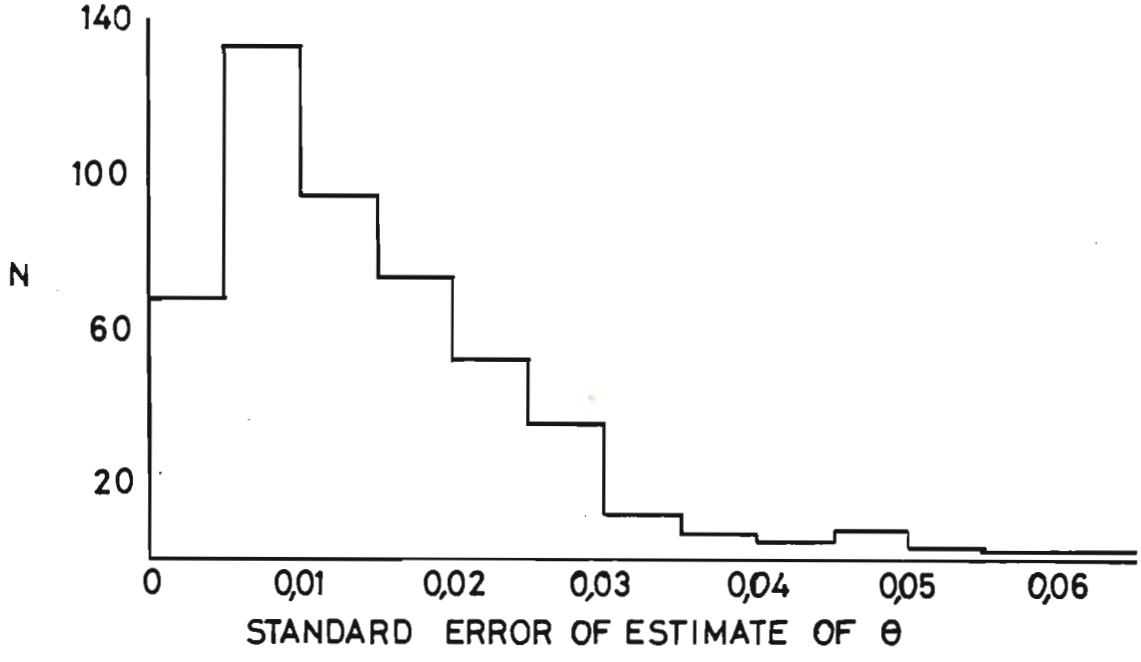

FIGURE 3.8 Distribution of standard errors of the estimate of θ, obtained by fitting the two-part function to data from sources 1 to 8

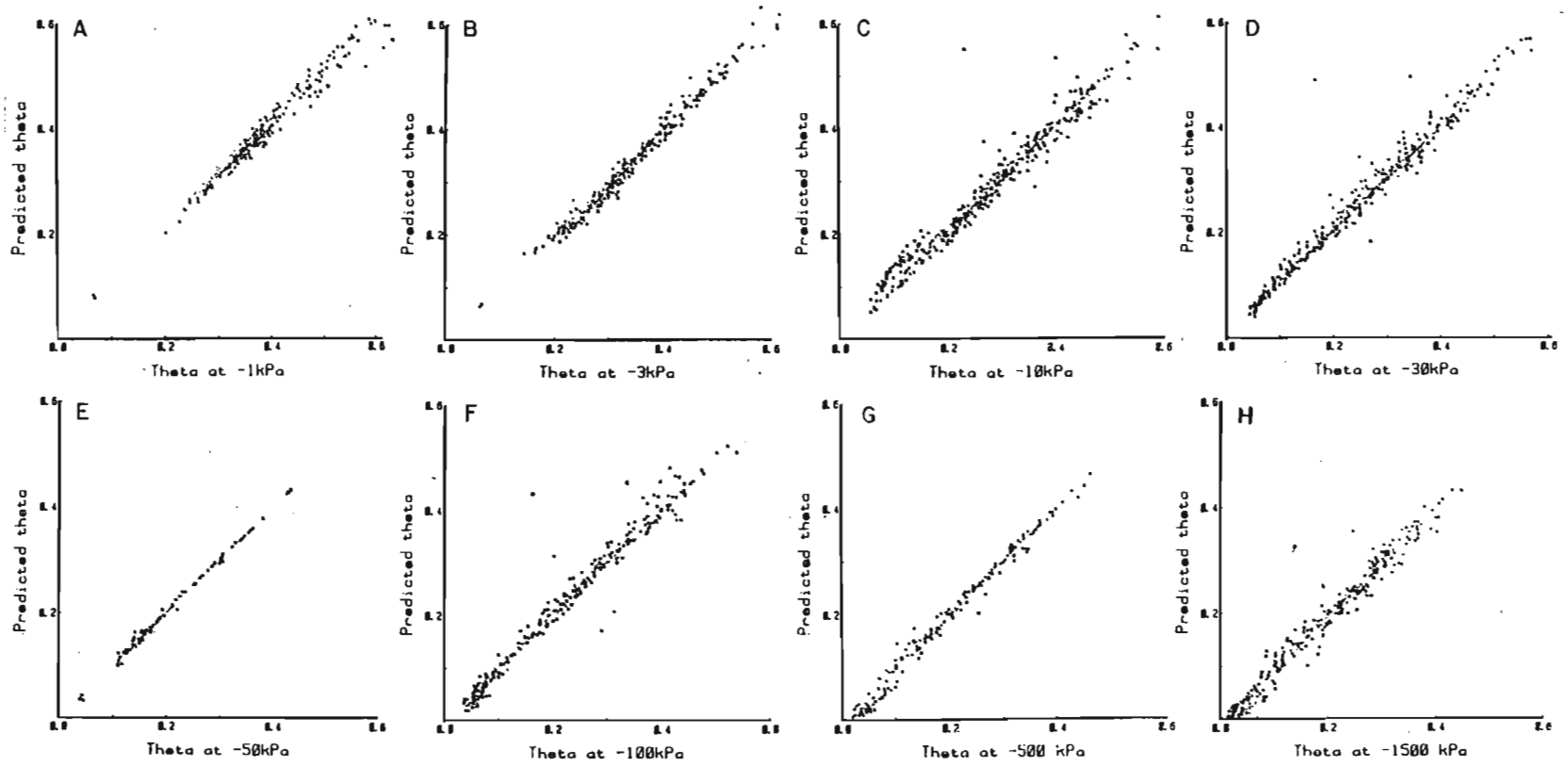

FIGURE 3.9 Measured θ (m^3/m^3) in relation to values predicted by a fitted retentivity function. E is based on source 1 data only, all others based on sources 1 to 8

are bound to be other functions which can be fitted more precisely to some of the data but the object of this work was to examine the range of parameter combinations of this particular retentivity function in relation to soil properties. The same procedure could be followed for any other function.

The distribution of retentivity constants a and b for the core and clod data is shown in Fig. 3.10. A third parameter, θ_s, is associated with each combination of a and b but is less variable and is assumed to be a measured soil property.

The range of a and b values is far wider than those reported by Ghosh (1980) or Clapp and Hornberger (1978). Both a and b influence the shape of a retentivity curve and it is not justifiable to claim, for example, that the value of b is related to textural class. In practice a wide range of combinations of a and b values can represent typical retentivity curves for a textural class.

For practical application, especially in modelling, one must know how to predict the values of the constants a and b from a knowledge of bulk density, particle size distribution and soil type. One way of estimating retentivity constants is to calculate all combinations of parameters leading to a particular value of the ratio θ/θ_s at any desired potential ψ. Since θ_ψ may be estimated from the regression equations relating retentivity to particle size criteria, especially at low potentials, the constants a and b may be obtained by inserting the desired values of θ, θ_s and ψ in Eq. 3.26 and solving for a and b. This is easily done graphically, using a diagram similar to Fig. 3.6.

In modelling, one often wishes to simulate the effects of changes in soil characteristics on retentivity. This may be accomplished by an appropriate change in a, b and θ_s. Regression equations may be used

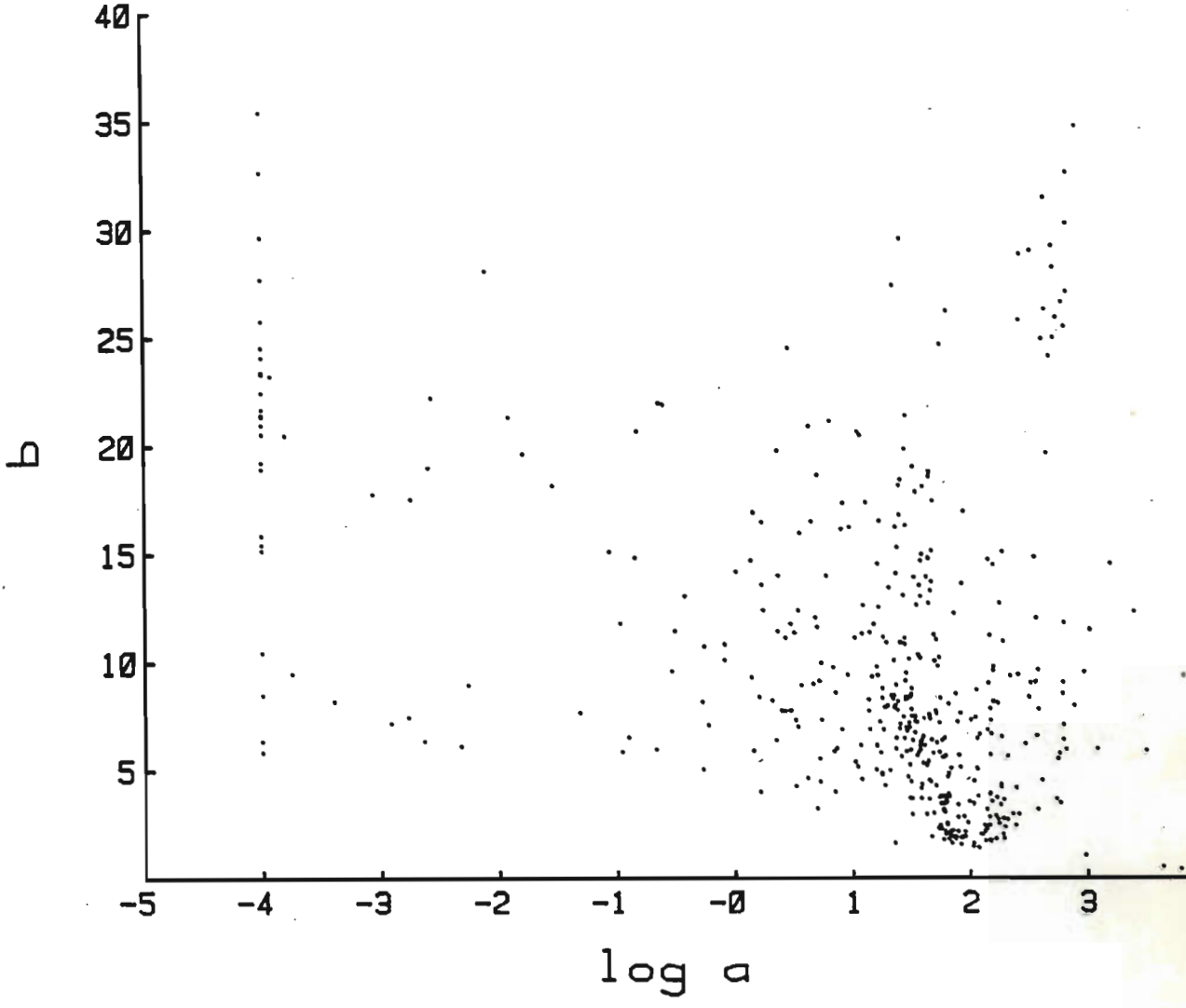

FIGURE 3.10 Distribution of retentivity parameters a and b for data from sources 1 to 8

to predict θ at various potentials for several combinations of bulk density, clay and silt content. Fitting the retentivity function to the predicted θ_ψ values enables the relationship between soil properties and retentivity parameters to be studied. Retentivity parameters derived using a model and coefficients listed in Table 3.8 are shown in relation to some properties of South African soils in Fig. 3.11. In Fig. 3.12 results of a similar exercise using Eq. 3.3 for British subsoils are displayed. These diagrams provide a means of estimating retentivity parameters and predicting the effects of changes in soil properties. Several points should be considered when interpreting or comparing these diagrams.

1) The regression equations used for predicting the retentivity curves, and hence retentivity parameters, account for only between about 60 and 80% of the variance of θ_ψ, depending upon the pressure potential. Predictions may thus vary markedly from actual measured retentivity at a particular site. Even over large areas of soil having a wide range of textures, a uniform characteristic such as parent material, organic matter, clay mineralogy, etc. may cause a constant bias away from the predicted values, which are averages for the range of soils included in the regression analysis.

2) The regression equations are valid only within the range of soil properties used in their derivation. Outside this range predictions may be incorrect and often illogical, for example at high bulk density values predicted θ at -10 kPa may be higher than calculated pore space for soils of high clay content. Such anomalous combinations are omitted from Figs. 3.11 and 3.12.

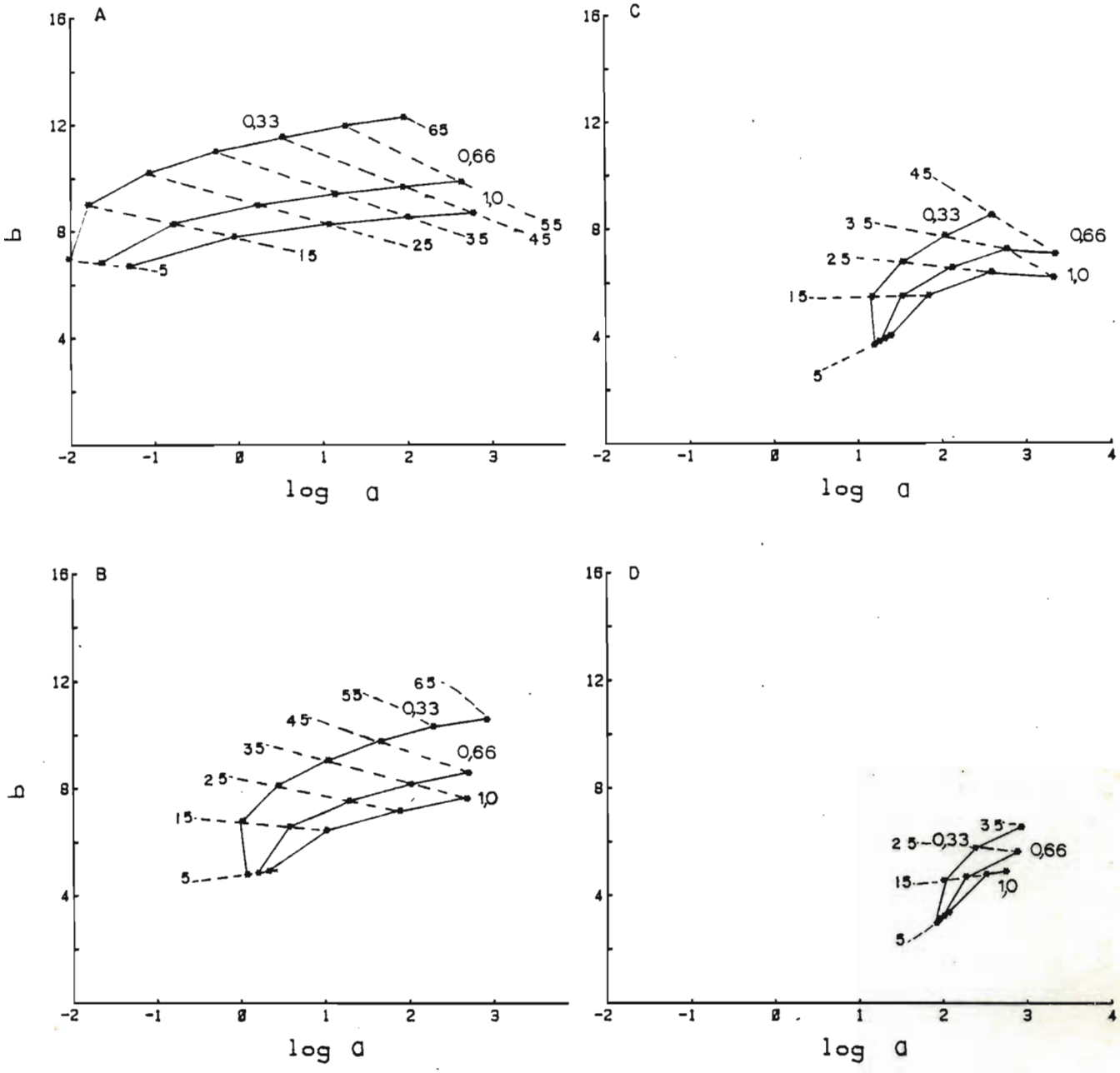

FIGURE 3.11 The effect of bulk density, clay and silt on retentivity parameters for South African soils

A: 1,2 Mg m^{-3}; θ_s = 0,547

B: 1,4 Mg m^{-3}; θ_s = 0,472

C: 1,6 Mg m^{-3}; θ_s = 0,396

D: 1,8 Mg m^{-3}; θ_s = 0,320

Silt/clay ratios denoted ——— and clay content (%) as -----

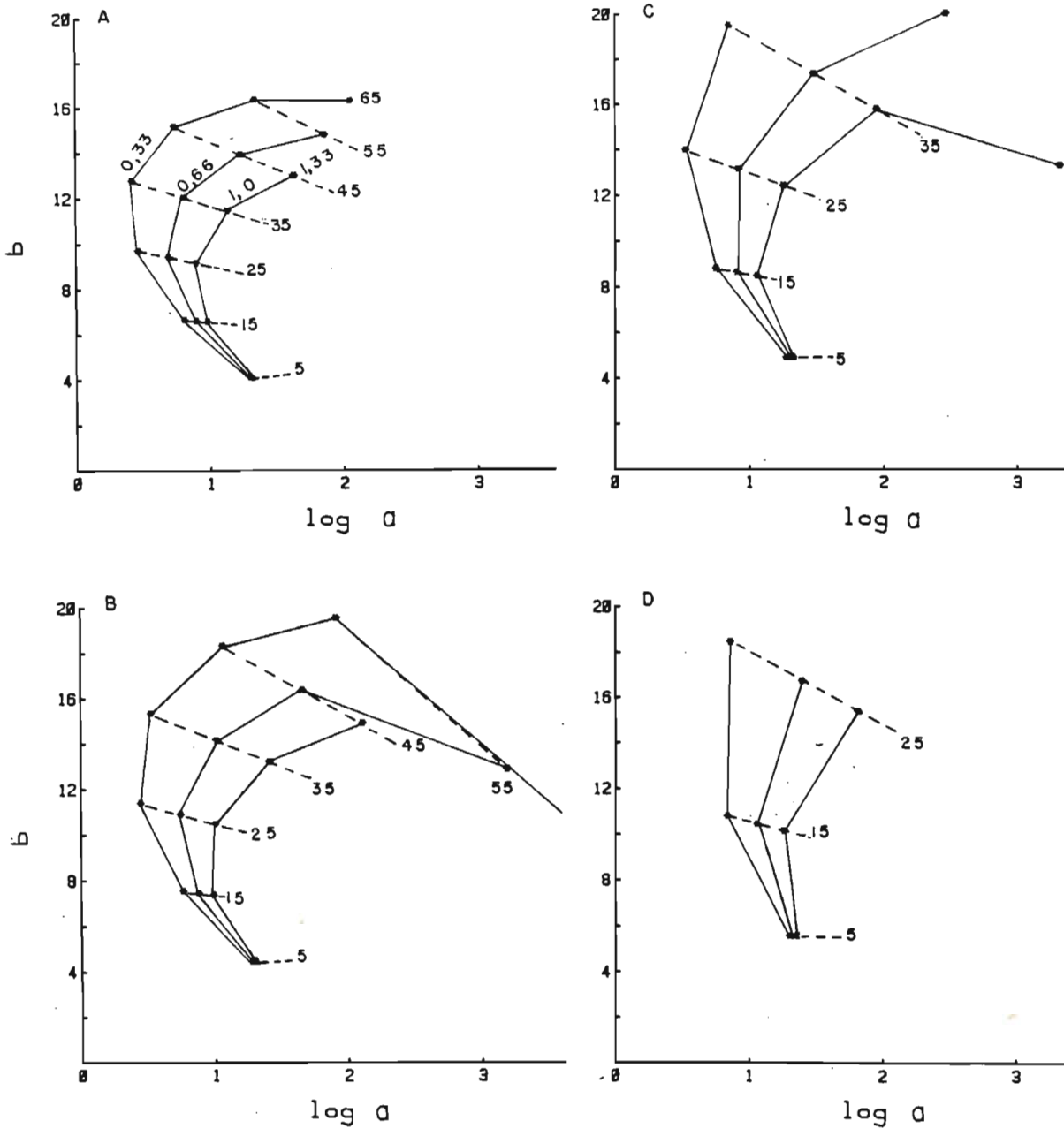

FIGURE 3.12 The effects of bulk density, clay and silt on retentivity parameters for British soils

A: ρ_b = 1,2 Mg m^{-3}; θ_s = 0,547

B: ρ_b = 1,4 Mg m^{-3}; θ_s = 0,472

C: ρ_b = 1,6 Mg m^{-3}; θ_s = 0,396

D: ρ_b = 1,8 Mg m^{-3}; θ_s = 0,320

Silt/clay ratios denotied ———— and clay content (%) as ----------

3) The apparently large effect of bulk density on the retentivity parameters is caused more by the large influence of bulk density on θ_s, and hence the ratio θ/θ_s, rather than on θ itself. In the case of the British regression equations, bulk density is excluded from regression at -200 and -1500 kPa.

4) Both clay, silt and bulk density are incorporated in the regression equation predicting θ_{-1500} for South African soils, whereas clay content only is used in the equation for British soils. This is probably the main reason for the differences in distribution of parameter combinations in Figs. 3.11 and 3.12. Note that different definitions of silt are used.

5) Swelling soils, such as vertic horizons, and structurally unstable soils such as prismacutanic horizons, were excluded from the regression analysis of Table 3.8. The results reported here thus apply only to stable soils which do not exhibit appreciable structural and density changes owing to swelling.

6) The highest potential for which a regression equation for the calculation of θ was available was -10 kPa for South African soils and -5 kPa for British soils. This means that the shape of the predicted retentivity curve between these potentials and saturation may not be correct, as was demonstrated in Fig. 3.7. This effect is most marked in sandy soils and arises from the steepness of the $\theta(\psi)$ curve at these potentials. It is a factor to consider before hydraulic conductivities, for example, are calculated from predicted retentivity curves, as small differences in retentivity at high pressure potentials have a large influence on calculated conductivity.

Characterizing retentivity by means of a function does enable simple computer storage and manipulation of data. For modelling purposes, especially finite difference modelling, retentivity parameters may be estimated for each depth node, using any available measured data for adjusting the estimates to values more suitable for the particular soil type. The curves defined by these parameters will be self-consistent and will reflect the effects of soil properties in a realistic manner.

CHAPTER 4

PREDICTING HYDRAULIC CONDUCTIVITY

4.1 HYDRAULIC CONDUCTIVITY MODELS - A REVIEW

4.1.1 Introduction

Most soil water simulation models require soil hydraulic conductivity data. Soil hydraulic conductivity is difficult to measure particularly under unsaturated conditions. In addition, many measurements are required for a reliable estimate of the mean value. Consequently, simple predictive techniques have received much attention and are especially attractive for modelling field hydrologic processes as it is not feasible to measure conductivity for all soil types and horizons which may be included in the exercise.

Many simulations concern hypothetical situations for which approximate data are satisfactory, provided that conductivity and retentivity data are consistent and reflect the properties of the soil to be simulated.

Three approaches have been followed in order to predict or simulate the conductivity characteristics of soils:

1) capillary models utilize pore size distributions calculated from retentivity curves to predict the contribution of each pore size class to total conductivity;
2) empirical or regression equations relate conductivity to soil water content, matric potential or textural properties;
3) qualitative or semi-quantitative estimates are based upon horizon or profile morphology.

Models of each type are described in this section, with the emphasis on those likely to be useful in soil water modelling.

In this discussion, the following symbols are used:

K for hydraulic conductivity;

K_s for hydraulic conductivity at saturation;

K_r is hydraulic conductivity relative to that at saturation (K_s);

$K(\theta)$ refers to hydraulic conductivity as a function of water content;

K(S) is hydraulic conductivity as a function of degree of saturation S.

4.1.2 Capillary models

In capillary models, the soil pore space is visualized as a system of capillary tubes, parallel to the direction of water flow. K may be calculated in various ways, using:

1) the number and size distribution of water-filled pores, calculated from the retentivity curve using the capillary law relating matric potential to the radius of the largest water-filled pore;
2) the relative sizes of a sequence of pores, calculated from the probability of a pore of a given radius connecting pores of other radii;
3) various assumptions concerning pore tortuosity and pore continuity or correlation across planes perpendicular to flow;
4) Poiseuille's equation relating flow to capillary tube radius, fluid density and viscosity.

Developments and modifications of this type of model concern the calculation of effective pore radius and the introduction of several ways of accounting for tortuosity and pore continuity. The limitations of this approach lie partly in its basic assumptions, especially those concerning the relationships between retentivity, pore size distribution and flow, and the simplified geometry of the porous system which prohibits by-pass flow. Mualem and Dagan (1978) derived common capillary models from basic principles and discussed the differences between them. They classified those models into three groups, namely:

1. Burdine (1953), cited in Brooks and Corey (1966);
2. Childs and Collis-George (1950);
3. Mualem (1976).

4.1.2.1 Burdine Models

A general equation for Burdine-type models derived by Mualem and Dagan (1978) is:

$$K_r(\theta) = S_e^p \int_0^{\theta} \frac{d\theta}{\psi^{2+y}} \Big/ \int_0^{\theta_s} \frac{d\theta}{\psi^{2+y}} \qquad (4.1)$$

Effective saturation S_e is defined as

$$S_e = \frac{\theta - \theta_r}{\theta_s - \theta_r} \qquad (4.2)$$

where θ_r is residual water content, below which the terms $d\theta/d\psi$ and $K(\theta)$ are effectively zero. The tortuosity or pore interaction parameter p usually lies between 0 and 2. Another tortuosity factor (y) is included if it is assumed that tortuosity is inversely proportional to a power function of pore radius. Neither p nor y can be derived theoretically for any but the simplest porous systems.

$K(\theta)$ may be calculated from:

$$K(\theta)= \frac{\gamma^2 \varepsilon^p}{2\rho g\eta} \int_o^{\theta} \frac{d\theta}{\psi^{2+y}} \qquad (4.3)$$

where ε is a function of water-filled porosity, and density ρ, viscosity η and surface tension γ define the properties of the fluid.

4.1.2.2 Childs and Collis-George models

In this type of capillary model (Childs and Collis-George, 1950; Marshall, 1958) random distribution of pore diameters in planes perpendicular to the direction of flow is assumed. The probability of obtaining any sequence of pore diameters across such a plane may be calculated. All effective resistance to flow in a sequence of two pores is confined to the smaller of the two pores.

$$K_r(\theta) = S_e^p \int_o^{\theta} \frac{(\theta - \xi)\, d\xi}{\psi^{2+y}} \Big/ \int_o^{\theta_s} \frac{(\theta - \xi)\, d\xi}{\psi^{2+y}} \qquad (4.4)$$

where ξ is a variable of integration representing effective water content as a function of ψ. A number of different values have been assigned to the tortuosity factor p. Childs and Collis-George (1950) assumed p to be zero; Kunze, Vehara and Graham (1968) used a value of 1; Millington and Quirk (1961) used a value of 1,33 and Marshall (1958) assumed p to be 2. In general, the factor p is preferred to y, the latter being assigned a value of zero.

Marshall's (1958) derivation is similar in concept to Eq. 4.4, but the integrals are replaced by finite sums. This enables measured retentivity curves to be used without having to fit a retentivity function to the measured data. Green and Corey (1971) formulated a general finite sums equation for calculating $K(\theta)$,

$$K(\theta)_i = \frac{MF\ \gamma^2\ \varepsilon^p}{2\rho\ g\eta\ n^2} \Big/ \sum_{j=1}^{m} \left[(2j + 1 - 2i)\ \psi_j^{-2}\right] \qquad (4.5)$$

where $K(\theta)_i$ is calculated for a specified water content θ_i. The retentivity curve is divided into n segments, or pore classes of an equal fractional pore volume, each having an average pressure potential ψ_j. The last water-filled pore class on the wet end of the retentivity curve is designated i. The pore class corresponding to saturation is identified by i = 1, while i = m identifies the pore class corresponding to the lowest water content for which K is calculated.

Surface tension γ, density ρ and viscosity η define the properties of the wetting fluid. A matching factor MF is used to bring the measured and calculated values into coincidence. MF is usually the ratio of measured to calculated K_s although it may be calculated at any convenient water content. The variables ε and n have been given various definitions (Table 4.1).

The integral form of Eq. 4.5 is

$$K(\theta) = \frac{\gamma^2}{\rho g \eta}\ \varepsilon^p \int_{\theta_m}^{\theta_i} \frac{(\theta - \xi)\ .\ d\xi}{\psi^2} \qquad (4.6)$$

which enables $K(\theta)$ to be calculated if a retentivity function is available.

4.1.2.3 Mualem models

Mualem (1976) proposed a model which includes the effect of the larger pore in a sequence of two pores:

$$K_r(\theta) = S_e^p \left[\int_o^{\theta} \frac{d\theta}{\psi^{1+y}} \Big/ \int_o^{\theta_s} \frac{d\theta}{\psi^{1+y}}\right]^2 \qquad (4.7)$$

Table 4.1 Variations in the conductivity equation for three methods of computation (Modified after Green and Corey, 1971)

Definition of ε	Definition of n	Value of p	Reference
$\varepsilon = \theta$ variable	Number of water-filled pore classes corresponding to θ; variable.	2	Marshall (1958)
		2	Nielsen et al., (19
		2	Jackson et al., (19
$\varepsilon = \theta$ variable	Total number of pore classes at saturation; constant.	1	Kunze et al., (1968
		1,33	Millington & Quirk (1959)
		1	Jackson et al., (19
$\varepsilon = \theta_s$ constant	Total number of pore classes at saturation; constant.	2	Green & Corey (1971

and $$K(\theta) = \frac{\gamma^2 \varepsilon^p}{2\rho g \eta} \left[\int_0^\theta \frac{d\theta}{\psi^{1+y}} \right]^2 . \qquad (4.8)$$

He claimed that agreement between measured and calculated $K(\theta)$ values was better using this model than the others he tested, but the difference was not marked and was probably not significant.

4.1.2.4 Morphometric techniques

Instead of using retentivity curves, Bouma and Anderson (1973) used statistical models of pore size distributions obtained from thin sections and polished surfaces of plastic impregnated soils to calculate hydraulic conductivity. The probability of obtaining continuous pores was calculated and their effective size was estimated on this basis, together with the effect of swelling (predicted from coefficient of linear expansion measurements) on plane width. For comparative purposes K was calculated from pore size distribution based on water retention data and was measured on cores using a crust infiltration procedure. Calculated and measured values were in reasonable agreement providing a matching factor was used. Neither physical nor morphometric methods gave good results for clayey soils. The morphometric method did not work well when observed porosity is only a small fraction of total porosity. They concluded that the physical method based on pore size distribution is preferable as it is simpler and cheaper.

Anderson and Bouma (1973) calculated K_s values for a Batavia silt loam using morphometric data. The results obtained agreed fairly well with measured data. Measured and calculated K_s values decreased as core thickness increased owing to the reduced probability of pores extending the length of the cores.

4.1.2.5 Matching Factors

From the numerous comparisons between measured and predicted $K(\theta)$ curves published in the literature (e.g. Green and Corey, 1971; Mualem, 1976; Jackson, Reginato and Van Bavel, 1965; Parkes and Waters, 1980) it is clear that the capillary models have serious shortcomings.

While the shapes of predicted and measured $K(\theta)$ curves often agree well, absolute values differ considerably, necessitating the use of matching factors to bring the curves into coincidence. Matching factors (the ratio of measured to calculated conductivity at a specified water content) range from 0,2 to 0,004 and bear no obvious relationship to soil properties. The use of matching factors should not be necessary if the theory were complete and correct.

Matching is generally performed at saturation as it is easier to measure saturated conductivity than unsaturated conductivity. Ideally, at least two measured values, at different water contents, should be used so that the shape of the $K(\theta)$ curve may be checked.

4.1.3 Empirical equations

Many empirical functions relating conductivity to water content or pressure potential have been reported (see for instance Mualem, 1978). These formulae have proved extremely useful, especially in analytical solutions to the flow equation, but are of little use for modelling purposes unless the function parameters can be related to soil properties. The parameters are usually obtained by fitting the function to measured data. The only empirical equation to be discussed here is one of the simplest, the case in which K_r is a power function of effective saturation S_e or matric potential ψ.

$$K_r(S_e) = S_e^{\beta} \tag{4.9}$$

$$K_r(\psi) = (a/\psi)^n. \tag{4.10}$$

Mualem (1978) examined measured $K(\theta)$ curves for 50 soils and used a best-fit procedure to derive β for each soil. The majority of β values lay between 2,5 and 9, but values as high as 24,5 were found. Extreme values appeared to be linked to the range of matric potentials for which data were available. In an attempt to relate the value of β to some property of the retentivity curve, regardless of its complexity, Mualem calculated the work w required to drain a unit volume of saturated soil to a lower pressure potential.

$$w = \int_{\psi_1}^{\psi_o} \gamma_w \psi \, . \, d\theta \tag{4.11}$$

where γ_w is the specific weight of water and ψ_1 is the final matric potential.

Correlation between w and β was highest when $\psi_1 = -1\,500$ kPa ($r = 0,874$). The equation suggested for predicting β is,

$$\beta = 0,015W + 3,0 \tag{4.12}$$

and

$$K_r = S_e^{0,015W + 3,0}. \tag{4.13}$$

Eq. 4.13 was competitive with the best capillary models when verified

using experimental data for 50 soils. However, the experimental results used for verification were also used for obtaining the constants in Eq. 4.12 so the performance of this model is not unexpected. The important feature of this equation is that the exponent incorporates a parameter that can be related to soil properties.

Equations of the same form as Eq. 4.9 and Eq. 4.10 may be derived by applying the capillary models to retentivity functions of the type,

$$\psi = a\ (S_e)^{-b} \tag{4.14}$$

which were discussed in Chapter 3. Using the Childs and Collis-George model, Campbell (1974) obtained for $\theta_r = 0$

$$K_r\ (S) = S^{p+2+2b} \tag{4.15}$$

$$K_r(\psi) = (a/\psi)^{2+(2+p)/b}. \tag{4.16}$$

Brooks and Corey (1966) using the Burdine equation with p = 2, derived

$$K_r\ (S_e) = S_e^{2b+3} \tag{4.17}$$

$$K_r\ (\psi) = (a/\psi)^{2+3/b} \tag{4.18}$$

so that

$$K_r\ (S_e) = S_e^{2b+1+p} \tag{4.19}$$

$$K_r\ (\psi) = (a/\psi)^{2+(1+p)/b}. \tag{4.20}$$

Bloemen (1980) fitted Eq. 4.10 to measured $K(\psi)$ curves for 22 Netherlands soils and obtained values for n. These were correlated with values of n_B calculated from the exponent in Eq. 4.18. Values of b were obtained by fitting Eq. 4.14 to the measured retentivity data. If θ_r was assumed zero (Campbell, 1974), then

$$n_B = 0{,}76n + 0{,}864 \tag{4.21}$$

but if θ_r was included as a curve-fitting parameter (Brooks and Corey, 1966) then

$$n_B = 0{,}988n + 0{,}628 \tag{4.22}$$

4.1.4 Conductivity in relation to soil properties

Soil texture and organic matter, through their influence on pore size distribution, must influence the conductivity characteristics of soils. Many approximate relationships between soil texture and hydraulic conductivity have been published, for example, that of Bloemen (1980).

Bloemen (1980) related the parameters n, a and K_s of Eq. 4.10 to particle size criteria. He defined a grain size distribution index f, calculated from a cumulative particle size distribution, as

$$f = \frac{\sum_{i=1}^{n} (P_{i+1} - P_i)\, G_i}{\sum_{i=1}^{n} (P_{i+1} - P_i)} \tag{4.23}$$

where $G_i = \log (P_{i+1}/P_i)/\log (S_{i+1}/S_i)$, and P_i are cumulative mass percentages between particle size interval limits S.

For undisturbed soils, Bloemen found that the exponent n was related to f and organic matter content OM (mass %) so that

$$n = 1,4 + 4,536\ (e^{0,3f} - 1) - 0,75f \log OM. \qquad (4.24)$$

The parameter a in Eq. 4.10 is sometimes defined and measured as an air-entry potential ψ_a and at other times used as a curve-fitting parameter. Bloemen used measured ψ_a values, which were related to f and median particle size M_d by

$$\psi_a = 2914 M_d^{-0,96}\ f^{0,79}\ cm \qquad (4.25)$$

where SD was 12,7 cm when ψ_a had units of cm.

A regression of saturated conductivity K_s on f and M_d produced

$$K_s = 0,2 M_d^{1,93}\ f^{-7,4}\ cm/d \qquad (4.26)$$

where SD was 167 cm/d.

High standard deviations are probably caused by aggregation and packing differences between samples.

4.1.5 Discussion

Conductivity models reflect the dependance of K on θ and are easily incorporated into soil water flow simulation models. Gardner (1974) in a critical review of developments since Childs and Collis-George first published their procedure cautions against blindly applying the capillary models, regarding them as a means of obtaining hydrological data suitable for many applications, but at best as a guide to the properties of field soils. The fact that a wide range of matching factors have to be used to bring experimental and calcu-

lated K values into coincidence and that the capillary model does not nearly account for the temperature dependence of retentivity and permeability indicate the limitations of our present concepts (e.g. Haridasan and Jensen, 1972)

Models for predicting K have never been more than partially successful. It is preferable to consider them as representing simple porous media, which display many of the conductivity properties of real soils, which are of greater geometrical and physico-chemical complexity. The models do not account for hysteresis effects or for the changes in pore geometry that accompany swelling and shrinking.

If one is fortunate, K relationships generated from a model may coincide with those of a real soil, but this is no guarantee that the model will be as successful for other soils. Nonetheless, the models may be valuable for theoretical studies as well as water flow simulations, especially when combined with a retentivity function having parameters which may be related to soil type.

For water flow modelling purposes, the simpler capillary models or empirical equations are preferable. More complex K models require more data and parameter values which are usually unavailable. At present the biggest problem in using even the simplest empirical equation lies in the selection of parameter values which reflect soil hydrological properties correctly. These limitations favour the use of the simplest pore model or conductivity equation suitable for a particular application. For example, a theoretical study investigating effects of changes in pore size distribution on water flow would require a capillary model. A similar study investigating particle size effects could utilize Bloemen's equations or others of a similar type, while a simulation for which some measured K data is available merely requires the fitting of an empirical equation in order to obtain a mathematical description of the $K(\theta)$ relationship.

Development of more sophisticated concepts of soil pore size distribution and geometry (for example, Bevan and Germann, 1981) indicates that the search for better models is continuing. Improvements will be beneficial if they are based on an improved understanding of the mechanism of water flow. The greatest need at present is to relate the constants in existing capillary models to soil properties. For this purpose models having only a few constants are preferred to more complex models.

In section 4.3, it was mentioned that it is possible to derive some of the empirical equations by applying the capillary models to certain retentivity function. The relationship between the parameters of a simple retentivity function and soil properties was described in a previous section. Applying the capillary models to this function enables the derivation of K equations in terms of these retentivity parameters. In the next section, such equations will be derived and compared.

4.2 PREDICTING CONDUCTIVITY FROM RETENTIVITY PARAMETERS

4.2.1 Introduction

In Chapter 3 it was shown how the retentivity of most soils could be described by a two-part retentivity function (Table 3.12). This function is based on that of Campbell (1974) but has a parabolic portion at the wet end of the curve to facilitate computer simulation modelling and to remove the discontinuity at a potential ψ_e. The parameters $\underline{a}$ and $\underline{b}$ have been related to silt and clay contents and methods of estimating these parameters were suggested.

In this section the capillary models described in the previous section are combined with the two-part retentivity function to give equations for K_s and $K(\theta)$. The effect of the value of $\underline{b}$ on K_r is demonstrated and the values predicted by the three capillary models are compared.

Van Genuchten (1980) used a similar procedure, using a retentivity function having three parameters, in conjunction with the Burdine and Mualem models. The advantage of using a retentivity function having fewer parameters is that they are more easily related to soil properties, as was done in Chapter 3.

4.2.2 Theory

Two retentivity functions were used in this work:

1) an exponential function described by Brooks and Corey (1966) and Campbell (1974);
2) a two-part function (Table 3.12) in which the exponential function is replaced by a parabolic section at high water contents.

Writing these functions in terms of saturation,

$$\psi = a\, S^{-b} \tag{4.27}$$

where $S = \left(\frac{\theta - \theta_r}{\theta_s - \theta_r}\right)$ (Brooks and Corey, 1966)

or $S = \frac{\theta}{\theta_s}$ (Campbell, 1974).

In the two-part function, at water contents greater than a point of inflection S_i,

$$\psi = a\, (1 - S)^{\frac{1}{2}}\, S_i^{-b}/(1 - S_i)^{\frac{1}{2}} \tag{4.28}$$

where $S_i = 2b/(1 + 2b)$. (4.29)

These retentivity equations may be used in conjunction with the pore models of Burdine, Childs and Collis-George, and Mualem to derive equations for K. The derivation of these equations based on the Childs and Collis-George model illustrates this procedure.

4.2.2.1 Derivation of a K equation by applying the Childs and Collis-George model to an exponential retentivity function

Combining the fluid properties into a constant, M, where,

$$M = \gamma^2/2\rho g\eta \tag{4.30}$$

and combining Eq. 4.27, 4.30 and 4.6, gives

$$K(S) = 2\, M\epsilon^p \int_o^S \frac{(S-\xi)}{(a\xi^{-b})^2} \cdot d\xi \tag{4.31}$$

$$= \frac{2M\epsilon^p}{a^2} \int_o^S (S-\xi)\, \xi^{2b} \cdot d\xi \,. \tag{4.32}$$

Integrating,

$$K(S) = \frac{2M\epsilon^p}{a^2} \left[\frac{S^{2b+2}}{2b+1} - \frac{S^{2b+2}}{2b+2}\right] \tag{4.33}$$

$$= \frac{2M\epsilon^p\, S^{2b+2}}{a^2\,(2b+1)(2b+2)} \,. \tag{4.34}$$

At saturation, S = 1 and Eq. 4.34 reduces to

$$K_s = \frac{2M\epsilon^p}{a^2\,(2b+1)(2b+2)} \,. \tag{4.35}$$

Since $K_r(\theta) = K(\theta)/K_s$, and if $\epsilon = \theta - \theta_r$

$$K_r(S) = S^{2b+2+p} \tag{4.36}$$

Eq. 4.36 is identical to Eq. 4.15, Campbell's (1974) conductivity equation.

4.2.2.2 Derivation of a K equation by applying the Childs and Collis-George model to a two-part retentivity function

Substituting Eq. 4.27, 4.28 and 4.30 into 4.6,

$$K(S) = 2M\epsilon^p \left[\int_0^{\min S,S_i} \frac{(S-\xi)\xi^{2b}}{a^2} \cdot d\xi + \int_{S_i}^{\max S,S_i} \frac{(S-\xi)(1-S_i)}{(1-\xi)a^2 S_i^{-2b}} \cdot d\xi\right]. \tag{4.37}$$

On integrating, the righthand integral is zero if $S \leq S_i$ and

$$K(S) = \frac{2M\epsilon^p}{a^2} \left(\frac{S^{2b+2}}{2b+1} - \frac{S^{2b+2}}{2b+2}\right) . \tag{4.38}$$

If $S \geq S_i$ then

$$K(S) = \frac{2M\epsilon^p}{a^2} \left[\frac{S\, S_i^{2b+1}}{2b+2} - \frac{S_i^{2b+2}}{2b+2} + \frac{1-S_i}{S_i^{-2b}} \left(S - S_i + (1-S)\ln\left(\frac{1-S}{1-S_i}\right)\right)\right] \tag{4.39}$$

$$K_s = \frac{2M\epsilon^p}{a^2} \left[\frac{S_i^{2b+1}}{2b+1} - \frac{S_i^{2b+2}}{2b+2} + \frac{(1-S_i)^2}{S_i^{-2b}}\right] . \tag{4.40}$$

4.2.3 Comparison of K equations

In 4.2.2.1 and 4.2.2.2 K equations were derived by applying the capillary model of Childs and Collis-George (C-CG) to two retentivity functions, an exponential function (Eq. 4.27) (designated C-BC, from Campbell-Brooks and Corey) and a two-part function (Table 3.12, Eq. 4.28 and 4.29). The Burdine and and Mualem models can be applied in a similar way. In addition to these integral equations for K, a finite sums equation can be written for each model, similar to Eq. 4.5 for the Childs and Collis-George model.

in Table 4.2 and those developed using the Mualem model, in Table 4.3.

All integral K equations are of the same form,

$$K(S) = \frac{2M\epsilon^p}{a^2} f(b,S,m) \qquad (4.41)$$

where M is a constant incorporating fluid properties, $\underline{a}$ is a retentivity parameter which may be regarded as a scaling factor, and ϵ^p accounts for porosity, tortuosity and pore interaction. The constant M has a value of 2,689 x 10^{-4} m^3 s^{-1} at 20°C. For modelling convenience, all K values in this work are expressed in mm d^{-1}, thus M becomes 2,323 x 10^{10} mm^3 d^{-1}.

The term f(b,S,m) is a function of the shape of the retentivity curve, reflected by parameter $\underline{b}$, degree of saturation S, and capillary model m. The function f (b,S,m) is dimensionless and represents relative water-filled pore radius.

In this section the relative importance of choice of model, value of tortuosity factor and definition of ϵ is examined.

The effect of choice of model on predicted K may be examined by comparing values of f(b,S,m) calculated for various combinations of model, b value and degree of saturation. In Table 4.4 (column 3) values of f(b,S,m) are tabulated for several combinations of $\underline{b}$ and S using the C-CG model in conjunction with the C-BC retentivity function. These values are the reference values against which the other models are compared. Ratios of f(b,S,m) values, obtained using other model/ retentivity function combinations, to the reference values are listed in subsequent columns.

The C-CG and Mualem models predicted K values between 1,6 times and twice that of the C-CG model. K(S) values predicted by both models are identical for the C-BC function. Using the two-part retentivity function causes a slight increase in calculated K as saturation is

TABLE 4.2 Conductivity equations derived by combining the Campbell-Brooks and Corey (C-BC), two-part and finite sums retentivity models with the Burdine capillary model

Retentivity function	Saturation range	Conductivity equation
	$S = 1$	$K_s = M\varepsilon^p/a^2\ (2b + 1)$
C-BC	$0 \leq S \leq 1$	$K(S) = M\varepsilon^p\ S^{2b+1}/a^2\,(2b + 1)$
	$0 \leq S \leq 1$	$K_r(S) = S^{2b+1+p}$ for $\varepsilon = \theta$
Two-part	$S_i \leq S < 1$	$K(S) = \frac{M\varepsilon^p}{a^2}\left[\frac{S_i^{2b+1}}{2b + 1} + \frac{1 - S_i}{S_i^{-2b}} \cdot \ln\frac{1 - S_i}{1 - S}\right]$
	$0 \leq S \leq S_i$	$K(S) = M\varepsilon^p S^{2b+1}/a^2\,(2b+1)$
Finite sums	$0 < S < 1$	$K(S)_i = \frac{M\varepsilon^p}{n} \sum_{j=i}^{m} \psi_j^{-2}$

TABLE 4.3 Conductivity equations derived by combining the Campbell-Brooks and Corey (C-BC), two-part and finite sums retentivity models with the Mualem capillary model.

Retentivity function	Saturation range	Conductivity equation
	$S = 1$	$K_s = M\varepsilon^p/a^2\ (b+1)^2$
C-BC	$0 \leqq S \leqq 1$	$K(S) = \frac{M\varepsilon^p}{a^2}\left[\frac{S^{b+1}}{b+1}\right]^2$
	$0 < S \leqq 1$	$K_r(S) = S^{2b+2+p}$ for $\varepsilon = \theta$
	$S_i < S < 1$	$K(S) = \frac{M\varepsilon^p}{a^2}\left[\frac{S_i^{b+1}}{b+1} + \frac{(1-S_i)^{\frac{1}{2}}}{S^{-b}} \cdot 2((1-S_i)^{\frac{1}{2}} - (1-S)^{\frac{1}{2}})\right]^2$
Two-part	$0 < S < S_i$	$K(S) = \frac{M\varepsilon^p}{a^2}\left[\frac{S^{b+1}}{b+1}\right]^2$
Finite sums	$0 < S \leqq 1$	$K(S)_i = \frac{M\varepsilon^p}{n^2}\left[\sum_{j=1}^{m} \psi^{-1}\right]^2$

TABLE 4.4 The influence of saturation, pore model (C-CG-Childs and Collis-George, M-Mualem, B-Burdine) and retentivity function (C-BC-Campbell, Brooks and Corey and two-part function) on the value of f(S,b,m) using the C-CG model and C-BC function as a reference

Saturation	b	f(b,S,m) for C-CG model and C-BC function	$f(b,S,m)/f(b,S)_{CCG,C\text{-}BC}$					
			C-BC function			Two-part function		
			C-CG	M	B	C-CG	M	B
1,00	2	$6,07\times10^{-2}$	1	1,67	3,00	1,15	-	-
	4	$2,22\times10^{-2}$	1	1,80	5,00	1,13	-	-
	8	$6,54\times10^{-3}$	1	1,89	9,00	1,12	-	-
	12	$3,08\times10^{-3}$	1	1,92	13,00	1,11	-	-
	20	$1,16\times10^{-3}$	1	1,95	21,00	1,11	-	-
0,98	2	$5,91\times10^{-2}$	1	1,67	3,06	1,07	2,02	4,30
	4	$1,82\times10^{-2}$	1	1,80	5,10	1,03	2,01	6,21
	8	$4,54\times10^{-3}$	1	1,89	9,18	1,01	1,97	9,91
	12	$1,82\times10^{-3}$	1	1,92	13,3	1	1,95	13,6
	20	$4,97\times10^{-4}$	1	1,95	21,4	1	1,95	21,4
0,90	2	$3,54\times10^{-2}$	1	1,67	3,33	1	1,70	3,45
	4	$7,75\times10^{-3}$	1	1,80	5,56	1	1,80	5,56
	8	$9,81\times10^{-4}$	1	1,89	10,0	1	1,89	10,0
	12	$1,99\times10^{-4}$	1	1,92	14,0	1	1,92	14,4
	20	$1,39\times10^{-5}$	1	1,95	23,3	1	1,95	23,3
0,70	2	$7,84\times10^{-3}$	1	1,67	4,29	1	1,67	4,29
	4	$1,13\times10^{-3}$	1	1,80	7,14	1	1,80	7,14
	8	$1,06\times10^{-5}$	1	1,89	12,9	1	1,89	12,9
	12	$2,89\times10^{-7}$	1	1,92	18,6	1	1,92	18,6
	20	$3,62\times10^{-10}$	1	1,95	30,0	1	1,95	30,0
0,40	2	$2,73\times10^{-4}$	1	1,67	7,50	1	1,67	7,50
	4	$2,33\times10^{-6}$	1	1,80	12,5	1	1,80	12,5
	8	$4,49\times10^{-10}$	1	1,89	22,5	1	1,89	22,5
	12	$1,39\times10^{-13}$	1	1,92	43,3	1	1,92	43,3
	20	$2,25\times10^{-20}$	1	1,95	52,5	1	1,95	52,5

approached, since the two-part function predicts pores larger than the maximum allowed by the C-BC function. This increase is small for the C-CG model since the probability of two large pores being in sequence decreases as pore size increases. The two-part function cannot be used to calculate a K_s value using the Burdine model unless a maximum matric potential corresponding to a maximum pore size is specified. At S = 0,98 and b = 2, K calculated using the two-part function is 1,07 times (C-CG model); 1,21 times (Mualem's model) and 1,43 times (Burdine's model) that calculated using the C-BC function.

The Burdine model differs from the C-CG model by a factor (b + 1)/S for the C-BC function; the deviation thus becomes greater as degree of saturation decreases and the value of b increases. The data listed in Table 4.4 show that the C-CG and Mualem models, applied to either the C-BC or two-part function, predict K values which do not differ by more than a factor of three.

Choice of a value for p and the definition of ε can influence predicted K to a greater extent than choice of model. Values between 0 and 2 have been assigned to p. ε can represent total or water-filled porosity. For a soil having a total porosity (θ_s) of 0,5, the term ε^p can vary from 1 to 0,25 at saturation and from 1 to 0,04 when θ is 0,2. Thus the definition of p and ε is as, if not more, important than the choice of capillary model.

The finite sums equations are intended for application to measured retentivity data to which a retentivity function cannot be fitted. If the measured curve corresponds exactly to a retentivity function then the finite sum and integral equations will predict the same K values, providing that the number of pore class intervals into which the curve is divided is sufficiently large. The effect of the number of pore class intervals, the value of b and the choice of model is demonstrated in Table 4.5, which lists ratios of finite sum to integral

TABLE 4.5 Effect of the number of pore class intervals (N) and the value of retentivity parameter b on the ratio of K_s predicted by finite sums to K_s predicted by an integral equation

Model	Retentivity function	b	K_s (finite sums)/K_s (integral) N=4	N=8	N=16	N=32	N=64	N=128
		2	1,07	1,02	1,01	1	1	1
		4	1,17	1,05	1,01	1	1	1
Childs		8	1,14	1,14	1,05	1,02	1	1
Collis-George	C-BC	12	0,83	1,19	1,09	1,03	1,01	1
		20	0,26	1,03	1,16	1,06	1,02	1
		2	0,99	1	1	1	1	1
		4	1,04	1	1	1	1	1
Childs &		8	1,03	1,02	1	1	1	1
Collis-George	Two-part	12	0,74	1,07	0,99	1	1	1
		20	0,23	0,93	1,05	1	1	1
		2	0,97	1	1	1	1	1
		4	0,90	0,99	1	1	1	1
Mualem	C-BC	8	0,68	0,98	0,99	1	1	1
		12	0,44	0,95	0,99	1	1	1
		20	0,13	0,87	0,97	0,99	1	1
		2	0,95	0,99	1	1	1	1
		4	0,83	0,95	0,99	1	1	1
Burdine	C-BC	8	0,50	0,84	0,96	0,99	0,99	1
		12	0,25	0,69	0,91	0,98	0,99	1
		20	0,05	0,39	0,77	0,94	0,98	1

equation predictions of K_s for curves corresponding to the two retentivity functions used.

The C-CG model requires the fewest pore class intervals; more than 8 classes produce satisfactory convergence, especially at lower $\underline{b}$ values. An increase in the number of pore classes increases the average potential of the pore class nearest saturation. In the C-CG model this is of little consequence since the probability of two large pores being in sequence decreases as pore size increases. If no largest pore size or maximum pressure potential is specified and the retentivity function is of a type for which the term $d\theta/d\psi = 0$ at $S = 1$, then the largest pore size increases to infinity. This is the reason the Burdine model cannot be used with the two-part function without specifying a maximum potential.

In general, about 30 pore class intervals should produce K_s values which are within 5% of the integral value. This is especially so if the retentivity curve has a definite "air-entry" value which defines the maximum pore size.

4.2.4 Discussion

Conductivity models can be of great value provided users are aware of their limitations. These models simulate the dependence of K on θ realistically and the relative effects of changes in pore size distribution are accounted for. Furthermore, they are easily incorporated into computer models. The equivalent closed-form K equations are useful in analytical solutions to the flow equation. The retentivity functions used to derive these equations have only two parameters which can be related to soil properties. The relationship between these parameters and the shape of the retentivity curve is easily visualized. Conductivity models provide a useful first estimate of K_s but are actually more useful in predicting $K_r(\theta)$.

Predicted K values can only be brought into coincidence with measured values by manipulating matching and tortuosity parameters. This is not surprising since so many parameter values in the model are chosen empirically. In addition, the choice of model is subjective. Real soils are far more complex in their behaviour than is predicted by capillary models. Pore geometry is simplified for modelling purposes and swelling and shrinkage is ignored.

The lack of agreement between measured and predicted K values raises doubts as to whether these models should be used at all. Gardner (1974) suggested that a simple empirical function with few parameters is often preferable to a more complex model and can be as accurate. Some of the capillary models, when applied to simple retentivity functions, do reduce to simple exponential equations of the same form as some of the commonly used empirical functions. These simple K equations, expressed in terms of retentivity parameters, are preferable to purely empirical equations as the retentivity parameters can be related to soil properties, as described in Chapter 3.

In water flow modelling such equations are valuable for predicting the effects of changes in soil properties through the profile on K. In real soils $\theta(\psi)$ and $K(\psi)$ relationships change with depth in response to changes in texture, organic matter content, bulk density and other factors. In a finite difference model the hydrologic effects of changes in soil properties are reflected in the values of the retentivity and conductivity parameters defined for each depth node. If soil properties are linked to $K(\psi)$ and $\theta(\psi)$ through suitable functions and parameter values then complex profiles may easily be simulated.

The conductivity models are a simplification of real soils. They should be regarded as a means of describing the behaviour of hypothetical soils which may have features in common with real soils.

In the next chapter K values are calculated using some of these predictive equations using textural and retentivity data for South African soils.

CHAPTER 5

ESTIMATES OF HYDRAULIC CONDUCTIVITY FOR SOUTH AFRICAN SOILS

5.1 INTRODUCTION

Several methods for predicting K were discussed in Chapter 4. They were based on various capillary models for predicting $K(\psi)$ from retentivity data or on regression equations relating K to textural criteria. Published comparisons of measured and predicted K show that none of these methods are reliable predictors of K. Although the capillary models often predict the shape of $K(\psi)$ curves, matching factors are required to bring measured and calculated $K(\psi)$ curves into coincidence.

In order to calculate K values which correspond to calculated pressure potentials in the soil profile, estimated or measured $K(\psi)$ functions must be incorporated in water flow models. In the absence of measured K data, an estimation procedure must be used to obtain this function. In this chapter some predictive procedures are applied to several sets of retentivity and textural data described in previous chapters. To test predictive methods sufficient measured data must be available. Conductivity of South African soils is rarely measured which means that predictive methods are difficult to evaluate.

Two predictive techniques are used.

1) The capillary model of Childs and Collis-George in conjunction with the two-part retentivity equation (Table 3.12) assuming $p = 1$. The term $K_{\psi}(CCG)$ refers to conductivity at pressure potential ψ calculated using Eq. 4.38 and 4.39. The relationship between $K_{\psi}(CCG)$ values and those predicted using other capillary models is given in Table 4.4.

2) Bloemen's equation (Eq. 4.26) is used to predict saturated K, designated K_s(Bloemen), from median particle size and a size distribution index. This equation was originally derived using data from the Netherlands. It is based on textural indices and may correlate with K in South African soils.

One or both of these techniques are applied to three sets of data, the object being:

1) to compare K_ψ(CCG) values, based on retentivity values calculated from core data, to K_s(Bloemen) values calculated from corresponding textural data;
2) to compare K_s values, measured on repacked columns of fragmented soil, with K_s values predicted from textural criteria;
3) to examine K_ψ(CCG) values calculated from retentivity parameters corresponding to soils of various textures and bulk densities.

5.2 PROCEDURE

5.2.1 Core data

Retentivity and textural data for core samples of South African soils (Table 3.3) were used. K_s(Bloemen) values were calculated using Eq. 4.26 based on median particle size and a size distribution index (Bloemen, 1980). K_ψ(CCG) values were calculated (Eq. 4.38 and 4.39) at pressure potentials of 0; -1; -3 and -10 kPa using retentivity parameters calculated for each core as described in 3.3.3.2.

5.2.2 Land Type Survey data

K_s values were measured on packed columns of fragmented soil samples collected during a Land Type Survey of South Africa (2.2.2.4). K_s(Bloemen) values were calculated from particle size distribution data. Median diameters less than 1 μm were excluded owing to uncertainty as to the shape of the cumulative particle size curve in this region.

5.2.3 Soil properties in relation to calculated $K(\psi)$

In Chapter 3, regression equations relating retentivity to bulk density, clay content and silt content were derived using British and South African retentivity data. These equations were used to generate retentivity data for combinations of six clay contents, five silt/clay ratios and four bulk densities (Table 3.13). Corresponding retentivity parameters were obtained by fitting a two-part retentivity function to the generated retentivity curves. These determinations were made for three sets of data (Table 5.1), two of which were discussed in Chapter 3 (Figs. 3.11 and 3.12). These three retentivity parameter systems represent three families of hypothetical soils which display the main retentivity characteristics of the real soils on which they are based. K_ψ(CCG) values were calculated for each clay/silt/bulk density combination at pressure potentials of 0, -1 and -100 kPa.

5.3 RESULTS AND DISCUSSION

5.3.1 Core data

Both K_s(Bloemen) values and median particle diameters were significantly correlated with K_ψ(CCG) values at ψ values of

TABLE 5.1 Retentivity data used for deriving the relationship between retentivity parameters and soil properties

	Data source	Pressure potentials (kPa) for which retentivity data were available	Retentivity parameters displayed
I	Source 1 - 8 Table 3.8	0 -10 -30 -100 -500 -1500	Fig. 3.11
II	Hall, et al. (1977) (British data)	0 -5 -10 -40 -200 -1500	Fig. 3.12
III	Source 1 only Table 3.9	0 -3 -10 -30 -50	Fig. 5.5

TABLE 5.2 Correlation between K_ψ (CCG) values, median particle diameter (M) and K_s (Bloemen) values (**significant at 1% level, *significant at 5% level with N = 397).

ψ (kPa)	Correlation coefficient between log K_ψ (CCG) and log M	log K_s (Bloemen)
0	0,114	0,115
-1	0,320**	0,318**
-3	0,333**	0,318**
-10	0,221*	0,213*

-1; -3 and -10 kPa (Table 5.2), but scattergrams of K_{-1}(CCG) versus K_s(Bloemen) (Fig. 5.1) and median particle diameter (Fig. 5.2) show a wide scatter of points.

The reason why K_{-1}(CCG) and K_{-3}(CCG) rather than K_s(CCG) should be most closely correlated with K_s(Bloemen) is probably a result of the shape of the retentivity function at high potentials in particular between saturation and the highest measured potential, generally -5 to -10 kPa. Since the parabolic shape of the extreme wet end of the function is empirical, and was introduced to fulfil mathematical modelling requirements, its exact shape will depend on the choice of retentivity parameters, which in turn depend on the distribution of measured retentivity values to which the function was fitted. This was illustrated in Fig. 3.7. If the value of parameter a corresponds to a measured air-entry value then the size of the largest pore is defined. In this case, Campbell's exponential function (Eq. 3.26) could be used in place of the two-part function and K_s(CCG) should correlate with measured K_s. If parameter a is used as a curve-fitting parameter, as was done here, then there is no reason why K_s(CCG) should be related to measured K_s unless these are measured retentivity values near saturation which influence the values of the retentivity parameters.

The retentivity function is more likely to match the real retentivity curve in the -1 to -3 kPa region than at higher potentials, since it is in this region that the exponential portion of the function starts, which is generally closely matched to measured retentivity. In most soils θ_{-1} is close to θ_s and K_{-1}(CCG) will be correlated with K_s.

The correlation between K_{-1}(CCG) and K_s(Bloemen) was the same as that between K_{-1}(CCG) and median particle diameter. Median particle diameter is as good a predictor of K_s but is simpler than Bloemen's equation, which incorporates a size distribution index. At low

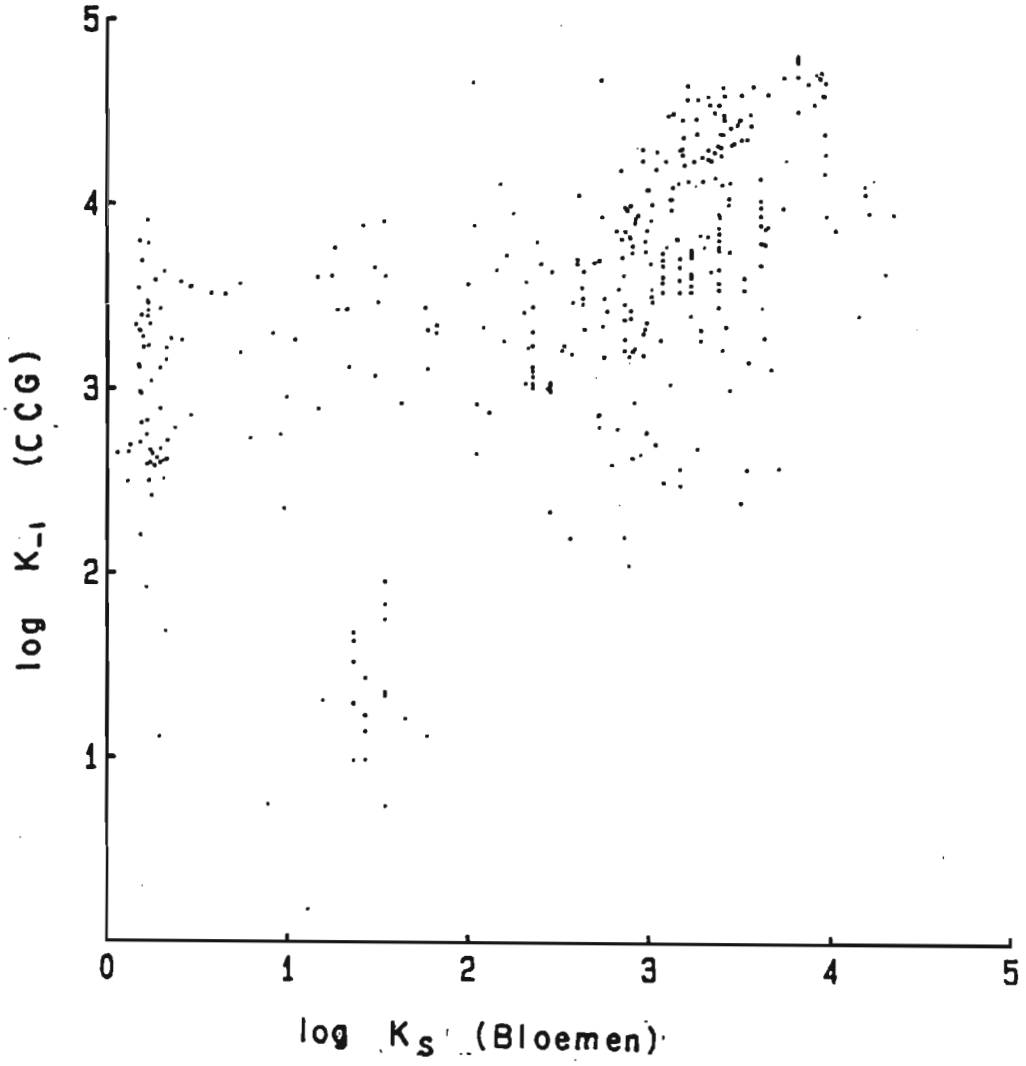

FIGURE 5.1 Scattergram of K_s(Bloemen) values against K_{-1}(CCG) values (mm/d), calculated using data from sources 1 - 8 (Table 3.3)

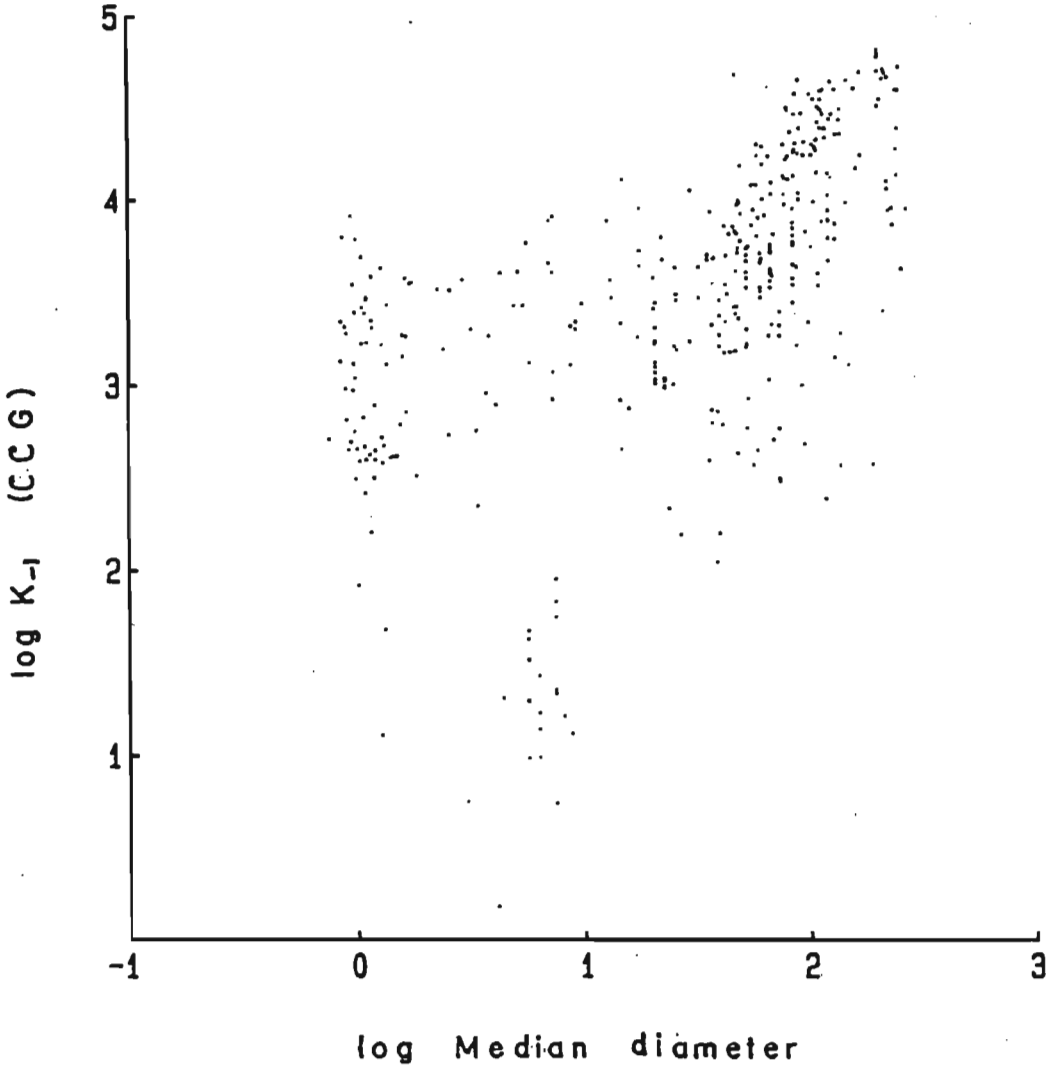

FIGURE 5.2 Scattergram of median particle diameter (μm) against K_{-1}(CCG) (mm/d), calculated using data from sources 1 - 8 (Table 3.3)

median diameters K_s(Bloemen) values are generally lower than K_{-1}(CCG) values, probably owing to aggregation effects which are not accounted for in Bloemen's equation.

These data show that:

1) the value of K_{-1}(CCG) is within an order of magnitude of K_s(Bloemen) at K values greater than about 20 mm/d;
2) median particle diameter is correlated with both K_{-1}(CCG) and K_{-3}(CCG) but the association weakens at median diameters less than 2 μm;
3) an equation based on texture for predicting K_s will be more reliable in coarse-textured soils in which particle size rather than aggregate size determines pore size distribution;
4) predictions are approximate and are probably unlikely to be better than an order of magnitude.

5.3.2 Land Type Survey data

Measured K_s values for the Land Type Survey samples were obtained as part of the air-to-water permeability ratio test described earlier (2.2.2.4). Short columns of fragmented soil, of unknown bulk density and aggregate size distribution, were used.

Scattergrams of measured K_s values against K_s(Bloemen) values (Fig. 5.3) and median particle diameters (Fig. 5.4) show trends similar to those observed for core data. K_s(Bloemen) values less than about 20 mm/d (and median particle diameters less than 2 μm) correspond to higher measured K_s values. The remaining K_s(Bloemen) and measured values are clustered in the 10^2 to 10^4 mm/d region, there being no significant correlation. Elimination of swelling or dispersed soils (air-to-water permeability ratios above ten) did not improve the correlation. These results indicate that K_s predictions based on

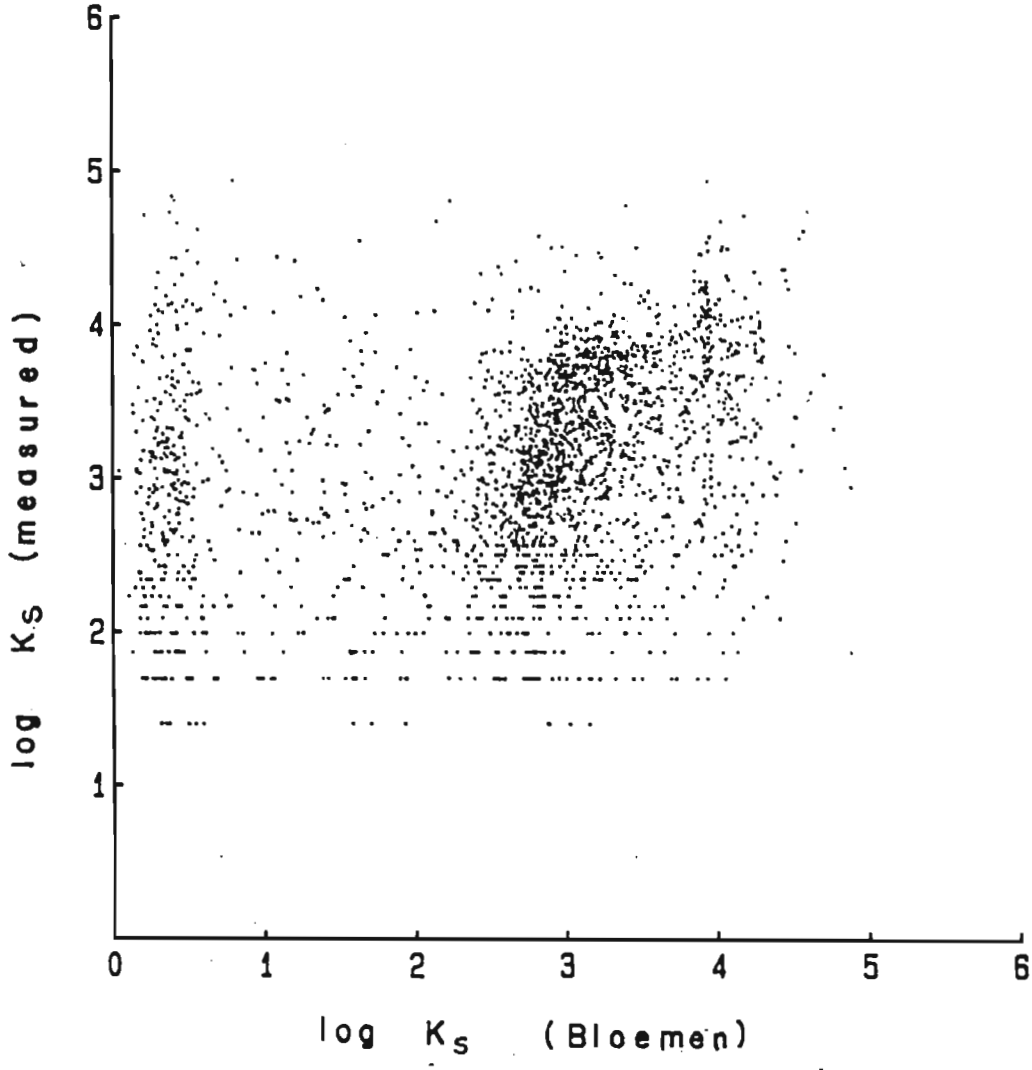

FIGURE 5.3 Scattergram of K_s(Bloemen) values against measured K_s (mm/d). Data from Land Type Survey (Source 9, Table 3.3)

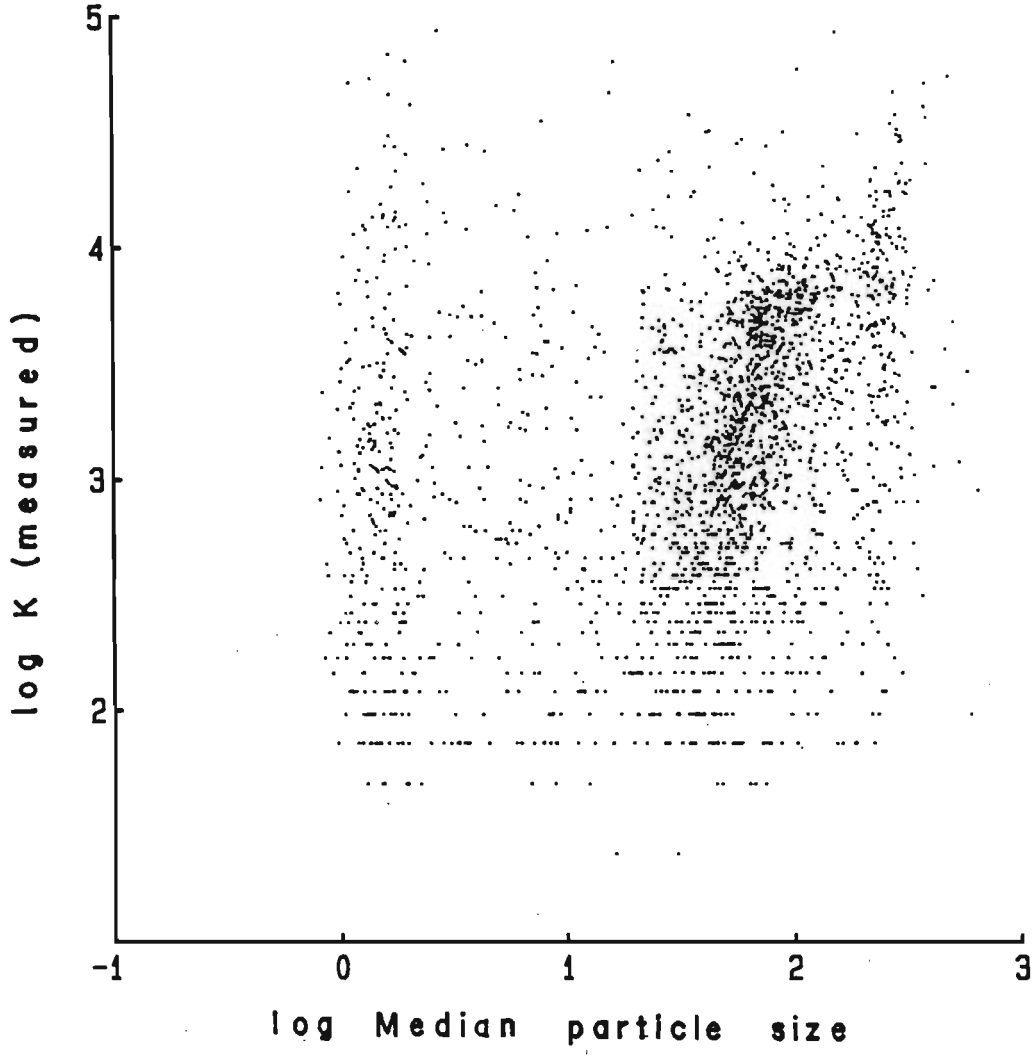

FIGURE 5.4 Scattergram of median particle diameter (μm) against measured K_s (mm/d). Data from Land Type Survey (Source 9, Table 3.3)

texture or simple K_s measurements are unreliable and should not be extrapolated to field soils, where factors such as bulk density, structure and aggregation influence K to an unknown extent.

5.3.3 Soil properties in relation to calculated $K(\psi)$

The object of this work is to derive a general relationship between soil properties (specifically, clay content, silt content and bulk density) and retentivity and conductivity characteristics. In the absence of measured data, or for demonstration purposes, such a framework can provide estimates of $K(\psi)$ and $\theta(\psi)$ for modelling purposes.

In Chapter 3, regression equations were derived relating retentivity at several pressure potentials to clay content, silt/clay ratio and bulk density. Using these equations, retentivity curves corresponding to various combinations of clay, silt and bulk density (Table 3.13) were generated. The two-part retentivity function was fitted to these curves in order to relate the values of the retentivity parameters to soil properties. This procedure was applied to three sets of data, summarized in Table 5.1. Results for systems I and II were discussed earlier (3.3.3.3, Figs. 3.11 and 3.12).

Retentivity parameters for system III are displayed in Fig. 5.5. These were not discussed in Chapter 3 as the parameters were derived from data obtained over a narrow pressure potential range of 0 to -50 kPa. The object in Chapter 3 was to draw up general retentivity relationships for the whole range of plant available water rather than a limited range. However, for the purpose of calculating $K(\psi)$ at high pressure potentials these data are useful as the fitted $\theta(\psi)$ curve is likely to be more accurate near saturation.

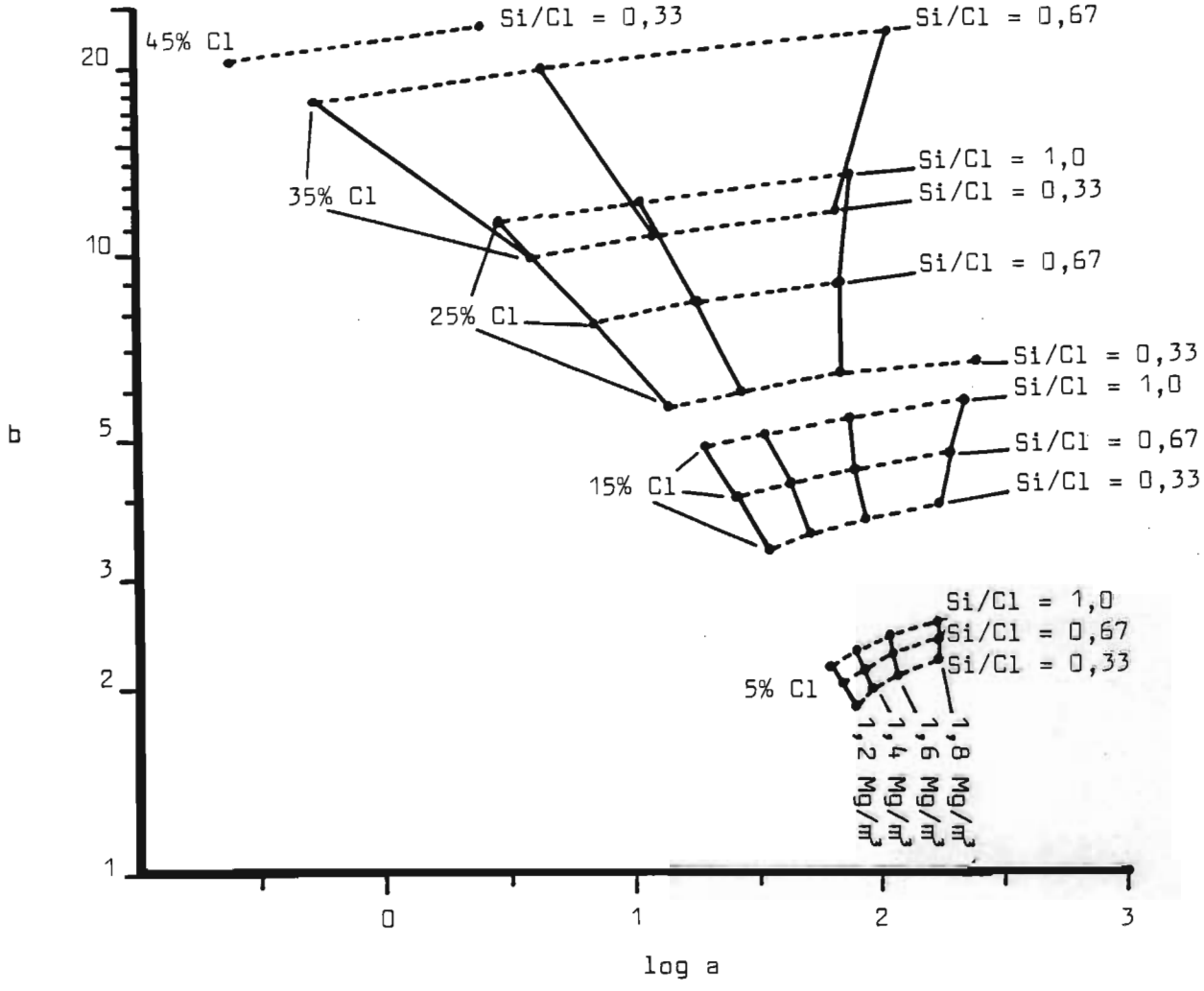

FIGURE 5.5 Retentivity parameters for two-part retentivity function, derived from regression equations relating θ_ψ to clay content, silt content and bulk density. (regression coefficients listed in Table 3.10). Originally retentivity data from source 1 (Table 3.3)

For each of the three systems best-fit retentivity parameters corresponding to various clay, silt and bulk density values are known. These are approximate relationships since the multiple correlation coefficients for the original regression analyses ranged from 0,6 to 0,8. An additional source of error arises from fitting the retentivity function to the generated retentivity curves.

K_ψ(CCG) values were calculated for all retentivity parameters, at ψ values of 0, -1, -10 and -100 kPa. Thus for each of the three soil systems, $K(\psi)$ was calculated for various combinations of clay content, silt/clay ratio and bulk density.

In the absence of measured K values against which the calculated values may be compared, the following criteria were chosen to evaluate K_ψ(CCG) values:

1) An increase in value of any one of clay content, silt content or bulk density should lead to a decrease in K_s(CCG) and, since θ is near saturation, K_{-1}(CCG);

2) The slope of the $K(\psi)$ function (i.e. the term $d\log K/d\log(-\psi)$) should decrease with increasing clay content, silt content or bulk density. For the two-part function at pressure potentials less than the inflection point, the slope has the value (3/b) + 2.

These criteria are based upon an assumption that any factor which shifts pore size distribution so as to increase the proportion of small pores should lead to a reduction in K_s and the slope of $K(\psi)$.

There is no means of evaluating absolute K_ψ values without experimental measurements. The above criteria will ensure that calculated $K(\psi)$ functions for the various clay, silt/clay ratio and bulk density combinations have a qualitative or relative relationship which would be expected in real soils.

An evaluation of K_ψ(CCG) values for the three systems is summarized in Table 5.3. System III provides the best framework for modelling purposes as it meets both criteria except for K_s values at bulk densities of 1,2 and 1,4 Mg/m. The calculated values of K_ψ(CCG) at 0, -1 and -100 kPa are listed in Table 5.4 for system III.

System III was superior to systems I and II for calculating conductivity because the shape of the retentivity function at high potentials was defined more exactly. Systems I and II should be better for describing retentivity over a wider potential range but for flow modelling purposes the 0 to -50 kPa range is of greatest importance. Extrapolating the retentivity curves predicted by system III to -1500 kPa may lead to errors in estimating available water. Providing soils are non-swelling, apedal and lie within the density, clay, silt and organic matter limits of the source 1 data, system III could provide a good framework from which preliminary soil hydrological data may be extracted.

There is no means of assessing the validity of the absolute values of K_ψ listed in Table 5.4 as there is no measured data against which they may be compared. As shown earlier, K_s values may be inaccurate owing to an arbitrary retentivity function near saturation. It is necessary to examine the whole $K(\psi)$ relationship before rejecting it. If a K_s value for example, calculated at 0 kPa is unrealistically high, it does not necessarily imply that the rest of the $K(\psi)$ curve is unrealistic. Similarly, if a measured K_s value is available and a matching factor is calculated, it does not mean that the matching factor can be used over the whole potential range, but the uncertainties are likely to be very much less.

At present K calculation procedures are not sufficiently reliable

TABLE 5.3 A qualitative evaluation of K_ψ (CCG) values calculated from retentivity parameters corresponding to three sets of soil data. (System I is Sources 1 - 8 data, System II is British data (Hall et al. 1977), System III is source 1 data only. Favourable response indicated by ✓, unfavourable by x)

System	I				II				III			
Bulk density (Mg/m^3)	1,2	1,4	1,6	1,8	1,2	1,4	1,6	1,8	1,2	1,4	1,6	1,8
K_s decreases with												
i) increasing Cl	✓	✓	✓	✓	x	x	x	x	x	x	✓	✓
ii) increasing Si	✓	✓	✓	✓	✓	✓	✓	✓	x	x	✓	✓
K_{-1} decreases with												
i) increasing Cl	x	x	x	✓	✓	✓	✓	✓	✓	✓	✓	✓
ii) increasing Si	x	x	x	✓	x	x	x	x	✓	✓	✓	✓
K_s decreases with increasing ρ_b		✓				✓				✓		
K_{-1} decreases with increasing ρ_b		x				✓				✓		
Log (K/ψ) decreases with												
i) increasing Cl		✓				✓				✓		
ii) increasing Si		x				x				✓		
iii) increasing ρ_b		x				✓				✓		

TABLE 5.4 Values of K_ψ (CCG) in mm/d at pressure potentials of 0, -1 and -100 kPa for various combinations of clay content, Si/Cl ratio and bulk density (ρ_b). Calculated using Eq. 4.38 and 4.39 and the retentivity parameters for System III (Fig. 5.5)

Clay (%)	ψ (kPa)	ρ_b = 1,2 (Mg/m³)			ρ_b = 1,4 (Mg/m³)			ρ_b = 1,6 (Mg/m³)			ρ_b = 1,8 (Mg/m³)		
		Si/Cl =			Si/Cl =			Si/Cl =			Si/Cl =		
		0,33	0,66	1,00	0,33	0,66	1,00	0,33	0,66	1,00	0,33	0,66	1,00
5	0	$1,9\times10^{5}$	$2,0\times10^{5}$	$2,1\times10^{5}$	$1,0\times10^{5}$	$1,1\times10^{5}$	$1,1\times10^{5}$	$4,7\times10^{4}$	$4,5\times10^{2}$	$4,4\times10^{4}$	$1,6\times10^{4}$	$1,4\times10^{4}$	$1,3\times10^{4}$
	-1	$6,1\times10^{4}$	$5,4\times10^{4}$	$4,7\times10^{4}$	$4,7\times10^{4}$	$4,4\times10^{4}$	$4,1\times10^{4}$	$2,9\times10^{4}$	$2,7\times10^{4}$	$2,5\times10^{4}$	$1,2\times10^{4}$	$1,1\times10^{4}$	$1,0\times10^{4}$
	-100	$4,5\times10^{-2}$	$5,5\times10^{-2}$	$6,6\times10^{-2}$	$5,9\times10^{-2}$	$7,0\times10^{-2}$	$8,2\times10^{-2}$	$7,7\times10^{-2}$	$9,1\times10^{-2}$	$1,0\times10^{-1}$	$1,0\times10^{-1}$	$1,2\times10^{-1}$	$1,4\times10^{-}$
15	0	$3,5\times10^{5}$	$4,5\times10^{5}$	$6,0\times10^{5}$	$1,3\times10^{5}$	$1,4\times10^{5}$	$1,5\times10^{5}$	$3,5\times10^{4}$	$3,0\times10^{4}$	$2,4\times10^{4}$	$6,0\times10^{3}$	$3,6\times10^{3}$	$1,9\times10^{3}$
	-1	$2,0\times10^{4}$	$1,4\times10^{4}$	$9,9\times10^{3}$	$2,0\times10^{4}$	$1,4\times10^{4}$	$9,9\times10^{3}$	$1,7\times10^{4}$	$1,3\times10^{4}$	$9,6\times10^{3}$	$4,8\times10^{3}$	$3,0\times10^{3}$	$1,6\times10^{3}$
	-100	$1,2\times10^{-1}$	$1,4\times10^{-1}$	$1,5\times10^{-1}$	$1,4\times10^{-1}$	$1,6\times10^{-1}$	$1,7\times10^{-1}$	$1,7\times10^{-1}$	$1,8\times10^{-1}$	$1,9\times10^{-1}$	$2,1\times10^{-1}$	$2,2\times10^{-1}$	$2,2\times10^{-}$
25	0	$8,6\times10^{5}$	$1,8\times10^{6}$	$5,7\times10^{6}$	$1,8\times10^{5}$	$2,2\times10^{5}$	$2,9\times10^{5}$	$2,1\times10^{4}$	$1,1\times10^{4}$	$4,2\times10^{3}$	$1,1\times10^{3}$		
	-1	$7,5\times10^{3}$	$4,3\times10^{3}$	$2,3\times10^{3}$	$7,5\times10^{3}$	$4,2\times10^{3}$	$2,2\times10^{3}$	$7,6\times10^{3}$	$4,2\times10^{3}$	$1,9\times10^{3}$	$9,8\times10^{2}$		
	-100	$1,4\times10^{-1}$	$1,3\times10^{-1}$	$1,0\times10^{-1}$	$1,6\times10^{-1}$	$1,4\times10^{-1}$	$1,0\times10^{-1}$	$1,8\times10^{-1}$	$1,5\times10^{-1}$	$1,1\times10^{-1}$	$2,2\times10^{-1}$		
35	0	$4,4\times10^{6}$	$7,2\times10^{7}$	$1,1\times10^{2}$	$3,1\times10^{5}$	$7,7\times10^{5}$	$6,3\times10^{7}$	$7,5\times10^{3}$	$7,2\times10^{2}$				
	-1	$2,8\times10^{3}$	$1,0\times10^{3}$	$1,9\times10^{2}$	$2,7\times10^{3}$	$9,1\times10^{2}$	$1,3\times10^{2}$	$2,6\times10^{3}$	$4,9\times10^{2}$				
	-100	$1,1\times10^{-1}$	$5,9\times10^{-2}$	$1,6\times10^{-2}$	$1,1\times10^{-1}$	$5,7\times10^{-2}$	$1,1\times10^{-2}$	$1,2\times10^{-1}$	$5,4\times10^{-2}$				
45	0	$2,8\times10^{8}$	$1,8\times10^{14}$		$1,7\times10^{6}$			$4,7\times10^{2}$					
	-1	$7,6\times10^{2}$	$9,9\times10^{1}$		$6,6\times10^{2}$			$3,2\times10^{2}$					
	-100	$4,8\times10^{-2}$	$8,5\times10^{-3}$		$4,5\times10^{-2}$			$4,1\times10^{-2}$					

a means of generating conductivity data which exhibit similar qualitative characteristics to those displayed by real soils. In the following chapter a method of estimating K_s from core outflow data is described which will enable a "best-fit" $K(\psi)$ relationship to be defined for a specific pressure potential range.

CHAPTER 6

AN OUTFLOW/INFLOW METHOD OF ESTIMATING HYDRAULIC CONDUCTIVITY

6.1 INTRODUCTION

The review of methods of estimating unsaturated hydraulic conductivity showed that procedures based solely on retentivity or textural properties of soils were neither precise nor reliable. At least one measurement of K is required so that a matching factor may be calculated. This is normally done at saturation, but maintaining full saturation while preserving the structure of soil core samples is difficult. Ideally, K measurements should be carried out at several water contents so that both the matching factor and the shape of the $K(\theta)$ curve may be ascertained. In this chapter a method for determining $K(\psi)$ is described, which utilizes the rate of outflow or inflow of water after an abrupt change of suction or pressure upon a cell containing a soil core supported by a porous plate or membrane.

Commonly used methods of measuring $K(\psi)$ were summarized by Klute (1972). The outflow methods in which K is calculated from the rate of outflow from a core after a pressure or suction increment is applied to it, are convenient as they can easily be incorporated in the normal procedure for measuring retentivity, provided each core is contained in a separate pressure cell. Outflow techniques described in the literature are of two kinds, the short column - small increment and short column - large increment methods.

In the short column - small increment method (Gardner, 1956) the pressure increment is assumed sufficiently small to justify assumptions of constant diffusivity and a linear $\theta(\psi)$ function over the range of the increment. Modifications by Miller and Elrick (1958), Rijtema (1959), Kunze and Kirkham (1962), Peck (1966) and Collis-George and Rosenthal (1966) were aimed primarily at accounting for the impeding effects of

the ceramic plate or membrane supporting the soil core and poor contact between core and plate. The effect of gravity is ignored but this is negligible except at water contents near saturation. A practical problem of this method is measurement of the small outflow volumes associated with small pressure increments.

In the short column - large increment method (Doering, 1965) diffusivity and water content are assumed uniform through the core at any instant in time. Diffusivity is calculated from instantaneous outflow flux rate assuming negligible boundary and plate impedance. Gupta, Farrell and Larson (1974) described an improved but somewhat involved calculation procedure which accounts for the non-uniform distribution of water through the core. Membrane and gravity effects were ignored.

Passioura (1976) described a method for calculating K from large-increment outflow experiments in which he identified three stages of outflow. Initially, flow rate is determined by the conductivity of the supporting plate or membrane and cumulative outflow is proportional to elapsed time. As the soil dries, membrane or plate resistance becomes negligible in comparison with reduced soil hydraulic conductivity. The soil core behaves as a semi-infinite column in which matric potential adjacent to the plate has reached a final potential. Cumulative outflow is then linearly related to $\sqrt{t}$. The third stage begins when the water content at the top of the core begins to decrease. This stage is used to calculate conductivity based on the rate at which the approximately uniform water content distribution in the core decreases with time. Jaynes and Tyler (1980) compared Passioura's method with an *in situ* crust infiltration technique. Agreement was satisfactory, especially considering that the crust test measures K while the soil is wetting and the outflow method is a drying procedure. Plate impedance

limited the range of third-stage outflow. Longer cores would have improved the range but would invalidate the assumption of constant water content distribution.

The method to be described involves matching a measured outflow curve to a series of simulated curves, reflecting a range of conductivity values. Numerical simulation of outflow can include the effects of core length, gravity and plate resistance, thus eliminating the need for most of the simplifying assumptions necessary for analytical solutions to the flow equation. There are several advantages to such a method.

1) there are no limitations on core size, plate conductivity or matric potential range which cannot be ascertained beforehand by means of simulation studies;
2) gravity is accounted for;
3) both outflow and inflow may be measured and simulated, enabling hysteresis to be studied;
4) once the computer programs are available, calculations are reduced to a minimum.

There are several assumptions inherent in this method:

1) the water flow simulation model correctly simulates outflow from or absorption by a core supported on a ceramic plate of known conductivity;
2) the retentivity function incorporated in the model accurately reflects measured retentivity;
3) the conductivity function is of the same form as the real $K(\psi)$ curve and can be matched to it if the correct values of one or two parameters can be estimated;
4) conductivity of the ceramic plate remains constant over the whole range of potentials of interest and no resistance to

flow is caused by poor contact between core and plate;

5) retentivity and conductivity functions are valid for equilibrium, steady-state and transient flow in the core.

6.2 HYPOTHESIS

Any retentivity and conductivity functions may be incorporated into a water flow simulation model. In this work a Brooks and Corey (1966) retentivity function was used,

$$\psi = a \left(\frac{\theta - \theta_r}{\theta_s - \theta_r}\right)^{-b} \tag{6.1}$$

in which constants a and b and residual saturation θ_r may be used as curve-fitting parameters. Campbell's (1974) conductivity function,

$$K(\theta) = K_s \, (\theta/\theta_s)^{2b+2+p} \tag{6.2}$$

or

$$K(\psi) = K_s \, (a/\psi)^{2+(2+p)/b} \tag{6.3}$$

was used. The value of b is determined by the shape of the retentivity curve and is one of the parameters of the retentivity function. The tortuosity factor p is normally chosen between 0 and 2, small in comparison to the usual values of 2b + 2. Water inflow or outflow between desired matric potential limits is simulated using several K_s values, or combinations of K_s and p, if a value for p is not assumed. By matching a measured outflow or inflow curve to the simulated curves, best-fit values of K_s, or K_s and p, are obtained which may be used to estimate $K(\theta)$ over the matric potential range used.

If the impedance of the porous plate supporting the core is negligible then the time required for outflow is inversely proportional

to K_s. When plate resistance is not negligible this inverse relationship is no longer maintained (Table 6.1), but high plate resistance are required to mask the effect of changes in soil K.

6.3 PROCEDURE

6.3.1 Measurements of outflow and inflow

The apparatus used for measuring outflow and inflow was designed so that it could easily be attached to a Tempe Cell[1)] during retentivity measurements. The main components (Fig. 6.1) were a pressure control system capable of maintaining pressure constant to within 1 mm hydraulic head over a range of 0 to 2 000 mm, the Tempe cell (Fig. 6.2) in which the sample was contained and a horizontal tube attached to the cell outlet for measuring outflow or absorption of water. The tube which was 2,25 mm diameter, was graduated in 0,05 ml divisions but volume could be estimated to 0,01 ml. Calibration was performed with the aid of a microburette from which known volumes were released into the dry tube. The horizontal tube could be detached and replaced rapidly. If, during outflow, a tube became nearly filled with water, it was replaced with a clean dry tube. A burette enabled the volume absorbed from the tube during inflow to be replenished and hence measured. A dummy tube, closed at one end and filled with water, was used to estimate evaporation losses from the open-ended tubes, but this was negligible.

Hydraulic conductivity of the ceramic plates was measured before mounting cores in the Tempe cells and again after they were removed. The plates were saturated under vacuum, using de-aired water and a burette of water attached to the inlet to form a vertical standpipe.

---

1) (Manufactured by Soil Moisture Equipment Co., Santa Barbara, California)

TABLE 6.1 An example of the effect of K_p and K_s on $t_{\frac{1}{2}}$ values.
(a = 31,62mm ; b = 6,0 ; θ_s = 0,4217 m/m)

K_p mm/d	$t_{\frac{1}{2}}$ values (days) for outflow from -3 to -10 kPa at K_s values (mm/d)				$t_{\frac{1}{2}}$ values (days) for inflow from -10 to -3 kPa at K_s values (mm/d) of			
	10^2	10^3	10^4	10^5	10^2	10^3	10^4	10^5
0,15	0,247	0,070	0,057	0,056	0,33	0,126	0,090	0,085
1,5	0,213	0,025	0,0071	0,0048	1,65	0,032	0,013	0,009
15	0,210	0,022	0,0026	0,0008	0,136	0,016	0,0033	0,0014
150	0,210	0,021	0,0022		0,132	0,0137	0,0017	

TABLE 6.2 Properties of soil used for cores

Locality: Horticultural Research Institute, Roodeplaat

Horizon: Red apedal

Series: Shorrocks

Form: Hutton

Soil taxonomy (USDA): Rhodic paleustalf

Depth of sampling: 300 mm

Water content at compaction: 9,6 g/100 g

Particle size distribution %:

Cl : 23
Si : 6
fSa : 37
mSa : 25
cSa : 8

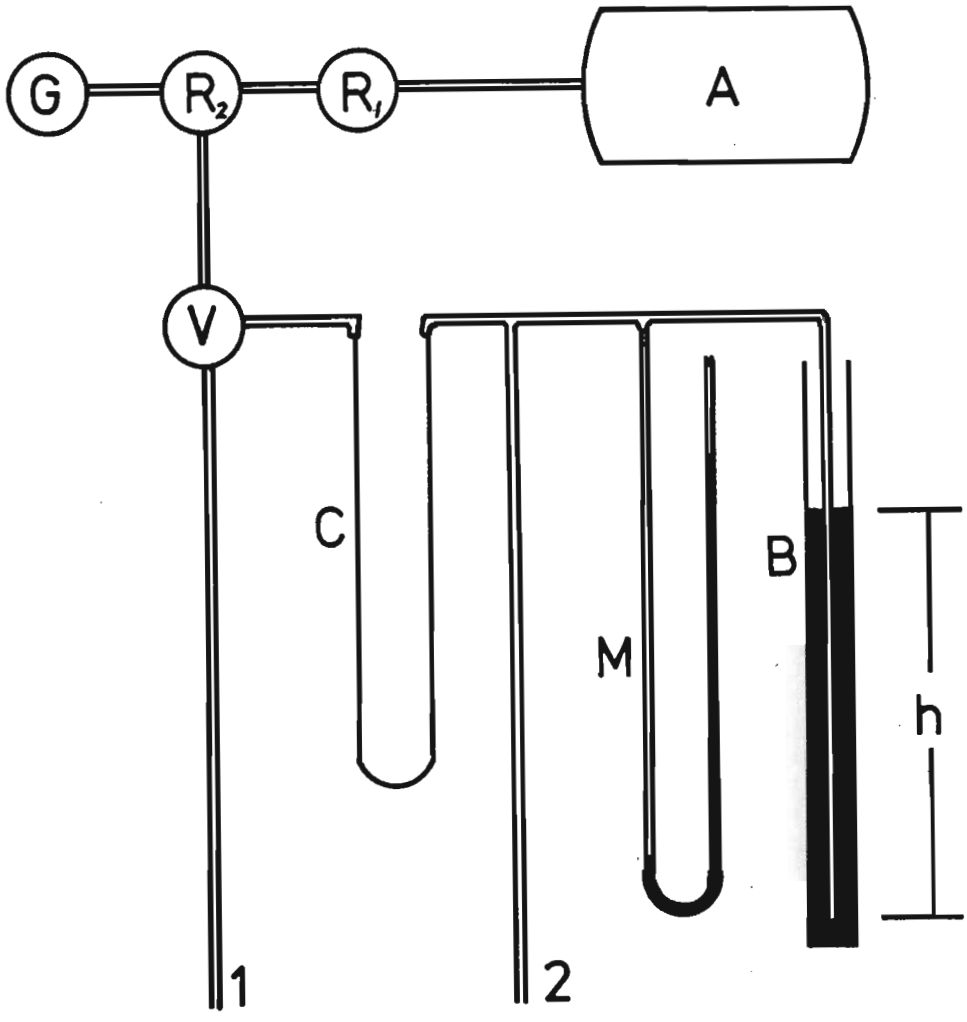

FIGURE 6.1 Pressure control system for retentivity and outflow/inflow apparatus. A - compressed air source, R_1 - regulator, R_2 - "Nullmatic" regulator, G - pressure gauge, C - capillary tubing (1 m x 0,7 mm i.d.), M - water manometer, B - bubble tower, V - valve for selecting port 1 (constant pressure between 20 and 100 kPa) or 2 (constant pressure between 0 and 20 kPa, controlled by water column h in B, monitored by M)

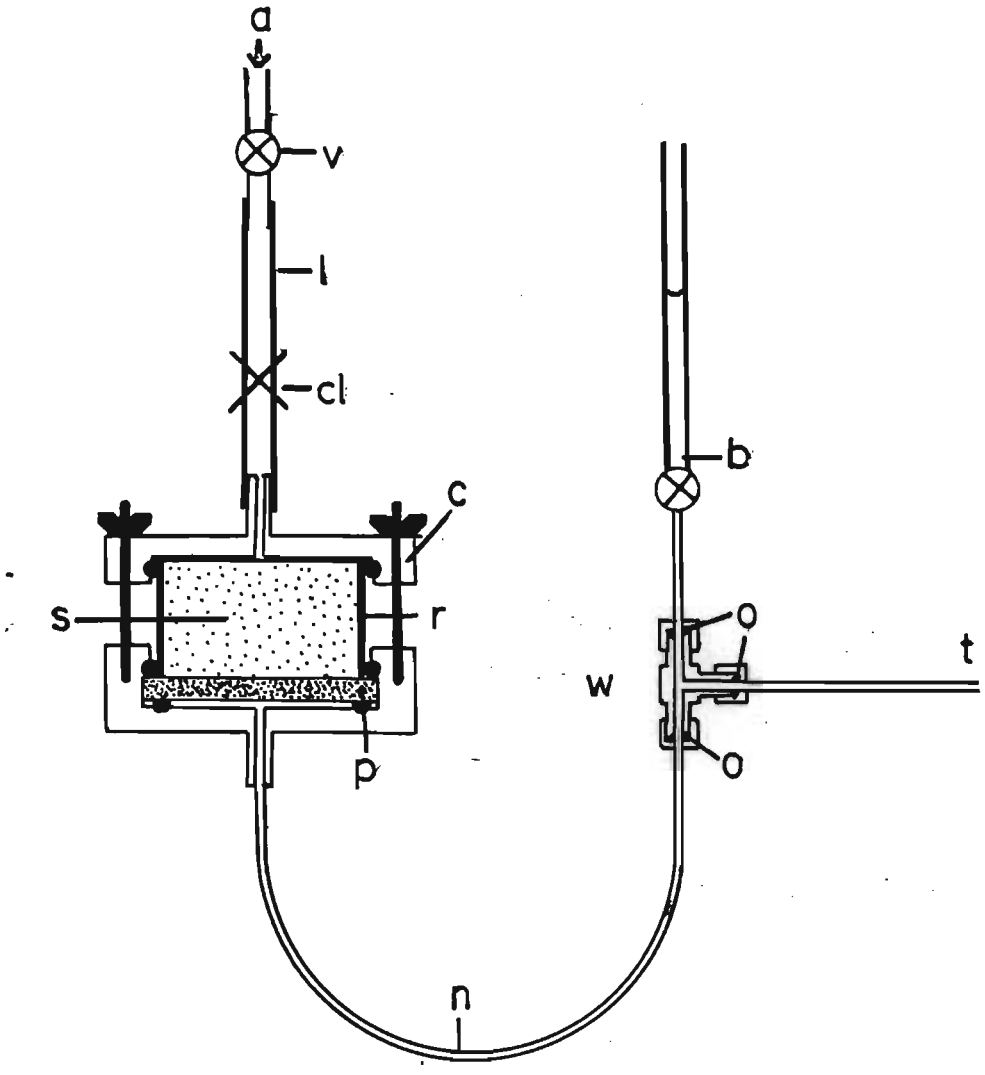

FIGURE 6.2 Apparatus for measuring core retentivity and rates of outflow or inflow of water. a - constant pressure from port 1 or 2 (Fig. 6.1); v - valve; ℓ - latex tubing; cl - clamp; c - Tempe cell; r - brass retaining ring; s - soil core; p - porous ceramic plate; n - nylon tubing; t - 2,25 mm i.d. graduated glass tube; b - burette; w - brass T-piece; 0 - neoprene "O"-rings

Flow from the burette in relation to the hydraulic head enabled plate conductivity to be calculated by a falling head method (Klute, 1965).

Soil cores of two sizes, 54 mm diameter x 30 mm, and 85,5 x 30 mm were prepared by packing soil directly onto the ceramic plates to ensure good contact. A brass core-retaining ring was mounted on the base of the Tempe cell and an extension ring of identical size taped to it. Well-mixed damp soil of the Shorrocks series (Table 6.2) was dumped into the ring assembly, excess soil being struck off. The soil was compressed by applying pressure to an aluminium disc placed on the soil surface. All cores were compressed a uniform amount. The extension ring was removed, the cores pared to the dimensions of the remaining ring and the cell lid bolted into place. Before doing any outflow measurements, the cores were saturated, desorbed to a matric potential of -30 kPa and resaturated, so that their structure would stabilize.

Retentivity and conductivity were measured at 21° ± 0,5 °C. Cores were saturated by partly immersing the assembled cells in de-aired tap water after ensuring that the space between the lower surface of the ceramic plate and its support was completely filled with water. Saturation to constant mass normally required about four days. The cells were connected and the cores were allowed to drain. The cells were massed after outflow ceased. The cell inlets were connected to closed pressure ports; dry outflow tubes were attached and an initial volume of water run into the tubes from the burettes to ensure that the T-pieces and connecting tubing were free of air bubbles.

Pressure ports were opened at 5,3 minute intervals. This enabled the first stages of outflow to be measured frequently on each cell before the next was started. Outflow was measured after 1, 2, 4, 8, 16 and 30 minutes; 1, 2, 4, 8, 16 and 24 hours and twice daily thereafter

until equilibrium was reached after about 5 days. To avoid the confusion which could result from these readings being taken on each of ten cells starting at 5,3 minute intervals, a computer program was written to predict order and times of measurement. Outflow tubes were replaced with clean, dry tubes when they were nearly full. At equilibrium, indicated by a negligible volume change, the pressure ports were closed and the cell pressure inlet tubes clamped to maintain pressure in the cell. Air bubbles, rarely present, were flushed from the space beneath the ceramic plate and the mass of the cells recorded. The pressure control system was adjusted to a new level and the next series of measurements started.

Pressure changes in the Tempe cells at the start of outflow were as abrupt as possible. This was accomplished by pinching the latex tube connecting a cell to its pressure port so that the port could be opened and the tubing clamp removed a few seconds before the desired starting time. At the correct time the tube was released.

Inflow measurements were done in a similar way. The horizontal tube was filled to a reference mark. After reduction of pressure in the cell the core absorbed water from the tube; the volume was measured directly and checked whenever water was released from the burette to refill the tube to the reference mark.

Outflow was measured between the matric potential ranges -3 to -10 and -10 to -30 kPa. Absorbtion or inflow was measured between -30 to -10 and -10 to -3 kPa.

6.3.2 Simulation model

Simulations of outflow and inflow were performed using a modified version of the model described in Chapter 1. Features of this version (Appendix 2) were:

1) data were recorded and printed after simulated times of 1, 2, 4, 8, 16 and 30 minutes, 1, 2, 4, 8, 16 and 24 hours and daily thereafter;
2) the simulation was repeated for each of four K_s values;
3) a node spacing of 2 mm was used (Fig. 6.3) as prior sensitivity studies showed this to be satisfactory for cores of 30 mm length and longer;
4) time intervals were chosen so that the maximum volumetric water content change ($\Delta\theta$) at any node did not exceed 0,01 m/m during a time interval;
5) the ceramic plate was simulated by specifying appropriate retentivity parameters and the measured plate conductivity for the depth nodes corresponding to the ceramic plate which ensured that over the matric potential range 0 to -33 kPa the simulated plate water content remained very nearly saturated while conductivity remained close to measured K_p (Table 6.3).

The only input data required to run this model are

1) core dimensions;
2) core retentivity parameters a, b, θ_s and θ_r;
3) plate thickness and conductivity;
4) initial and final matric potentials at the plate surface;
5) log K_s range and interval;
6) values of the tortuosity factor p.

The simulations were usually performed for K_s values of 10^2, 10^3, 10^4 and 10^5 mm/d. The program allows for several p values to be specified, in which case outflow or inflow is simulated for all combinations of p

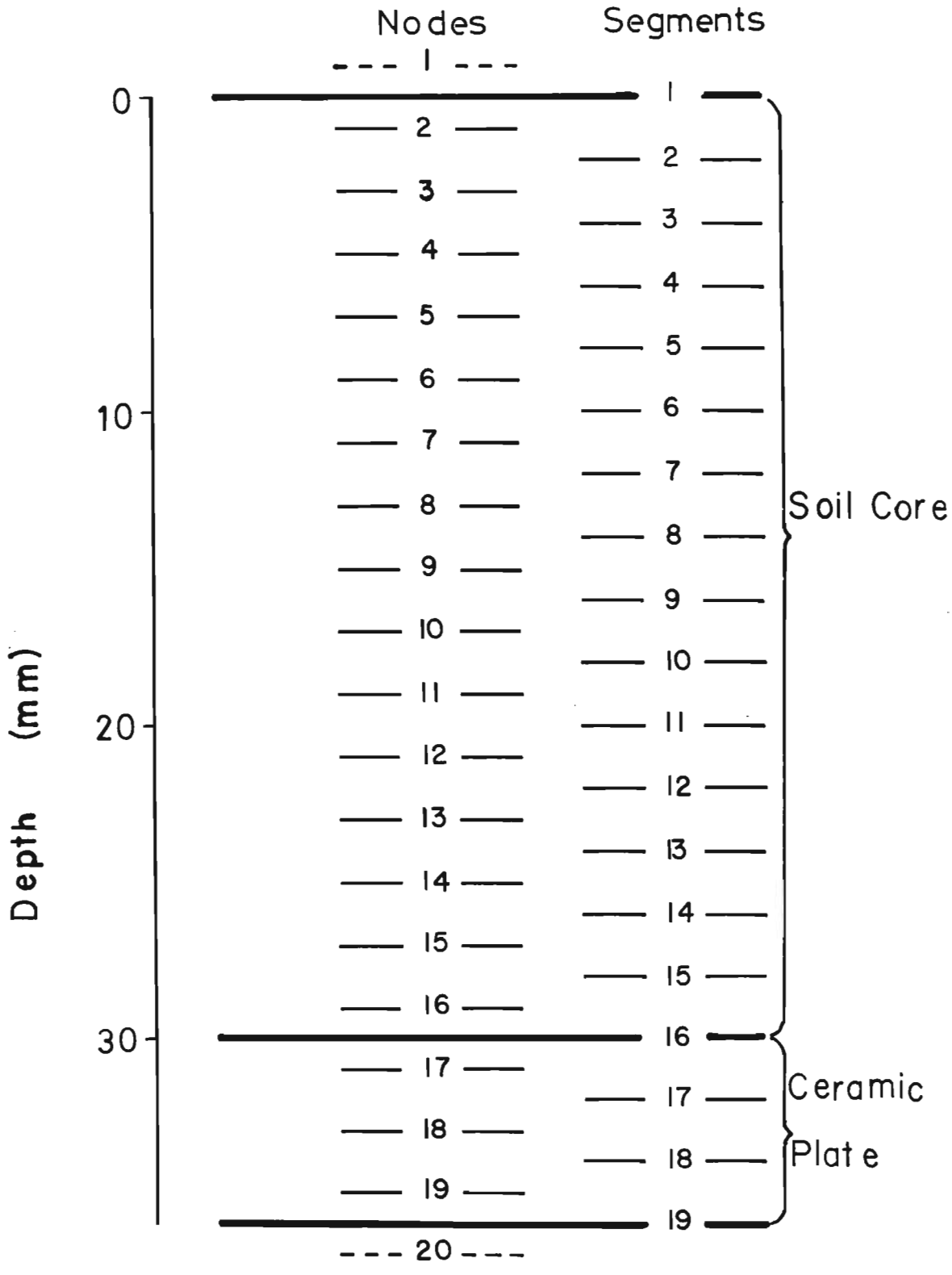

FIGURE 6.3 Subdivision of soil core and ceramic plate into segments for finite difference simulation of water outflow and inflow

TABLE 6.3 Retentivity and conductivity characteristics of simulated ceramic plate ($a = -1 \times 10^4$ mm; $b = 10$; $\theta_s = 0,3$ m/m; $\theta_r = 0$)

ψ kPa	θ m/m	K_r
0	0,3000	1,000
-10	0,2999	0,995
-20	0,2998	0,983
-30	0,2995	0,961

and K_s. In this work a constant value of 1 was assigned to p.

6.3.3 Data processing

The steps involved in assessing $K(\theta)$ were:

1) calculation of core water contents at each equilibrium matric potential;
2) values for the retentivity parameters $\underline{a}$, $\underline{b}$ and θ_r were obtained by fitting Eq. 6.1 to the measured retentivity values;
3) simulation of outflow or inflow for each of four K_s values, assuming p = 1; the time required for half the total water content change to occur, $t_{\frac{1}{2}}$, was calculated in the program;
4) plotting measured outflow or inflow volume against log time to obtain a measured $t_{\frac{1}{2}}$ value;
5) plotting simulated $t_{\frac{1}{2}}$ against K_s to determine an interpolated K_s value corresponding to the measured $t_{\frac{1}{2}}$ value, provided the magnitude of the plate resistance did not mask the effect of K_s;
6) calculation of $K(\theta)$ over the relevant matric potential range using the interpolated K_s value and Eq. 6.2;
7) for demonstration purposes outflow and inflow was simulated for one core using the interpolated K_s values, measured plate conductivity and a high plate conductivity of 150 mm/d. Passioura's (1976) method of calculating conductivity was applied to the best-fit simulated and measured outflow curves for this core. A computer program was written to calculate $K(\theta)$ and $K(\psi)$ according to Passioura (1976) and Jaynes and Tyler (1980). Their graphical method of estimating θ at the upper surface of the core from $\bar{\theta}$ was replaced by a computer routine. The program is listed in Appendix 3.

6.4 RESULTS AND DISCUSSION

Core dimensions, measured plate conductivities and retentivity parameters for the ten cores are listed in Table 6.4. Measured and fitted retentivity data are plotted for core AS (Fig. 6.4). For these cores an almost perfect fit of the retentivity function to the measured retentivity points was obtained. A good fit is desirable so that the simulated inflow or outflow volumes will be similar to those measured.

Simulated $t_{\frac{1}{2}}$ values, measured $t_{\frac{1}{2}}$ and the interpolated best-fit K_s value are listed in Table 6.5 for each of four K_s values, and the two pressure potential ranges over which both outflow and inflow were measured. An example of a computer simulation is shown in Table 6.6 for core AS. Measured and simulated outflow (Fig. 6.5) and inflow (Fig. 6.6) curves for core AS show the displacement dependent on the values of K_s and K_p and the agreement between measured outflow or inflow and that simulated using the best-fit K_s values.

The match between measured outflow or inflow and the best-fit simulated curve is generally good, with the exception of the inflow curve between matric potentials of -30 and -10 kPa possibly owing to an inaccurate assessment of equilibrium. Plate impedance generally prevented discrimination of K_s effects on outflow between -3 and -10 kPa, but inflow from -10 kPa to -3 kPa was not affected to the same extent. This can be ascribed to the difference between K_p and soil K at the start of outflow or inflow. At the start of outflow, at -3 kPa, soil K is higher than K_p and the plate controls outflow. At the start of inflow, at -10 kPa, soil K is low and the soil controls the rate of absorption. Towards the final stages of inflow, soil K increases, but potential gradients are low and the plate offers negligible resistance to the resulting low flow rates.

TABLE 6.4 Dimensions and retentivity parameters of Shorrocks cores and hydraulic conductivity K_p of ceramic plates

Core	Diameter	Depth	Retentivity parameters								K_p
			desorption				absorption				
	mm	mm	$\underline{a}$ mm	$\underline{b}$	θ_s m/m	θ_r	$\underline{a}$ mm	$\underline{b}$	θ_s m/m	θ_r	mm/day
JL	85,5	30	-133,0	0,837	0,5360	0,1220	-101,7	0,796	0,5360	0,1259	2,14
FL	85,5	30	-126,6	0,827	0,5327	0,1139	- 94,4	0,815	0,5327	0,1168	0,90
DL	85,5	30	-117,6	0,863	0,5510	0,1172	- 96,7	0,765	0,5510	0,1223	0,50
ES	54	30	-107,1	0,912	0,5562	0,1088	- 94,7	0,774	0,5562	0,1150	1,70
FS	54	30	-152,6	0,778	0,5136	0,1253	- 94,0	0,906	0,5136	0,1256	1,20
KS	54	30	-138,3	0,805	0,5300	0,1100	-104,0	0,788	0,5300	0,1132	1,20
GS	54	30	-142,8	0,787	0,5294	0,1203	-102,9	0,796	0,5294	0,1228	0,70
AS	54	30	-147,6	0,802	0,5174	0,1200	- 98,8	0,860	0,5174	0,1217	0,60
NS	54	30	-136,5	0,810	0,5277	0,1126	-100,9	0,807	0,5277	0,1153	0,53
JS	54	30	-133,8	0,815	0,5309	0,1216	- 98,2	0,822	0,5309	0,1241	0,50

TABLE 6.5 Simulated $t_{\frac{1}{2}}$ values for each of four K_s values and K_s value corresponding to measured $t_{\frac{1}{2}}$ listed for two inflow ranges (* indicates that plate impedance masked soil K)

	Outflow: -3 to -10 kPa						Outflow: -10 to -30 kPa					
Cores	Simulated $t_{\frac{1}{2}}$ (days) for K_s (mm/d) values of				Measured $t_{\frac{1}{2}}$ days	Best-fit K_s mm/d	Simulated $t_{\frac{1}{2}}$ (days) for K_s (mm/d) values of				Measured $t_{\frac{1}{2}}$ days	Best K_s mm/
	10^2	10^3	10^4	10^5			10^2	10^3	10^4	10^5		
JL	0,470	0,502	0,010	0,007	0,010	*	>4	3,125	0,301	0,030	0,386	7 9
FL	0,620	0,069	0,019	0,016	0,018	*	>4	>4	0,408	0,041	0,407	10 0
DL	0,766	0,090	0,031	0,028	0,052	2 500	>4	>4	0,440	0,045	0,389	11 5
ES	0,972	0,100	0,015	0,008	0,011	*	>4	>4	0,396	0,040	0,272	14 6
FS	0,304	0,037	0,015	0,014	0,014	*	>4	1,880	0,184	0,019	0,323	5 8
KS	0,552	0,059	0,015	0,013	0,015	*	>4	4,0	0,396	0,040	0,404	9 8
GS	0,436	0,056	0,024	0,023	0,033	2 700	>4	2,717	0,263	0,027	0,344	7 6
AS	0,349	0,051	0,028	0,026	0,026	*	>4	2,013	0,197	0,020	0,131	15 1
NS	0,479	0,064	0,030	0,028	0,048	1 750	>4	3,473	0,332	0,034	0,342	9 7
JS	0,519	0,068	0,031	0,029	0,040	3 000	>4	2,926	0,281	0,029	0,357	7 9

	Inflow: -30 to -10 kPa						Inflow: -10 to -3 kPa					
Cores	Simulated $t_{\frac{1}{2}}$ (days) for K_s (mm/d) values of				Measured $t_{\frac{1}{2}}$ days	Best-fit K_s mm/d	Simulated $t_{\frac{1}{2}}$ (days) for K_s (mm/d) values of				Measured $t_{\frac{1}{2}}$ days	Best K_s mm/
	10^2	10^3	10^4	10^5			10^2	10^3	10^4	10^5		
JL	>4	>4	0,579	0,064	0,505	11 500	0,864	0,136	0,041	0,018	0,043	9 3
FL	>4	>4	0,703	0,084	0,499	14 100	1,171	0,214	0,071	0,035	0,075	8 9
DL	>4	>4	1,030	0,125	0,668	15 800	1,497	0,313	0,110	0,059	0,338	8
ES	>4	>4	0,919	0,102	0,615	14 000	1,352	0,203	0,055	0,024	0,069	6 1
FS	>4	2,761	0,301	0,039	0,502	5 800	0,749	0,142	0,048	0,025	0,062	5 3
KS	>4	>4	0,648	0,071	0,713	9 050	0,964	0,169	0,054	0,028	0,077	4 3
GS	>4	2,717	0,496	0,065	0,508	9 700	0,952	0,205	0,079	0,044	0,134	2 7
AS	>4	3,198	0,360	0,051	0,217	16 500	0,866	0,200	0,080	0,047	0,076	12 0
NS	>4	3,473	0,571	0,076	0,547	11 000	1,059	0,241	0,096	0,055	0,179	1 8
JS	>4	2,926	0,500	0,070	0,580	8 600	1,075	0,245	0,098	0,056	0,138	4 2

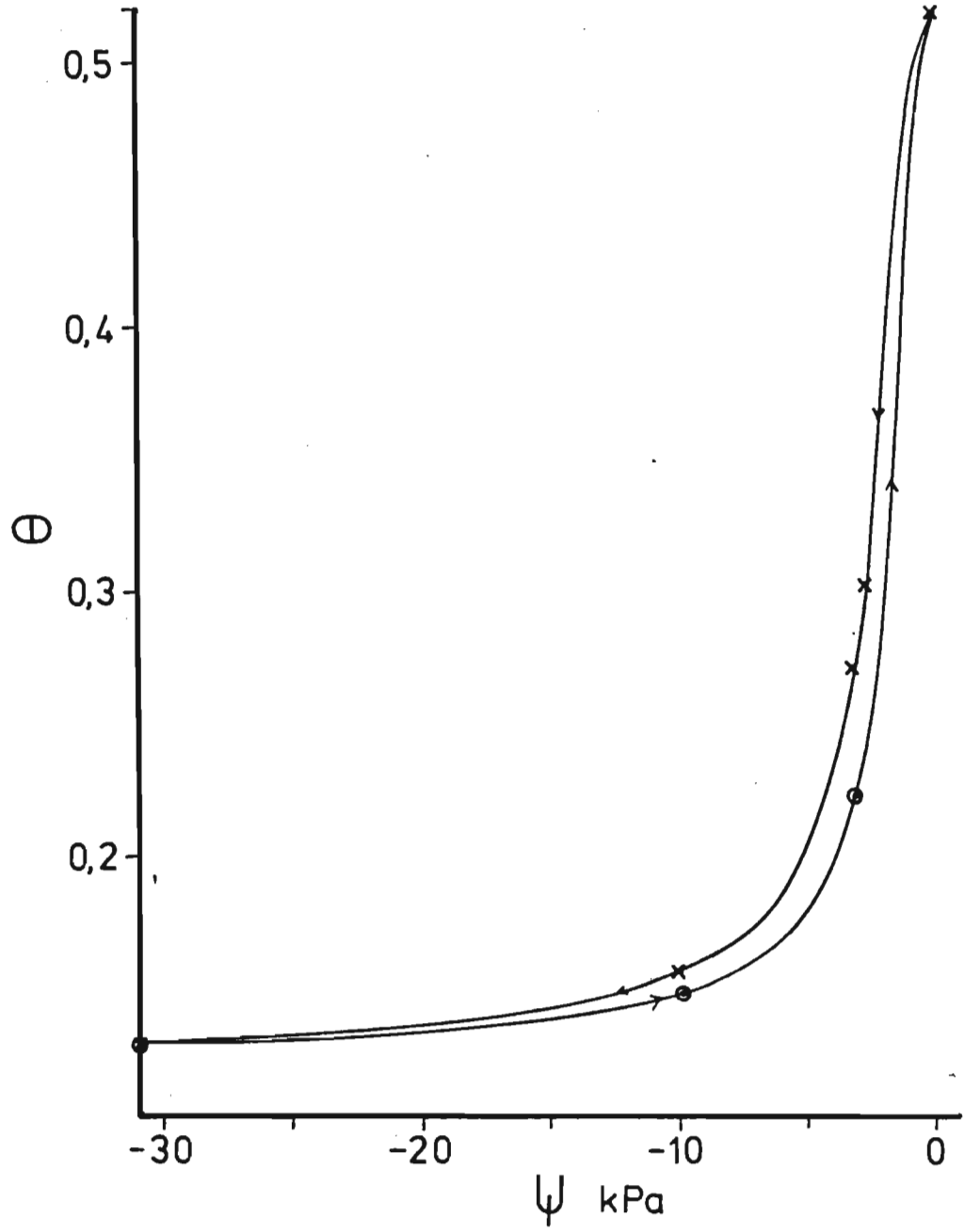

FIGURE 6.4 Measured retentivity values for core AS during desorption (x) and absorption (0). Solid lines represent fitted retentivity function

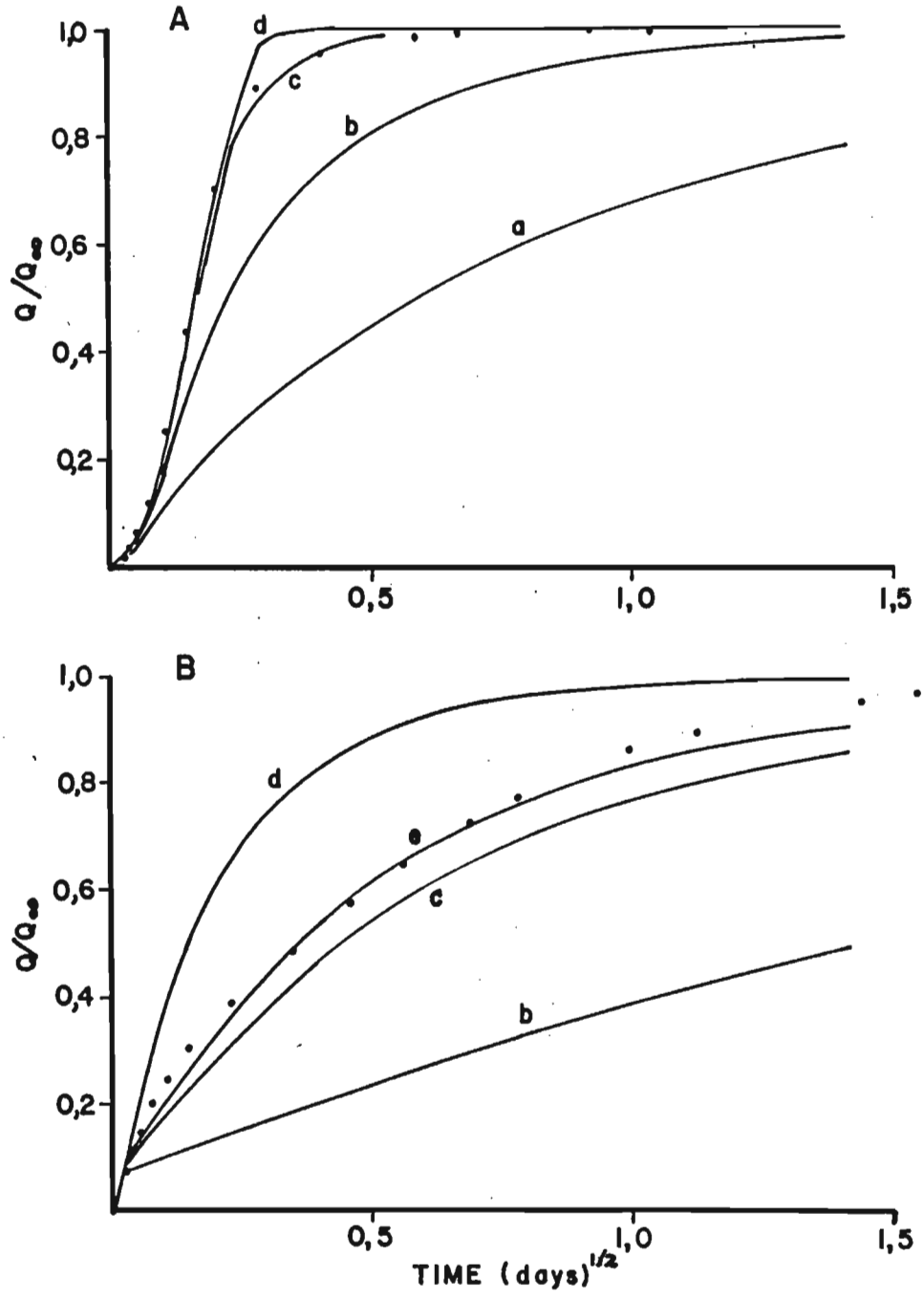

FIGURE 6.5 Measured (·) and simulated (—) outflow data for core AS between -3 and -10 kPa (A) and -10 and -30 kPa (B). K_p was 0,6 mm/d. K_s values used in simulations are indicated as: 10^2 mm/d(a), 10^3 mm/d(b), 10^4 mm/d(c), 10^5 mm/d(d) and best-fit value (e)

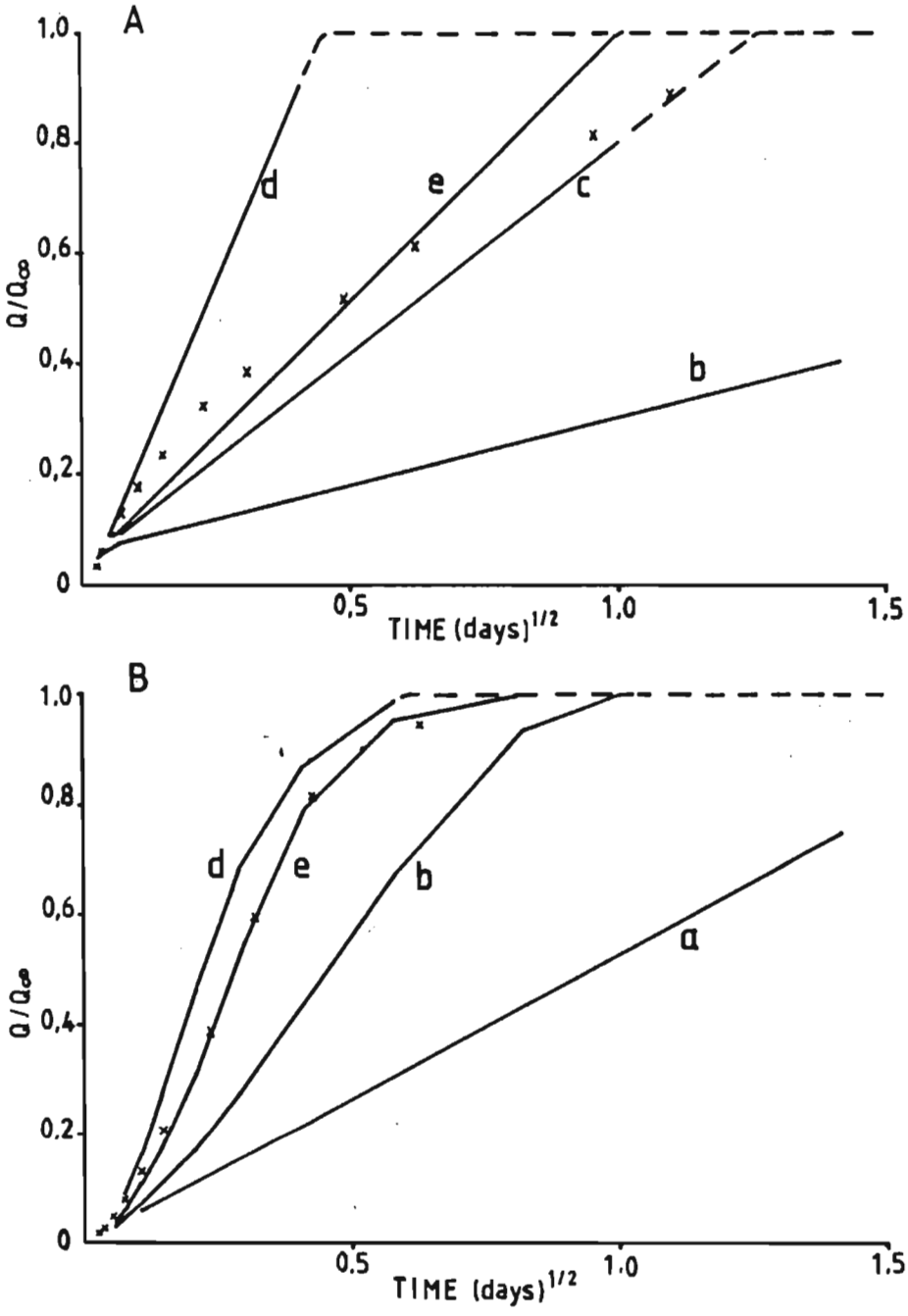

FIGURE 6.6 Measured (x) and simulated (solid lines) inflow data for core AS between -30 and -10 kPa (A) and -10 and - 3 kPa (B). Plate conductivity was 0,6 mm/d. K_s values used in simulations are indicated as 10^2 mm/d(a), 10^3 mm/d(b), 10^4 mm/d(c), 10^5 mm/d(d) and best-fit value (e)

$K(\psi)$ relationships over each pressure potential range are shown for both outflow (Fig. 6.7) and inflow (Fig. 6.8) and were calculated by substituting the retentivity parameters of Table 6.4, a p value of one and the best-fit K_s value into Eq. 6.3. The calculated $K(\theta)$ relationship (Eq. 6.2) is plotted for core AS only (Fig. 6.9). If Eq. 6.1 and Eq. 6.2 were valid over the total measurement range of -3 to -30 kPa then $K(\psi)$ would be continuous across the -10 kPa boundary and the best-fit K_s values would be identical for the -3 to -10 kPa and -10 to -30 kPa segments. This is nearly true for cores AS and FS while cores DL and NS show the greatest deviation. For most modelling purposes the use of a mean K_s value is usually adequate, although for more accurate work both K_s and p may be varied for a better fit between measured and simulated data.

Comparison of Fig. 6.7 (desorption data) with Fig. 6.8 (absorption data) shows a considerable hysteresis effect. $K(\psi)$ values obtained during desorption are in all cases higher than those determined during absorption. Hysteresis of $K(\theta)$ is less pronounced (Fig. 6.9 for AS.

As a demonstration of the water distribution pattern within cores during outflow and inflow, simulated data for core AS are plotted in Figs. 6.10 to 6.13. The data were obtained using the best-fit K_s values. Two plate conductivity values were compared, namely the measured value of 0,6 mm/d and a very high value of 150 mm/d corresponding to negligible plate impedance. Outflow between -3 and -10 kPa was almost completely controlled by plate conductivity at a K_p value of 0,6 mm/d, whereas at a K_p value of 150 mm/d the lower node of the core reached the final potential very quickly, outflow being controlled by the conductivity distribution through the core. Between -10 and -30 kPa plate conductivity had no influence on water content distribution in the core.

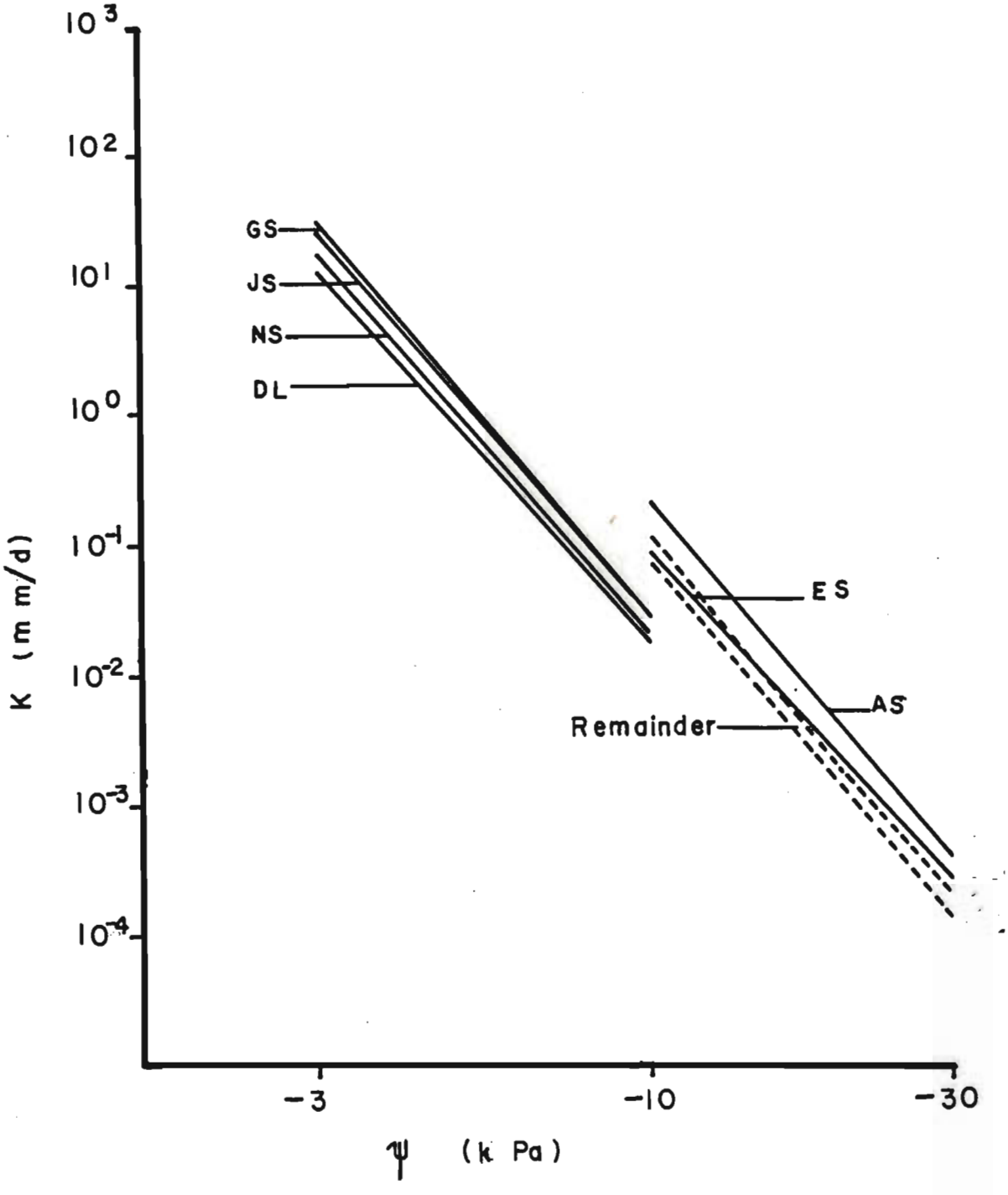

FIGURE 6.7 Predicted hydraulic conductivities (K) for the pressure potential ranges -3 to -10 kPa and -10 to -30 kPa, calculated from Eq. 6.3 using fitted retentivity parameters and K_s values estimated from outflow data. Soil cores coded according to Table 6.4

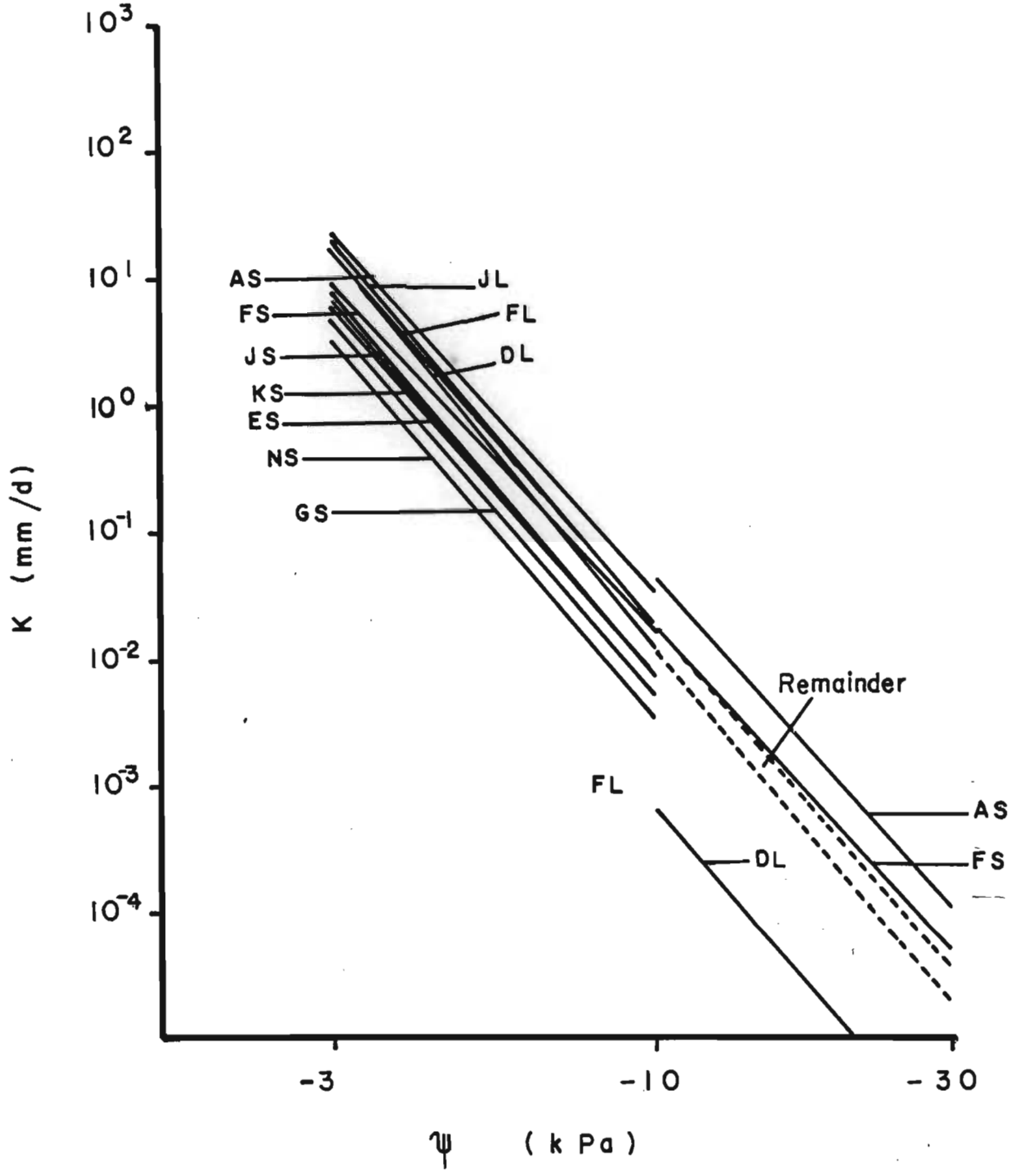

FIGURE 6.8 Predicted hydraulic conductivities (K) for the pressure potential ranges - 3 to -10 kPa and -10 to -30 kPa, calculated from Eq. 6.3, using fitted retentivity parameters and K_s values estimated from inflow data. Soil cores coded according to Table 6.4

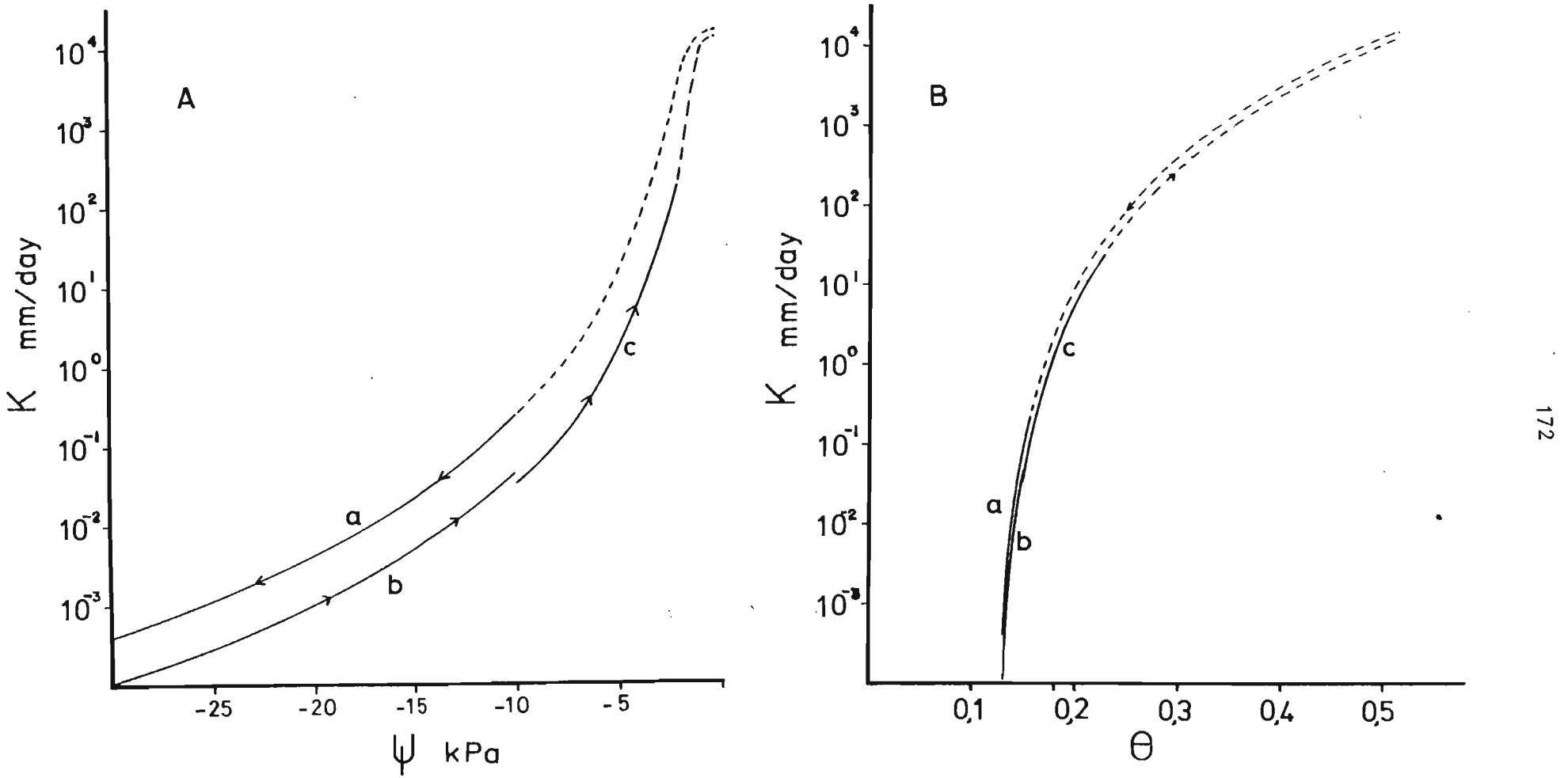

FIGURE 6.9 Conductivity relationships for core AS. $K(\psi)$ curves (A) calculated using Eq. 6.3 and $K(\theta)$ curves (B) using Eq. 6.2, together with fitted retentivity data and K_s values estimated from outflow and inflow data. Corresponding θ and ψ ranges used for K estimation (—) designated as a (outflow from -10 to -30 kPa),

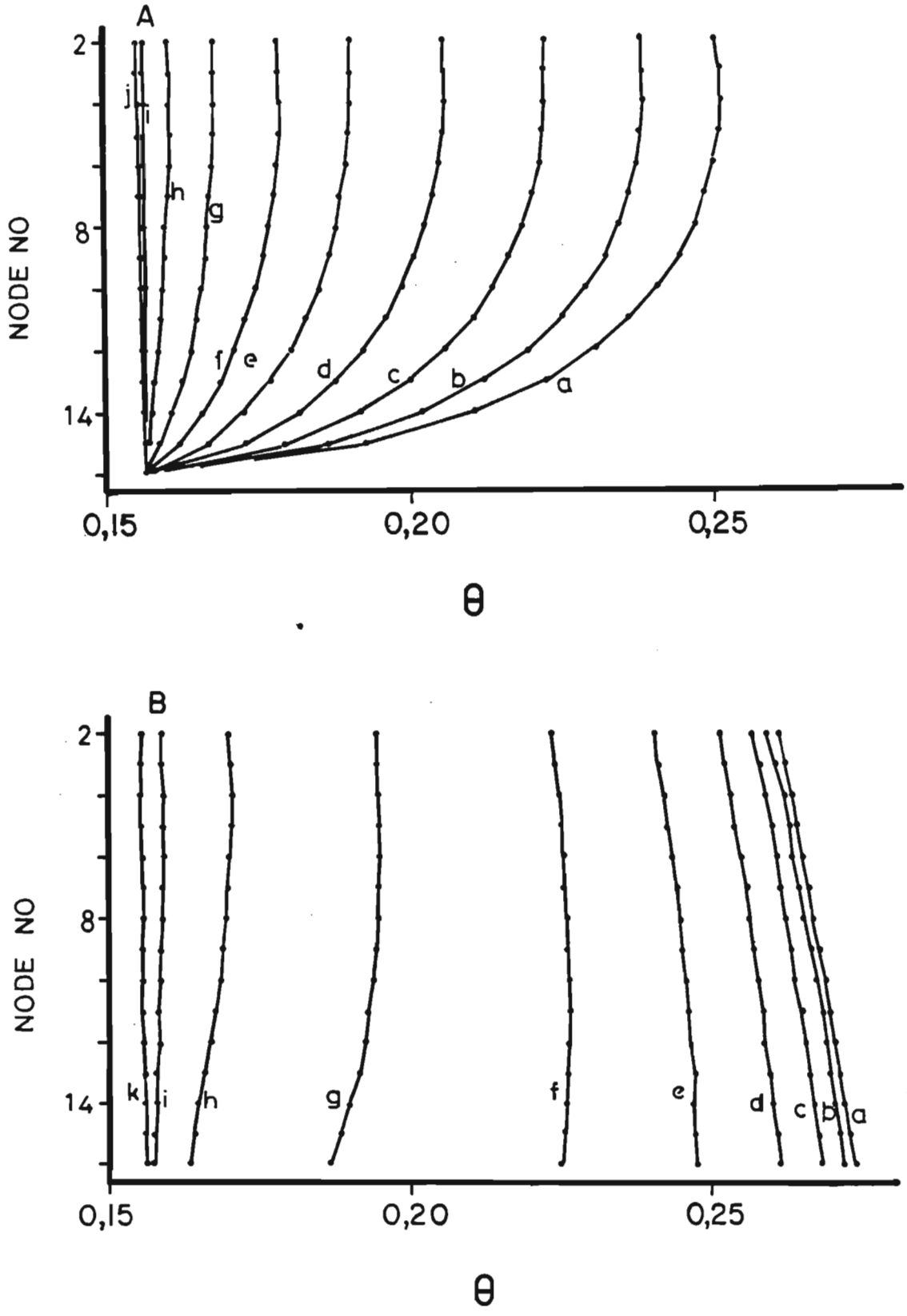

FIGURE 6.10 Simulated water content (θ) distributions through core AS during outflow between -3 and -10 kPa for each of two plate conductivities, 150 mm/d (A) and 0,6 mm/d (B). Elapsed time is indicated as: 1 min (a), 2 min (b), 4 min (c), 8 min (d), 16 min (d), 30 min (f), 1 hour (g), 2 hours (h), 4 hours (i),

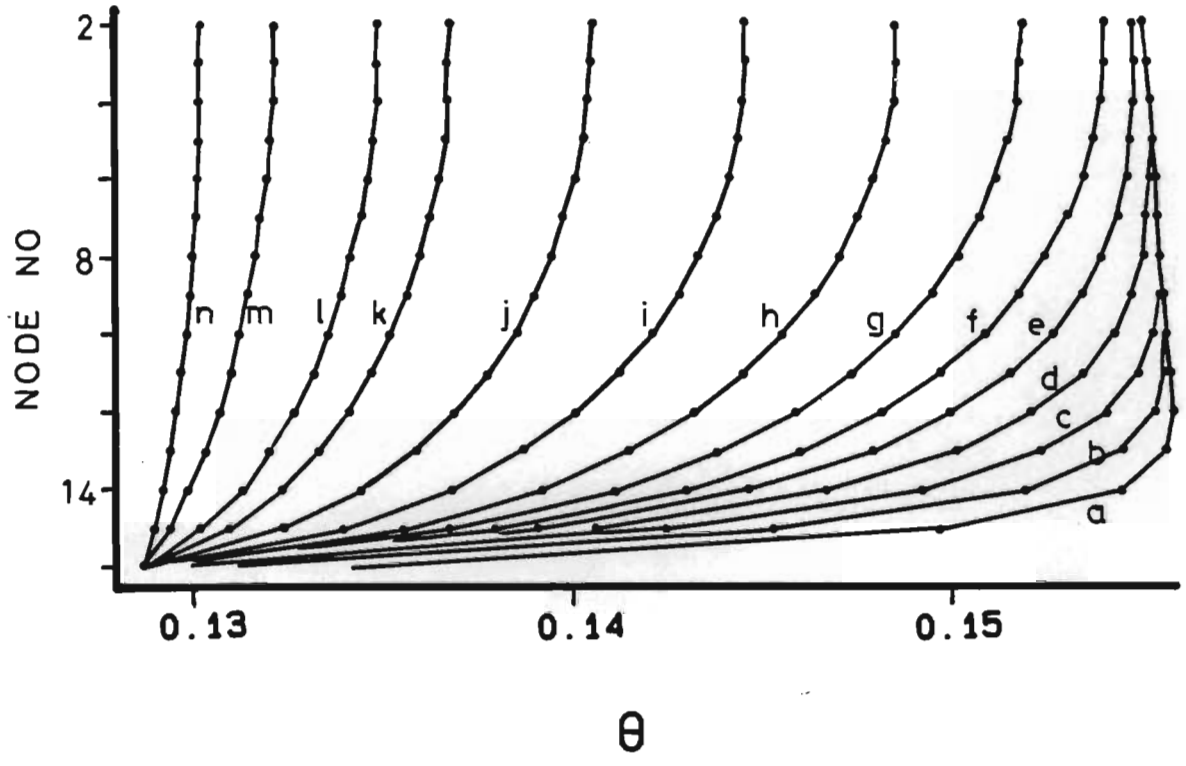

FIGURE 6.11 Simulated water content (θ) distributions through core AS during outflow between -10 and -30 kPa, with negligible plate impedance effects. Elapsed times as for Fig. 6.10 with the addition of 1 day (l), 2 days (m) and 4 days (n)

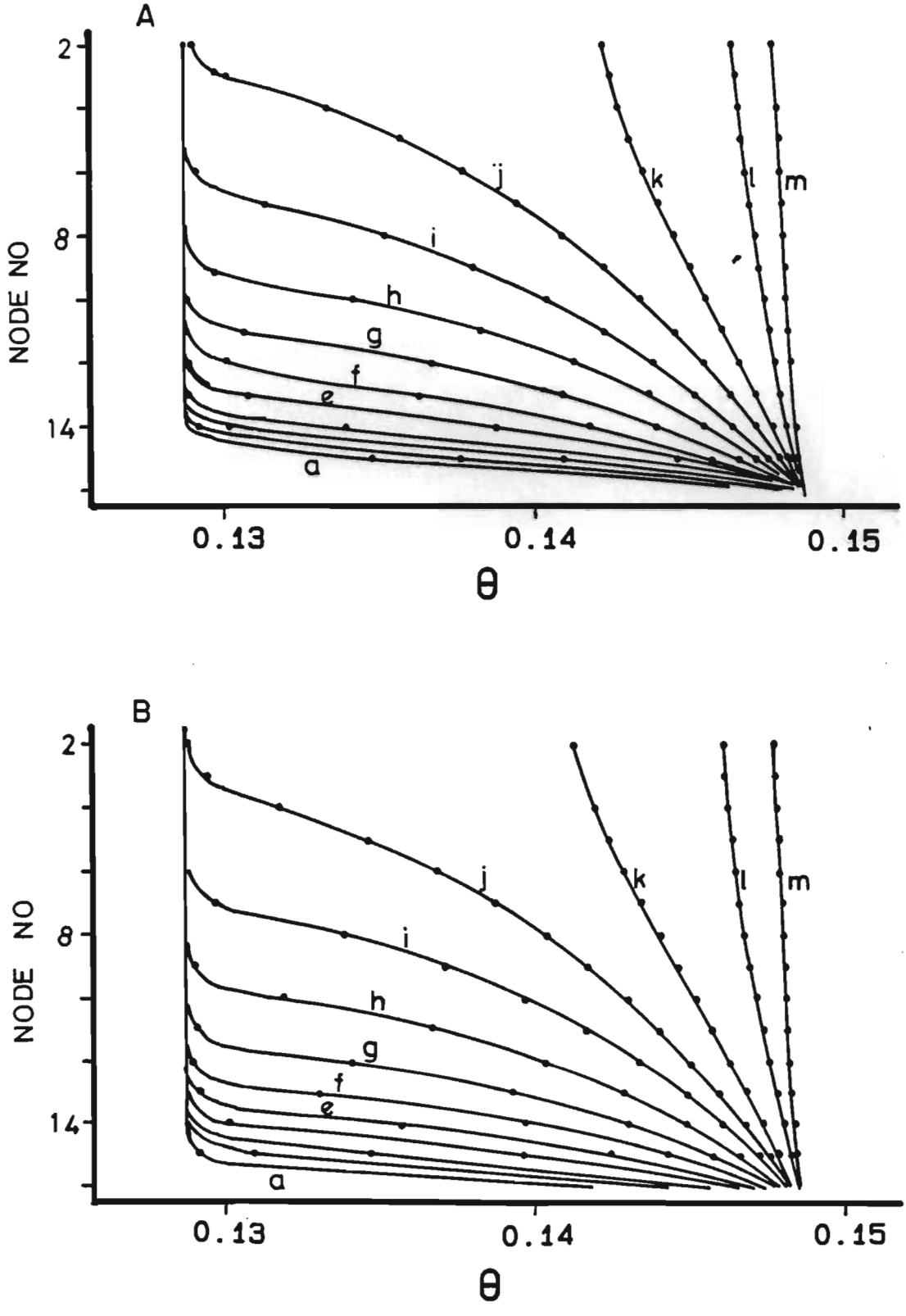

FIGURE 6.12 Simulated water content (θ) distributions through core AS during inflow between -30 and -10 kPa for each of two plate conductivities, 150 mm/d (A) and 0,6 mm/d (B). Elapsed times as for Figs. 6.10 and 6.11

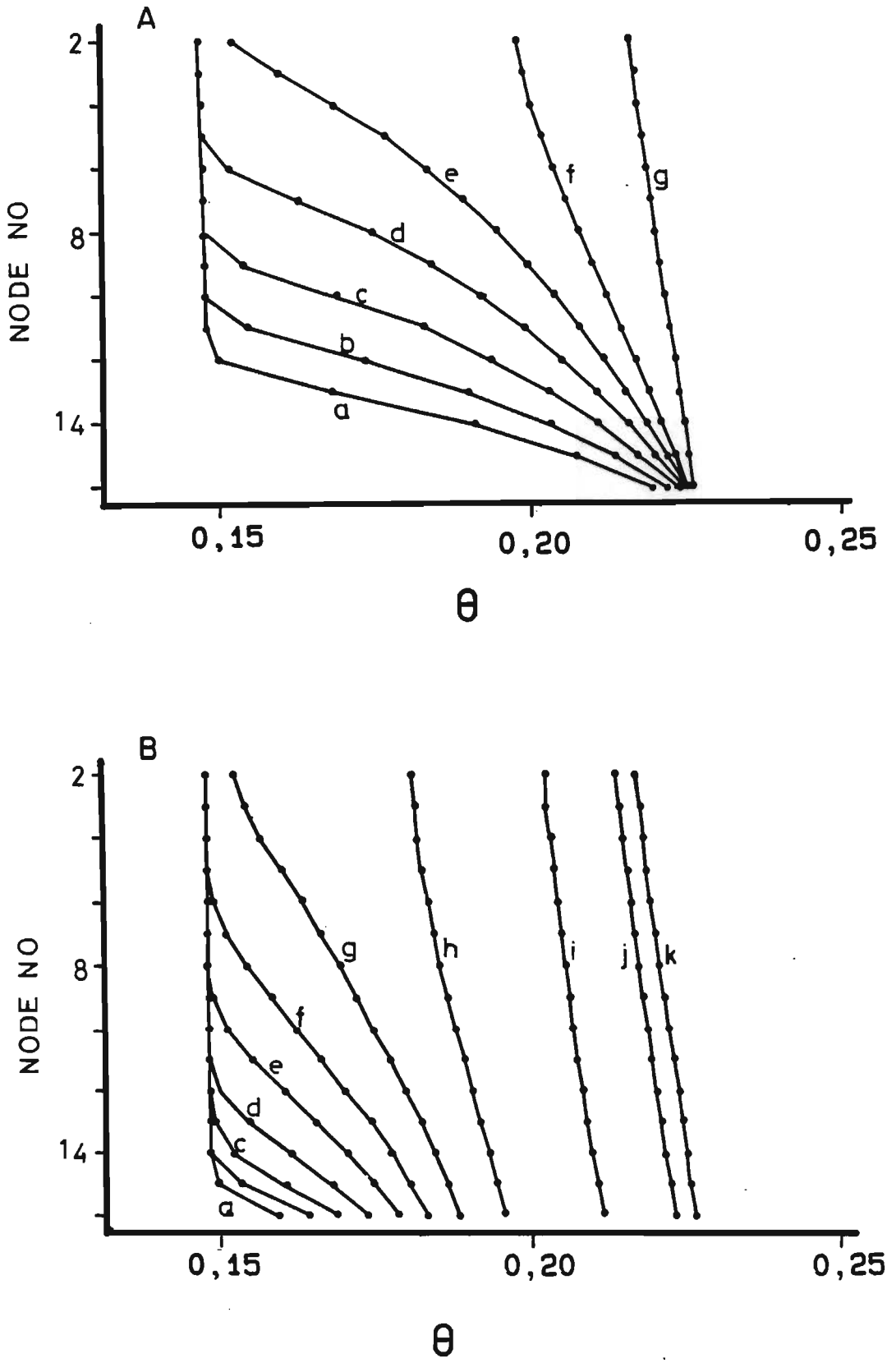

FIGURE 6.13 Simulated water content (θ) distributions through core AS during inflow between -10 and -3 kPa for each of two plate conductivities, 150 mm/d (A) and 0,6 mm/d (B). Elapsed times

There is a small but significant gradient of water content in the cores, which is more pronounced at higher potentials. At equilibrium, the matric potential at the surface of a 30 mm core is about 0,3 kPa less than that at the plate surface. For core AS at -3,02 kPa and using desorption curves, K is 23,1 mm/d and θ is 0,252 while at -3,31 kPa K falls to 14 mm/d and θ to 0,2146. One of the advantages of this method is that no assumptions need be made regarding the distributions of K, θ or diffusivity through the core. The analytical methods of calculating conductivity from outflow data depend upon such assumptions, which become less valid as core length and θ increases. $K(\psi)$ values for core AS, using Passioura's method, designated K(Passioura), are compared to K(simulated) values which were used in the best-fit outflow simulation (Fig. 6.14). K(simulated) values, the solid line in Fig. 6.14, were calculated according to Eq. 6.3 using K_p = 15 100 mm/d. The outflow curves to which Passioura's method was applied, were

1) measured, -3 to -10 kPa;
2) measured, -10 to -30 kPa;
3) simulated, -3 to -10 kPa, K_p = 0,6 mm/d;
4) simulated, -3 to -10 kPa, K_p = 150 mm/d;
5) simulated, -10 to -30 kPa, K_p = 0,6 mm/d.

K(Passioura) values calculated from simulated outflow curves were similar to those calculated from measured outflow curves, providing that the measured K_p value (0,6 mm/d) was used in the simulations. Slight differences in shape between measured and best-fit simulated outflow curves (Figs. 6.5 and 6.6) caused negligible differences in K(Passioura) values.

The validity of Passioura's method can be judged by comparing K(Passioura) values to K(simulated) values. Outflow between -3 and

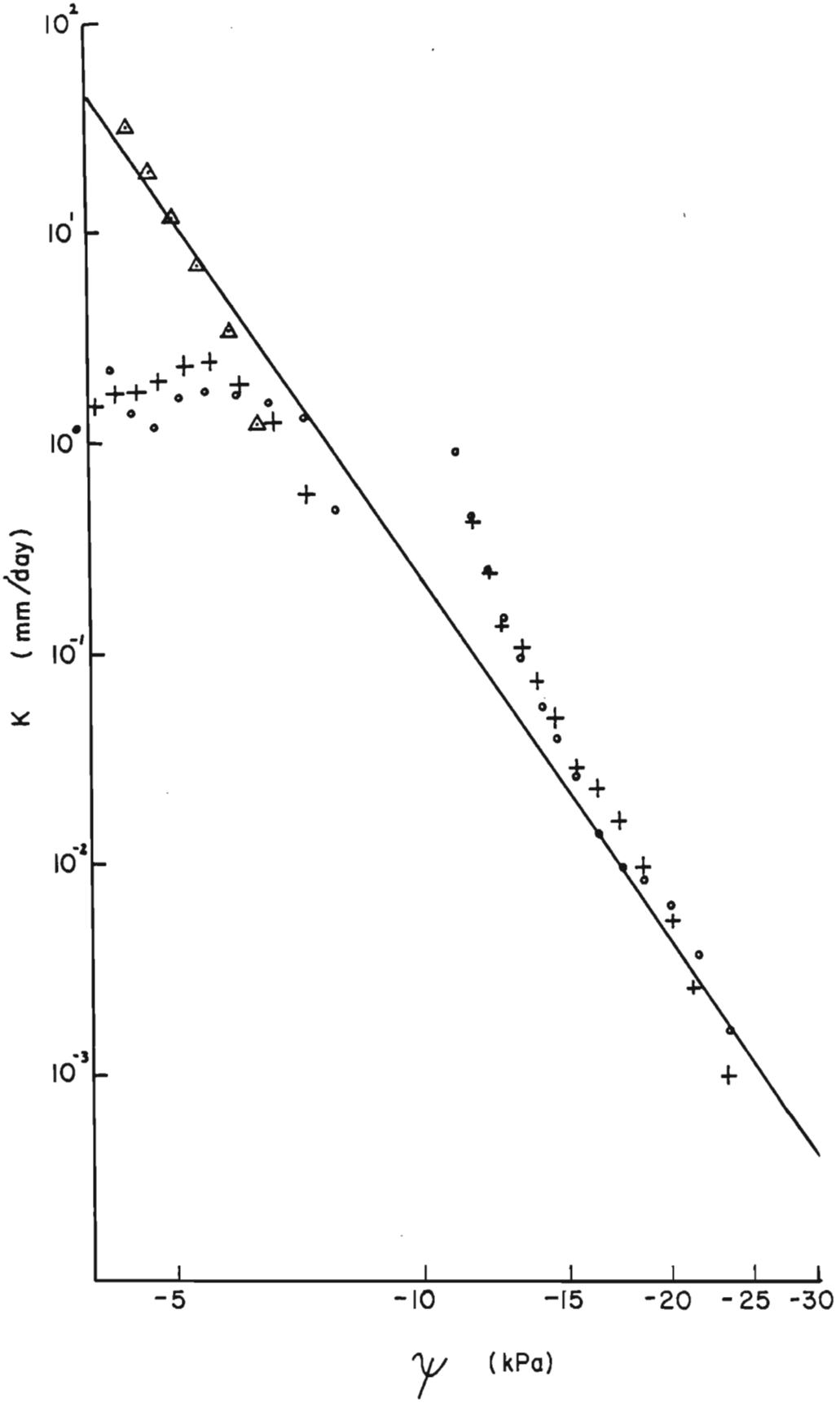

FIGURE 6.14 $K(\psi)$ for core AS calculated according to: 1) Eq. 6.3 with K_s = 15100 mm/d (solid line); 2) Passioura's method applied to measured outflow curves (o) and 3) Passioura's method applied to simulated outflow curve using Eq. 6.3,

-10 kPa was controlled by the ceramic plate when K_p = 0,6 mm/d, thus the requirements for Passioura's method are not met. Only at -7 kPa do the K(Passioura) values show the same trend as the K(simulated) line. K(Passioura) calculated from an outflow curve simulated for negligible plate impedance (K_p = 150 mm/d) matched the K(simulated) line closely but not exactly, being too high at potentials above -5 kPa and too low at lower potentials.

Between -10 and -30 kPa plate impedance (at K_p = 0,6 mm/d) was negligible but K(Passioura) values matched the K(simulated) line over the centre of the ψ range only. Deviations are probably caused by the fact that the water content distribution pattern through the core does not remain constant (Fig. 6.12) as is assumed in Passioura's method. Longer cores and higher pressure increments should improve the range of ψ values over which Passioura's method is valid.

The results recorded here were obtained using laboratory packed cores. Good contact between core and plate was ensured by packing the soil directly onto the plate. Core samples from the field could be used but good contact between core and plate is essential. This can be accomplished by using a contact material, such as diatomaceous earth, which has high retentivity coupled with high conductivity in the matric potential range 0 to -30 kPa. Contact between core and plate may be evaluated by comparing simulated and measured outflow for a short initial period; the initial 60 seconds is suitable. At high potentials, when plate impedance determines outflow, measured and simulated results should be similar. Any sources of impedance additional to that of the plate will reduce measured outflow. There is no reason why a similar approach should not be used for field determinations of $K(\psi)$. All that is required is a defined situation in which the movement and distribution of water can be simulated and

measured. Prior simulations using a range of estimated K_s values will show whether measurement of K using the intended experimental procedure will be feasible or not.

CHAPTER 7

APPLICATION OF THE SIMULATION MODEL

7.1 INTRODUCTION

The aim of this chapter is to show how retentivity parameters and conductivity can be estimated and then applied to a soil water simulation model. It is assumed that measured retentivity and conductivity data are not available, hence estimation is a prerequisite. The example taken is the simulation of the water regime in a lysimeter tank.

Three weighing lysimeters are installed at the Sundays River Research Station, Addo, Cape Province as described by Green and Bruwer (1979). Each lysimeter contains a mature citrus tree (Citrus sinensis, var. Valencia). During November 1981 a combined Israeli-South African workshop on water relations of citrus orchards was held at Addo (Green and Fuchs, 1982) during which the soils were sampled, particle size distribution measured and root distribution estimated. Owing to the restricted volume of the lysimeter tanks, their depth and the desirability of minimum soil disturbance it was not possible to take core samples for laboratory determination of retentivity and conductivity. Hydrological parameters required for the simulation model had therefore to be estimated.

There are two main aims in this chapter:

1) to show how data for the water flow model can be estimated from easily measured soil properties;
2) to compare simulated and measured water regimes and evaluate the initial parameter estimates.

7.2 PROCEDURE

7.2.1 Soil characterization

The relevant soil data for lysimeter B was extracted from the Israeli-South African Orchard Workshop data set. This consisted of particle size distributions of samples from several depths at each of three sampling points, the root concentration in each sample and some bulk density values measured at a nearby site in the orchard.

For modelling purposes values of the parameters $\underline{a}$, $\underline{b}$ and θ_s are required for each node in the profile. In this example, nodes were spaced at 50 mm intervals from the surface to 1800 mm, the depth of the lysimeter tank. Values of the parameters together with an estimate of saturated conductivity, K_s, were obtained as follows:

1) measured values of clay, silt and fine sand percentages were plotted against depth, and nodal values were obtained by interpolation;
2) nodal bulk density values were obtained in a similar way using field data;
3) water content (θ) values at pressure potentials of -1; -3; -10; -30 and -50 kPa were predicted for each node using the regression equations listed in Table 3.10;
4) water content at -1500 kPa was predicted using the third equation in Table 3.7;
5) the two-part retentivity function (Table 3.12) was fitted to the predicted $\theta(\psi)$ data using a least-squares technique described in 3.3.3.2, in order to obtain values for the parameters $\underline{a}$ and $\underline{b}$;
6) saturated conductivity, K_s, and K values at each pressure potential were calculated using the conductivity equation derived by combining the Childs and Collis-George capillary model with the two-part retentivity function (Table 4.2).

Steps (1) and (2) above were performed graphically, while steps (3) to (6) were combined in a computer program listed in Appendix 1.

7.2.2 Soil water simulation model

The model used is based upon that described in Chapter 1. The program and flowchart are discussed in Appendix 1. Briefly, the model consists of a data file, a program enabling examination of the input data and predicted retentivity and conductivity values, and a processing program. The model results may be printed in full or in a summarized form. A FORTRAN version, written for a Burroughs 7800 was used in this work but a version is available for Hewlett-Packard 9825 or 9826 desk-top computers, written in HPL.

7.2.3 Lysimeter measurements

Gains or losses of water were recorded daily. Resolution and accuracy of the weighing system correspond to a water content change of 0,15 mm over the surface of the lysimeter. Tensiometers were installed at 300 mm depth intervals and were read daily.

7.2.4 Simulations

Simulations for October 1981 were run using the estimated soil hydrological properties together with evapotranspiration, irrigation and rainfall data obtained from the lysimeter record. Since conductivity is the least reliable of the soil hydrological properties the simulation was performed for each of three matching factors (10^{-3}, 10^{-4} and 10^{-5}) with the estimated $K(\psi)$ data.

7.3 RESULTS AND DISCUSSION

Fig. 7.1 shows measured clay, silt and fine sand contents, and bulk density values for several depths in the lysimeter profile,

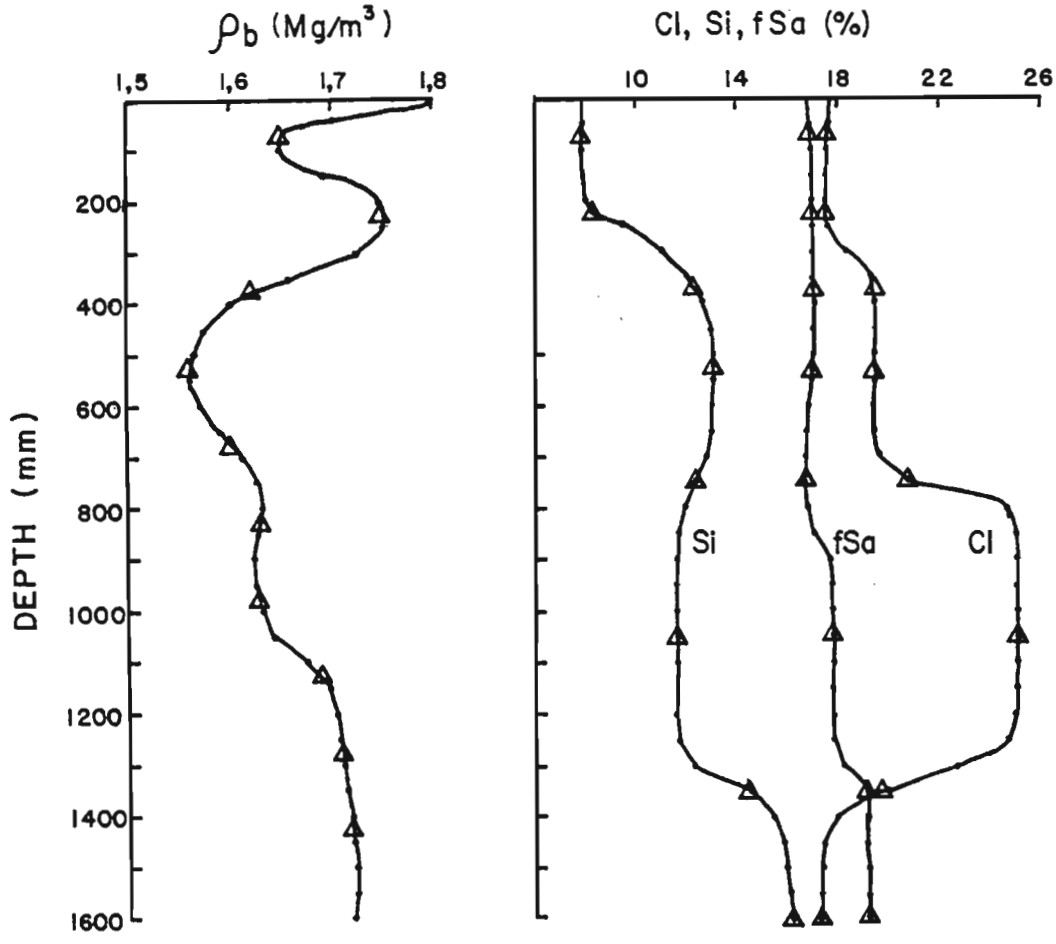

FIGURE 7.1 Measured clay, silt and fine sand contents and bulk density values for several depths in the lysimeter profile. Interpolated values for nodes are also shown

together with interpolated values from which nodal values were obtained. The nodal values are those for 50 mm depth intervals, starting at the surface. The interpolated lines are subjective and are intended to reflect layering which may have occurred during filling of the tanks. Bulk density values were measured in a field profile and do not necessarily correspond to the bulk density distribution in the lysimeter tanks. They are used to illustrate how a non-uniform bulk density profile is treated in the model. Surface bulk density was increased to 1,8 Mg/m^3 to represent a surface crust.

Nodal values of clay, silt and fine sand content and bulk density were substituted in a regression model to predict θ at six ψ values. Predicted nodal θ values at these potentials are shown in Fig. 7.2 as solid lines. Retention parameters *a* and *b* for each node, obtained by fitting the two-part retentivity function to the predicted $\theta(\psi)$ data, are plotted in Fig. 7.3. These two parameters, together with θ_s, calculated from bulk density, form the soil hydrological input data for the water flow model.

The fit of the two-part retentivity function to the predicted $\theta(\psi)$ data is indicated in Fig. 7.2 by means of dashed lines. Differences between the fitted function and the predicted $\theta(\psi)$ data are greatest at -10 to -30 kPa but do not exceed a θ value of 0,015. The textural features of the profile are reflected in both sets of data.

There are other ways in which retentivity parameters could have been obtained. The simplest way would be to assume a uniform profile, estimate average silt and clay contents and bulk density and obtain values of *a* and *b* by interpolation from Figs. 3.11, 3.12 or 5.5. Another method is to fit the retentivity function directly to measured $\theta(\psi)$ data, if available. The retentivity function can be made to fit more closely to measured or estimated retentivity data by including

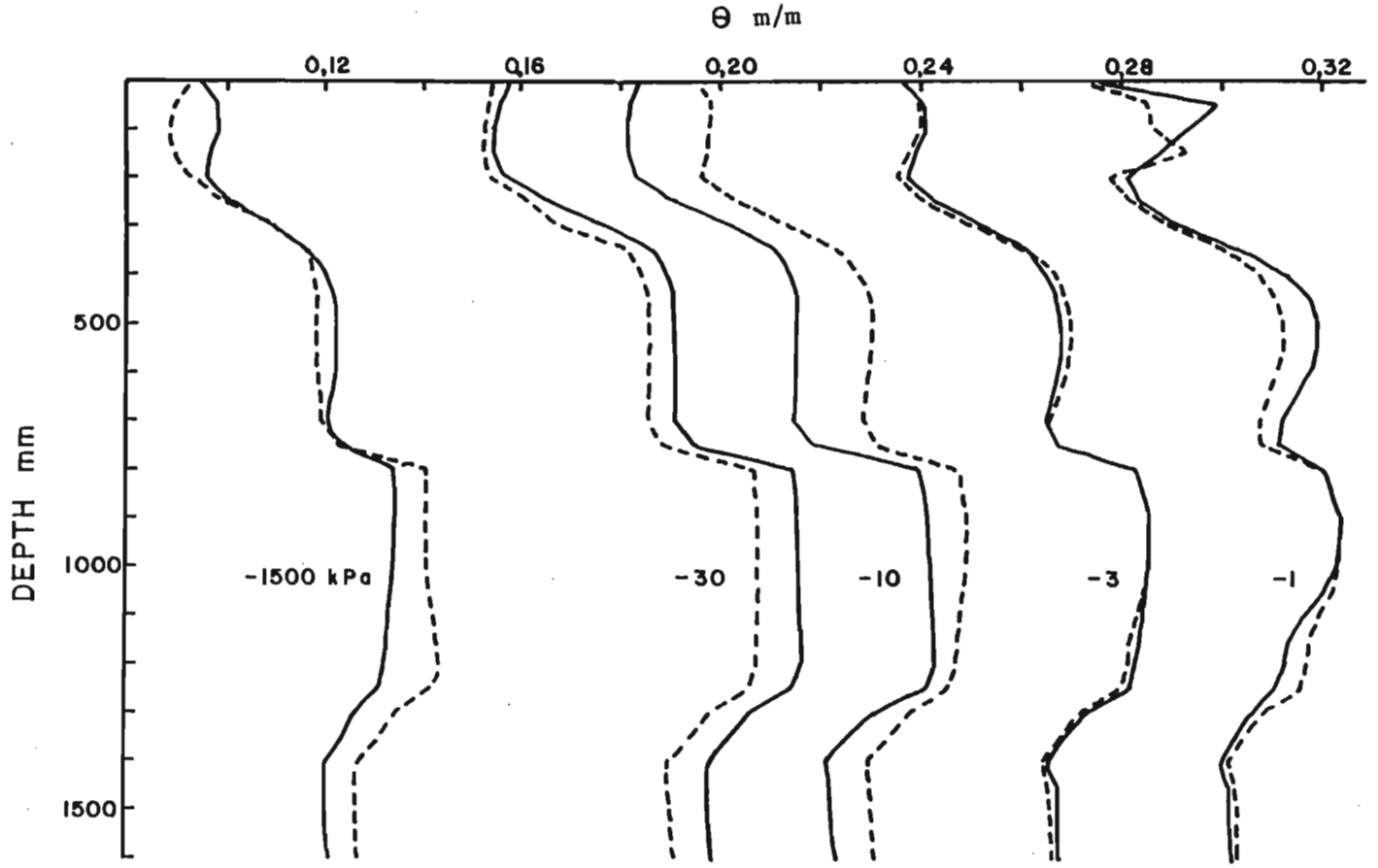

FIGURE 7.2 Predicted nodal values of θ at ψ_s values of -1500, -30, -10, -3 and -1 kPa (—)

Fit of two-part retentivity function to predicted $\theta(\psi)$ data is indicated (---)

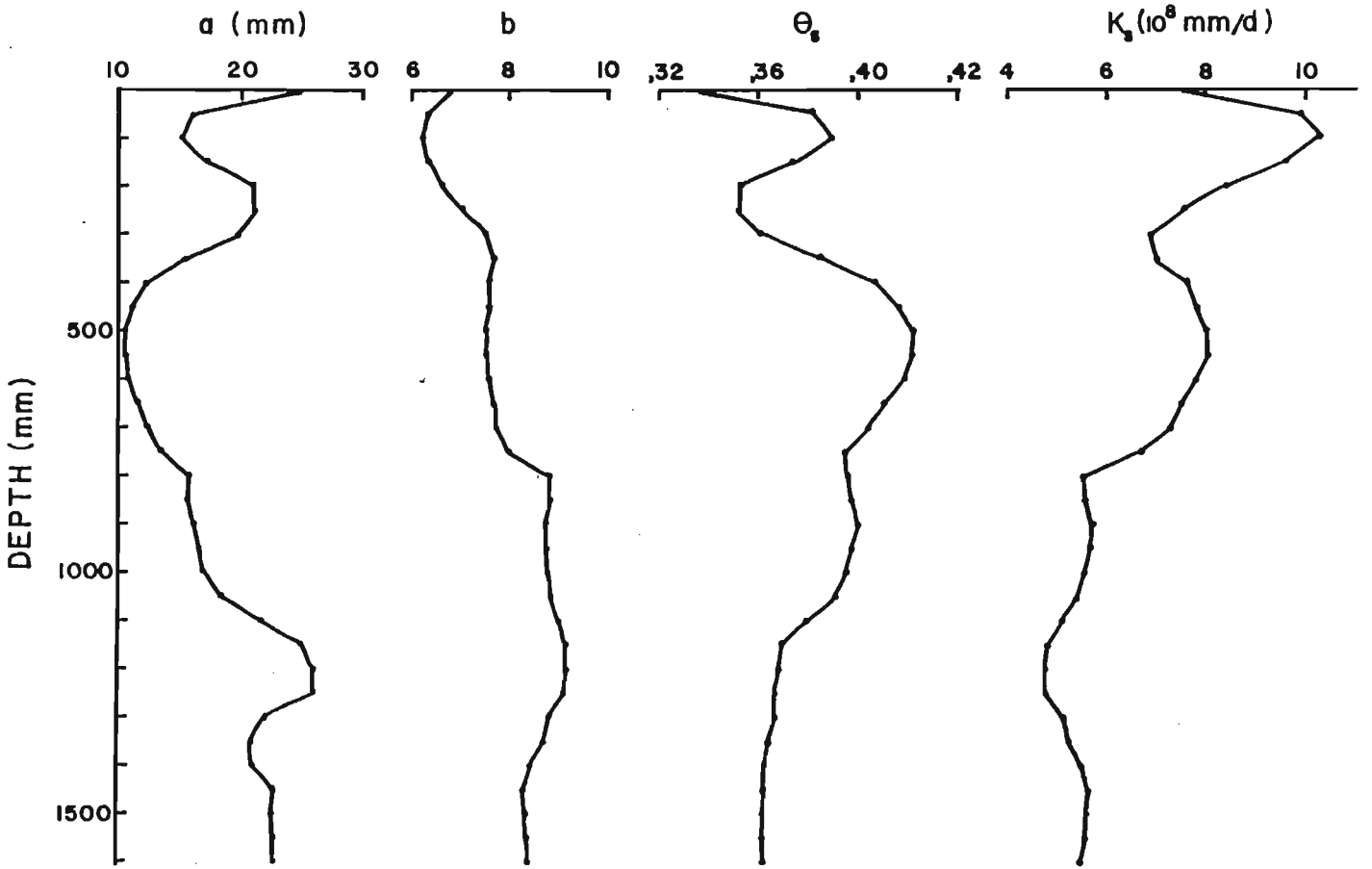

FIGURE 7.3 Nodal values of retentivity and conductivity parameters a, b, θ_s and K_s for Addo lysimeter profile

residual saturation as a curve-fitting parameter, as was done in Chapter 6. This detracts from the simpler relationship between soil properties and retentivity which is more easily visualized when $\underline{a}$, $\underline{b}$ and θ_s only are used.

However determined, it is the retentivity parameters that provide the means of incorporating soil properties in the flow model. The regression models and graphical techniques discussed in Chapter 3 provide methods of estimating these parameters for South African soils.

Prediction and description of conductivity is more difficult than is retentivity. As shown in Chapters 4 and 5, conductivity is not closely related to any easily measured soil property. K_s values for the lysimeter profile calculated by the method of Childs and Collis-George (Eq. 4.40) using the retentivity parameters are extremely high (Fig. 7.3). Relative K_s values through the profile follow the expected pattern, decreasing with increasing clay content and bulk density.

Since there was no means of estimating K_s, the simulation of the lysimeter water regime was performed three times using calculated K_s values multiplied by each of three conductivity matching factors, 10^{-3}, 10^{-4} and 10^{-5}. In this way the sensitivity of various simulated phenomena could be demonstrated and a value for K_s which leads to a close match between measured and simulated water regimes may be chosen.

Measured and simulated water regimes in these lysimeters may be influenced by:

1) the single tensiometer installed at each depth being unlikely to represent average water potential at that depth;
2) flood irrigation which increases the risk of channelling of water through macropores, leading to non-uniform infiltration;
3) assumptions regarding the relationship between root distribution, soil water potential and water absorption by roots;

4) the one-dimensional nature of the model applied to a system which must display both horizontal and vertical variability.

Initial pressure potentials through the profile were obtained by interpolation from actual tensiometer readings at the end of September 1981. The data required to run the water flow model is listed in Appendix 1. These data are printed by program WATDAT (Appendix 1) which calculates retentivity and conductivity from retentivity parameters for a range of potentials to enable data to be checked before the simulation program is run.

Measured and simulated pressure potentials for October 1981 at five depths in the lysimeter are plotted in Fig. 7.4. Gaps in the measured record are a result of technical staff being unavailable for weekend measurements. There are three sets of simulated data, referred to here as simulation 1 (matching factor 10^{-3}), simulation 2 (MF = 10^{-4}) and simulation 3 (MF = 10^{-5}). Thus the only differences between the simulations are those arising from differences in hydraulic conductivity. This range of matching factors was chosen after prior simulations of the first infiltration event had shown that values outside this range bore no resemblance to the measured data.

During the first day simulated ψ values changed in response to gradients which were introduced in the initial ψ data. Simulation 1 showed the greatest changes as K values were highest. Simulated ψ values decreased over the next three days, following the measured trend, with the exception of simulation 1 at 600 mm. In this case high K values caused fluxes from both above and below which added water to this level faster than it was absorbed by roots.

Application of 38 mm of water on day 5 increased measured ψ values at 300 mm and 600 mm. Simulation 1 showed slight wetting at 1200 mm

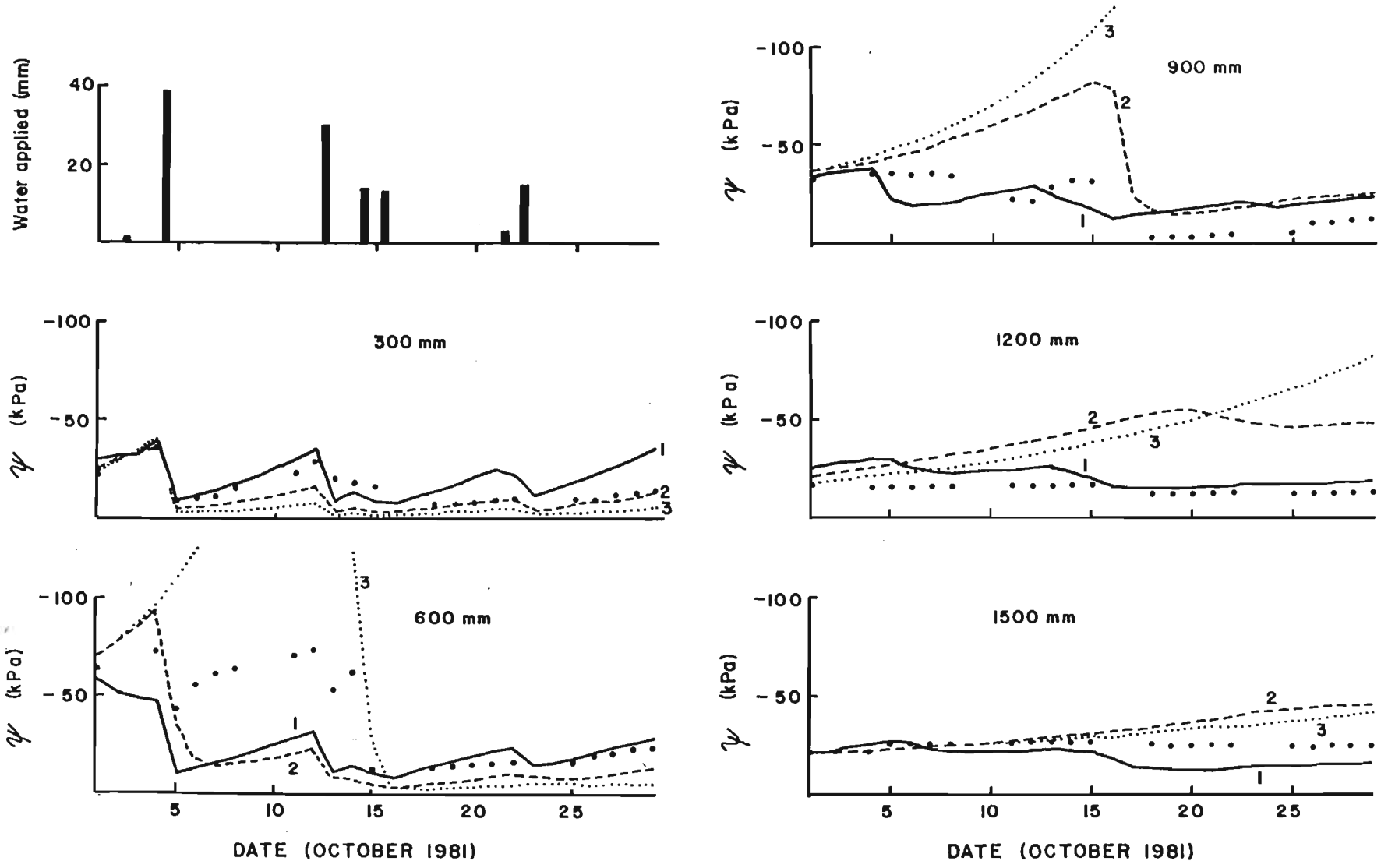

FIGURE 7.4: Measured and simulated daily pressure potentials at five depths in a lysimeter for each of 3 matching factors (M.F.). Measured values are denoted as ...; simulated values for M.F. = 10^{-3} as ——; M.F. = 10^{-4} as ---- and M.F. = 10^{-5} as ..... Water applied (mm) is also given. Numerals indicate

and 1500 mm but the largest increases in ψ were at 300 to 900 mm. Simulation 2 showed wetting at 600 mm and simulation 3 at 300 mm only. During the subsequent redistribution and drying to day 12, simulation 1 followed measured trends most closely.

Water applications on days 12, 14 and 15 caused marked increases in measured ψ values at 300, 600 and 900 mm. High measured values at 900 mm between days 18 and 25 may have been caused by a tensiometer fault or preferential channelling of water. Simulation 1 predicted wetting to 1500 mm, simulation 2 to 900 mm by day 16 and to 1200 mm by day 20, whereas simulation 3 predicted wetting to 600 mm only.

Small water applications on days 21 and 22 coincided with a two-day gap in the measured tensiometer record, but simulation 1 predicted wetting beyond 600 mm. Simulations 2 and 3 predict gradual drying at 1200 mm and 1500 mm whereas the tensiometer record indicates nearly constant ψ values.

Of the three simulations, simulation 1 corresponded most closely with the measured data. A matching factor between 5×10^{-4} and 8×10^{-4} which would give predictions between those of simulations 1 and 2 would probably give the best results. Another way of matching predicted data to measured is to change the root distribution and water uptake pattern. After initial infiltration and redistribution is complete, absorption of water by roots plays the largest role in determining profile water content and distribution. In this example a measure of root distribution was available but the response of roots to changing water potentials was assumed. Defining root distribution, which in an annual crop varies through the growing season, and water absorption mechanisms is as important to the success of a model as is the measurement of soil hydrological properties.

Considering the possible inaccuracies in the tensiometer record and the uncertain root distribution and withdrawal pattern, simulation 1

and to a lesser extent 2, are satisfactory and produce adequate medium term water distribution predictions. If more accurate short-term simulations are required, or if fluxes in the profile need to be predicted accurately, then the limitations of the data used in this example should be appreciated and they must be augmented by measured data.

This example has illustrated how a soil water flow model can be used starting with easily-available soil data. Errors are introduced at all stages: from the regression model, the shape of the retentivity and conductivity functions and the assumptions regarding water withdrawal by roots. The model does reflect soil profile characteristics such as textural and density changes and, within the limitations of a one-dimensional model, provides a method of predicting the temporal variation of soil water content through a profile. The model is flexible in that it is possible to run the same model, incorporating fixed retentivity and conductivity functions, using any level of soil information. In this example particle size and bulk density data were used, data which are commonly available from soil survey reports. Increasing the level of soil data does not change the model, it merely changes the method used to obtain the retentivity and conductivity parameters.

The overall objective of this work was to develop methods which could simplify the task of obtaining the soil hydrological data required by soil water flow simulation models. The methods described in Chapters 3 and 4, augmented if necessary by rapid methods such as that described in Chapter 6, provide a means of estimating soil hydrological data for South African soils. The example described in this chapter shows how these techniques are applied. A similar procedure can be followed for any other field soil. Used in this way the soil water simulation model becomes a valuable and easily-used tool for acquiring information on the water regime in soils.

CONCLUDING REMARKS

In general, hydrological data for South African soils are lacking with the result that the use of models in planning, development and management of soil water projects is restricted. Because of this restriction the main objective of this work was the estimation and prediction of values of the retentivity function parameters in relation to soil type enabling their inclusion in hydraulic conductivity and water flow models.

Broadly speaking, the water flow model described above is similar to other soil water flow models. It differs in that soil hydrological properties are defined by retentivity function parameters, the values of which can be varied with depth to reflect vertical inhomogeneity. The use of a standard retentivity function, rather than a table of θ and ψ values and an interpolation routine, simplifies the representation of inhomogeneous soils but sacrifices the ability to describe complex $\theta(\psi)$ relationships.

The suite of retentivity curves defined by the two-part retentivity function essentially apply to a range of hypothetical soils. Application of the function requires identification of that curve (or combination of parameters producing that curve) which corresponds most closely to the retentivity properties of the real soil. The relationship between function parameter values, curve shape and properties of South African soils (retentivity being estimated from soil texture, bulk density and soil type data) was also examined in this thesis .

The validity and applicability of the model and hydrological relationships described depend on the scale and complexity of the real system. Simulations are necessarily simplifications of real processes. In water flow modelling the inclusion of all factors which significantly influence the soil water regime is as important as accurate description of the various processes that occur during water flow. Small-scale phenomena are masked in field-scale investigations by spatial variability, complex flow behaviour and the tendency of plant roots to equalise water contents through the profile. In such systems accurate representation of soil hydrological properties is impossible and the methods described in this work should be adequate. As the scale decreases and hydrological properties can be defined more accurately, so the need for measured rather than estimated data increases. Similarly, the finite difference flow model is most valid for simple systems in which water moves in accordance with Darcy's law. It is less applicable to field soils in which macropore flow and lateral movement of water occur. The model does not take account of the effects of temperature, hysteresis and vapour flux which can be important under certain conditions.

The model is nonetheless a valuable aid in field soil water investigations, providing a dynamic, continuous overlay to what is often a discontinuous and arbitrary monitoring programme. In addition, simulations may suggest more efficient and discriminating measurement programmes. Calibrating the model output with observed field data enables the model to be used as a management tool. Initial estimates for the various model parameters can be obtained using the techniques outlined in this thesis.

Models such as the water flow model developed in this thesis are mathematical descriptions of processes and their interaction which occur

in nature. They provide an understanding of complex interactions between processes as well as predictions of soil water conditions. Certain processes are either poorly understood or difficult to describe quantitatively. In South Africa there are several areas in which further research is needed. These include the determination of

1) conductivity data for South African soils;
2) flow patterns within soil profiles for major soil forms;
3) the effects of surface hydrology and surface sealing and
4) root growth and distribution and root-water interaction for different crops and soils.

The data and procedures described can be used in any model, such as irrigation return flow, effluent disposal and plant nutrient simulations, which require a soil water flow subroutine. While not claiming to represent all facets of water flow accurately this work provides a relatively simple means of representing the major hydrological features of South African soils.

REFERENCES

Allison, L.E. 1965. Organic carbon. In Black, C.A. (ed.). *Methods of Soil Analysis. Part II. Chemical and Microbiological Properties.* Agronomy No. 9, 1367-1378, Am. Soc. Agron., Madison, Wisconsin.

Amerman, C.R. 1971. Numerical solution of the flow equation. In Hillel, D: *Soil and Water - physical principles and practices.* Academic Press, New York.

Anderson, J.L. and Bouma, J., 1973. Relationships between saturated hydraulic conductivity and morphometric data of an argillic horizon. *Soil Sci. Soc. Amer. Proc. 37*, 408-413.

Ayars, J.E. 1976. *Salt transport in irrigated soils.* Unpub. PhD thesis. Colorado State Univ., Fort Collins, Colorado.

Bartelli, L.J. and Peters, D.B. 1959. Integrating soil moisture characteristics with classification units of some Illinois soils. *Soil Sci. Soc. Amer. Proc. 23*, 149-151.

Beven, K. and Germann, P. 1981. Water flow in soil macropores II. A combined flow model. *J: Soil Sci. 32*, 15-29.

Bouma, J. and Anderson, J.L. 1983. Relationships between soil structure characteristics and hydraulic conductivity. In: R.R. Bruce, ed., *Field soil water regime.* Soil Sci. Soc. Amer. Proc. Special Publ. No. 5, pp. 77-105.

Bloemen, G.W. 1980. Calculation of hydraulic conductivities of soils from texture and organic matter content. *Z: Pflanzenernaehr. Bodenkd. 143*, 581-605.

Brooks, R.H. and Corey, A.T. 1966. Properties of porous media affecting fluid flow. *J: Irrig. Drain Div. 92*, 61-88.

Bruce, R.R. 1972. Hydraulic conductivity evaluation of the soil water retention relations. *Soil Sci. Soc. Am. J.* 36, 555-561.

Burdine, N.T. 1953. Relative permeability calculations from pore-size distribution data. *Petroleum Transactions 198*, 71-77 (cited in Brooks and Corey, 1966).

Burger, R. du T., Bennie, A.T.P., Botha, F.J.P. and du Preez, C.C. 1979. *Grondverdigting onder besproeiing op die Vaalhartsbesproeiing-skema.* Dept. of Soil Sci., Univ. of the Orange Free State, Bloemfontein.

Cameron, D.R. 1978. Variability of soil water retention curves and predicted hydraulic conductivities on a small plot. *Soil Sci. 126*, 364-371.

Campbell, G.S. 1974. A simple method for determining unsaturated conductivity from moisture retention data. *Soil Sci. 117*, 311-314.

Childs, E.C. and Collis-George, N. 1950. The permeability of porous materials. *Proc. Roy. Soc. London A: 201*, 392-405.

Clapp, R.B. and Hornberger, G.M. 1978. Empirical equations for some soil hydraulic properties. *Water Resources Res. 14*, 601-604.

Collis-George, N. and Rosenthal, M.J. 1966. Proposed outflow method for the determination of the hydraulic conductivity of unsaturated porous materials. *Austr. J. Soil Res. 4*, 165-180.

Day, P.R. 1965. Particle fractionation and particle-size analysis. In Black, C.A. (ed.). *Methods of Soil Analysis. Part I: Physical and mineralogical properties.* Agronomy No. 9, 545-567. Am. Soc.. Agron., Madison, Wisconsin.

Dekker, D.A., Jeffrey, R.A. and Scotney, D.M. 1980. *Soil survey of the Tala Valley area.* Natal region, Dept. of Agriculture and Fisheries, Rept. N11/80.

Doering, E.J. 1965. Soil water diffusivity by the one step method. *Soil Sci. 99*, 322-326.

Donaldson, G.W. 1975. The occurrence of dispersive soil piping in central South Africa. *Proc. Sixth Reg. Conf. for Africa on Soil Mechanics and Foundation Engineering Durban*, 229-235.

Draper, N.R. and Smith, H. 1966. *Applied regression analysis.* John Wiley and Sons, New York.

Dutt, G.R., Shaffer, M.J. and Moore, W.J. 1972. *Computer simulation model of dynamic bio-physicochemical processes in soils.* Tech. Bull., 196. Dept. of Soils, Water and Engineering, Univ. of Arizona, Tucson.

Erh, K.T. 1972. Application of the spline function to soil science. *Soil Sci. 114*, 333-338.

Feddes, R.A., Bresler, E. and Neuman, S.P. 1974. Field test of a modified numerical model for water uptake by root systems. *Water Resources Res.* 10, 1199-1206.

Feddes, R.A., Kowalik, P., Kolinska-Malinka, K. and Zaradry, H. 1976. Simulation of field water uptake by plants using a soil water dependent root extraction function. *J. Hydrology 31*, 13-26.

Gardner, W.R. 1956. Calculation of capillary conductivity from pressure plate outflow data. *Soil Sci. Soc. Amer. Proc. 20*, 317-320.

Gardner, W.R. 1960. Dynamic aspects of water availability to plants. *Soil Sci. 89*, 63-73.

Gardner, W.R. 1974. The permeability problem. *Soil Sci. 117*, 243-249.

Gardner, W.R., Hillel, D. and Benyamini, Y. 1970. Post-irrigation movement of soil water: I. Predistribution. *Water Resources Res. 6*, 851-861.

Ghosh, R.K. 1980. Estimation of soil moisture characteristics from mechanical properties of soils. *Soil Sci. 130*, 60-63.

Green, G.C. and Bruwer, W. 1979. An improved weighing lysimeter facility for citrus evapotranspiration studies. *Water SA 5*, 189-195.

Green, G.C. and Fuchs, M. 1982. Of trees, water and men-experimental workshop on water in the soil-tree-atmosphere continuum. *S. Afr. J. Sci. 78*, 226-228.

Green, R.E. and Corey, J.C. 1971. Calculation of hydraulic conductivity: a further evaluation of some predictive methods. *Soil Sci. Soc. Amer. J. 35*, 3-8.

Gupta, S.C., Farrell, D.A. and Larson, W.E. 1974. Determining effective soil water diffusivities from one-step outflow experiments. *Soil Sci. Soc. Amer. Proc. 38*, 710-716.

Gupta, S.C. and Larson, W.E. 1979. Estimating soil water retention characteristics from particle size distribution, organic matter percent and bulk density. *Water Resources Res. 15*, 1633-1635.

Hall, D.G.M., Reeve, M.J., Thomasson, A.J. and Wright, V.F. 1977. *Water retention, porosity and density of field soils.* Tech. Monograph No. 9, Soil Survey of England and Wales.

Hanks, R.J. and Bowers, S.A. 1962. Numerical solution of the moisture flow equation for infiltration into layered soils. *Soil Sci. Soc. Am. Proc. 26*, 530-535.

Haridasan, M. and Jensen, R.D. 1972. Effect of temperature on pressure head - water content relationship and conductivity of two soils. *Soil Sci. Soc. Amer. Proc. 36*, 703-708.

Haverkamp, R., Vauchin, M., Touma, J., Wierenga, P.J. and Vachaud, G. 1977. A comparison of numerical simulation models for one dimensional infiltration. *Soil Sci. Soc. Amer. J. 41*, 285-294.

Hensley, M. 1969. *Selected properties affecting the irrigable value of some Makatini soils.* Unpub. MSc. (Agric.) dissertation, Univ. of Natal, Pietermaritzburg.

Hensley, M. 1980. A comparison of two methods for determining plant available water in a soil profile. *Agrochemophysica 12*, 39-43.

Hill, J.N.S. and Sumner, M.E. 1967. Effect of bulk density on moisture characteristics of soils. *Soil Sci. 103*, 234-238.

Hillel, D. 1971. *Soil and water: physical principles and processes.* Academic Press, New York.

Hillel, D. 1977. *Computer simulation of soil-water dynamics: a compendium of recent work.* Inter. Dev. Research Centre, Ottawa.

Hillel, D. and Talpaz, H. 1977. Simulation of soil water dynamics in layered soils. *Soil Sci. 123*, 54-62.

Jackson, R.D. 1972. On the calculation of hydraulic conductivity. *Soil Sci. Soc. Amer. Proc. 36*, 380-382.

Jackson, R.D., Reginato, R.J. and van Bavel, C.H.M. 1965. Comparison of measured and calculated conductivities of unsaturated soils. *Water Resources Res. 1*, 375-380.

Jamison, V.C. and Kroth, E.M. 1958. Available moisture storage capacity in relation to textural composition and organic matter content of several Missouri soils. *Soil Sci. Soc. Amer. Proc. 22*, 189-192.

Jaynes, D.B. and Tyler, E.J. 1980. Comparison of one-step outflow laboratory method to an in situ method for measuring hydraulic conductivity. *Soil Sci. Soc. Amer. J. 44*, 903-907.

Johnston, M.A. 1973. Physical properties of sugar belt soils with particular reference to moisture release characteristics. *Proc. S.A. Sugar Tech. Assoc., 47th Congr., Durban*, 115-119.

Klute, A. 1965. Laboratory measurement of hydraulic conductivity of saturated soil. In Black, C.A. (ed.). *Methods of soil analysis: Part I. Physical and minerological properties.* Agronomy No. 9, 210-221. Am. Soc. Agron., Madison, Wisconsin.

Klute, A. 1972. The determination of the hydraulic conductivity and diffusivity of unsaturated soils. *Soil Sci. 113*, 264-276.

Kunze, R.J. and Kirkham, D. 1962. Simplified accounting for membrane impedance in capillary conductivity determinations. *Soil Sci. Soc. Amer. Proc. 26*, 421-426.

Kunze, R.J., Vehara, G. and Graham, K. 1968. Factors important in the calculation of hydraulic conductivity. *Soil Sci. Soc. Amer. Proc. 32*, 760-765.

Lenhard, R.J. and Bloomberg, G.L. 1979. Capillary pressure - saturation relationships for a forest soil. *Trans. Amer. Soc. agric. Engrs. 22*, 357-360.

Loxton, R.F. 1961. A modified chart for the determination of basic soil textural classes in terms of the International classification for soil separates. *S. Afr. J. Agr. Sci. 4*, 507-512.

Lund, Z.F. 1959. Available water holding capacity of alluvial soils in Louisiana. *Soil Sci. Soc. Amer. Proc. 23*, 1-3.

MacLean, A.H. and Yager, T.U. 1972. Available water capacities of Zambian soils in relation to pressure plate measurements and particle size analysis. *Soil Sci. 113*, 23-29.

MacVicar, C.N., de Villiers, J.M., Loxton, R.F., Verster, E., Lambrechts, J.J.N., Merryweather, F.R., Le Roux, J., van Rooyen, T.H. and Harmse, H.J. von M. 1977. *Soil classification. A binomial system for South Africa.* Science Bull., 390. Dept. of Agric. Tech. Services, Pretoria.

Marshall, T.J. 1958. A relation between permeability and size distribution of pores. *J. Soil Sci. 9*, 1-8.

Millington, R.J. and Quirk, J.P. 1959. Permeability of porous media. *Nature 183*, 387-388.

Millington, R.J. and Quirk, J.P. 1960. Transport in porous media. *Trans. 7th Inter. Congr. Soil Sci., Madison, Wisconsin, 1.3*, 97-106.

Miller, E.E. and Elrick, D.E. 1958. Dynamic determination of capillary conductivity extended for non-negligible membrane impedance. *Soil Sci. Soc. Amer. Proc. 22*, 483-486.

Mottram, R., Hutson, J.L. and Goodman, P.S. 1981. Water retention of some Natal soils as related to soil texture and organic matter content. *Crop Production 10*, 47-50.

Mualem, Y. 1976. A new model for predicting the hydraulic conductivity of unsaturated porous media. *Water Resources Res. 12*, 513-522.

Mualem, Y. 1978. Hydraulic conductivity of unsaturated porous media: generalized macroscopic approach. *Water Resources Res. 14*, 325-334.

Mualem, Y. and Dagan, G. 1978. Hydraulic conductivity of soils: unified approach to the statistical models. *Soil Sci. Soc. Amer. J. 42*, 392-395.

Nielsen, D.R., Kirkham, D. and Perrier, E.R. 1960. Soil capillary conductivity: comparison of measured and calculated values. *Soil Sci. Soc. Amer. Proc. 24*, 157-160.

Nielsen, D.R., Biggar, J.W. and Erh, K.T. 1973. Spatial variability of field measured soil water properties. *Hilgardia 42*, 215-259.

Nimah, M.N. and Hanks, R.J. 1973. Model for estimating soil water, plant and atmospheric interrelations 1. Description and sensitivity. *Soil Sci. Soc. Amer. J. 37*,522-527.

Parkes, M.E. and Waters, P.A. 1980. Comparison of measured and estimated unsaturated hydraulic conductivity. *Water Resources Res. 16*, 749-754.

Passioura, J.B. 1976. Determining soil water diffusivities from one-step outflow experiments. *Aust. J. Soil Res. 15*, 1-8.

Peck, A.J. 1966. Diffusivity determination by a new outflow method. In: *Water in the unsaturated zone*. Vol 1. Publ. No. 82, 191-202. Int. Assoc. Sci. Hydrol.

Petersen, G.W., Cunningham, R.L. and Matelski, R.P. 1968. Moisture characteristics of Pennsylvania soils: 1. Moisture retention as related to texture. *Soil Sci. Soc. Amer. Proc. 32*, 271-275.

Reeve, R.C. 1953. A method for determining the stability of soil structure based upon air and water permeability tests. *Soil Sci. Amer. Proc. 17*, 324-329.

Reeve, R.C. 1965. Air-to-water permeability ratio. In: Black, C.A. (ed.). *Methods of Soil Analysis Part I: Physical and minerological properties*. Agronomy No. 9, 520-531., Am. Soc. Agron., Madison, Wisconsin.

Rijtema, P.E. 1959. Calculation of capillary conductivity from pressure plate outflow data with non-negligible membrane impedance. *Netherlands J. Agric. Sci. 7*, 209-215.

Rivers, E.D. and Shipp, R.F. 1972. Available water capacity of sandy and gravelly North Dakota soils. *Soil Sci. 113*, 74-80.

Rivers, E.D. and Shipp, R.F. 1978. Soil water retention as related to particle size in selected sands and loamy sands. *Soil Sci. 126*, 94-100.

Rogowski, A.S. 1971. Watershed physics: model of the soil moisture characteristic. *Water Resources Res. 7*, 1575-1582.

Russo, D. and Bresler, E. 1980a. Scaling soil hydraulic properties of a heterogenous soil. *Soil Sci. Soc. Amer. J. 44*, 681-684.

Russo, D. and Bresler, E. 1980b. Field determination of soil hydraulic properties for statistical analysis. *Soil Sci. Soc. Amer. J. 44*, 697-702.

Salter, P.J., Berry, G. and Williams, J.B. 1966. The influence of texture on the moisture characteristics of soils. III. Quantitative relationships between particle size, composition and available water capacity. *J. Soil Sci. 17*, 93-98.

Salter, P.J. and Williams, J.B. 1965a. The influence of texture on the moisture characteristic of soils. I. A critical comparison of techniques for determining the available water capacity and moisture characteristic curve of a soil. *J. Soil Sci. 16*, 1-15.

Salter, P.J. and Williams, J.B. 1965b. The influence of texture on the moisture characteristics of soils. II. Available - water capacity and moisture release characteristics. *J. Soil Sci. 16*, 310-317.

Savage, M.J. and McGee, O.S. 1980. The equation of time and the photoperiod. *S. Afr. J. Sci. 76*, 281-282.

Scotney, D.M. 1970. *Soils and land-use planning in the Howick extension area.* Unpub. PhD. thesis, Univ. of Natal, Pietermaritzburg.

Shaykewich, C.F. and Zwarich, M.A. 1968. Relationships between soil physical constants and soil physical components of some Manitoba soils. *Can. J. Soil Sci. 48*, 199-204.

Skopp, J., Gardner, W.R. and Tyler, E.J. 1981. Solute movement in structured soils: two region model with small interaction. *Soil Sci. Soc. Amer. J. 45*, 837-842.

Tillotson, W.R., Robbins, C.W., Wagenet, R.J. and Hanks, R.J. 1980. *Soil water, solute, and plant growth simulation.* Bull. Utah Agr. Exp. Stn. 502, Logan, Utah.

Turner, D.P. 1976. *A study of water infiltration into soils.* Unpub. M.Sc. (Agric) Dissertation, Univ. of Natal, Pietermaritzburg.

Van der Eyk, J.J., MacVicar, C.N. and De Villiers, J.M. 1969. *Soils of the Tugela Basin.* Natal Town and Regional Planning Report 15, Pietermaritzburg.

Van der Merwe, A. 1973. *Physico-chemical relationships of selected OFS soils - a statistical approach based on taxonomic criteria.* Unpub. PhD thesis, Univ. of Orange Free State, Bloemfontein.

Van der Ploeg, R.R. 1974. Simulation of moisture transfer in soils: one-dimensional infiltration. *Soil Sci. 118*, 349-357.

Van der Watt, H.V.H. 1971. Verwantskap tussen vog retensie en partikelgrootteverdeling van grond. *Agrochemophysica 3*, 33-34.

Van Genuchten, R. 1980. A closed-form equation for predicting the hydraulic conductivity of unsaturated soils. *Soil Sci. Soc. Amer. J. 44*, 892-898.

Van Shaik, J.C. 1974. Oil:water permeability ratios as a measure of stability of soil structure. *Can. J. Soil Sci. 54*, 331-332.

Wilcox, J.C. 1962. Rate of soil drainage following an irrigation, IV: Effects of consumptive use and soil depth on upper limit of available moisture. *Can. J. Soil Sci. 42*, 129-136.

APPENDICES

Note: The computer programs listed in Appendices 1, 2 and 3 were originally written in HPL for Hewlett-Packard 9825 or 9826 desk-top computers. They were later rewritten in FORTRAN for a Burroughs B7800 computer. The FORTRAN versions, presented here, contain a large number of variables corresponding to the numbered r-variables used in HPL, which were merely capitalized during translation.

APPENDIX 1

COMPUTER PROGRAMS AND FILES FOR SOIL WATER FLOW SIMULATION MODEL

In this appendix the computer programs comprising the water flow model and the associated data files are listed. Data used as an example are those for the simulation of water flow in a lysimeter (Chapter 7). The soil water flow model consists of three programs, each of which may be used independently:

1) RETFUN, a program for estimating retentivity parameters for the two-part retentivity function and hydraulic conductivity at saturation from clay, silt and fine sand contents and bulk density;
2) WATDAT, a program which tabulates the input data for the simulation model together with calculated θ and K values at several ψ values;
3) WATFLO, the water flow simulation program.

The arrangement of programs and data files is shown in Fig. A1.1. Data file names are those used for the simulation in Chapter 7. Details of programs and data files appear in the following figures and tables:

Program	Flowchart	Program listing	Input data format	Input file example	Output file example
RETFUN	Fig. A1.2	Table A1.1	Table A1.2	Table A1.3	Table A1.4
WATDAT	Fig. A1.3	Table A1.5	Table A1.6	Table A1.7	Table A1.8
WATFLO	Fig. A1.4	Table A1.9	Table A1.6	Table A1.7	Table A1.10

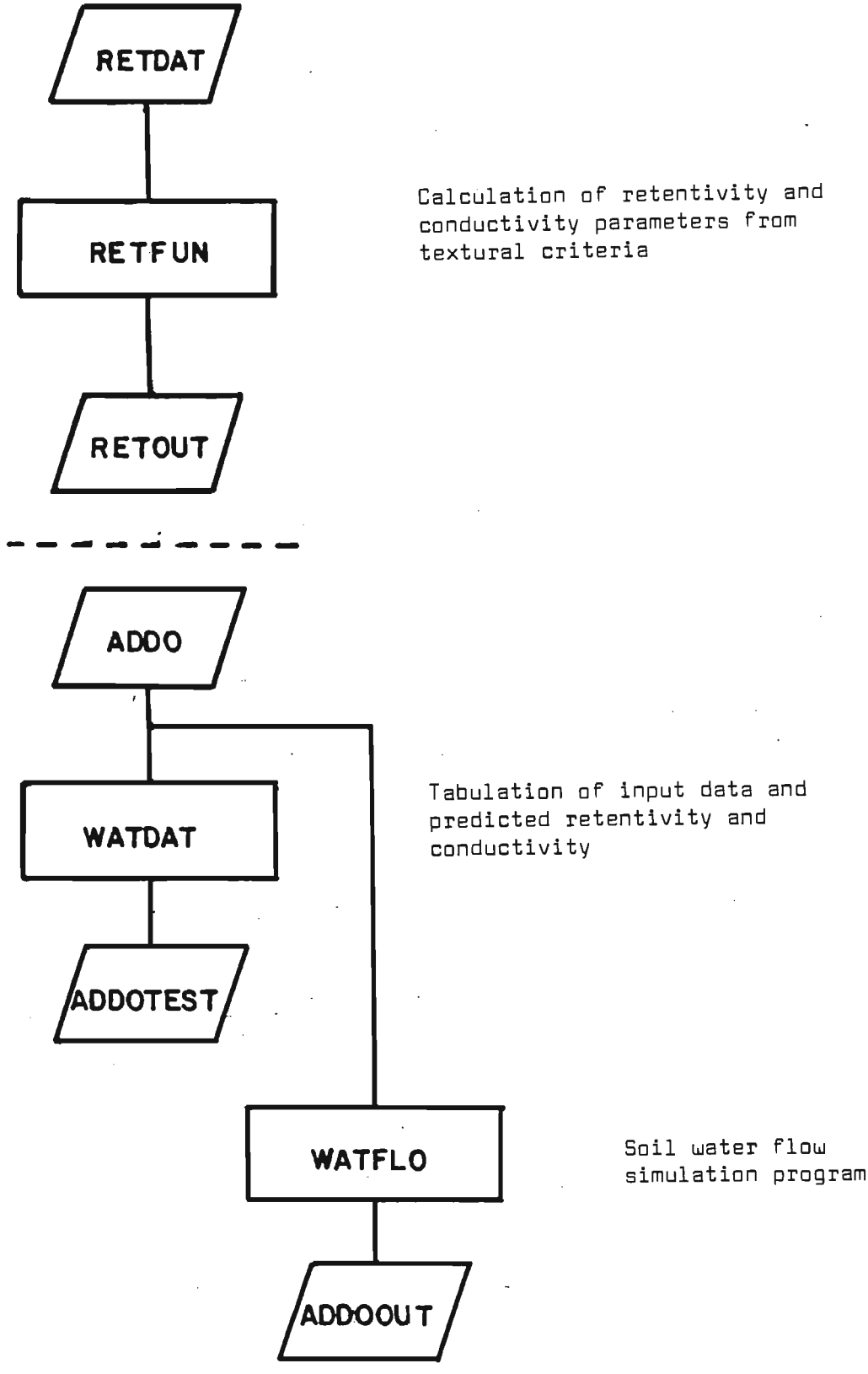

FIGURE A1.1 Programs and data files used to simulate water flow in soils

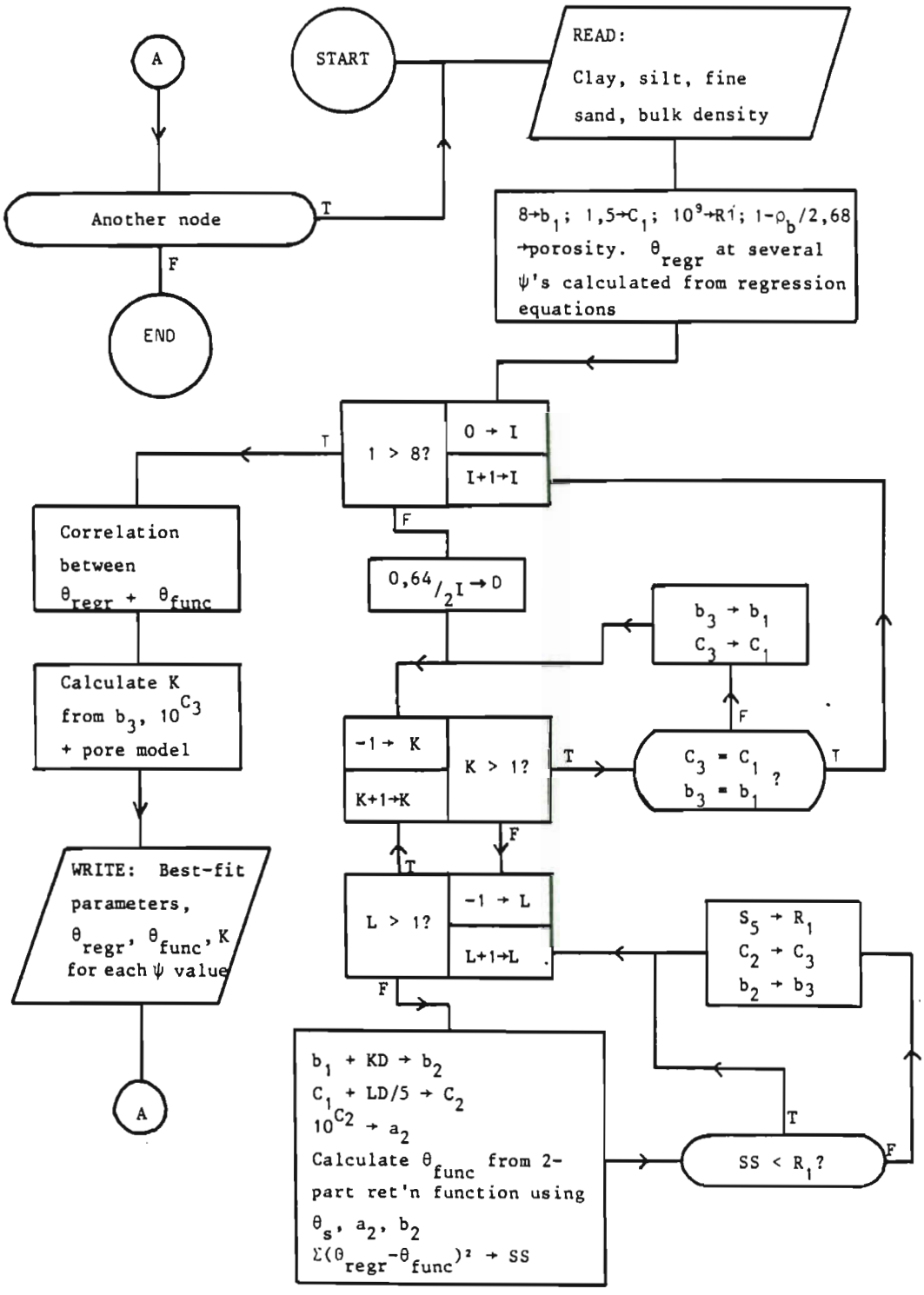

FIGURE A1.2 Flowchart for RETFUN, a program for estimating retentivity and conductivity parameters

TABLE A1.2 Data format for file RETDATA

RECORD	FORMAT	VARIABLE NAME	DESCRIPTION
1	F4.0	TOTAL	No. of nodes or no. of samples
2 to TOTAL	F6.1	CL	Clay content (%)
	F6.1	SI	Silt content (%)

TABLE A1.1 A FORTRAN program for RETFUN

```
100 $RESET FREE
200 C FITTING TWO PART RETENTIVITY FUNCTION
250 C TO CALCULATE WATER CONTENT FROM MATRIC POTENTIAL
300       FUNCTION THETA(FH,FF,FQ,FI,FL)
400       IF(FH-FQ*(FL/FF)**(-FI))6060,6050,6050
500  6050 THETA=FF*(FH/FQ)**(-1/FI);GO TO 6061
600  6060 THETA=FF-(FF*(1-FL/FF)*(FH**2))/(FQ*FQ*((FL/FF)**(-2*FI)))
700  6061 RETURN
800       END
890       REAL K,L
890 C H=POTENTIAL (MM WATER IN CALCULATIONS), T=THETA, COND(UCTIVITY)MM/D
900       DIMENSION H(30),T(30),COND(30)
900       N=6;R17=1
100       READ(1,9510)TOTAL
200       DO 500 Z=1,TOTAL
300       READ(1,9500)CL,SI,FSA,BD
305 C STARTING VALUES FOR RETN PARAMETERS B,C(=LOG A) &R=SUM OF SQUARES
310       B=8;C=1.5;R1=10**9
320 C F=POROSITY;BD=BULK DENSITY (MG/M**3)
400       F=(1-BD/2.7)
455 C APPROPRIATE REGRESSION EQUATIONS ARE INCORPORATED FOR CALCULATING
460 C THETA FROM TEXTURE AND BULK DENSITY. ALTERNATIVELY ACTUAL THETA
470 C VALUES CAN BE SPECIFIED IN WHICH CASE THE PARTICLE SIZE DATA IS
480 C NOT REQUIRED
500       T(1)=.4244+.00246*CL+.00188*SI+.00134*FSA-.1294*BD
500       T(2)=.1620+.00408*CL+.00317*SI+.00212*FSA-.0328*BD
500       T(3)=-.0029+.00562*CL+.00477*SI+.00151*FSA+.0133*BD
500       T(4)=-.0035+.00548*CL+.00505*SI+.00051*FSA+.0148*BD
500       T(5)=-.0146+.00548*CL+.00525*SI+.00040*FSA+.0149*BD
550       T(6)=.06023+.00322*CL+.00309*SI-.02598*BD
560 C POTENTIALS (-KPA*102.2=MM WATER) CORRESPOND TO REGRESSION EQUATIONS
570 C USED.  OTHER APPROPRIATE VALUES MAY BE SPECIFIED.
600       H(1)=1*102.2;H(2)=3*102.2;H(3)=10*102.2;H(4)=30*102.2
600       H(5)=50*102.2;H(6)=1500*102.2
650 C START OF SEARCH FOR OPTIMUM COMBINATION OF RETENTIVITY PARAMETERS
700       DO 100 I=0,8
750 C     WRITE(2,9999)I,D,R1,A,B
760 C STEP SIZE D STARTS AT .64/2 AND ENDS AT .64/256
800       D=.64/(2**I)
900       R13=B
900       R14=C
979    96 A=A
000       DO 99 K=-1,1
000       B=AMAX1(0.01,R13+K*D)
050       DO 98 L=-1,1
100       C=AMAX1(-4,R14+L*D/5)
150       A=10**C
200       P=2*B*F/(1+2*B)
250       DO 97 J=R17,N
300       S=S+(THETA(H(J),F,A,B,P)-T(J))**2
350    97 CONTINUE
360 C TEST WHETHER SS IS LESS THAN PREVIOUS LOWEST VALUE
3510     90 R10=B
3520        R11=C
3530        R1=S
3600     91 S=0
3700     98 CONTINUE
3800     99 CONTINUE
3900        IF(R10.EQ.R13.AND.R11.EQ.R14)GO TO 60
4000        R13=R10;R14=R11
4100        GO TO 96
4150     60 B=R10;C=R11;A=10**R11
4200    100 CONTINUE
4300        R4=0;R5=0;R6=0;R7=0;R8=0
4400        DO 200 J=R17,N
4500        R4=T(J)*THETA(H(J),F,A,B,P)+R4
4600        R5=T(J)+R5
4700        R6=THETA(H(J),F,A,B,P)+R6
4800        R7=T(J)*T(J)+R7
4900        R8=THETA(H(J),F,A,B,P)**2+R8
5000    200 CONTINUE
5100        R=(R4-R5*R6/(N+1))/SQRT((R7-R5*R5/(N+1))*(R8-R6*R6/(N+1)))
5108 C CALCULATE CONDUCTIVITY USING CHILDS & COLLIS-GEORGE MODEL APPLIED
5109 C TO THE TWO-PART RETENTIVITY FUNCTION
5110        PS=P/F
5111        CSAT=2*2.323*10**10*F/A*A
5112        CSAT=CSAT*((PS**(2*B+1))/(2*B+1)-(PS**(2*B+2))/(2*B+2)+((1-PS)
5113       1**2)/(PS**(-2*B)))
5114        PS=P/F
5115        DO 600 J=1,N
5116        SAT=T(J)/F
5118        COND(J)=2*2.323*10**10*F/(A*A)
5119        IF(T(J).LT.P)GO TO 590
5120        COND(J)=COND(J)*(SAT*PS**(2*B+1)/(2*B+1)-PS**(2*B+2)/(2*B+2)
5122       1+(1-PS)*(SAT-PS+(1-SAT)*ALOG((1-SAT)/(1-PS)))/(PS**(-2*B)))
5124    590 COND(J)=COND(J)*SAT**(2*B+2)/((2*B+1)*(2*B+1))
5129    600 CONTINUE
5200        WRITE(6,9000)10**C,B,R,CSAT
5300        WRITE(6,9010)
5400        WRITE(6,9030)
5500        DO 300 J=1,N
5550 C POTENTIALS CONVERTED TO -KPA FOR OUTPUT
5600        WRITE(6,9020)H(J)/102.2,T(J),THETA(H(J),F,A,B,P),T(J)-THETA(
5700       1H(J),F,A,B,P),COND(J)
5800    300 CONTINUE
5850        WRITE(6,9010)
5860        WRITE(6,9010)
5900     500 CONTINUE
6000    9000 FORMAT(1X,"     A="E10.3,"    B=",F7.3,"    R=",F6.4,"    KS=",E10.3)
6100    9010 FORMAT(1X)
6200    9020 FORMAT(1X,F8.1,2F9.4,F10.5,E11.3)
6290    9500 FORMAT(3F6.1,F8.4)
6300    9510 FORMAT(F4.0)
```

TABLE A1.3 An example of RETDAT, an input data file for RETFUN

```
33
17.7    7.9   16.8   1.8000
17.7    7.9   16.8   1.6700
17.6    7.9   16.8   1.6500
17.5    7.9   16.9   1.6900
17.5    8.1   16.9   1.7500
17.6    9.6   17.0   1.7500
18.4   11.1   17.0   1.7250
19.4   12.0   17.0   1.6600
19.4   12.7   17.0   1.6000
19.4   13.1   17.0   1.5750
19.4   13.1   17.0   1.5600
19.4   13.1   17.0   1.5600
19.4   13.1   16.9   1.5700
19.4   13.1   16.8   1.5900
19.6   12.8   16.7   1.6100
20.7   12.4   16.6   1.6300
24.7   11.9   16.8   1.6300
25.1   11.6   17.0   1.6250
25.1   11.6   17.7   1.6200
25.1   11.6   17.8   1.6250
25.1   11.6   17.8   1.6300
25.1   11.6   17.8   1.6450
25.1   11.6   17.8
25.1   11.6   17
 5.1   11.6
```

TABLE A1.4 An example of RETOUT, an output data file of RETFUN

A= .259E+02 B= 6.848 R=0.9984 KS= .750E+08

POT'L	THETA	THETA-EST	DEV	COND MM/D
1.0	0.2742	0.2728	0.00134	.497E+04
3.0	0.2358	0.2324	0.00343	.467E+03
10.0	0.1836	0.1949	-0.01137	.915E+01
30.0	0.1687	0.1660	0.00264	.243E+01
50.0	0.1575	0.1541	0.00339	.826E+00
1500.0	0.0948	0.0938	0.00102	.286E-03

A= .160E+02 B= 6.385 R=0.9965 KS= .988E+08

POT'L	THETA	THETA-EST	DEV	COND MM/D
1.0	0.2909	0.2846	0.00632	.697E+04
3.0	0.2401	0.2393	0.00085	.418E+03
10.0	0.1818	0.1978	-0.01601	.708E+01
30.0	0.1668	0.1663	0.00041	.199E+01
50.0	0.1556	0.1535	0.00210	.717E+00
1500.0	0.0982	0.0897	0.00846	.828E-03

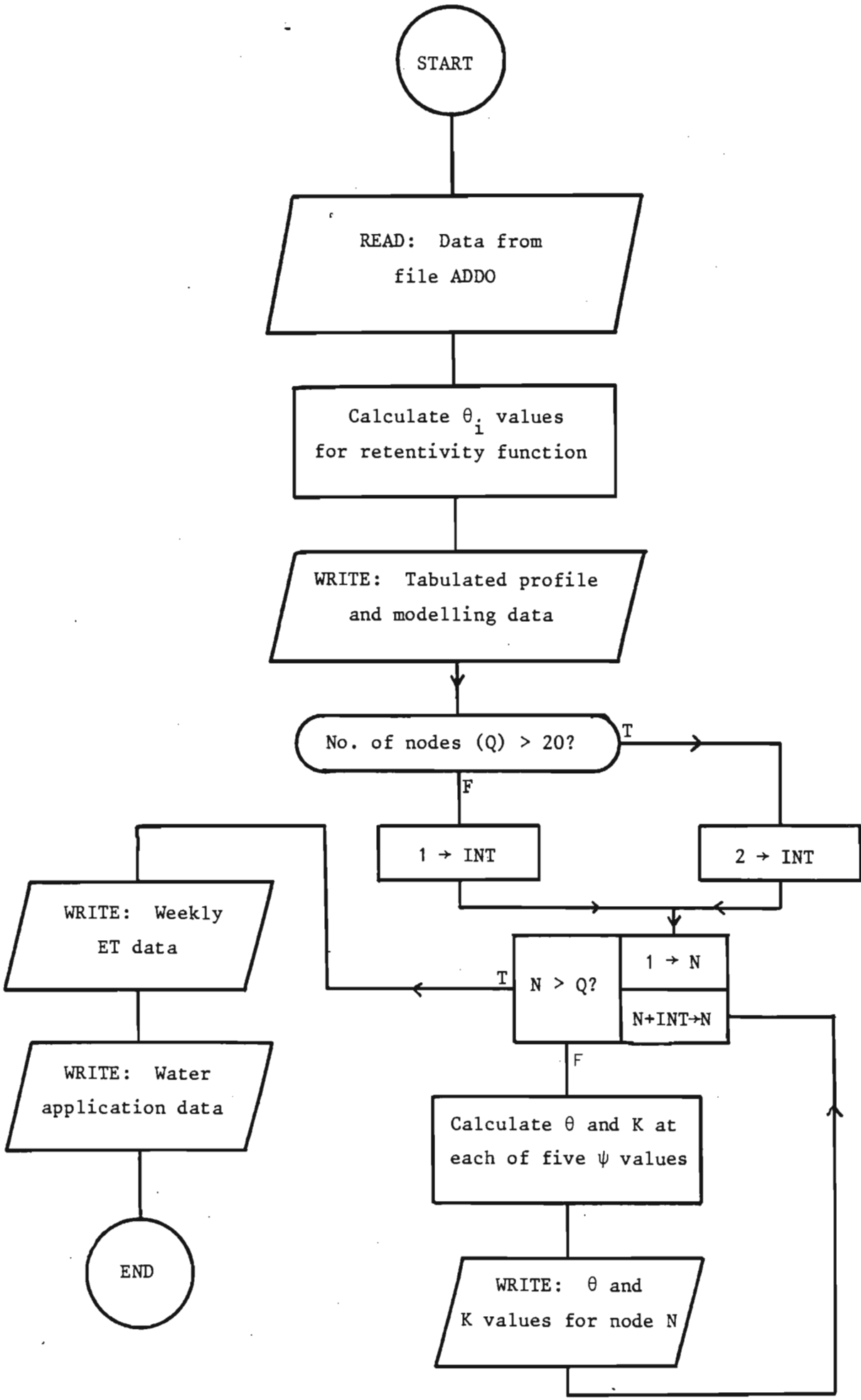

FIGURE A1.3 Flowchart for WATDAT, a program for tabulating input

TABLE A1.5 A FORTRAN program for WATDAT

```
10 FILE  6=JLH/ADDOTEST,UNIT=DISK,RECORD=14,BLOCKING=420
20 FILE  1=JLH/ADDO,UNIT=DISK,RECORD=14,BLOCKING=420
30 $RESET FREE
40 C
50 C
60 C
70 C
80 C  R1=FIRST DAY NO, R2=LAST DAY NO, R3=MIN.NO TIME INTERVALS/DAY,
90 C  R4=NO OF IRRIGATIONS, R5=DEPTH NODE INTERVALS, R6=BOTTOM BOUNDARY,
00 C  R7=MIN. WATER POTL(MM), R8=PROFILE DEPTH, R44=PRINT INTERVAL(DAYS),
10 C  R47=NO.OF PRINTS/PAGE(1-4)
20 C
30       FUNCTION THETA(R13,FQ,FF,FQ,FI,FL)
40       IF(R13-FQ)6050,6050,6060
50  6050 THETA=FF*(AMIN1(FQ,R13)/FQ)**(-1/FI);GO TO 6061
60  6060 THETA=FF-(FF*(1-FL/FF)*((AMIN1(R13,-10))**2))/(FQ*FQ*((FL/FF)**(-2
61      1*FI)))
70  6061 RETURN
80       END
90       FUNCTION POTL(R13,FL,FF,FQ,FI)
00       IF(R13-FL)6040,6030,6030
10  6030 POTL=(SQRT(1-R13/FF))*FQ*((FL/FF)**(-FI))/SQRT(1-FL/FF)
20  6040 IF(R13.LT.FQ)POTL=FQ*(R13/FF)**(-FI)
30       RETURN
40       END
50 C
60 C
70       FUNCTION HC(R13,FQ,FW,FQ,FI,FF,FL)
80       IF(R13.LE.FQ)HC=AMIN1(FW,FW*(FQ/AMIN1(FQ,R13))**(2+3/FI))
90       IF(R13.GT.FQ)HC=FW*((THETA(R13,FQ,FF,FQ,FI,FL)/FF)**FI)**
91      1(2+3/FI)
92       RETURN
10       END
20 C
30       FUNCTION DWC(R13,FQ,FF,FI,FL,FQ)
40       IF(R13-FQ)6070,6070,6080
50  6070 DWC=FF*(-R13)**(-1/FI-1)/(FI*(-FQ)**(-1/FI));GO TO 6081
60  6080 DWC=-2*FF*(1-FL/FF)*AMIN1(-10,R13)/(FQ*FQ*((FL/FF)**(-2*FI)))
70  6081 RETURN
80       END
90       REAL L,N,I,K,M
00       INTEGER R1,R2,R3,R4,R6,R8,R47,Q,R45,R14,W,A,R30,R46,R9,
10      1R49,R50,R51,R52,Z
20       DIMENSION A(50),B(50),N(50),I(50),RQ(50),RW(50),F(50),
30      1Q(50),L(50),D(50),E(50,6),H(50),K(50,6),M(50),P(50),S(50),
40      2T(50),U(50),V(50),O(50),Y(11,2),R(50),X(52)
50      3,Y1(50,2),Y2(50,2),Y3(50,2),Y4(50,2),RR(50),ER(50),IRATE(50)
51      4,SURF(50),DZ(50)
60 STATION=181;
70 C  A=WATER APPL DAY, B=MM WATER APPLIED, N=NEW WATER POTL, O=OLD WATER
80 C  POTL, I,RQ,F,RW,G&L=SOIL HYDROLOGIC CONSTANTS, E=WATER CONTENT,
90 C  H,X=ETRANS MM/LAYER/DAY, K=HYDR COND, D=ETRANS/TIME PERIOD, T=WATER
10 C  Y=DAILY OUTPUT DATA,IRATE=IRRIG RATE(MM/D),MAXDT=MAX DEL THETA
15 C  SURF=MAX SURFACE WATER STORAGE(MM)
18       PI=3.14159
20       READ(1,9510)R1,R2,R3,R4,R6,R7,R8,Q,PRINT,MAXDT
30       R45=AINT((R2-1)/7)-AINT((R1-1)/7)+1
35       R5=R8/(Q-1)
40       Q=AINT(R8/R5)+1
45       R5=R8/(Q-1)
50 C
60 C  READ SOIL HYDROLOGIC DATA
70 C
80       READ(1,9520)(DZ(J),N(J),R(J),RQ(J),I(J),F(J),RR(J),RW(J), J=1,Q)
90 C
96 C
97 C
98 C
00 C  READ WATER APPLICATION DATA
10 C
20       READ(1,9530)(A(J),B(J),IRATE(J),SURF(J),J=1,R4)
30 C
40 C  READ EVAPOTRANSPIRATION DATA X=TRANS/WEEK(MM) ER=MAX EVAP FLUX(MM/D)
50 C
60       READ(1,9540)(X(J),ER(J) ,J=1,R45)
70 C
80 C
90 C  CALCULATE CONSTANTS FOR SPECIAL FUNCTIONS
00 C
10       DO 500 J=1,Q
20       L(J)=2*I(J)*F(J)/(1+2*I(J))
30       G(J)=RQ(J)*(L(J)/F(J))**(-I(J))
40   500 CONTINUE
50 C
60    10 FORMAT(19X,'SOIL WATER MODEL - INPUT DATA'//)
70       WRITE(6,10)
80 C
90 C
00    30 FORMAT(' STARTING DAY NO  :',I3,'   NO OF NODES:  ',I5)
10       WRITE(6,30)R1,Q
20    40 FORMAT(' LAST DAY NO.       :',I3,'   BOTTOM BOUNDARY COND :',I5)
30       WRITE(6,40)R2,R6
40    50 FORMAT(' TIME INTERVALS/DAY:',I3,'   MIN WATER POTNL   :'I6,'KPA')
50       WRITE(6,50)R3,R7
60    60 FORMAT(' WATER APPLICATIONS:'I3,'   DEPTH OF PROFILE  :',I5,'MM')
70       WRITE(6,60)R4,R8
80    70 FORMAT(///6X,'INITIAL')
90       WRITE(6,70)
00    80 FORMAT(' DEPTH  WATER  FRACTION  HYDROLOGIC PARAMETERS')
10       WRITE(6,80)
20    90 FORMAT(7X,'POTNL  OF ROOTS')
30       WRITE(6,90)
40   100 FORMAT(' (MM)  (KPA)',14X,'A     B     WSAT     K'/)
50       WRITE(6,100)
60   110 FORMAT(I5,I6,F8.3,F8.2,F5.2,F7.3,I6)
70       DO 1000 J=1,Q
80       WRITE(6,110)DZ(J),N(J),R(J),RQ(J),I(J),F(J),RW(J)
```

```
)00    120 FORMAT(////10X,' PREDICTED RETENTIVITY AND CONDUCTIVITY DATA'//)
)10        WRITE(6,120)
)20    130 FORMAT(' DEPTH',21X,'WATER RETENTION')
)30        WRITE(6,130)
)40    140 FORMAT('   (MM)'19X,'(CONDUCTIVITY MM/DAY)'/)
)50        WRITE(6,140)
)60    150 FORMAT(9X,'SATRN',6X,'-3KPA     -10KPA     -30KPA    -100KPA    -500K
)65       1PA'//)
)70        WRITE(6,150)
)80        R10=1
)90 C      IF(Q.GT.20)R10=2
)92        P(1)=0
)94        P(2)=-306.6
)96        P(3)=-1022
)98        P(4)=-3066
 00        P(5)=-10220
 10        P(6)=-51100
 20    160 FORMAT(F5.0,6F10.3)
 30    170 FORMAT(5X,6E10.3)
 40        DO 2000 Z=1,6
 50        DO 2500 J=1,Q,R10
 55        R13=P(Z)
 60        E(J,Z)=THETA(R13,Q(J),F(J),RQ(J),I(J),L(J))
 70        K(J,Z)=HC(R13,Q(J),RW(J),RQ(J),I(J),F(J),L(J))
 80  2500  CONTINUE
 90  2000  CONTINUE
100        DO 3000 J=1,Q,R10
110        WRITE(6,160)DZ(J),(E(J,Z),Z=1,6)
120        WRITE(6,170)(K(J,Z),Z=1,6)
125  3000  CONTINUE
130    180 FORMAT(////10X,'WATER APPLIED'/)
140        WRITE(6,180)
150    190 FORMAT(5X,'TIME   DEPTH    RATE   SURF STORE')
160        WRITE(6,190)
170    200 FORMAT(7X,'D      MM       MM/H    MM'/)
180        WRITE(6,200)
190    210 FORMAT(F9.3,F6.1,F7.1,F6.1)
200        DO 3050 J=1,R4
210        WRITE(6,210)A(J),B(J),IRATE(J),SURF(J)
220  3050  CONTINUE
230    220 FORMAT(/// 7X,'EVAPOTRANSPIRATION'//)
240        WRITE(6,220)
250    230 FORMAT('     WEEK   TRANSPRN   MAX EVAP RATE')
260        WRITE(6,230)
270    240 FORMAT(11X,'MM/W',5X,'MM/D AT 12H00'/)
300        WRITE(6,240)
310    250 FORMAT(I6,F9.1,8X,F5.1)
320        R46=AINT((R2-1)/7)-AINT((R1-1)/7)+1
330        DO 4000 J=1,R46
340        WRITE(6,250)J,X(J),ER(J)
350  4000  CONTINUE
360  9510  FORMAT(4I5,I4,2I6,I5,F5.1,F6.3)
370  9520  FORMAT(I5,F8.1,F6.3,E11.3,F7.3,2F7.4,I7)
380  9530  FORMAT(F9.3,2F6.1,F6.1)
390  9540  FORMAT(2F6.1)
```

TABLE A1.6 Data format for file ADDO

RECORD	FORMAT	VARIABLE NAME	DESCRIPTION
1	I5	R1	First day number
	I5	R2	Last day number
	I5	R3	Minimum no. of time intervals per day
	I5	R4	No. of water applications
	I4	R6	Bottom boundary
	I6	R7	Minimum water potential (kPa) for root uptake
	I6	R8	Profile depth (mm)
	I5	Q	No. of nodes
	F5.1	PRINT	Print interval (days)
	F6.3	MAXDT	Maximum change in θ per time interval
For each node	I5	DZ	Depth of node below surface (mm)
	F8.1	N	Initial water potential (kPa)
	F6.3	R	Fraction of roots
	E11.3	RQ	Retentivity parameter a (mm)
	F7.3	I	Retentivity parameter b
	F7.4	F	Porosity or θ_s
	F7.4	FR	Residual saturation (if used)
	I7	RW	Hydraulic conductivity at saturation (mm d^{-1})
For each water appli- cation	F9.3	A	Time at start of water application (day)
	F6.1	B	Depth of water applied (mm)
	F6.1	IRATE	Rate of application (mm/d))not used in
	F6.1	SURF	Maximum surface storage (mm))this model
For each week	F6.1	X	Weekly evapotranspiration (mm)
	F6.1	ER	Potential surface evaporation rate (mm/d) at 12h00

TABLE A1.7 An example of ADDO, an input data file for WATDAT and WATFLO

```
  1   30   20    8   4 -1500  1800   37  1.0  .010
 00   -30.0 0.000 -0.259E+02  6.848 0.3333 0.0000  75000
050   -25.0 0.000 -0.160E+02  6.335 0.3815 0.0000  98800
100   -21.0 0.055 -0.150E+02  6.240 0.3889 0.0000 103000
150   -18.0 0.066 -0.171E+02  6.360 0.3741 0.0000  96200
200   -17.0 0.069 -0.210E+02  6.643 0.3519 0.0000  83600
250   -17.0 0.068 -0.212E+02  7.035 0.3519 0.0000  75400
300   -19.0 0.066 -0.196E+02  7.508 0.3611 0.0000  68700
350   -30.0 0.061 -0.153E+02  7.698 0.3852 0.0000  70000
400   -41.0 0.054 -0.121E+02  7.613 0.4075 0.0000  75600
450   -53.0 0.049 -0.110E+02  7.603 0.4167 0.0000  77500
500   -61.0 0.045 -0.105E+02  7.540 0.4222 0.0000  79700
550   -62.0 0.042 -0.105E+02  7.540 0.4222 0.0000  79700
600   -63.0 0.039 -0.108E+02  7.588 0.4185 0.0000  78100
650   -63.0 0.037 -0.115E+02  7.678 0.4111 0.0000  75100
700   -61.0 0.034 -0.123E+02  7.743 0.4037 0.0000  72600
750   -51.0 0.031 -0.136E+02  8.003 0.3963 0.0000  67000
800   -41.0 0.029 -0.157E+02  8.855 0.3963 0.0000  55600
850   -36.0 0.027 -0.157E+02  8.840 0.3981 0.0000  56000
900   -32.0 0.025 -0.161E+02  8.777 0.4000 0.0000  57100
950   -38.0 0.023 -0.166E+02  8.795 0.3981 0.0000  56600
1000  -35.0 0.021 -0.170E+02  8.820 0.3963 0.0000  56000
1050  -23.0 0.020 -0.184E+02  8.893 0.3907 0.0000  54400
1100  -20.0 0.019 -0.217E+02  9.042 0.3796 0.0000  51200
1150  -18.0 0.017 -0.251E+02  9.170 0.3704 0.0000  48700
1200  -16.0 0.016 -0.259E+02  9.195 0.3685 0.0000  48200
1250  -15.0 0.014 -0.261E+02  9.145 0.3667 0.0000  48500
1300  -15.0 0.013 -0.220E+02  8.828 0.3667 0.0000  51800
1350  -16.0 0.012 -0.209E+02  8.715 0.3648 0.0000  52700
1400  -19.0 0.010 -0.210E+02  8.480 0.3630 0.0000  55200
1450  -20.0 0.009 -0.226E+02  8.352 0.3630 0.0000  56700
1500  -21.0 0.008 -0.226E+02  8.380 0.3630 0.0000  56400
1550  -22.0 0.007 -0.227E+02  8.405 0.3630 0.0000  56100
1600  -22.0 0.006 -0.228E+02  8.433 0.3630 0.0000  55800
1650  -23.0 0.005 -0.228E+02  8.433 0.3638 0.0000  55800
1700  -24.0 0.003 -0.228E+02  8.433 0.3630 0.0000  55800
1750  -24.0 0.001 -0.228E+02  8.433 0.3630 0.0000  55800
1800  -24.0 0.000 -0.228E+02  8.433 0.3630 0.0000  55800
   2.000   1.5   0.0   0.0
   3.000   1.8   0.0   0.0
   5.000  37.9   0.0   0.0
  13.000  30.3   0.0   0.0
  15.000  14.2   0.0   0.0
  16.000  13.6   0.0   0.0
  22.000   3.3   0.0   0.0
  23.000  14.9   0.0   0.0
  25.1   0.0
  30.3   0.0
  31.2   0.0
```

SOIL WATER MODEL - INPUT DATA

STARTING DAY NO : 1 NO OF NODES: 37
LAST DAY NO. : 30 BOTTOM BOUNDARY COND : 4
TIME INTERVALS/DAY: 20 MIN WATER POTNL : -1500KPA
WATER APPLICATIONS: 8 DEPTH OF PROFILE : 1800MM

DEPTH (MM)	INITIAL WATER POTNL (KPA)	FRACTION OF ROOTS	HYDROLOGIC PARAMETERS A	B	WSAT	K
0	-30	0.000	-25.90	6.95	0.333	75000
50	-25	0.000	-16.00	6.34	0.381	98900
100	-21	0.055	-15.00	6.24	0.389	103000
150	-18	0.066	-17.10	6.36	0.374	96200
200	-17	0.069	-21.00	6.64	0.352	83500
250	-17	0.068	-21.20	7.04	0.352	75400
300	-19	0.066	-19.60	7.51	0.361	68700
350	-30	0.061	-15.30	7.70	0.385	70000
400	-41	0.054	-12.10	7.61	0.407	75600
450	-53	0.049	-11.00	7.60	0.417	77500
500	-61	0.045	-10.50	7.54	0.422	79700
550	-62	0.042	-10.50	7.54	0.422	79700
600	-63	0.039	-10.80	7.59	0.419	78100
650	-63	0.037	-11.50	7.68	0.411	75100
700	-61	0.034	-12.30	7.74	0.404	72600
750	-51	0.031	-13.60	8.00	0.396	67000
800	-41	0.029	-15.70	8.96	0.396	55600
850	-36	0.027	-15.70	8.94	0.398	56000
900	-32	0.025	-16.10	8.78	0.400	57100
950	-38	0.023	-16.60	8.80	0.398	56600
1000	-35	0.021	-17.00	8.92	0.396	56000
1050	-23	0.020	-18.40	8.99	0.391	54400
1100	-20	0.019	-21.70	9.04	0.380	51200
1150	-18	0.017	-25.10	9.17	0.370	48700
1200	-16	0.016	-25.90	9.19	0.369	48200
1250	-16	0.014	-26.10	9.15	0.367	48500
1300	-15	0.013	-22.00	8.93	0.367	51900
1350	-16	0.012	-20.90	8.72	0.365	52700
1400	-19	0.010	-21.00	8.48	0.363	55200
1450	-20	0.009	-22.60	8.35	0.363	56700
1500	-21	0.008	-22.60	8.38	0.363	56400
1550	-22	0.007	-22.70	8.41	0.363	56100
1600	-22	0.006	-22.80	8.43	0.363	55800
1650	-23	0.005	-22.80	8.43	0.364	55800
1700	-24	0.003	-22.80	8.43	0.363	55800

TABLE A1.8 An example of ADDOTEST, an output data file of WATDAT

PREDICTED RETENTIVITY AND CONDUCTIVITY DATA

DEPTH (MM)	WATER RETENTION (CONDUCTIVITY MM/DAY)					
	SATRN	-3KPA	-10KPA	-30KPA	-100KPA	-500K PA
0.	0. 332	0. 232	0. 195	0. 166	0. 139	0. 110
	. 703E+05	. 181E+03	. 963E+01	. 661E+00	. 351E-01	. 694E-03
50.	0. 377	0. 239	0. 198	0. 166	0. 139	0. 107
	. 832E+05	. 565E+02	. 339E+01	. 223E+00	. 114E-01	. 212E-03
100.	0. 384	0. 240	0. 198	0. 166	0. 137	0. 106
	. 846E+05	. 578E+02	. 292E+01	. 191E+00	. 964E-02	. 179E-03
150.	0. 371	0. 239	0. 197	0. 165	0. 137	0. 106
	. 828E+05	. 767E+02	. 391E+01	. 259E+00	. 132E-01	. 247E-03
200.	0. 350	0. 235	0. 196	0. 166	0. 139	0. 109
	. 757E+05	. 117E+03	. 611E+01	. 413E+00	. 216E-01	. 417E-03
250.	0. 350	0. 241	0. 203	0. 174	0. 146	0. 116
	. 695E+05	. 115E+03	. 621E+01	. 432E+00	. 233E-01	469E-03
300.	0. 359	0. 250	0. 213	0. 184	0. 157	0. 127
	. 614E+05	. 936E+02	. 521E+01	. 373E+00	. 207E-01	. 436E-03
350.	0. 381	0. 261	0. 223	0. 193	0. 165	0. 134
	. 583E+05	. 542E+02	. 305E+01	. 221E+00	. 124E-01	266E-03
400.	0. 401	0. 267	0. 228	0. 197	0. 169	0. 136
	. 564E+05	. 329E+02	. 184E+01	. 133E+00	. 745E-02	159E-03
450.	0. 409	0. 269	0. 230	0. 199	0. 170	0. 137
	. 543E+05	. 268E+02	. 150E+01	. 108E+00	. 605E-02	. 129E-03
500.	0. 413	0. 270	0. 230	0. 199	0. 170	0. 137
	. 539E+05	. 244E+02	. 136E+01	. 977E-01	. 544E-02	115E-03
550.	0. 413	0. 270	0. 230	0. 199	0. 170	0. 137
	. 539E+05	. 244E+02	. 136E+01	. 977E-01	. 544E-02	. 115E-03
600.	0. 410	0. 269	0. 230	0. 199	0. 170	0. 137
	. 540E+05	. 258E+02	. 144E+01	. 104E+00	. 581E-02	. 123E-03
650.	0. 404	0. 269	0. 229	0. 199	0. 170	0. 138
	. 543E+05	. 293E+02	. 165E+01	. 119E+00	. 670E-02	. 143E-03
700.	0. 398	0. 266	0. 228	0. 198	0. 169	0. 138
	. 547E+05	. 336E+02	. 190E+01	. 138E+00	. 777E-02	. 167E-03
750.	0. 392	0. 269	0. 231	0. 201	0. 173	0. 142
	. 532E+05	. 410E+02	. 235E+01	. 173E+00	. 991E-02	. 217E-03
800.	0. 393	0. 283	0. 247	0. 218	0. 191	0. 159
	. 459E+05	. 533E+02	. 319E+01	. 244E+00	. 146E-01	339E-03
850.	0. 395	0. 284	0. 248	0. 219	0. 191	0. 159
	. 472E+05	. 536E+02	. 320E+01	. 245E+00	. 147E-01	. 340E-03
900.	0. 397	0. 286	0. 249	0. 220	0. 192	0. 160
	. 485E+05	. 575E+02	. 343E+01	. 262E+00	. 156E-01	. 360E-03
950.	0. 395	0. 286	0. 249	0. 220	0. 192	0. 160
	. 486E+05	. 614E+02	. 366E+01	. 280E+00	. 167E-01	. 386E-03
1000.	0. 394	0. 286	0. 249	0. 220	0. 192	0. 160
	. 484E+05	. 644E+02	. 385E+01	. 294E+00	. 176E-01	. 407E-03
1050.	0. 388	0. 285	0. 249	0. 220	0. 192	0. 160
	. 481E+05	. 758E+02	. 455E+01	. 349E+00	. 209E-01	. 486E-03
1100.	0. 378	0. 283	0. 248	0. 220	0. 192	0. 161
	. 468E+05	. 107E+03	. 643E+01	. 496E+00	. 300E-01	. 702E-03
1150.	0. 369	0. 282	0. 247	0. 219	0. 192	0. 161
	. 456E+05	. 144E+03	. 874E+01	. 678E+00	. 411E-01	. 972E-03
1200.	0. 367	0. 282	0. 247	0. 219	0. 192	0. 161
	. 453E+05	. 154E+03	. 938E+01	. 725E+00	. 440E-01	. 104E-02
1250.	0. 366	0. 280	0. 246	0. 218	0. 191	0. 160
	. 456E+05	. 157E+03	. 950E+01	. 736E+00	. 446E-01	. 105E-02
1300.	0. 365	0. 272	0. 237	0. 210	0. 183	0. 152
	. 475E+05	. 109E+03	. 651E+01	. 498E+00	. 298E-01	. 689E-03
1350.	0. 363	0. 268	0. 233	0. 206	0. 179	0. 149
	. 479E+05	. 971E+02	. 578E+01	. 440E+00	. 261E-01	. 601E-03
1400.	0. 361	0. 265	0. 230	0. 202	0. 175	0. 145
	. 502E+05	. 100E+03	. 590E+01	. 444E+00	. 261E-01	. 591E-03
1450.	0. 361	0. 266	0. 230	0. 202	0. 175	0. 144
	. 522E+05	. 121E+03	. 705E+01	. 528E+00	. 308E-01	. 692E-03
1500.	0. 361	0. 266	0. 230	0. 202	0. 175	0. 144
	. 519E+05	. 120E+03	. 705E+01	. 528E+00	. 309E-01	. 695E-03
1550.	0. 362	0. 266	0. 231	0. 202	0. 175	0. 145
	. 517E+05	. 121E+03	. 711E+01	. 534E+00	. 313E-01	. 704E-03
1600.	0. 362	0. 267	0. 231	0. 203	0. 176	0. 145
	. 515E+05	. 122E+03	. 719E+01	. 540E+00	. 316E-01	714E-03
1650.	0. 362	0. 267	0. 232	0. 203	0. 176	0. 146
	. 515E+05	. 122E+03	. 719E+01	. 540E+00	. 316E-01	. 714E-03
1700.	0. 362	0. 267	0. 231	0. 203	0. 176	0. 145
	. 515E+05	. 122E+03	. 719E+01	. 540E+00	. 316E-01	. 714E-03
1750.	0. 362	0. 267	0. 231	0. 203	0. 176	0. 145
	. 515E+05	. 122E+03	. 719E+01	. 540E+00	. 316E-01	. 714E-03
1800.	0. 362	0. 267	0. 231	0. 203	0. 176	0. 145

EVAPOTRANSPIRATION

WEEK	TRANSPRN MM/W	MAX EVAP MM/D AT
1	25. 1	0. 0
2	30. 3	0. 0
3	31. 2	0. 0
4	30. 1	0. 0
5	29. 9	0. 0

WATER APPLIE

TIME D	DEPTH MM	RAT MM/
2. 000	1. 5	0. 0
3. 000	1. 8	0. 0
5. 000	37. 9	0. 0
13. 000	30. 3	0. 0
15. 000	14. 2	0. 0
16. 000	13. 6	0. 0
22. 000	3. 3	0. 0
23. 000	14. 9	0. 0

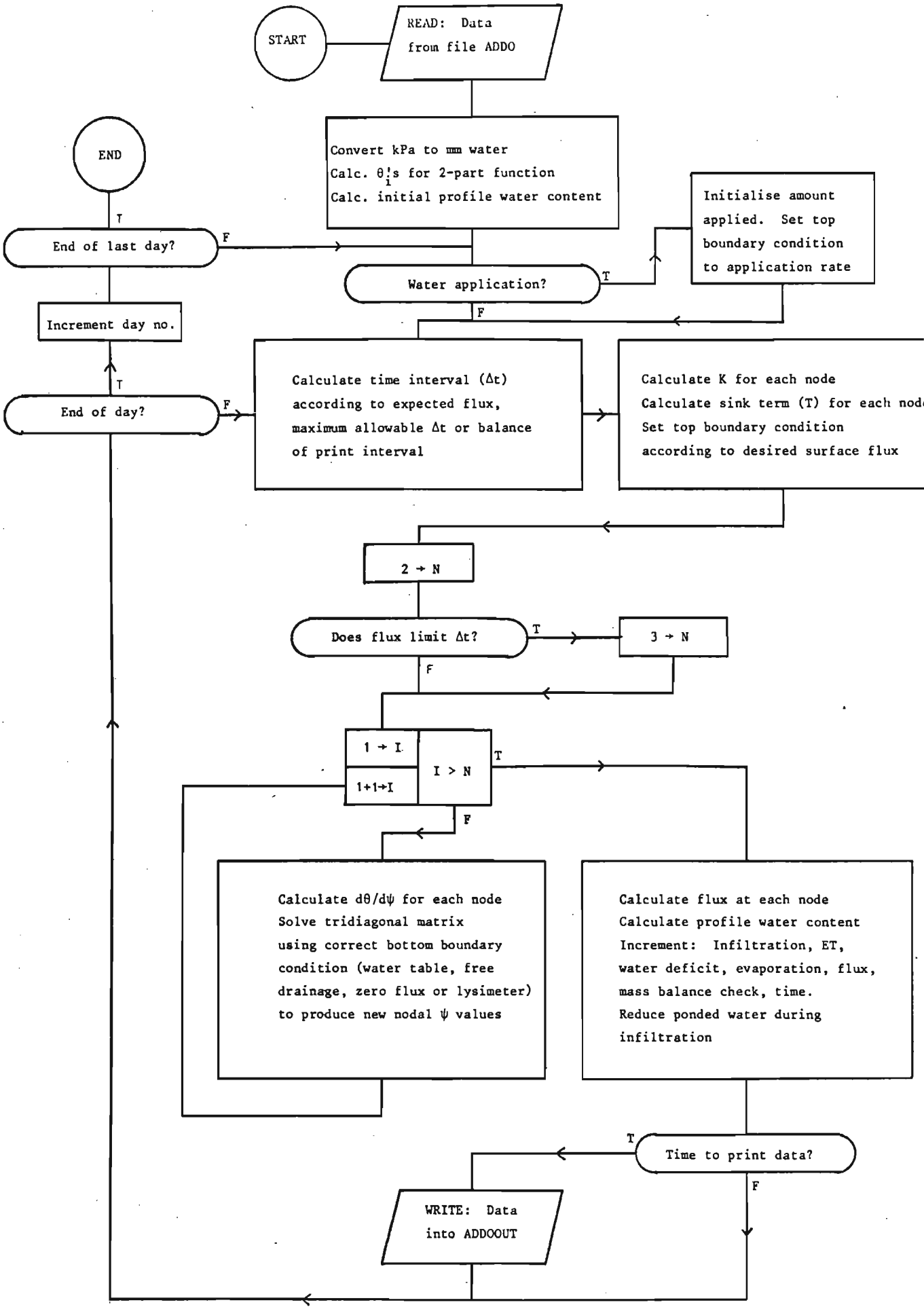

FIGURE A1.4 Flowchart for WATFLO, a soil water simulation program

TABLE A1.9 A FORTRAN program for WATFLO

```
) FILE   6=JLH/ADDOOUT,UNIT=DISK,RECORD=14,BLOCKING=420
) FILE   1=JLH/ADDO,UNIT=DISK,RECORD=14,BLOCKING=420
) FILE   5=JLH/ADDOOUT1,UNIT=DISK,RECORD=22,BLOCKING=660
) $RESET FREE
) C
) C
) C
) C
) C  R1=FIRST DAY NO, R2=LAST DAY NO, R3=MIN.NO TIME INTERVALS/DAY,
) C  R4=NO OF IRRIGATIONS, R5=DEPTH NODE INTERVALS, R6=BOTTOM BOUNDARY,
) C  R7=MIN. WATER POTL(MM), R8=PROFILE DEPTH, R44=PRINT INTERVAL(DAYS),
) C  R47=NO.OF PRINTS/PAGE(2 IN THIS VERSION)
) C  RATE OF WATER APPLICATION & SURFACE STORAGE NOT INCLUDED
)       FUNCTION THETA(R13,FG,FF,FQ,FI,FL)
)       IF(R13-FG)6050,6050,6060
)  6050 THETA=FF*(AMIN1(FQ,R13)/FQ)**(-1/FI);GO TO 6061
)  6060 THETA=FF-(FF*(1-FL/FF)*((AMIN1(R13,-10))**2))/(FQ*FQ*((FL/FF)**(-2
)     1*FI)))
)  6061 RETURN
)       END
)       FUNCTION POTL(R13,FL,FF,FQ,FI)
)       IF(R13-FL)6040,6030,6030
)  6030 POTL=(SQRT(1-R13/FF))*FQ*((FL/FF)**(-FI))/SQRT(1-FL/FF)
)  6040 IF(R13.LT.FQ)POTL=FQ*(R13/FF)**(-FI)
)       RETURN
)       END
) C
) C
)       FUNCTION HC(R13,FG,FW,FQ,FI,FF,FL)
)       IF(R13.LE.FG)HC=AMIN1(FW,FW*(FQ/AMIN1(FQ,R13))**(2+3/FI))
)       IF(R13.GT.FG)HC=FW*((THETA(R13,FG,FF,FQ,FI,FL)/FF)**FI)**
)      1(2+3/FI)
)       RETURN
)       END
) C
)       FUNCTION DWC(R13,FG,FF,FI,FL,FQ)
)       IF(R13-FG)6070,6070,6080
)  6070 DWC=FF*(-R13)**(-1/FI-1)/(FI*(-FQ)**(-1/FI));GO TO 6081
)  6080 DWC=-2*FF*(1-FL/FF)*AMIN1(-10,R13)/(FQ*FQ*((FL/FF)**(-2*FI)))
)  6081 RETURN
)       END
)       REAL L,N,I,K,M,MAXDT,IRATE
)       INTEGER R1,R2,R3,R4,R5,R9,R47,Q,R45,R14,W,A,R30,R46,R9,
)      1R49,R50,R51,R52
)       DIMENSION A(60),B(60),N(60),I(60),RQ(60),RW(60),F(60),
)      1G(60),L(60),D(60),E(60),H(60),K(60),M(60),P(60),S(60),
)      2T(60),U(60),V(60),O(60),Z(60),Y(11,2),R(60),X(62)
)      3,Y1(60,2),Y2(60,2),Y3(60,2),Y4(60,2),FR(60),ER(60),IRATE(60)
) C  A=WATER APPL DAY, B=MM WATER APPLIED, N=NEW WATER POTL, O=OLD WATER
) C  POTL, I,RQ,F,RW,G&L=SOIL HYDROLOGIC CONSTANTS, E=WATER CONTENT,
) C  H,X=ETRANS MM/LAYER/DAY, K=HYDR COND, D=ETRANS/TIME PERIOD, T=WATER
) C  DEFICIT, U=FLUX RATE, V=FLUX, Z=DIF WATER CAP., P,M=GAUSS CONSTANTS
) C  Y=DAILY OUTPUT DATA,IRATE=IRRIG RATE(MM/D),MAXDT=MAX DEL THETA
) C  SURF=MAX SURFACE WATER STORAGE(MM)
)       PI=3.14159
)       READ(1,9510)R1,R2,R3,R4,R6,R7,R8,Q,PRINT,MAXDT
)       R45=AINT((R2-1)/7)-AINT((R1-1)/7)+1
)       R5=R8/(Q-1)
) C
) C
) C  READ SOIL HYDROLOGIC DATA
) C
)       READ(1,9520)(DZ(J),N(J),R(J),RQ(J),I(J),F(J),FR(J),RW(J), J=1,Q)
) C  CONVERT KPA TO MM WATER
)       DO 100 J=1,Q
)       N(J)=N(J)*102.2
)  100 CONTINUE
)       R7=102.2*R7
) C  READ WATER APPLICATION DATA
) C
)       READ(1,9530)(A(J),B(J),IRATE(J),SURF(J),J=1,R4)
) C
) C  READ EVAPOTRANSPIRATION DATA X=TRANS/WEEK(MM) ER=MAX EVAP FLUX(MM/D)
) C
)       READ(1,9540)(X(J),ER(J),J=1,R45)
)       WRITE(6,9999)
) C
) C  CALCULATE POINT OF COINCIDENCE OF EXP. & PARABOLIC FUNCTIONS
) C
)       DO 500 J=1,Q
)       L(J)=2*I(J)*F(J)/(1+2*I(J))
)       G(J)=RQ(J)*(L(J)/F(J))**(-I(J))
)  500 CONTINUE
) C
) C  INITIALIZE VARIABLES
) C
)       R15=0
)       R16=1.0/FLOAT(R3)
)       R18=R16
)       R14=1
)       R21=R5
)       R19=10**10
)       R20=10**(-10)
)       DO 600 J=1,Q
)       T(J)=0
)       O(J)=N(J)
)       R13=N(J)
)       E(J)=THETA(R13,G(J),F(J),RQ(J),I(J),L(J))
```

```
300 C  CALCULATE INITIAL PROFILE WATER CONTENT, R22
400 C
500       DO 700 J=2,Q-1
600       R22=R22+E(J)
700   700 CONTINUE
800 C
900 C  START OF DAILY CYCLE
000 C
100
200       DO 1000 W=R1,R2
300 C
400 C  ASSIGNMENT OF DAILY ETRANS/LAYER TO H(J), WEIGHTED ACCORDING TO
500 C  ROOT DISTRIBUTION AND WATER POTENTIAL.  CHANGE TO SUIT THE
550 C  ROOT UPTAKE/POTENTIAL RELATIONSHIP DESIRED
600       IF(W.NE.R1.AND.AMOD((W-1),7.0).NE.0)GO TO 1100
700       R45=AINT((W-1)/7)-AINT((R1-1)/7)+1
800   1100 DO 1200 J=1,Q
900       TR=TR+R(J)
000
100   1200 CONTINUE
200       DO 1250 J=1,Q
300       H(J)=2.5*X(R45)*R(J)/(7*TR)
400       H(J)=H(J)
500   1250 CONTINUE
600       TR=0
700 C
800 C  SET PONDED WATER TO CORRECT DEPTH
900 C
100       R25=0
200       IF(R4.EQ.0)GO TO 1300
300       IF(W.NE.A(R14))GO TO 1800
400       IF(R27)1600,1600,1500
500   1500 R27=R27+B(R14)
600       J=1
700       GO TO 1700
800   1600 R27=B(R14)
900   1700 R10=0
950 C  PRINT: TIME & PONDED WATER ON SURFACE (ONLY DURING INFILTRATION)
000       WRITE(6,9100)
.00       WRITE(6,9110)W
200       WRITE(6,9120)
300       WRITE(6,9130)R25,R27
400       O(1)=0
500       E(1)=F(1)
600   1300 R19=10**10
700       IF(R14.EQ.R4)GO TO 1800
800       R14=R14+1
900 C TIMES ELAPSED:   R24=PRINT INTERVAL R25=PER DAY R20=PER.1DAY
000   1800 R28=R18
.00       IF(AINT(R20*10**8).GE..1*10**8)R20=0
200       R30=2
```

```
15500       R18=AMAX1(10**(-10),R18)
15600       R19=10**(-10)
15700       IF(R20+R18-.1)2100,2100,2050
15800   2050 R18=.1-R20
15900   2100 R20=R20+R18
16000       R24=R18+R24
16100       R25=R25+R18
16200 C
16300 C  SET TOP BOUNDARY CONDITION
16400       IF(R27)2550,2550,2500
16500   2550 M(1)=1
16600 C EVAP RATE (EV) SET ACCORDING TO TIME OF DAY
16700       EV=-ER(R45)*AMAX1(0,SIN(2*PI*(R25-R18/2-.25)))
16800       J=1;K(J)=HC(R13,Q(J),RW(J),RQ(J),I(J),F(J),L(J))
16900       J=2;K(J)=HC(R13,Q(J),RW(J),RQ(J),I(J),F(J),L(J))
17000       K(1)=(K(1)+K(2))/2
17100       IF(EV-K(1)*(N(1)-300000-2*N(2))/(2*R5))2490,2490,2495
17200   2490 P(1)=-300000-N(2);M(1)=1
17300       GO TO 2600
17400   2495 M(1)=1
17500       P(1)=AMIN1(-R5,(EV-K(1))*2*R5/K(1)-N(1)+N(2))
17600       GO TO 2600
17700   2500 E(1)=F(1)
17800       N(1)=0
17900       M(1)=0
18000       P(1)=0
18100   2600 CONTINUE
18200       R46=0
18300       J=1
18400       R13=O(1)
18500       K(1)=HC(R13,Q(J),RW(J),RQ(J),I(J),F(J),L(J))
18600 C
18700 C  INITIALIZE HYDRAULIC CONDUCTIVITIES
18800 C
18900       DO 2800 J=2,Q
19000       R13=O(J)
19100       K(J)=HC(R13,Q(J),RW(J),RQ(J),I(J),F(J),L(J))
19200       K(J-1)=(K(J)+K(J-1))/2
19300   2800 CONTINUE
19400 C
19500 C  SIMULTANEOUS EQUATION SOLUTION- FORWARD
19600 C
19700   3500 DO 3600 J=1,Q
19800       R13=AMIN1(-10.0(J)+.58*(N(J)-O(J)))
19900       Z(J)=DWC(R13,Q(J),F(J),I(J),L(J),RQ(J))
20000   3600 CONTINUE
20100       DO 3900 J=2,Q-1
20200       S(J)=0
20300       IF(R25-R18.GE..3.AND.R25.LE..7)S(J)=R18*H(J)/R5
20400   3660 R32=K(J)
20500       R34=K(J-1)
20600       R33=2*R5*R5*Z(J)/R18+R32+R34
```

```
      IF(D(J).LT.R7)S(J)=0
      IF(R46-R30)3700,3750,3700
 3750 IF(R25-R18.LT..3.OR.R25.GT..7)GO TO 3700
      T(J)=T(J)+(H(J)*R18-S(J)*R5)
      R36=R36+S(J)*R5
 3700 S(J)=S(J)/R18
      R35=R32*D(J+1)+R34*D(J-1)+(R33-2*R32-2*R34)*D(J)
      R35=R35+2*R5*(K(J-1)-K(J))-S(J)*2*R5*R5
      M(J)=R32/(R33-R34*M(J-1))
      P(J)=(R35+R34*P(J-1))/(R33-R34*M(J-1))
 3900 CONTINUE
C  SOLUTION OF SIMULTANEOUS EQUATIONS-REVERSE
C
C  SET BOTTOM BOUNDARY CONDITIONS
C
      IF(R6.EQ.4.AND.N(Q).GT.0)N(Q)=0
      IF(R6.NE.4)R9=R6
      IF(R9.NE.1)GO TO 4100
      N(Q)=0
      R13=0
      E(Q)=THETA(R13,G(Q),F(Q),RG(Q),I(Q),L(Q))
      GO TO 4200
 4100 IF(R9.NE.3)GO TO 4150
      N(Q)=(2*R5-D(Q)+D(Q-1)+P(Q-1))/(1-M(Q-1))
      R13=N(Q)
      E(Q)=THETA(R13,G(Q),F(Q),RG(Q),I(Q),L(Q))
      GO TO 4200
 4150 IF(R9.NE.2)GO TO 4200
      N(Q)=(P(Q-1)-D(Q)+D(Q-1))/(1-M(Q-1))
      R13=N(Q)
      E(Q)=THETA(R13,G(Q),F(Q),RG(Q),I(Q),L(Q))
 4200 J=Q
 4210 J=J-1
      N(J)=M(J)*N(J+1)+P(J)
      R13=N(J)
      IF(R46.LT.R30.AND.J.GT.1)GO TO 4210
      IF(R46-R30)4250,4300,4300
 4250 R46=R46+1
      GO TO 3500
 4300 E(J)=THETA(R13,G(J),F(J),RG(J),I(J),L(J))
      U(J)=(K(J)-K(J)*(N(J+1)+D(J+1)-N(J)-D(J))/(2*R5))*R18
      R37=ABS(U(J)/R18)
C  RECORD MAXIMUM FLUX
      R19=AMAX1(R19,R37)
      V(J)=V(J)+U(J)
 4500 IF(J.GT.1)GO TO 4210
      DO 4550 J=1,Q
      D(J)=N(J)
 4550 CONTINUE
C INCREMENT LEACHATE R38, INFILTRATION R40, SURFACE FLUX R39
      ETRANS=-R39+R36
      IF(R9.NE.3)R38=R38+U(Q-1)
      IF(R6-4)4600,4650,4600
 4650 R9=3
      IF(N(Q-1).GT.-R5)R9=1
 4600 IF(U(1).LE.0)GO TO 4700
      R40=R40+U(1)
      R27=R27-U(1)
      IF(R27.LE.0)R27=0
      IF(R27.GT.0)R10=R10+1
      IF(R27.GT.0.AND.R10.EQ.4)WRITE(6,9130)R25,R27
      IF(R10.EQ.4)R10=0
 4700 IF(AINT(R20*10**8).LT.1*10**7)GO TO 1800
      IF(AINT(R24*10**3+5).GE.PRINT*10**3)GO TO 5500
      IF(AINT(R25*10**3+5).GE.1*10**3)GO TO 1000
      GO TO 1800
 5500 R41=0
      R47=R47+1
      DO 5600 J=2,Q-1
      R41=R41+E(J)
 5600 CONTINUE
C
C  MASS BALANCE CHECK
C
      R42=(R41-R22)*R5
      R43=R40-R42-ETRANS
C
      Y(1,R47)=W
      Y(2,R47)=R25
      Y(3,R47)=R40
      Y(4,R47)=R38
      Y(5,R47)=-R39
      Y(6,R47)=R27
      Y(7,R47)=R43
      Y(8,R47)=R5*R41
      Y(9,R47)=R14
      Y(10,R47)=ETRANS
      Y(11,R47)=R42
      DO 5700 J=1,Q
      Y1(J,R47)=E(J)
      Y3(J,R47)=V(J)
      Y2(J,R47)=N(J)/102.2
      Y4(J,R47)=T(J)
C
C
C
C
      T(J)=0
      V(J)=0
 5700 CONTINUE
```

```
1200        WRITE(5,9060)
1300        WRITE(5,9053)
1400        DO 7000 J=1,Q,6
1500        DE(J)=J*R5-R5
1600   7000 CONTINUE
1700        WRITE(5,9065)W,R40,R39,ETRANS,R38,R5*R41,R42,R43,(DE(J),J=1,Q,6)
1800        WRITE(5,9070)(N(J)/102.2,J=1,Q,6)
1900        WRITE(5,9075)(E(J),J=1,Q,6)
2000        WRITE(5,9080)(Y3(J,R47),J=1,Q,6)
2100        WRITE(5,9085)(Y4(J,R47),J=1,Q,6)
2200        WRITE(5,9053)
2300   9060 FORMAT(1X," DAY   INF    E     ET    D     PWC  DPWC   CHECK
2400       1     DEPTH/POTENTIAL/THETA/FLUX DENSITY/WATER DEFICIT")
2500   9065 FORMAT(F7.1,4F6.1,2F7.1,F6.1,8F8.1)
2600   9070 FORMAT(51X,7F8.1)
2700   9075 FORMAT(51X,7F8.1)
2800   9080 FORMAT(51X,7F8.3)
2900   9085 FORMAT(51X,7F8.3)
2950        R24=0
3000        IF(R47-2)6100,5800,6100
3100   5800 WRITE(6,9010)Y(1,1),Y(1,2)
3200        R49=AINT(Y(2,1)*24.0)
3300        R51=AINT(Y(2,2)*24.0)
3400        R50=60*(Y(2,1)*24.0-AINT(Y(2,1)*24.))
3500        R52=60*(Y(2,2)*24.-AINT(Y(2,2)*24.))
3600        WRITE(6,9020)R49,R50,Y(2,1),R51,R52,Y(2,2)
3700        WRITE(6,9030)Y(3,1),Y(3,2)
3800        WRITE(6,9032)Y(4,1),Y(4,2)
3900        WRITE(6,9034)Y(5,1),Y(5,2)
4000        WRITE(6,9036)Y(6,1),Y(6,2)
4100        WRITE(6,9038)Y(10,1),Y(10,2)
4200        WRITE(6,9044)Y(11,1),Y(11,2)
4300        WRITE(6,9040)Y(8,1),Y(8,2)
4400        WRITE(6,9042)Y(9,1),Y(9,2)
4500        WRITE(6,9046)Y(7,1),Y(7,2)
4600 C
4700        WRITE(6,9050)
4800        WRITE(6,9052)
4900        R54=AINT(Q/20)+1
5000        DO 6000 J=1,Q,R54
5100        R55=J*R5-R5
5200        WRITE(6,9054)R55,Y1(J,1),Y2(J,1),Y3(J,1),Y4(J,1),R55,Y1(J,2),
5300 C
5400       1Y2(J,2),Y3(J,2),Y4(J,2)
5500   6000 CONTINUE
5600        R47=0
5700   6100 IF(AINT(R25*10**3+5).LT.10**3)GO TO 1800
5800 C
5900 C
```

```
36300 C
36400 C  FORMATS
36500 C
36600        WRITE(6,9999)
36700   9010 FORMAT(////13X,'DAY',I3,31X,'DAY',I3)
36800   9020 FORMAT(/2(6X,'TIME',I2,'H',I2,F8.3,'DAY',12X))
36900   9030 FORMAT(//2(3X,'  CUM.  INFILTRATION: ',F6.1,9X))
37000   9032 FORMAT(2(3X,'  CUM. LEACHATE     : ',F6.1,9X))
37100   9034 FORMAT(2(3X,'  CUM. EVAPORATION  : ',F6.1,9X))
37200   9036 FORMAT(2(3X,'  PONDED WATER      : ',F6.1,9X))
37300   9038 FORMAT(2(3X,'  CUM. EVAPOTRANS   : ',F6.1,9X))
37400   9040 FORMAT(2(3X,'PROFILE WATER CONT.: ',F6.1,9X))
37500   9042 FORMAT(2(3X,'  WATER APPL. NO.   : ',I4,11X))
37600   9044 FORMAT(2(1X,'   PROF. WATER CHANGE: ',F6.1,9X))
37700   9046 FORMAT(2(3X,'  CHECK'12X,': ',F6.1,11X))
37800   9050 FORMAT(//2(1X,'DEPTH THETA  POTL. FLUX  WATER',5X))
37900   9052 FORMAT(2(1X,'  MM',10X,'KPA    MM  DEFICIT',4X)/)
38000   9054 FORMAT(2(1X,I4,F6.3,F7.1,F7.2,F5.1,7X))
38100   9053 FORMAT(1X)
38200   9100 FORMAT(////1X,3X,'INFILTRATION')
38300   9120 FORMAT(1X,'  TIME    MM WATER'/)
38400   9130 FORMAT(1X,F7.3,F8.1)
38500   9510 FORMAT(4I5,I4,2I6,I5,F5.1,F6.3)
38600   9520 FORMAT(I5,F8.1,F6.3,E11.3,F7.3,2F7.4,I7)
38700   9530 FORMAT(F9.3,3F6.1 )
38800   9540 FORMAT(2F6.1)
38900   9110 FORMAT(1X,'   DAY',F4.0)
39000   9999 FORMAT('****')
39100        LOCK(5)
39200        LOCK(6)
39300        END
39400
39500
```

TABLE A1.10 An example of ADDOOUT, an output data file of WATFLO

DAY 5

TIME23H59 1.000DAY

CUM. INFILTRATION:	41.8
CUM. LEACHATE :	0.0
CUM. EVAPORATION :	0.4
PONDED WATER :	0.0
CUM. EVAPOTRANS :	16.6
PROF. WATER CHANGE:	24.3
PROFILE WATER CONT. :	379.8
WATER APPL. NO. :	4
CHECK :	1.0

DEPTH MM	THETA	POTL. KPA	FLUX MM	WATER DEFICIT
0	0.193	-10.7	39.13	0.0
100	0.198	-9.8	33.89	0.0
200	0.199	-9.0	29.25	0.0
300	0.219	-8.2	24.57	-0.0
400	0.235	-7.7	19.59	0.0
500	0.237	-8.1	14.40	-0.0
600	0.231	-9.5	9.49	0.0
700	0.222	-12.4	5.48	-0.0
800	0.233	-16.6	2.67	0.0
900	0.228	-22.0	0.89	0.0
1000	0.222	-27.9	0.02	-0.0
1100	0.219	-30.6	-0.29	0.0
1200	0.219	-30.4	-0.39	0.0
1300	0.210	-29.3	-0.41	0.0
1400	0.203	-27.9	-0.37	0.0
1500	0.205	-26.5	-0.30	-0.0
1600	0.207	-25.2	-0.20	0.0
1700	0.208	-24.1	-0.09	-0.0
1800	0.209	-23.6	0.00	0.0

DAY 6

TIME23H59 1.000DAY

CUM. INFILTRATION:	41.8
CUM. LEACHATE :	0.0
CUM. EVAPORATION :	0.4
PONDED WATER :	0.0
CUM. EVAPOTRANS :	19.7
PROF. WATER CHANGE:	21.1
PROFILE WATER CONT. :	376.6
WATER APPL. NO :	4
CHECK :	1.0

DEPTH MM	THETA	POTL. KPA	FLUX MM	WATER DEFICIT
0	0.186	-13.9	0.00	0.0
100	0.190	-13.0	0.68	0.0
200	0.190	-12.2	1.15	0.0
300	0.210	-11.4	1.64	0.0
400	0.225	-10.9	2.29	0.0
500	0.227	-11.2	3.01	0.0
600	0.223	-12.4	3.61	0.0
700	0.218	-14.3	3.91	-0.0
800	0.234	-16.5	3.80	0.0
900	0.232	-18.6	3.30	0.0
1000	0.229	-21.3	2.51	0.0
1100	0.225	-23.6	1.72	0.0
1200	0.224	-24.5	1.08	0.0
1300	0.214	-25.0	0.57	0.0
1400	0.206	-25.3	0.24	0.0
1500	0.206	-25.5	0.07	0.0
1600	0.207	-25.1	-0.00	0.0
1700	0.208	-24.3	-0.01	0.0
1800	0.209	-23.9	0.00	0.0

DAY 7

TIME23H59 1.000DAY

CUM. INFILTRATION:	41.8
CUM. LEACHATE :	0.0
CUM. EVAPORATION :	0.4
PONDED WATER :	0.0
CUM. EVAPOTRANS :	22.8
PROF. WATER CHANGE:	18.0
PROFILE WATER CONT. :	373.5
WATER APPL. NO. :	4
CHECK :	1.0

DEPTH MM	THETA	POTL. KPA	FLUX MM	WATER DEFICIT
0	0.191	-16.8	0.00	0.0
100	0.194	-15.9	0.42	0.0
200	0.194	-15.1	0.61	0.0
300	0.203	-14.3	0.81	0.0
400	0.218	-13.8	1.12	0.0
500	0.220	-14.1	1.51	0.0
600	0.217	-15.2	1.86	0.0
700	0.213	-16.8	2.11	-0.0
800	0.231	-19.3	2.23	0.0
900	0.231	-19.6	2.25	0.0
1000	0.229	-21.1	2.13	0.0
1100	0.227	-22.3	1.90	0.0
1200	0.226	-22.6	1.61	0.0
1300	0.216	-22.7	1.30	0.0
1400	0.208	-23.0	0.99	0.0
1500	0.209	-23.0	0.67	0.0
1600	0.210	-22.7	0.39	0.0
1700	0.211	-22.1	0.12	0.0
1800	0.211	-21.7	0.00	0.0

DAY 8

TIME23H59 1.000DAY

CUM. INFILTRATION:	41.8
CUM. LEACHATE :	0.0
CUM. EVAPORATION :	0.4
PONDED WATER :	0.0
CUM. EVAPOTRANS :	26.5
PROF. WATER CHANGE:	14.2
PROFILE WATER CONT. :	369.7
WATER APPL. NO. :	4
CHECK :	1.1

DEPTH MM	THETA	POTL. KPA	FLUX MM	WATER DEFICIT
0	0.176	-20.1	0.00	0.0
100	0.178	-19.2	0.34	0.0
200	0.179	-18.5	0.38	0.0
300	0.198	-17.7	0.44	0.0
400	0.212	-17.2	0.61	0.0
500	0.214	-17.4	0.86	0.0
600	0.212	-18.2	1.09	0.0
700	0.209	-19.5	1.26	0.0
800	0.228	-20.6	1.37	0.0
900	0.229	-21.4	1.42	0.0
1000	0.228	-22.2	1.40	0.0
1100	0.226	-22.7	1.31	0.0
1200	0.226	-22.5	1.18	0.0
1300	0.217	-22.1	1.03	0.0
1400	0.209	-22.0	0.84	0.0
1500	0.210	-21.5	0.62	0.0
1600	0.212	-20.9	0.38	0.0
1700	0.213	-20.1	0.12	-0.0
1800	0.213	-19.7	0.00	0.0

APPENDIX 2

COMPUTER PROGRAMS AND FILES FOR ESTIMATING K BY AN OUTFLOW/INFLOW METHOD

The method of estimating K_s and p described in Chapter 6 is based on matching measured outflow or inflow curves to a family of simulated curves. Simulated outflow or inflow data are generated using the program OUTFLO, for which a flowchart (Fig. A2.1) and program listing (Table A2.2) are presented. Input data (Table A2.3) are stored in file TEMPE according to the format listed in Table A2.1.

A sample simulation (Table A2.4) shows outflow data generated for each combination of four values of K_s and two values of p.

TABLE A2.1 Format for file OUTFLO

RECORD	FORMAT	VARIABLE NAME	DESCRIPTION
1	I4	TRUN	Number of simulations
2	F4.0	R4	Plate thickness
	F4.0	R5	Node interval (mm)
	F5.0	R8	Core depth (mm)
	F7.1	R50	Core diameter
	F7.3	R55	Maximum allowable $\Delta\theta$ per time period
3	E10.3	A	Retentivity parameter a (mm)
	F9.3	B	Retentivity parameter b
	F8.4	PORE	Fractional porosity or θ_s
	F6.2	R7	Plate conductivity (mm/d)
4	F9.2	R53	Initial pressure potential at plate surface (kPa)
	F9.2	R54	Final pressure potential at plate surface (kPa)
5	F6.2	CLO	Lowest value of log K_s (mm/d)
	F6.2	CHI	Highest value of log K_s (mm/d)
	F6.2	CINT	(CHI-CLO)/3
	F6.2	PLO	Lowest value of tortuosity parameter p
	F6.2	PHI	Highest value of tortuosity parameter p
	F6.2	PINT	(PHI-PLO)/3
6 to	Repetition of records 2, 3, 4 and 5 containing data for next		

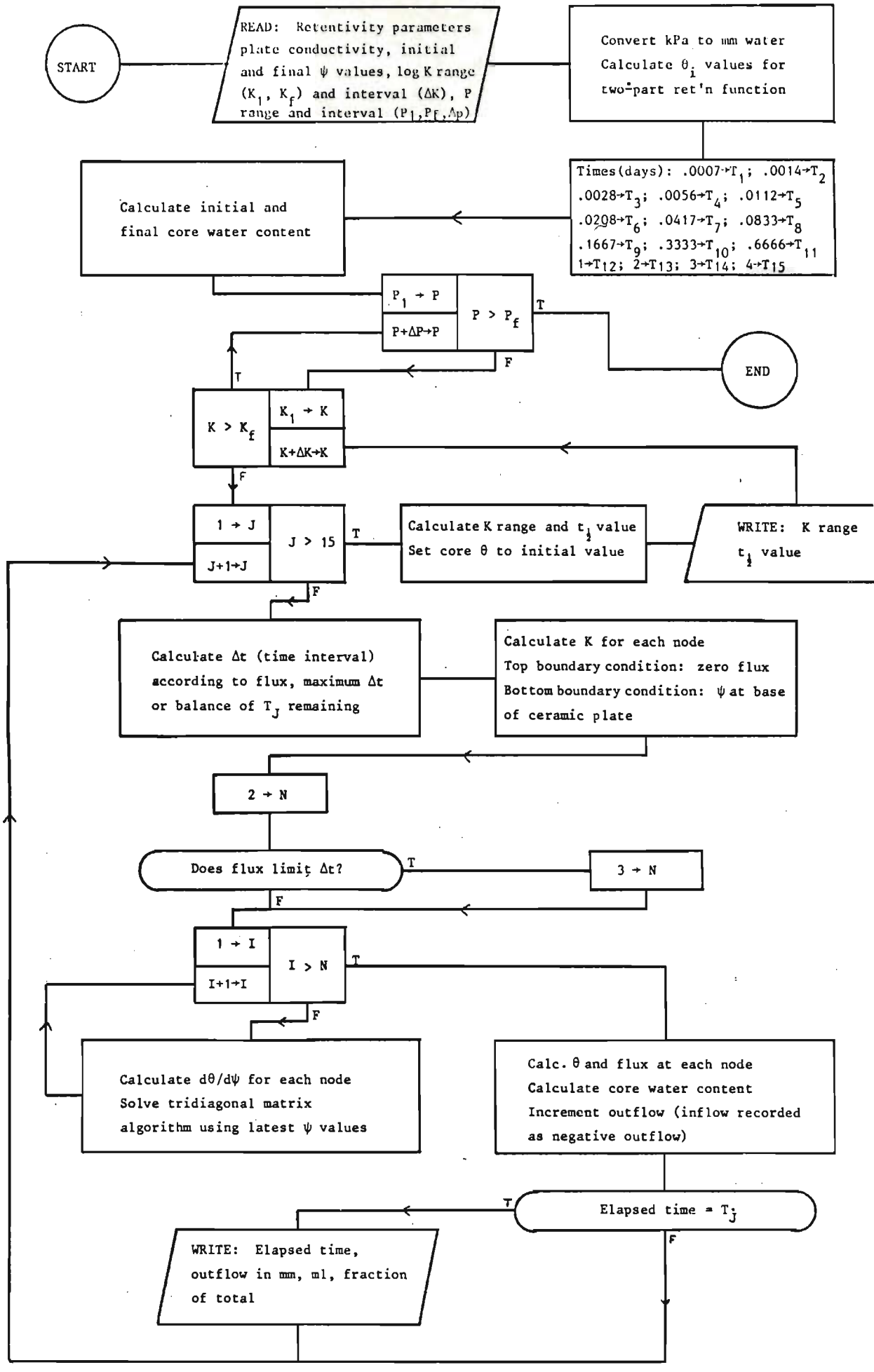

FIGURE A2.1 Flowchart for OUTFLO, a program for simulating outflow or inflow of water in soil cores

TABLE A2.2 A FORTRAN program for OUTFLO

```
 50 FILE  2(KIND=REMOTE)
100 FILE  6=PRINTER,UNIT=PRINTER,RECORD=80
200 FILE  1=TEMPE/KS,UNIT=DISK,RECORD=14,BLOCKING=420
300 *RESET FREE
400 C THIS PROGRAM SIMULATES OUTFLOW OR INFLOW FROM A SOIL CORE
500 C SUPPORTED ON A CERAMIC PLATE OF SPECIFIED CONDUCTIVITY.  SIMULATIONS
600 C ARE PERFORMED AT EACH OF SEVERAL COMBINATIONS OF SOIL K AND PORE
700 C INTERACTION PARAMETER VALUES
900 C  R5=DEPTH NODE INTERVALS
000 C  R53,R54=INITIAL AND FINAL POTENTIALS
100 C
150 C FUNCTIONS ARE BASED ON TWO-PART RETENTIVITY EQUATION (TABLE 3.12)
200       FUNCTION THETA(R13,FQ,FF,FQ,FI,FL)
300       IF(R13-FQ)6050,6050,6060
400  6050 THETA=FF*(AMIN1(FQ,R13)/FQ)**(-1/FI);GO TO 6061
500  6060 THETA=FF-(FF*(1-FL/FF)*((AMIN1(R13,-10))**2))/(FQ*FQ*((FL/FF)**(-2
600     1*FI)))
700  6061 RETURN
800       END
900       FUNCTION POTL(R13,FL,FF,FQ,FI)
000       IF(R13-FL)6040,6030,6030
100  6030 POTL=(SQRT(1-R13/FF))*FQ*((FL/FF)**(-FI))/SQRT(1-FL/FF)
200  6040 IF(R13.LT.FQ)POTL=FQ*(R13/FF)**(-FI)
300       RETURN
400       END
500 C
600 C
700       FUNCTION HC(R13,FQ,FW,FQ,FI,FF,FL,PP)
800       IF(R13.LE.FQ)HC=AMIN1(FW,FW*(FQ/AMIN1(FQ,R13))**(2+(2+PP)/FI))
900       IF(R13.GT.FQ)HC=FW*((THETA(R13,FQ,FF,FQ,FI,FL)/FF)**FI)**
000      1(2+(2+PP)/FI)
100       RETURN
200       END
300 C
400       FUNCTION DWC(R13,FQ,FF,FI,FL,FQ)
500       IF(R13-FQ)6070,6070,6080
600  6070 DWC=FF*(-R13)**(-1/FI-1)/(FI*(-FQ)**(-1/FI));GO TO 6081
700  6080 DWC=-2*FF*(1-FL/FF)*AMIN1(-10,R13)/(FQ*FQ*((FL/FF)**(-2*FI)))
300  6081 RETURN
900       END
100       REAL L,N,I,K,M,MM,ML,K1,K2,KM
200       INTEGER RS,Q,R30,R46,R9,R27,R47,TRUN,RUN
300 C
400       DIMENSION N(50),I(50),RQ(50),RW(50),F(50),
500      1G(50),L(50),D(50),E(50),K(50),M(50),P(50),
600      2T(50),U(50),V(50),O(50),Z(50),Y(20,3,4),
700      3Y1(4),Y2(4),Y3(20),TH(4),K1(4),K2(4),KM(4)
800 C
900 C    N=NEW WATER POTL,  O=OLD WATER
000 C  POTL,  I,RQ,F,RW,C1L=SOIL HYDROLOGIC CONSTANTS,  E=WATER CONTENT,
5300 C  Y=OUTPUT DATA
5400       PI=3.14159
5500 C
5550       READ(1,9595)TRUN
5590       DO 9999 RUN=1,TRUN
5600 C  READ CORE AND PLATE DIMENSIONS
5700 C
5800       READ(1,9550)R4,R5,R8,R50,R55
5900 C
6000 C  READ HYDROLOGIC DATA
6100 C
6200       READ(1,9560)A,B,PORE,R7
6300 C
6400 C  READ START AND END POTENTIALS
6500 C
6600       READ(1,9570)R53,R54
6700
6800       Q=AINT(R8/R5)+AINT(R4/R5)+2
7000       READ(1,9590)CLO,CHI,CINT,PLO,PHI,PINT
7100       R52 =102.2*R53+(R4+.5*R5)
7200       R6=102.2*R54+(R4+.5*R5)
8500       DO 250 J=1,Q-AINT(R4/R5)-1
8600       I(J)=8
8700       RQ(J)=A
8800       F(J)=PORE
9000   250 CONTINUE
9010       DO 100 J=Q-AINT(R4/R5),Q
9020       RQ(J)=-1*10**4
9030       I(J)=10
9040       F(J)=.3
9050       RW(J)=R7
9060   100 CONTINUE
9070 C  D VALUES ARE TIME INTERVALS(DAYS) AT WHICH OUTPUT IS PRINTED
9100       D(1)=.0007;D(2)=.0007;D(3)=.0014;D(4)=.0028
9200       D(5)=.0056;D(6)=.0096;D(7)=.0209;D(8)=.0416
9300       D(9)=.0834;D(10)=.1666;D(11)=.3334;D(12)=.3333
9400       D(13)=1.000;D(14)=1;D(15)=1
9500       R9=0;R10=0;R41=0;R39=0;R38=0;R40=0;R41=0;R42=0
9600       R43=0;R37=0;R25=0;TIME=0;R22=0
9700 C  CALCULATE CONSTANTS FOR SPECIAL FUNCTIONS
9800 C
9850       DO 500 J=1,Q
9900       L(J)=2*I(J)*F(J)/(1+2*I(J))
10100      G(J)=RQ(J)*(L(J)/F(J))**(-I(J))
10200  500 CONTINUE
10900 C  CALCULATE INITIAL CORE WATER CONTENT, R22
11000      DO 150 J=1,Q
11100      N(J)=R52-(Q-J)*R5
11200      O(J)=R6-(Q-J)*R5
11300  150 CONTINUE
```

```
1600        E(J)=THETA(R13,Q(J),F(J),RQ(J),I(J),L(J))
1700        R22=R22+E(J)
1800        R13=O(J)
1900        R41=R41+THETA(R13,Q(J),F(J),RQ(J),I(J),L(J))
2000    700 CONTINUE
2100        DO 900 J=1,Q
2200        O(J)=N(J)
2300    800 CONTINUE
2400 C
2500        MM=R5*(R22-R41)
2600        ML=(R22-R41)*R5*PI*R50*R50/4000
2700        WATER=(R22-R41)/(Q-AINT(R4/R5)-2)
2800        R9=0; R10=0; R41=0; R39=0; R38=0; R40=0; R41=0; R42=0
2900        R43=0; R37=0; R25=0; TIME=0
2990        WRITE(6,9200)A,R53,MM
2995        WRITE(6,9210)R50,B,R54,ML
3000        WRITE(6,9220)R8,PORE,WATER
3100        WRITE(6,9230)R5,R7
3200        WRITE(6,9240)R4
3400 C
3500        DO 6300 PP=PLO,PHI,PINT
3600        R47=0
3700        DO 6200 C=CLO,CHI,CINT
3750        R47=R47+1
3800        DO 210 J=1,Q
3900        N(J)=R52-(Q-J)*R5
3950        O(J)=N(J)
4100    210 CONTINUE
4150 C   INITIALIZE VARIABLES
4160        R9=0; R10=0; R41=0; R39=0; R38=0; R40=0; R41=0; R42=0
4170        R43=0; R37=0; R25=0; TIME=0
4200 C
4250        DO 220 J=1,Q-AINT(R4/R5)-1
4260        RW(J)=10**C
4270    220 CONTINUE
4300        R16=.05
4400        R18=R15
4500 C
4600        J=1
4700        R13=N(1)
4800        K(1)=HC(R13,Q(J),RW(J),RQ(J),I(J),F(J),L(J),PP)
4900        Z(1)=DWC(R13,Q(J),F(J),I(J),L(J),RQ(J))
5000        R20=0
5100        R19=10**(11)
5200 C   START OF TIME CYCLES
5300 C
5400        DO 1000 R27=1,15
5500        R20=0
5600        R25=0
5700        TIME=TIME+D(R27)
5800        Y3(R27)=TIME
```

```
18000    1800 R30=2
18100         R18=AMIN1(R55*R5/R19,R16)
18200         IF(R16.EQ.R18)R30=1
18300         R19=0
18400         IF(R20+R18-D(R27))2100,2100,2050
18500    2050 R18=D(R27)-R20
18600    2100 R20=R20+R18
18700         R25=R25+R18
18800 C   SET TOP BOUNDARY CONDITION
18900    2550 M(1)=1
19000         P(1)=(-K(1))*2*R5/K(1)-N(1)+N(2)
19100         R46=0
19200         J=1
19300         R13=N(1)
19400         K(1)=HC(R13,Q(J),RW(J),RQ(J),I(J),F(J),L(J),PP)
19500         Z(1)=DWC(R13,Q(J),F(J),I(J),L(J),RQ(J))
19600 C   INITIALIZE HYDRAULIC CONDUCTIVITIES
19700 C
19800         DO 2800 J=2,Q
19900         R13=N(J)
20000         K(J)=HC(R13,Q(J),RW(J),RQ(J),I(J),F(J),L(J),PP)
20100         K(J-1)=(K(J)+K(J-1))/2
20200    2800 CONTINUE
20300 C
20400 C   SIMULTANEOUS EQUATION SOLUTION- FORWARD
20500 C
20600    3500 DO 3600 J=1,Q
20700         R13=AMIN1(-10,O(J)+.99*(N(J)-O(J)))
20800         Z(J)=DWC(R13,Q(J),F(J),I(J),L(J),RQ(J))
20900    3600 CONTINUE
21000         DO 3900 J=2,Q-1
21100         R32=K(J)
21200         R34=K(J-1)
21300         R33=2*R5*R5*Z(J)/R18+R32+R34
21400         R35=R32*O(J+1)+R34*O(J-1)+(R33-2*R32-2*R34)*O(J)
21500         R35=R35+2*R5*(K(J-1)-K(J))
21600         M(J)=R32/(R33-R34*M(J-1))
21700         P(J)=(R35+R34*P(J-1))/(R33-R34*M(J-1))
21800    3900 CONTINUE
21900 C   SOLUTION OF SIMULTANEOUS EQUATIONS-REVERSE
22000 C
22100 C   SET BOTTOM BOUNDARY CONDITIONS
22200 C
22300         N(Q)=R6
22400    4200 J=Q
22500    4210 J=J-1
22600         N(J)=M(J)*N(J+1)+P(J)
22700         R13=N(J)
22800         IF(R46.LT.R30.AND.J.GT.1)GO TO 4210
22900         IF(R46-R30)4250,4300,4300
23000    4250 R46=R46+1
```

```
23200  4300 E(J)=THETA(R13,G(J),F(J),RG(J),I(J),L(J))
23300       U(J)=(K(J)-K(J)*(N(J+1)+O(J+1)-N(J)-O(J))/(2*R5))*R18
23400       R37=ABS(U(J)/R18)
23500       R19=AMAX1(R19,R37)
23600       V(J)=V(J)+U(J)
23700  4500 IF(J.GT.1)GO TO 4210
23800       DO 4550 J=1,G
23900       O(J)=N(J)
24000  4550 CONTINUE
24100 C INCREMENT OUTFLOW OR INFLOW  R39
24200 C
24300       R39=R39+U(1)
24400       R38=R39+U(G-AINT(R4/R5)-1)
24500       IF(R20*10**5+5.LT.O(R27)*10**5)GO TO 1800
25500 C
25600       Y(R27,1,R47)=R39
25700       Y(R27,2,R47)=R39*(PI*R50*R50)/4000
25800       Y(R27,3,R47)=R39/MM
25900       Y1(R47)=10**C
26000  1000 CONTINUE
26050  9660 FORMAT(2F6.2)
26051       WRITE(2,9660)PP,C
26053 C  MASS BALANCE CHECK
26054  5500 R41=0
26055       DO 5600 J=2,G-AINT(R4/R5)-1
26056       R41=R41+E(J)
26057  5600 CONTINUE
26060 C
26065       R42=(R41-R22)*R5
26070       Y2(R47)=R39-R42
26075 C CALC OF K RANGE
26077       J=2
26079       R13=R53*102.2
26091       K1(R47)=HC(R13,G(J),RW(J),RG(J),I(J),F(J),L(J),PP)
26093       R13=R54*102.2
26095       K2(R47)=HC(R13,G(J),RW(J),RG(J),I(J),F(J),L(J),PP)
26097       R13=102.2*(R53+R54)/2
26099       KM(R47)=HC(R13,G(J),RW(J),RG(J),I(J),F(J),L(J),PP)
26100  6200 CONTINUE
26200       WRITE(6,9310)
26300       WRITE(6,9260)Y1(1),Y1(2),Y1(3),Y1(4)
26400       WRITE(6,9270)PP,PP,PP,PP
26500       WRITE(6,9310)
26600       WRITE(6,9280)
26700       WRITE(6,9310)
26800       DO 5700 R27=1,15
26900       WRITE(6,9290)Y3(R27),Y(R27,1,1),Y(R27,2,1),Y(R27,3,1)
27000      1,Y(R27,1,2),Y(R27,2,2),Y(R27,3,2),Y(R27,1,3),Y(R27,2,
27100     23),Y(R27,3,3),Y(R27,1,4),Y(R27,2,4),Y(R27,3,4)
27300  5700 CONTINUE
27400 C  CALC OF TIME FOR HALF OUTFLOW
27500       DO 6500 R47=1,4
27550       TH(R47)=0
27600       DO 6400 R27=1,15
27700       IF(Y(R27,3,R47).LT..5)GO TO 6400
27750       IF(R27.EQ.1)GO TO 6500
27800       T2=ALOG10(Y3(R27))
27900       F2=Y(R27,3,R47)
28000       R27=R27-1
28100       T1=ALOG10(Y3(R27))
28200       F1=Y(R27,3,R47)
28300       TH(R47)=10**(T1+(.5-F1)*(T2-T1)/(F2-F1))
28400       GO TO 6500
28500  6400 CONTINUE
28600  6500 CONTINUE
28765       WRITE(6,9330)K1(1),K2(1),KM(1),K1(2),K2(2),KM(2),
28770      1K1(3),K2(3),KM(3),K1(4),K2(4),KM(4)
28800       WRITE(6,9300)TH(1),TH(2),TH(3),TH(4)
28890       WRITE(6,9340)Y2(1),Y2(2),Y2(3),Y2(4)
28900       WRITE(6,9320)
29000  6300 CONTINUE
29045       WRITE(6,9325)
29100 C
29150  9999 CONTINUE
29200 C  FORMATS
29300 C
29400  9200 FORMAT(/" CORE NO:"17X,"A:",F10.4,3X,"INITIAL POT'L:",F7.2," KPA"
29500      1,3X,"TOTAL OUTFLOW:"F8.4," MM")
29600  9210 FORMAT(3X,"DIAM :",F4.1," MM",10X,"B:",F9.3,6X,"FINAL POT'L:"
29700      1,F7.2," KPA",16X,":",F8.4," ML")
29800  9220 FORMAT(3X,"DEPTH:",F4.1," MM   POROSITY:",F10.4,6X,"(AT PLATE)",
29900      128X,":",F9.5," THETA")
30000  9230 FORMAT(3X,"NODES:",F4.1," MM",4X,"PLATE K:",F5.2," MM/D")
30100  9240 FORMAT(18X,"THICKNESS:" ,F7.0," MM")
30200  9260 FORMAT(" KSAT:   ",4(9X,F7.0," MM/D",5X))
30300  9270 FORMAT("     P:   ",4(12X,F4.2,10X))
30400  9280 FORMAT("  DAYS   ",4(5X,"MM",6X,"ML   FRACTION"))
30500  9290 FORMAT(F6.4,2X,4(F9.4,F8.4,F8.4,1X))
30600  9300 FORMAT(" T(0.5):",4(F11.4,15X))
30700  9310 FORMAT(1X)
30800  9320 FORMAT(//)
30850  9325 FORMAT(1H1)
30860  9330 FORMAT(" K RANGE",4(2X,3E8.3))
30900  9550 FORMAT(2F4.0,F5.0,F7.1,F7.3)
31000  9560 FORMAT(E10.3,F9.3,F8.4,F6.2)
31100  9570 FORMAT(2F9.2)
31200  9580 FORMAT(6F6.2)
31240  9340 FORMAT("CHECK    ",4(6X,F8.2,12X))
31250  9595 FORMAT(I4)
31300       END
```

TABLE A2.3 An example of TEMPE, an input data file for OUTFLO

```
  12
   6    2    30    85.5   0.010
-1.330E+02      0.837   0.4140   2.14
    -2.99     -9.98
  2.00   5.00   1.00   1.00   1.33   0.33
   6    2    30    85.5   0.010
-1.330E+02      0.837   0.4140   2.14
   -10.57    -30.82
  2.00   5.00   1.00   1.00   1.33   0.33
   6    2    30    85.5   0.010
-1.017E+02      0.796   0.4101   2.14
   -30.82    -10.16
  2.00   5.00   1.00   1.00   1.33   0.33
   6    2    30    85.5   0.010
-1.017E+02      0.796   0.4101   2.14
   -10.16     -3.03
  2.00   5.00   1.00   1.00   1.33   0.33
   6    2    30    85.5   0.010
-1.266E+02      0.827   0.4188   0.90
    -2.99     -9.98
  2.00   5.00   1.00   1.00   1.33   0.33
   6    2    30    85.5   0.010
-1.266E+02      0.827   0.4188   0.90
   -10.57    -30.82
  2.00   5.00   1.00   1.00   1.33   0.33
   6    2    30    85.5   0.010
-0.944E+02      0.815   0.4159   0.90
   -30.82    -10.16
  2.00   5.00   1.00   1.00   1.33   0.33
   6    2    30    85.5   0.010
-0.944E+02      0.815   0.4159   0.90
   -10.16     -3.03
  2.00   5.00   1.00   1.00   1.33   0.33
   6    2    30    85.5   0.010
-1.176E+02      0.863   0.4338   0.50
    -2.99     -9.98
  2.00   5.00   1.00   1.00   1.33   0.33
   6    2    30    85.5   0.010
-1.176E+02      0.863   0.4338   0.50
   -10.57    -30.82
  2.00   5.00   1.00   1.00   1.33   0.33
   6    2    30    85.5   0.010
-0.960E+02      0.765   0.4188   0.50
   -30.82    -10.16
  2.00   5.00   1.00   1.00   1.33   0.33
   6    2    30    85.5   0.010
-0.960E+02      0.765   0.4188   0.50
   -10.16     -3.03
  2.00   5.00   1.00   1.00   1.33   0.33
```

APPENDIX 3

CALCULATION OF HYDRAULIC CONDUCTIVITY FROM OUTFLOW DATA USING PASSIOURA'S METHOD

The computer program PASSIOURA for calculating K from outflow was developed from the procedure outlined by Passioura (1976) and Jaynes and Tyler (1981). The method used to estimate water content at the upper surface of the core, θ_L, from mean core water content, $\bar{\theta}$, is identical to their graphical technique. The essential steps in the program are outlined in Fig. A3.1 and the FORTRAN program (Burroughs B7700) is listed in Table A3.2.

Core dimensions, retentivity parameters and measured outflow data are stored in file PASSFLO according to the format listed in Table A3.1. A sample calculation, consisting of input data file PASSFLO and output file PASSOUT, is shown in Table A3.3.

TABLE A3.1 Format for file PASSFLO

RECORD	FORMAT	VARIABLE NAME	DESCRIPTION
1	F6.1	L	Core length (mm)
	F7.1	DIAM	Core diameter (mm)
	F7.4	WI	Initial mean core water content $\bar{\theta}_i$
	F7.4	WF	Final mean core water content $\bar{\theta}_f$
2	E11.3	A	Retentivity parameter a
	E7.3	B	Retentivity parameter b
	F7.4	WS	Porosity θ_s
	F7.4	WR	Residual saturation θ_r
	I5	N	Number of outflow observations
3toN+2	F8.4	T(J)	Time (days)
	F7.3	V(J)	Cumulative outflow volume (ml)

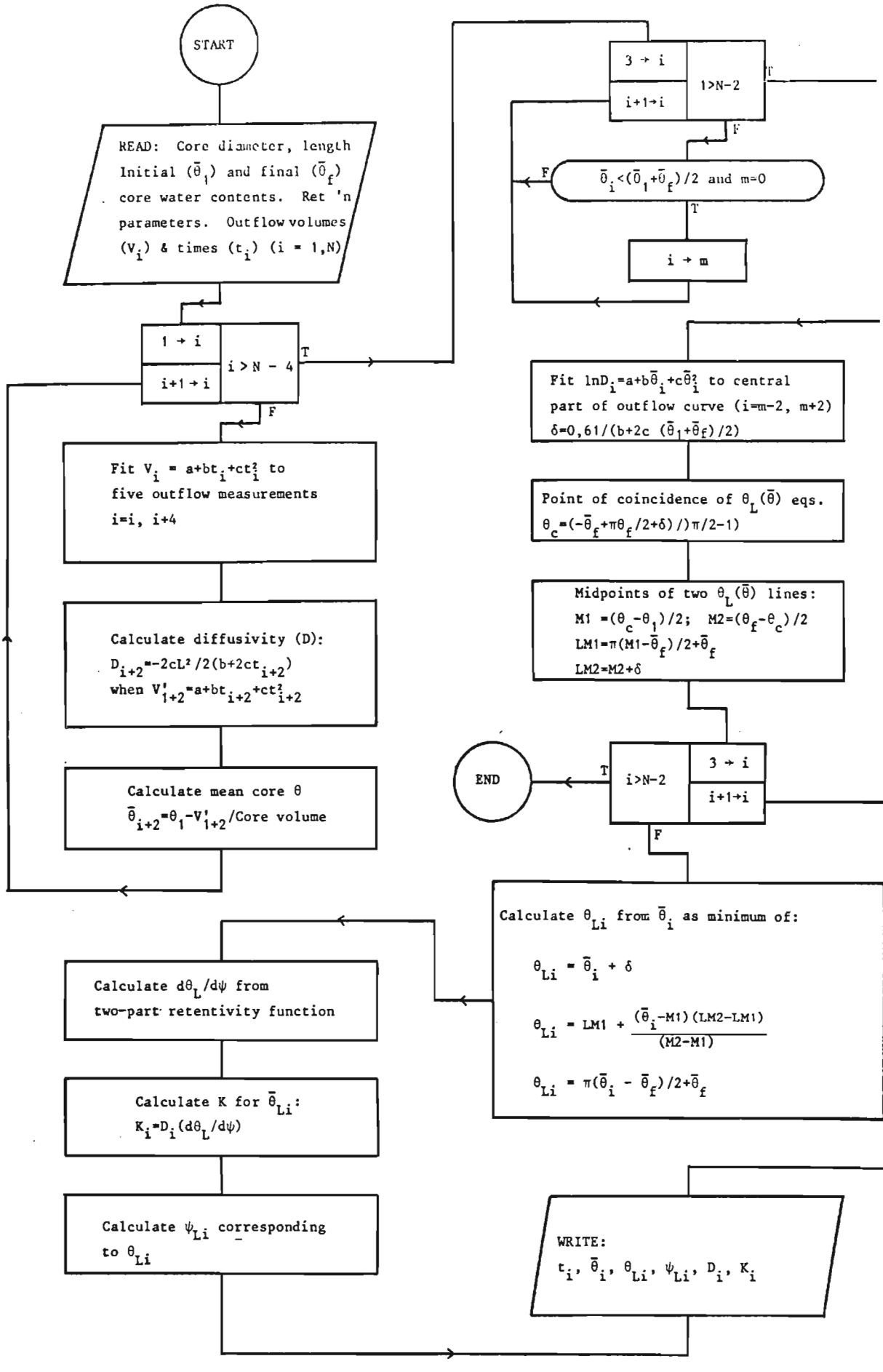

FIGURE A3.1 Flowchart for PASSIOURA, a program for calculating hydraulic conductivity from outflow data

TABLE A3.2 A FORTRAN program for PASSIOURA

```
PAGE 1          DATE 24/09/83 FILE: (LGROND)JLH/PASSIOURA

  100 FILE  6=PASSOUT,UNIT=DISK,RECORD=14,BLOCKING=420
  200 FILE  1=PASSFLO,UNIT=DISK,RECORD=14,BLOCKING=420
  250 FILE  2(KIND=REMOTE)
  300 $RESET FREE
  400 C CALCULATION OF K(THETA) FROM OUTFLOW USING PASSIOURAS METHOD
  500 C CORE LENGTH MM =L; INITIAL THETA=WI; FINAL THETA=WF;
  600 C ELAPSED TIME=T(J); OUTFLOW ML =V(J); DIFFUSIVITY=DIFF(J);
  700 C MEAN THETA=WM(J); THETA L=WL(J); BEST FIT V(J)=VE(J);
  800 C A,B,WS,WR=RETENTIVITY PARAMETERS; CORE DIAM MM =DIAM;
  900 C CORE VOL=VOL
 1000       REAL L,N,K,M1,M2,M1L,M2L,LND
 1100       DIMENSION T(50),V(50),DIFF(50),WM(50),VE(50),
 1200      1LND(50),WL(50),K(50),HL(50)
 1300       PI=3.14159
 1400 C READ CORE AND INITIAL DATA
 1500 C
 1600       READ(1,9500)L,DIAM,WI,WF
 1700       READ(1,9600)A,B,WS,WR,N
 1800       READ(1,9700)(T(J),V(J),J=1,N)
 1900       VOL=PI*L*(DIAM/2)**2
 2000 C
 2100 C CALCULATE 1ST AND 2ND DIFFERENTIALS OF OUTFLOW CURVE
 2200 C
 2300       DO 100 J=1,N-4
 2400       DO 110 Z=J,J+4
 2500       R25=R25+T(Z)*T(Z)
 2600       R21=R21+T(Z)
 2700       R33=R33+T(Z)**3
 2800       R35=R35+T(Z)**4
 2900       R36=R36+T(Z)*T(Z)*V(Z)
 3000       R28=R28+V(Z)
 3100       R14=R14+T(Z)*V(Z)
 3200   110 CONTINUE
 3300       R37=5*R25-R21**2
 3400       R38=5*R36-R25*R28
 3500       R39=5*R33-R21*R25
 3600       R40=5*R14-R21*R28
 3700       R41=5*R35-R25**2
 3800 C
 3900 C CONSTANTS IN QUADRATIC FIT: R1,R2,R3
 4000 C
 4100       R1=(R37*R38-R39*R40)/(R37*R41-R39*R39)
 4200       R2=(R40-R1*R39)/R37
 4300       R3=(R28-R25*R1-R21*R2)/5
 4400 C
 4500 C PREDICTED CENTRAL OUTFLOW VOL USING QUADRATIC FIT
 4600 C
 4700   105 VE(J+2)=R3+R2*T(J+2)+R1*T(J+2)**2
 4800 C
 4900 C IST DIFFERENTIAL
 5000       R4=R2+2*R1*T(J+2)
 5100 C 2ND DIFFERENTIAL
 5200       R5=2*R1
 5300 C DIFFUSIVITY
 5400       DIFF(J+2)=-R5*L*L/(2*R4)
 5451       WRITE(2,9999)R1,R2,R3,V(J+2),VE(J+2),DIFF(J+2)
 5500 C
 5800       R1=0; R2=0; R3=0; R4=0; R5=0; R14=0; R20=0; R25=0; R28=0; R33=0
 5900       R37=0; R38=0; R39=0; R40=0; R41=0; R35=0; R36=0; R21=0
 6000   100 CONTINUE
 6030   115 CONTINUE
 6100 C
 6110 C MEAN CORE WATER CONTENT
 6115       DO 130 J=1,N-4
 6120       WM(J+2)=WI-1000*VE(J+2)/VOL
 6125   130 CONTINUE
 6200 C CALCULATE LN DIFF AND MIDPOINT OF OUTFLOW
```

```
C
      DO 300 J=3,N-2
9999  FORMAT(6E11.3)
      LND(J)=ALOG(DIFF(J))
      IF(C.GT.0)GO TO 300
      IF(WM(J).LT.(WI+WF)/2)C=J
  300 CONTINUE
C
C CALC SLOPE OF LN DIFF/WM AT (WI-WF)/2
C
      DO 400 J=C-2,C+2
      R25=R25+WM(J)*WM(J)
      R21=R21+WM(J)
      R33=R33+WM(J)**3
      R35=R35+WM(J)**4
      R36=R36+WM(J)*WM(J)*LND(J)
      R28=R28+LND(J)
      R14=R14+WM(J)*LND(J)
  400 CONTINUE
      R37=5*R25-R21**2
      R38=5*R36-R25*R28
      R39=5*R33-R21*R25
      R40=5*R14-R21*R28
      R41=5*R35-R25**2
      R1=(R37*R38-R39*R40)/(R37*R41-R39**2)
      R2=(R40-R1*R39)/R37
      R3=(R28-R25*R1-R21*R2)/5
      R4=R2+2*R1*(WI-WF)/2
C CALC WL-WM=DW (ETA IN PASSIOURAS PAPER)
      DW=0.61/R4
C CALC POINT OF COINCIDENCE OF TWO THETAL/THETA LINES (WM VALUE)
      WCOIN=(-WF+PI*WF/2+DW)/(PI/2-1)
C CALC MIDPOINTS ON EACH LINE (M1 AND M2)
      M1=(WCOIN-WI)/2
      M2=(WF-WCOIN)/2
C WL VALUES CORRESPONDING TO M1 AND M2
      M1L=PI*(M1-WF)/2+WF
      M2L=M2+DW
C CALCULATE WL(J)VALUES FROM WM(J)
      DO 500 J=3,N-2
      IF(WM(J).LE.M1)GO TO510
      IF (WM(J).LE.M2)GO TO 520
      WL(J)=WM(J)+DW
      GO TO 550
  510 WL(J)=M1L+(WM(J)-M1)*(M2L-M1L)/(M2-M1)
      GO TO 550
  520 WL(J)=PI*(WM(J)-WF)/2+WF
C CALC K(THETA L) VALUES
  550 DWC=-((WS-WR)**(-B))*((WL(J)-WR)**(B+1))/(A*B)
      K(J)=DIFF(J)*DWC
C CALCULATE CORRESPONDING H VALUES
      HL(J)=(A*((WL(J)-WR)/(WS-WR))**(-B))/102.2
  500 CONTINUE
C PRINT RESULTS
      WRITE(6,9500)L,DIAM,WI,WF
      WRITE(6,9600)A,B,TS,TR,N
      WRITE(6,9030)
      WRITE(6,9030)
      WRITE(6,9010)
      WRITE(6,9020)
      WRITE(6,9030)
      DO 600 J=1,N
      WRITE(6,9040)T(J),WM(J),WL(J),HL(J),DIFF(J),K(J)
  600 CONTINUE
 9010 FORMAT("   TIME    MEAN    UPPER  POT'L    DIFF     CONDUCTIVITY")
 9020 FORMAT("   DAYS   THETA    THETA    KPA    SQMM/D       MM/DAY")
 9030 FORMAT(1X)
 9040 FORMAT(F8.4,2F7.4,F8.2,E9.2,E11.3)
 9500 FORMAT(F6.1,F7.1,F7.4,F7.4)
 9600 FORMAT(E11.3,F7.3,F7.4,F7.4,I5)
 9700 FORMAT(F8.4,F7.3)
 9800 LOCK(6)
      END
```

TABLE A3.3 A sample calculation using PASSIOURA, showing input and output data

```
 30.0    54.0 0.1566 0.1287
-1.476E+02  0.802 0.5174 0.1200    18
 0.0012  0.200
 0.0031  0.300
 0.0067  0.400
 0.0135  0.500
 0.0265  0.600
 0.0420  0.700
 0.0670  0.800
 0.1000  0.900
 0.1450  1.000
 0.2000  1.100
 0.2800  1.200
 0.3800  1.300
 0.4800  1.400
 0.6300  1.500
 0.8300  1.600
 1.1500  1.700
 1.7000  1.800
 3.6000  1.900
```

```
30.0    54.0 0.1566 0.1287
-.148E+03  0.802 0.0000 0.0000    18
```

TIME DAYS	MEAN THETA	UPPER THETA	POT'L KPA	DIFF SQMM/D	CONDUCTIVITY MM/DAY
0.0012	0.0000	0.0000	0.00	0.	0.
0.0031	0.0000	0.0000	0.00	0.	0.
0.0067	0.1511	0.1513	-11.09	.26E+05	.882E+00
0.0135	0.1496	0.1498	-11.53	.14E+05	.442E+00
0.0265	0.1479	0.1481	-12.09	.87E+04	.247E+00
0.0420	0.1465	0.1468	-12.57	.57E+04	.147E+00
0.0670	0.1450	0.1452	-13.18	.40E+04	.942E-01
0.1000	0.1436	0.1438	-13.82	.26E+04	.546E-01
0.1450	0.1420	0.1423	-14.56	.21E+04	.388E-01
0.2000	0.1407	0.1409	-15.33	.15E+04	.257E-01
0.2800	0.1392	0.1394	-16.27	.91E+03	.132E-01
0.3800	0.1376	0.1378	-17.40	.75E+03	.941E-02
0.4800	0.1363	0.1365	-18.49	.76E+03	.838E-02
0.6300	0.1348	0.1350	-19.96	.69E+03	.634E-02
0.8300	0.1334	0.1337	-21.55	.48E+03	.374E-02
1.1500	0.1321	0.1323	-23.41	.25E+03	.162E-02
1.7000	0.0000	0.0000	0.00	0.	0.
3.6000	0.0000	0.0000	0.00	0.	0.